Graphene-based flexible textile supercapacitor for wearable electronic applications

A thesis submitted in partial fulfilment of the requirements of the University of the West of England, Bristol for the degree of Doctor of Philosophy

College of Arts, Technology and Environment

December 2023

Md Rashedul Islam

Centre for Print Research (CFPR), School of Arts

Supervised by

Dr Nazmul Karim

TABLE OF CONTENTS

(Image and Article redacted for copyright reasons)

Word count (without reference): 47,426.

LIST OF FIGURES

LIST OF TABLES

ABBREVIATIONS

0D	zero-dimensional
1D	one-dimensional
2D	Two-dimensional
3D	Three-dimensional
AC	Activated carbon
AFM	Atomic Force Microscopy
BP	Black phosphorus
BSA	Bovine Serum Albumin
BSEN	British Standard European Norm
CB	Carbon black
CMC	Carboxy methyl cellulose
CNTs	Carbon nanotubes
CPs	Conducting polymers
CV	Cyclic voltammetry
CVD	Chemical vapor deposition
DI water	De-ionized water
DMP	Dimatix Material Printer
DMSO	Dimethyl sulfoxide
EDLC	Electric double-layer capacitor
EES	Electrochemical energy storage
EIS	Electrochemical impedance spectroscopy
E-textiles	Electronic textiles
GCD	Galvanostatic charge/discharge
GO	Graphene oxide
h-BN	Hexagonal boron nitride
IJP	Inkjet printing
LED	Light emitting diode
MOFs	Metal-organic frameworks
MoS_2	Molybdenum di-sulphide
MWCNTs	Multiwalled carbon nanotubes

P3HT	Poly(3-hexylthiophene)
PA	Polyamide or nylons
PANI	Polyaniline
PC	propylene carbonate
PDMS	Polydimethylsiloxane
PDMS	Polydimethylsiloxane
PEDOT	Poly (3,4-(ethylenedioxy) thiophene)
PEN	Polyethylene naphthalate
PEO	poly (ethylene oxide)
PET	Poly (ethylene terephthalate) or polyesters
PI	Polyimide
PMMA	poly (methyl methacrylate)
PP	Polypropylene
PPy	Polypyrrole
PSS	Poly(styrenesulfonate)
PSS	Poly (4-styrene sulfonate)
PVA	poly (vinyl alcohol)
PVC	Polyvinyl chloride
rGO	Reduced graphene oxide
SC	Supercapacitor
SDC	Sodium deoxycholate
SEM	Scanning electron microscope
SSF	stainless steel fibres
SWCNTs	Single-walled carbon nanotubes
TEM	Transmission Electron Microscopy
TMD	Transition metal dichalcogenide
TPU	Thermoplastic polyurethane
XG	Xanthan gum
XPS	X-ray Photoelectron Spectroscopy
XRD	X-ray diffraction

ABSTRACT

Smart electronic textiles (e-textiles) have drawn significant interests as lightweight, flexible and comfortable next-generation wearable devices due to their ability to continuously monitor, collect, and communicate various physiological parameters. They hold promise for diverse applications, including sportswear, military uniforms, safety instruments, environmental monitoring, and healthcare applications. However, a key challenge in integrating wearable devices into textiles lies in the demand for lightweight, flexible, and high-performance power supply units. Consequently, thin and flexible textile-based supercapacitors are being explored due to their inherent lightweight nature and remarkable power density. Nonetheless, the manufacture of high-performance textile supercapacitors for widespread industrial adoption in a scalable manner remains a formidable challenge.

To address this, the first study establishes an experimental protocol for traditional screen-printing of highly conductive graphene-based conductive inks on textiles showcasing their potential in applications like piezoresistive sensing, EEG electrodes, and supercapacitor electrodes. The resultant screen-printed in-plane textile supercapacitor achieves a notable aerial capacitance of approximately 3.2 mF $cm^{-2.}$ The second study focuses on the scalable exfoliations of two-dimensional materials, specifically graphene and MoS_2, and their integration onto textiles using an industrially viable high-speed pad-dry-cure technique for high-performance wearable supercapacitors applications. The graphene-MoS_2-graphene tri-layered heterostructure-based textile supercapacitors reveal an impressive areal capacitance of ~180 mF cm^{-2}. In the third study, sustainable digital manufacturing of 2D heterostructure-based textiles was investigated via layer-by-layer inkjet printing of 2D materials (graphene, MoS_2 and hBN) onto a rough and porous textile surface. The resulting graphene-hBN-graphene heterostructure textiles showcase a remarkable areal capacitance of ~32.5 mF cm^{-2}, surpassing existing literature on graphene-based inkjet-printed supercapacitors. Finally, the fourth study explores the utilization of a standalone Co/Zn-metal organic framework (MOF) for textile supercapacitor applications. Employing screen printing, pad-dry-cure, and inkjet printing, MOF-coated textiles achieve a remarkable areal capacitance of ~359.36 mF cm^{-2}. The findings from these four studies distinctly highlight the promise of textile-based supercapacitors for wearable electronics applications, signifying an important step toward moving from R&D-based textile supercapacitors to actual real-world applications.

DECLARATION AND COPYRIGHT

This PhD thesis includes chapters containing data from where either journal articles have already been published in peer-reviewed journals or to be submitted. The candidate is the first author for the journal papers as a principal contributor. The candidate declares that no other portion of the work referred to in this thesis has been submitted in support of an application for another degree or qualification at this or any other university or institute of learning.

DEDICATION

This thesis is dedicated to my beloved parents (Md Rafique Uddin Molla and Amena Khatun) for their unconditional love, support, and inspiration to be a better human being.

ACKNOWLEDGEMENT

It is my pleasure to acknowledge my gratefulness to my Director of studies (DoS), Associate Professor *Dr Nazmul Karim*, for his kind support and continuous guidance in carrying out this project. His availability, useful guidelines, constructive comments, and advice made this PhD journey worth accomplishing smoothly. With his guidance, I gradually developed the knowledge and understanding on my doctoral work and a great interest in this field of research. With his support, I had the opportunity to work with lab colleagues and collaborators on various- exciting projects and publish my work in peer-review journals and conferences. His own passion and enthusiasm towards work and research have inspired me to work hard with passion and enthusiasm. I will always cherish the opportunities he provided me to proof myself. In this instance, I would also want to take the opportunity to congratulate him for his recent appointment as a full Professor at the Nottingham Trent University, Nottingham, UK.

I also would like to thank my additional supervisors *Prof Carinna Parraman* and *Dr Shaila Afroj* for their helpful suggestions and guidance. Their advice helped me in designing the projects and their critical discussion on the experimental results helped me improve my experimental approach.

I would like to thank UWE-Augtex Partnership PhD program for funding the project. My heartiest gratitude goes to the Government of Bangladesh and Bangladesh University of Textiles (BUTEX), Dhaka, Bangladesh to allow me a study leave to pursue this PhD program.

I am very thankful to my lab-mates, colleagues, technical staffs and all the internal and external collaborators for their support and assistance throughout my PhD.

Finally, I would also like to sincerely thank my parents, my brother and sister for their inspiration throughout my life who always been there for me and have always been proud of my accomplishments.

BIOGRAPHICAL

Author

Md Rashedul Islam

Education

April 2014- October 2017	MSc Textile Engineering (Wet Processing) Bangladesh University of Textiles, Dhaka, Bangladesh
April 2007- August 2012	BSc Textile Engineering (Wet Processing) Bangladesh University of Textiles, Dhaka, Bangladesh

Professional Experience

December 2022- March 2023	Temporary Research Associate Centre for Print Research, University of the West of England (UWE), Bristol, UK
February 2022- June 2022	Temporary Research Associate Centre for Print Research, University of the West of England (UWE), Bristol, UK
February 2020- till date	Assistant Professor (currently on study leave), Department of Wet Process Engineering, Bangladesh University of Textiles, Dhaka, Bangladesh
September 2017- February 2020	Lecturer, Department of Wet Process Engineering, Bangladesh University of Textiles, Dhaka, Bangladesh
April 2016- September 2017	Assistant Professor, Department of Textile Engineering, Ahsanullah University of Science and Technology, Dhaka, Bangladesh
May 2013- April 2016	Lecturer, Department of Textile Engineering, Ahsanullah University of Science and Technology, Dhaka, Bangladesh
January 2013- April 2013	Lecturer, Department of Textile Engineering, Primeasia University, Dhaka, Bangladesh
November 2012- January 2013	Executive, Viyealltex Group, Dhaka, Bangladesh

Peer-reviewed journal articles published:[1-9]

(1) Islam, M. H.; **Islam, M. R.**; Dulal, M.; Afroj, S.; Karim, N. The effect of surface treatments and graphene-based modifications on mechanical properties of natural jute fibre reinforced composites: a review. *iScience* **2021**, 103597. DOI: 10.1016/j.isci.2021.103597.

(2) **Islam, M. R.**; Afroj, S.; Beach, C.; Islam, M. H.; Parraman, C.; Abdelkader, A.; Casson, A. J.; Novoselov, K. S.; Karim, N. Fully printed and multifunctional graphene-based wearable e-textiles for personalized healthcare applications. *iScience* **2022**, *25* (3), 103945. DOI: 10.1016/j.isci.2022.103945.

(3) **Islam, M. R.**; Afroj, S.; Novoselov, K. S.; Karim, N. Smart Electronic Textile-Based Wearable Supercapacitors. *Advanced Science* **2022**, *9* (31), 2203856. DOI: 10.1002/advs.202203856.

(4) Maiti, S.; **Islam, M. R.**; Uddin, M. A.; Afroj, S.; Eichhorn, S. J.; Karim, N. Sustainable Fiber-Reinforced Composites: A Review. *Advanced Sustainable Systems* **2022**, *6* (11), 2200258. DOI: 10.1002/adsu.202200258.

(5) Tan, S.; **Islam, M. R.**; Li, H.; Fernando, A.; Afroj, S.; Karim, N. Highly Scalable, Sensitive and Ultraflexible Graphene-Based Wearable E-Textiles Sensor for Bio-Signal Detection. *Advanced Sensor Research* **2022**, *1* (1), 2200010. DOI: 10.1002/adsr.202200010.

(6) Tan, S.; Afroj, S.; Li, D.; **Islam, M. R.**; Wu, J.; Cai, G.; Karim, N.; Zhao, Z. Highly sensitive and extremely durable wearable e-textiles of graphene/carbon nanotube hybrid for cardiorespiratory monitoring. *iScience* **2023**, *26* (4), 106403. DOI: 10.1016/j.isci.2023.106403.

(7) Dulal, M.; **Islam, M. R.**; Maiti, S.; Islam, M. H.; Ali, I.; Abdelkader, A. M.; Novoselov, K. S.; Afroj, S.; Karim, N. Smart and Multifunctional Fiber-Reinforced Composites of 2D Heterostructure-Based Textiles. *Advanced Functional Materials* **2023**, *33* (40), 2305901. DOI: 10.1002/adfm.202305901.

(8) **Islam, M. R.**; Afroj, S.; Karim, N. Scalable Production of 2D Material Heterostructure Textiles for High-Performance Wearable Supercapacitors. *ACS Nano* **2023**, *17* (18), 18481-18493. DOI: 10.1021/acsnano.3c06181.

(9) **Islam, M. R.**; Afroj, S.; Yin, J.; Novoselov, K. S.; Chen, J.; Karim, N. Advances in Printed Electronic Textiles. *Advanced Science* **2023**, *n/a* (n/a). DOI: 10.1002/advs.202304140.

Journal articles submitted for publication:

(1) Ali, I; **Islam, M.R.,** Junyi, Y.; Eichron, S.; Chen, J.; Karim, N.; Afroj, S. Advances in Smart Photovoltaic Textiles.

Journal articles ready for submission:

(1) **Islam, M. R.**; Afroj, S.; Karim, N. Ultra-flexible and machine-washable fully-inkjet-printed 2D heterostructures-based textiles for wearable supercapacitors applications.

(2) **Islam, M. R.**; Afroj, S.; Karim, N. Metal organic framework (MOF)-based wearable e-textiles for high-performance supercapacitors.

Conference poster presentations:

(1) **Islam, M. R.**; Afroj, S.; Karim, N. Screen-printed Multifunctional Wearable E-textiles1st International Future Textiles Conference (28 Feb-2 Mar 2023), UWE Bristol, UK.

(2) **Islam, M. R.**; Afroj, S.; Karim, N. Graphene-based Screen-printed Multifunctional Wearable E-textiles. 4th International Conference on the Challenges, Opportunities, Innovations and Applications in Electronic Textiles (8 – 10 November 2022), Nottingham, UK.

(3) **Islam, M. R.**; Afroj, S.; Karim, N. Graphene-based Multifunctional Wearable E-textiles. Faculty of ACE, Postgraduate Research PGR Conference (5 October 2021), UWE Bristol, UK.

1. General Introduction

1.1 Introduction

The realm of personalized healthcare has been transformed by wearable electronics, which allow for unobtrusive tracking of human health throughout daily activities.[1-3] The rapid progress in smart wearable technology and integrated electronics has significantly fuelled the growing demand for printed microelectronics with attributes like lightweight, high performance, and remarkable mechanical flexibility.[4, 5] Wearable electronic textiles (e-textiles), containing electronics and interconnections woven/knitted or printed/coated onto or into textiles,[6, 7] are of great interest in this regard, providing better comfortability, durability and lighter weight as well as maintaining the desirable electrical property.[8, 9]

Till date, one of the key challenges to integrate electronic components into textiles is the requirement of a lightweight, flexible, and high-performance power supply unit.[10] Among the different electrochemical energy storage (EES) devices, high energy density batteries and high power density supercapacitors stand out as the most successful contenders on the Ragone chart. Their unique properties and applications in portable electronic devices, electric automobiles, and other areas have accumulated significant attention.[11, 12] Supercapacitors or ultracapacitors have gained greater attention as energy storage devices compared to batteries, primarily because of their rapid charging and discharging rates, exceptional rate capability, long cycle life, and cost-effectiveness.[13-15] Flexible textiles supercapacitors (SCs) are promising due to their excellent lifetime, lightweight nature, high power density, and ability to deliver even under mechanically deformed conditions.[16] Recently, various types of flexible materials, including polymeric films, papers, fibres/yarns, and fabrics, carbon cloths, PET sheets have

been employed to produce all-solid-state supercapacitors, however, all of these materials are not suitable for clothing.[17] Fibers/yarns and fabrics, among them, are the most eye-catching substrates due to their integrate ability into clothes for direct manufacturing of wearable devices.[18] Textile materials, being highly flexible, show various advantages in mechanical properties like light weight, higher stretch ability and higher flexibility making them a favourable substrate in the application of energy storage devices. However, the main challenge to construct an energy-textiles is that flexible energy storage does not yet exist in a form, comparable with everyday fabrics, their feel, drape and thickness. In order to produce an "energy-textile" as part of a garment, it must be fabricated in a scalable and systematic manner allowing for multiple components of e-textiles to be integrated simultaneously.[19]

1.2 Research background

The most commonly used materials for supercapacitors electrodes are carbonaceous compounds (e.g. carbon black), metals and conductive polymers.[20, 21] Carbon black, composed of aggregated carbon nanoparticles in a three-dimensional structure, providing a conductive network typically has a high surface area, contributing to its capacitive performance. This is commonly used as a conductive additive in supercapacitor electrodes to enhance conductivity. Metal inks, though mostly used for their high conductivity; are expensive, environmentally unfriendly, not biocompatible and incompatible with heat sensitive textiles.[22] Metals typically possess a restricted surface area for charge storage, and characterized by rigidity, weight, and inflexibility, prone to corrosion potentially impacting their long-term stability. Conductive polymers exhibit lower electrical conductivity, with a moderate specific capacitance, and suffer from cycling stability issues.

The unique and often complementary properties of graphene and related two-dimensional (2D) materials offer an abundance of opportunities for next generation technologies. Transition metal dichalcogenides (TMDs), black phosphorus (BP) and hexagonal boron nitride (hBN) etc. are other such materials widely being studied for their tuneable properties.[23] Graphene, a single layer of sp2 bonded carbon atom,[24] has opened up a wide range of flexible electronics applications,[25] and thus graphene-based formulations are considered to be very promising for the next generation e-textiles.[26] The high mechanical flexibility, large surface area, good chemical stability, and superior electrical and thermal conductivities make it very competitive in new-generation energy application fields.[27]

In comparison to conventional carbon black, graphene, with its two-dimensional hexagonal lattice structure, offers an exceptionally high surface area, providing more sites for charge storage in supercapacitors. Macroscopic graphene, in contrast to metals, exhibits superior electrical conductivity (Appendix A), facilitating efficient charge and discharge cycles in supercapacitors. Graphene, renowned for its mechanical strength, flexibility, and lighter weight than metals, thus could be advantageous for applications in wearable electronic textiles. Being chemically stable, it contributes to the overall stability of supercapacitors. The remarkable combination of high conductivity and a large surface area also allow swift charging and discharging, rendering it suitable for applications requiring rapid energy release. Graphene thus can serve as an active material in supercapacitor electrodes. However, it is worth noting that traditional metals or conductive polymers are generally more cost-effective to produce, whereas the production of high-quality graphene can be expensive, potentially influencing the overall cost of graphene-based supercapacitors. The majority of the textile supercapacitors reported so far could only be produced at laboratory scale, such as fibre-like devices or synthesis on a carbon cloth.[8] Thin and flexible supercapacitors although gaining consideration,[28] still lagging behind the increasingly harsh requirements of industry. A key challenge is still the identification of ideal electrode materials satisfying the requirements of high energy-power densities and long cycle life.[29] Therefore, there still exists a strong need for the development of flexible and high-performance energy storage devices to be integrated with wearable electronics.

1.3 Research aim and objectives

The aim of the study is to develop scalable, low-cost, highly functional, and flexible graphene-based energy-storage textiles for powering personalized wearable garment. Specific objectives are:

- Developing functionalized and well-characterized graphene and other 2D materials for energy storage applications
- Developing a scalable and low-cost way of manufacturing textiles energy storage using existing manufacturing and fabrication methods (coating or printing)
- Analysing the electro-chemical and physical performance of developed energy storage fabrics in terms of energy density, charging-discharging and flexibility etc.
- Demonstration and validation of textile supercapacitors for wearable applications.

1.4 Thesis format and outline

This PhD thesis has been submitted in a format that includes chapters that contains the experimental methodologies and results from where journal articles have either already been published in peer-reviewed journals or are ready to submit. The references for all the chapters are included at the end of the thesis. As I was the principal contributor, I am the first author for the journal papers published from here. Due to the collaborative nature of the research, other authors have contributed towards the journal papers. However, my contribution to each chapter is presented at the beginning of each chapter (2,3, 4, 5 & 6). Chapter 1 introduces the topic for this PhD study, covering the research background, aims and objectives of this study. The literatures relevant to aims and objectives of this study are reviewed in Chapter 2. Chapter 3 reports the optimisation and application of versatile screen-printed graphene-based wearable e-textiles including supercapacitor for energy storage. In chapter 4, I report the scalable fabrication of 2D materials (graphene and MoS_2) and their heterostructure textiles for wearable supercapacitor application via highly scalable pad-dry coating technique [redacted] **(Texts redacted for copyright reasons)** Finally, the summary of the findings of this PhD study and the recommendations for future research are presented in Chapter 7.

2. Smart electronic textile-based wearable supercapacitors

Figure 2.1 Textile-based flexible supercapacitors for powering up wearable devices to monitor physiological parameters.

Wearable e-textiles have been going through significant evolutions in recent years, due to the continuous progress of material science and nanotechnology, miniaturization and wireless revolution.[30, 31] E-textiles possess functionalities such as sensing, computation, display and communication,[32-35] which facilitate the manufacturing of highly innovative and intelligent garments, able to perform as sensors, actuators, power generators, and energy storage devices all at the same time.[36, 37] Combining these electronic fibres/textiles with human skin can

potentially build an intelligent system that could be integrated with biological nerves, muscles, and ligaments in the future to endow us with more functions.[38] E-textiles inherit the advantages of being lightweight, flexible and air permeable with a certain degree of ductility of traditional fibres/textiles while possessing electronic functions.[39, 40] As a lightweight portable device to monitor vital health parameters *(Figure 2.1)*, e-textiles have become a focus of research interest due to their prospects in sportswear, military uniforms, safety instruments, environmental monitoring and health care applications.[41-43] However, one of the key challenges to integrate such electronic devices to textiles is the requirement of lightweight, flexible and high-performance power supply unit.[44, 45]

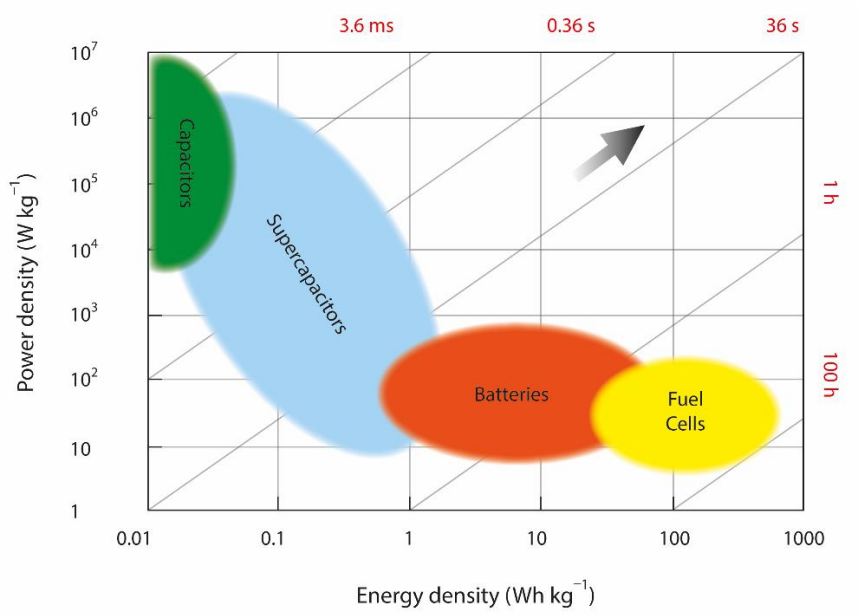

Figure 2.2 Ragone plot showing comparison of different electrochemical energy storage systems.

Conventional energy storage devices (e.g., batteries) can store a large amount of energy which cannot be delivered quickly owing to their higher internal resistance. Capacitors are another type of energy storage device, which can be charged and discharged quickly. However, capacitors have limited storage capacity. Therefore, the development of capacitors with high energy densities (i.e., supercapacitors) has become an exciting area of research for electrochemical energy storage/conversion systems. Supercapacitors (SC), also referred to as ultracapacitors, are promising electrochemical energy storage devices that can be charged and discharged within seconds, and possess high power density, long cycle life and outstanding cyclic stability.[46] As relatively new type of capacitors, they are distinguished by the phenomenon of electrochemical double-layer, diffusion and large effective area which lead to

extremely large capacitance per unit of geometrical area, taking their place in-between batteries and conventional capacitors. Considering energy and power densities, they also possess a wide area between batteries and conventional capacitors (*Figure 2.2*). The incorporation of flexible electrodes and/or substrate materials in SCs provides structural flexibility with their inherent high-power density, which are highly attractive for a large number of emerging portable and lightweight consumer devices.[47] Flexible plastic, elastomeric and textile substrates possess better biocompatibility, stretchability, transparency, and wearability.[48] In addition to intrinsic wearability and flexibility, a textile-based SC ensures better comfort when worn, better integration with the garment, and better wearability of the electronic components in comparison of the conventional rigid and bulky power supply units. It also ensures the enhanced mass loading of active materials, resulting in higher capacitance, energy and power density. Therefore, textile-based flexible SCs show a great potential for wearable electronic applications, due to miniaturized, portable, large-scale transparent and flexible consumer electronics in comparison with the current energy storage devices.[49] In this literature review, I focus on textiles-based flexible and wearable SCs due to their potential for next generation wearable e-textiles applications. I start with presenting an overview of electrochemical energy storage technologies and their working principles. I then discuss the basic parameters to evaluate SC performances and summarize electroactive materials required for the preparation of conductive textile electrodes and electrolytes for SC fabrications. I then review manufacturing techniques for conductive textile-based electrodes, followed by various forms of textile-based SCs and their integration techniques. The energy storage performances of recently developed textile based SCs in terms of capacitance, energy density, and power density are also summarized. Furthermore, key properties of textiles-based SCs for wearable e-textiles applications such as flexibility, safety and washability are discussed. I published this literature as two review article in *Advanced Science.*[10, 50]

2.1 Overview of electrochemical energy storage system

Energy storage is defined as the conversion of electrical energy from a power network into a form, that can be stored until converted back to its original electrical form.[51] The purpose of such system is to capture produced energy for a later use,[52] offering a number of significant benefits including achieving demand-side energy management, improved stability of power quality and the reliability of power supply on a long-term basis.[53] With the intensified energy crisis in recent years, energy storage has become a major research focus in both industry and academia[54] and are viewed as a promising solution for future highly renewable power

systems.[55] Among the various forms of energy storage, electrochemical energy storage (EES) systems are vitals, due to their versatility from assisting very large-scale electrical grid down to tiny portable devices to be used for various purposes.[56, 57] They offer the electrical energy accumulation for longer durability (even over 10^6 cycles) and higher specific power (more than 10 kW kg^{-1}), making them very useful for short-term pulses in hybrid electrical vehicles, digital telecommunications systems, uninterruptible power supply (UPS) for computers, pulse laser techniques, etc.[58] The electric energy is stored in the chemical bonds of electrode materials of the device, which involves the conversion reaction between chemical and electric energy. Now-a-days, EES devices are an integral part of telecommunication systems (cell phones, remote communication, walkie-talkies, etc.), standby power systems, and electric hybrid vehicles in the form of storage components such as batteries, SCs, and fuel cells.[59]

Two main parameters are important for energy storage: the energy density and the power density. The energy density is defined as the amount of energy to be stored per unit volume or weight, and the power density is described as the speed at which energy is stored or discharged from the device. An ideal storage device should simultaneously possess both high energy and power densities. Batteries and fuel cells are typical EES devices of small specific power, while conventional capacitors can have higher specific power but exhibit a very low specific energy. The performance parameters of EES such as energy density, power density and safety mostly depend on the electrode materials, which should have high electro activity, high electron/ion conductivity, and high structure/ electrochemical stability.[60] Many efforts have been made to develop advanced electrode materials in the last few decades, however it still requires further development regarding energy density, power density and lifespan. Additionally, it is desirable to fabricate EES with high electrochemical performance, ultra-flexibility and lightweight for wearable electronics applications.[61]

2.1.1 Structure of EES devices

EES devices are usually consist of electrode material, current collector, separator and electrolyte.[62] A thin layer of separator, sandwiched by a pair of electrodes and current collectors, filled with electrolyte make the device, *Figure 2.3*. Electrodes are composed of electrochemically active materials which store charges. Current collector, made of electrically conductive substrates, connects the electrodes with the external circuitry for the charge transfer. Separators physically and electrically separate electrodes to avoid short circuits. Electrolytes, either in liquid or in gel form, are used to carry and transport charged ions between electrodes. Finally, an encapsulation layer is applied to protect the full integration from any leakage of

electrolyte and oxidation of any material, ensuring the stability and safety of the device.[16] *Figure 2.4 (a-c)* represents the schematic of the basic structural components of different EES devices.

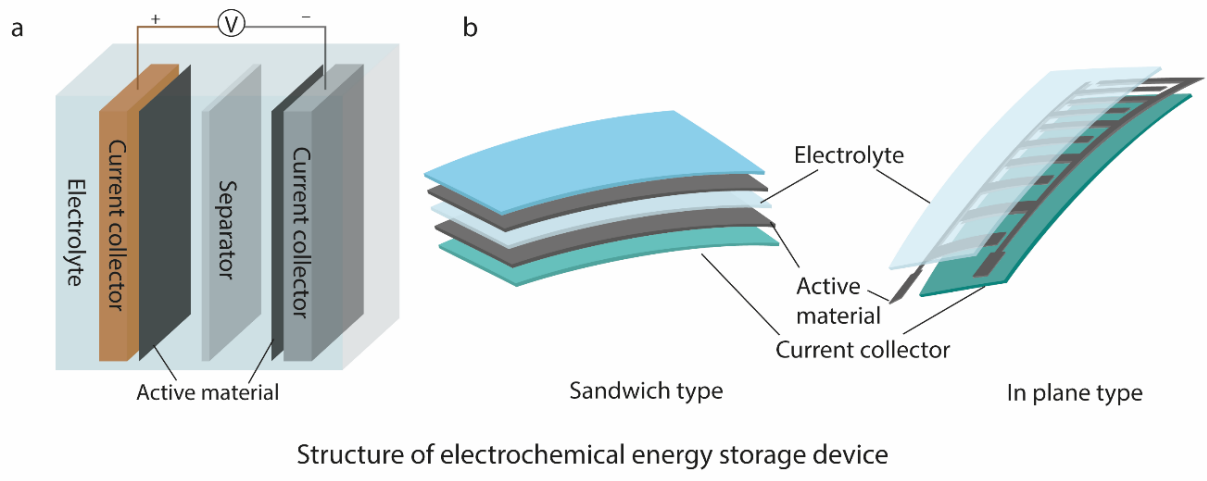

Figure 2.3 Schematic diagram of the structure of EES devices. a) conventional rigid form and b) flexible form.

2.1.2 Types and working principles of EES

EES devices are primarily classified as electrochemical capacitors (*Figure 2.4a*), batteries (*Figure 2.4b*) and fuel cells (*Figure 2.4c*). Due to a comparatively bulk structure, fuel cell is not considered suitable for wearable applications. Therefore, EES devices that are used in wearable systems, may either be electrochemical capacitors or batteries. Electrochemical capacitors, also known as supercapacitors or ultracapacitors, can be quickly charged and discharged with nearly 100% efficiency. They possess outstanding power performance, good reversibility, and very long life (>100,000 cycles). *Table 2.1* compares the characteristics of various EES devices.

Table 2.1 Comparison among various EESDs[63, 64]

Characteristics	**Li-ion battery**	**Capacitor**	**Supercapacitor**	**Fuel cell**
Storage mechanism	Chemical	Physical	Physical and chemical	N/A
Energy storage	High	Limited	Limited	High
Energy density (Wh kg^{-1})	8-600	0.01-0.05	1-10	300-3,000
Power density (kW kg^{-1})	0.005 to 0.4	0.25-10,000	10-120	0.001-0.1
Charge/discharge time	1-10 hours	ps-ms	ms-seconds	10-300 hrs
Operating temperature	-20°C to +65°C	-20°C to +100°C	-40°C to +85°C	+25°C to +90°C

Operating voltage	1.25 to 4.2V	6 to 800V	2.3 to 2.75V	0.6V
Cycle-life	150-1,500	>100,000	>50,000+ hrs, unlimited	1,500-10,000 hrs
Charge-discharge efficiency (%)	70-85	100	85-98	60
Charge stored determinants	Active mass and thermodynamics	Electrode area and dielectric	Electrode microstructure and electrolyte	N/A

Depending on the use of electrode materials, SCs are further divided into EDLCs, pseudocapacitors, and hybrid capacitors. There are two charge storage mechanisms involved in the operation of SCs: storing the charges electrostatically (at the interface of capacitor electrode as electric double layer capacitance) and storing the charges faradaically (at the electrode surface as pseudocapacitance).[65] *Table 2.2* compares the properties among various SC types.

Table 2.2. Comparison among various types of supercapacitors[66-68]

Parameters	**Electric double layer capacitor (EDLC)**	**Pseudo-capacitor (PC)**	**Hybrid capacitor (HC)**
Charge storage mechanism	Physical – Non faradic/electrostatic, electrical charge store at electrode/electrolyte interface	Chemical- faradic, reversible redox reaction	Physical and chemical (both faradic and non-faradic)
Electrode materials	Carbonaceous compounds	Conducting polymers and metal oxides	Combination of EDLC and PC type materials
Specific capacitance (Fg^{-1})	Lower (200-300)	Higher (200-1,340)	Higher (50-1,893)
Energy density (Wh kg^{-1})	Low (6.8-12)	High (167-223)	High (132-231)
Cyclability (cycles)	High (100,000)	Low (5,000)	Medium (12,000)
Capacitance retention (%)	60-100	52-96	80-95

2.1.2.1 Electrical double-layer capacitors (EDLCs)

Electric double layer (EDL) or Helmholtz double-layer (attributed to Helmholtz) involves the formation of two charged layers at the electrode-electrolyte interface. Thus, the ability of storing potential-dependent charge is termed as electric double layer capacitance, and the SCs based on this principle are termed as electric double layer capacitors (EDLCs). From a structural view, they are consist of three parts: two active material-loaded electrodes, an electrolyte, and a separator sheet,[69] *Figure 2.4d*. Energy is stored through charge separation

and can keep considerably more energy than a classic capacitor. A simple movement of ions migrate to and release from electrode surfaces is involved (*Figure 2.4g-i*), therefore can respond rapidly.[70] EDLCs are usually evaluated in terms of Farads (F), instead of picofarads (pF) and microfarads (μF) for the conventional dielectric and electrolytic capacitors due to their ability to store much more electricity. EDLCs have high power density, good reversibility and long cycle life, achieved by the use of high-surface-area activated carbon (AC) as the working medium in the capacitor system.[65]

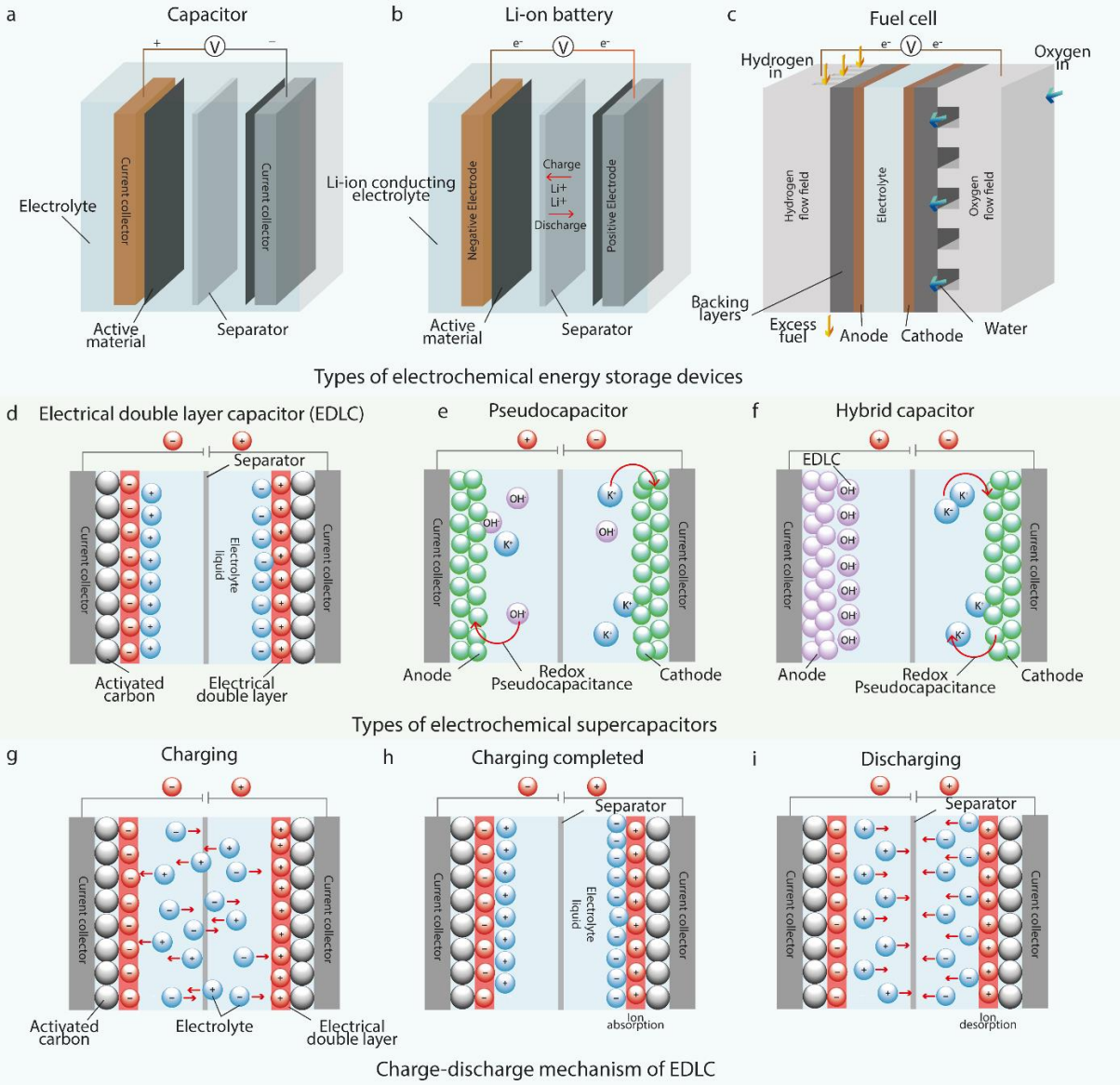

Figure 2.4 Basic schematic of electrochemical energy storage devices: a) a capacitor b) a Li-ion battery c) a fuel cell. Types of electrochemical supercapacitors: d) Electric double layer capacitor (EDLC) e) Pseudocapacitor f) Hybrid capacitor and g-i) Charge-discharge mechanism of an EDLC.

2.1.2.2 Pseudo capacitors

Pseudo capacitors defeat EDLCs in energy density for the reversible redox reactions between their electrode materials and electrolytes,[71] *Figure 2.4e*. They are also referred to as redox super capacitors, since they store charges, faradaically, through battery-like redox reactions but at a faster rate than the EDLCs, offering a pathway for achieving both high energy and high-power densities. Materials that combine these properties are in demand for the realization of fast-charging EES devices capable of delivering high power for long period of time.[72] Transition metal oxides such as MnO_2, conducting polymers like Polyaniline (PANI), Polypyrrole (PPy) or derivatives of Polythiophene (PTh) such as Poly (3,4-(ethylenedioxy) thiophene) (PEDOT) are being studied as prominent pseudocapacitive materials now-a-days. This faradaic charge transfer process is highly reversible. During charging, the surface region of redox-active electrode materials gets reduced to lower oxidation states coupled with adsorption/insertion of cations from the electrolyte at/near the electrode surfaces. Upon discharge, the process can be almost fully reversed,[65] similar to the charging and discharging processes that occur in batteries, resulting in faradaic current passing through the SC cell.[73, 74] Pseudo capacitors offer a higher energy density but a lower cycle life than EDLCs.

2.1.2.3 Hybrid capacitors

Hybrid SCs offer improved performance in energy density without altering the power density and has been in recent trends. They deliver higher specific capacitance in comparison to the existing EDLC and pseudocapacitors.[75] They are made by the hybridization of two types of electrodes to form a new capacitor, *Figure 2.4f*. This is a unique approach, which is used to enhance the electrochemical properties of a single cell. The exhibition of electrochemical behaviour over a wide voltage range will enhance the overall operating voltage window and increase specific energy density, which is larger than the cells containing single type of electrode. Among two types of electrodes in hybrid capacitors, one is an energy source electrode (i.e., battery like electrodes), and the other terminal contains a power source electrode (i.e., either an EDLC or a pseudo-capacitor electrode). The selection of the energy source electrode is important to enhance the cell voltage without sacrificing much energy and power densities. Such configuration offers the advantages of both SCs and the advanced batteries, resulting in a significant increase in the overall energy density of the system.[76]

2.1.2.4. Lithium-ion batteries

Batteries store charge through the conversion of electrical energy into chemical energy. In a lithium-ion battery (LIB), lithium ions move from the negative to the positive electrode during discharge, and travel back to the negative electrode when charging, *Figure 2.4b*. Unlike lithium primary batteries (which are disposable), LIBs use an intercalated lithium compound as the electrode materials instead of metallic lithium. LIBs are common in consumer electronics as rechargeable batteries for portable electronics, which provide one of the best energy-to-weight ratios, high open circuit voltage, low self-discharge rate, no memory effect, and a slow loss of charge when not in use. Beyond consumer electronics, LIBs are growing in popularity for military, electric vehicle and aerospace applications due to their high energy density.[77, 78] The diffusion-controlled electrochemical process of lithium-ion insertion/de-insertion in LIBs results in a much lower power density compared to SCs. However, they typically appear in a rigid form which makes them unfavourable for many applications, especially in the field of portable and highly integrated equipment. Several research groups also investigated flexible textile-based batteries for wearable electronics application.[79-83] Although this review does not focus on batteries, it is worth noting that in many cases, batteries are used in combination with supercapacitors for achieving high performance. The details of electrochemical performance evaluation of supercapacitors are discussed in Appendix B.

2.2 Components of textile-based supercapacitors

The performance of SC largely depends on the nature of electrode materials, type of electrolyte used, and the range of voltage windows employed. In this section, we will discuss about the basic textile materials used for wearable SC fabrication, as well as the electroactive materials for electrode preparation and electrolyte materials commonly used for textile-based SC fabrication.

2.2.1 Textiles as the substrate for supercapacitor fabrication

Multifunctional wearable electronics require a conformal platform close to the human body. Textiles or fabrics that are usually embedded with normal clothes and worn on various body parts, have emerged as promising substrates and platform for wearable electronics, due to its unique characteristics including lightweight, soft, flexible, stretchable, air-permeable, low-cost, chemically resistant, scalable production, and integrable with various forms of garments.[84] In addition to natural fibres (e.g., cotton, silk, wool), other polymeric substrates are commonly used to fabricate e-textiles including poly (ethylene terephthalate) or polyesters (PET), polyamide or nylons (PA), polyimide (PI), viscose, polyethylene naphthalate (PEN) and

thermoplastic polyurethane (TPU). Furthermore, some research groups studied papers (specifically for fabricating disposable devices) and polydimethylsiloxane (PDMS) for fabricating such wearable devices.[85, 86] However, these substrates vary in their physical, chemical, thermal and tensile properties.[87, 88] Therefore, the choice of any specific textiles substrate depends on the properties required for the end-products.

2.2.2 Electroactive materials for electrode preparation

As previously discussed in section 2.2, SCs are classified into two types, according to the charge-storage mechanism, which includes EDLCs based on carbon materials, and pseudocapacitors based on certain transition metal oxides or conducting polymers. The EDLCs usually display perfect cycling stability, but lower specific capacitance. In contrast, pseudocapacitors present high specific capacitance but poor cyclability. These undoubtedly limit their practical application as individual electrode material for SCs.[46] Therefore, to enhance the capacitive performance, developing composite materials combining both EDLC materials and pseudocapacitor materials becomes an inevitable trend.[89]

2.2.2.1 Carbonaceous materials

Carbonaceous compounds and their allotropes (*Figure 2.5a*) are currently of particular interest as key materials for multiple applications including nano- and optoelectronics, photonics, molecular separation and storage, nano mechanics, catalysis, and energy storage.[90] A unique combination of chemical and physical properties, including exceptionally high Young's modulus and mechanical strength, higher light transmittance, higher conductivity, higher surface-area range (~1 to >2000 $m^2\ g^{-1}$), good corrosion resistance, higher temperature stability, controlled pore structure, processability and compatibility with composite materials, and relatively lower cost make carbon-based materials attractive material for SC electrodes.[63, 91] Among five forms of carbon allotropes: 3-dimensional diamond (Csp^3), 2-dimensional graphite (Csp^2), 1-dimensional carbene (Csp^1), 0-dimensional fullerene (Csp^0), and transitional carbons (admixtures of Csp^3, Csp^2 and Csp^1), the first four are crystalline and first two are found naturally. Graphite and fullerene have attracted much attention as electrode materials due to their structures and functionalities.[92] Additionally, they have faster electron transfer kinetics with lower fabrication costs. However, their specific capacitances were found to be too low for commercial applications.

Carbon nanotubes (CNTs), a one-dimensional allotrope of carbon, are cylindrical large molecules consisting of a hexagonal arrangement of hybridized carbon atoms. Being nano-

meter in diameter and several millimetres in length, they are available in the form of single-walled carbon nanotubes, SWCNTs (formed by rolling up a single sheet of graphene) or multiwalled carbon nanotubes, MWCNTs (by rolling up multiple sheets of graphene).[93] Chemical vapor deposition (CVD), laser-ablation and carbon arc-discharge are three common techniques for producing CNTs. Structure, surface area, surface charge, size distribution, surface chemistry, agglomeration state and purity are the main parameters that affect the reactivity of CNTs.[94] Their exceptional physical, chemical, and electronic properties offer exciting possibilities for even nano-meter scale electronic applications.[59] Since its discovery in 1990s, CNTs have been utilized in a variety of applications including actuators, artificial muscles, and lightweight electromagnetic shields.[95] Additionally, CNTs have been investigated as SC electrodes by several research groups. [96-99]

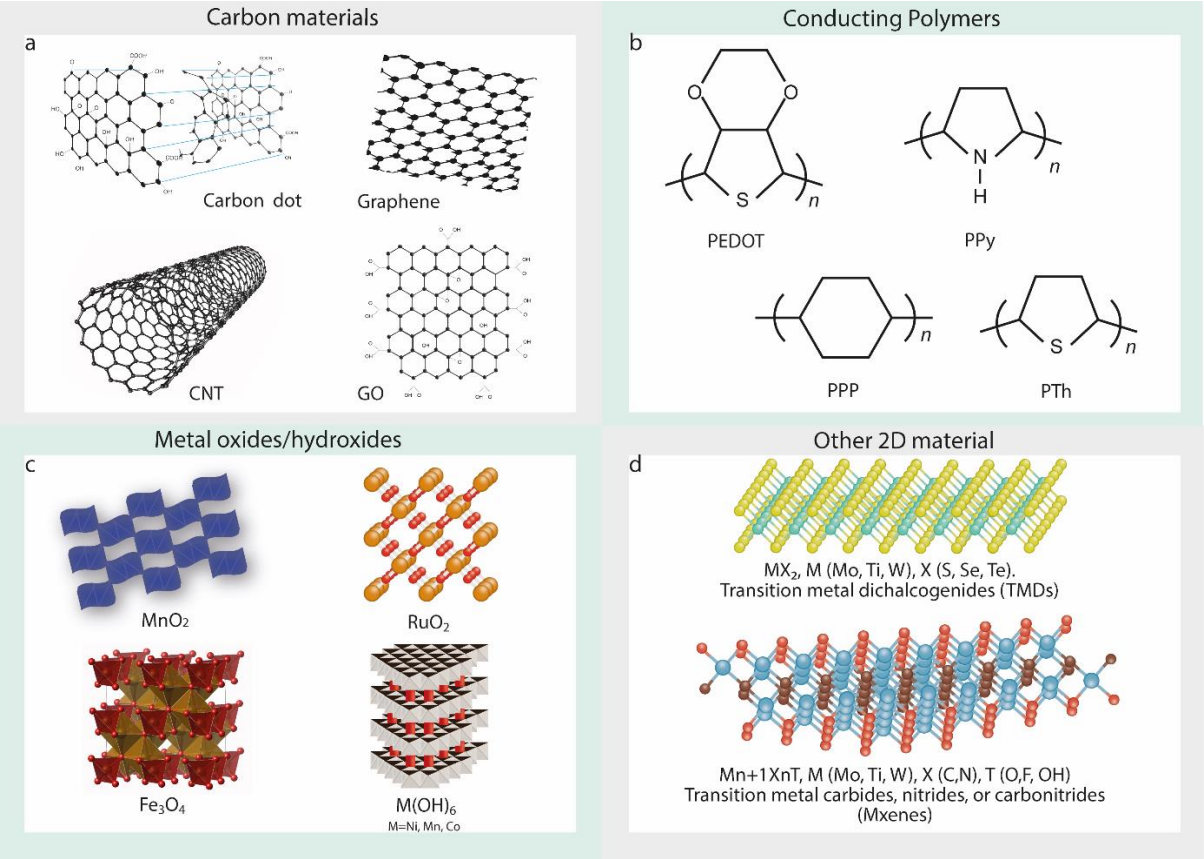

Figure 2.5. Electrode materials for textile-based supercapacitors a) carbonaceous materials b) conducting polymers c) metal oxides/hydroxides and d) other 2D materials.

Carbon black (CB), a common denomination for particles with a carbonaceous core, is manufactured by thermal decomposition, including detonation, or by incomplete combustion of carbon hydrogen compounds having a well-defined morphology with a minimum content of

tars or other extraneous materials.[100] In recent years, it has become an interesting modifier of sensors, due to its excellent conductive and electrocatalytic properties, as well as its cost-effectiveness.[101] Conductive carbon blacks which usually possess electrical conductivity in a range of 10^{-1} to 10^{2} $(\Omega\ cm)^{-1}$ are usually well-structured (i.e., aggregates with a highly branched open structure). They have higher porosity, smaller particle size, and chemically clean (oxygen free) surface.[63] In addition to using as electrode material itself,[102] carbon black is also used in combination with other materials to enhance the performance of SC.[103, 104]

Activated carbon (AC), in comparison with the other forms of carbonaceous materials, is preferred as electrode materials due to its low cost and environmentally friendly nature.[105] Carbonization and activation are the main steps for the synthesis of activated carbon. Due to the tuneable pore size and higher specific surface area as compared to other carbonaceous material, activated carbon has been widely used as electrode material for SC applications. The high surface area, hierarchical pore structure, and different morphology enable the formation of a bilayer of ions at electrode-electrolyte interfaces.[106] Activated carbon powder (ACP) is known as an inexpensive yet good electrode material with 1,000–2,000 m^2g^{-1} of specific surface area,[107] and have widely been studied for SC application.[108-110]

Graphene, since its isolation in 2004, has unveiled a wide range of other similar 2D materials and received much attention from the researcher community due to their outstanding mechanical, thermal, electrical and other properties.[25, 111-113] It is a two-dimensional allotrope of carbon, which is the basic structural element of carbon allotropes including graphite, carbon nanotubes, and fullerenes.[114] It has an isolated single layer of carbon hexagons consisting of sp^2 hybridized C-C bonding with π-electron clouds.[115] It can be considered the "mother" of all graphitic-based nanostructures, owing to the variety of sizes and morphologies onto which a single graphitic layer can be transformed. It can be wrapped up into the zero-dimensional (0D) "buckyball" structure and folded into one-dimensional (1D) carbon nanotubes (CNTs). It can also be stacked into multi-layer graphene sheets.[116] Mechanical, thermal, and liquid phase exfoliation, and the chemical vapor deposition (CVD) are the most common techniques to manufacture graphene.[117, 118] Due to its unique physicochemical properties including theoretical specific surface area (2,600 m^2g^{-1}), good biocompatibility, strong mechanical strength (130 GPa), excellent thermal conductivity (3000 $Wm^{-1}K^{-1}$), high electrical charges mobility (230,000 $cm^2\ V^{-1}\ s^{-1}$) and fast electron transportation makes it not only unique but also a promising material for next generation energy storage applications, particularly SC

devices.[119-123] Graphene and its derivatives have the capability to form chemical bonds with textiles and therefore, show great potential to be used in smart energy storage textiles.[124-126]

Graphene oxide (GO), a derivative of graphene[127] can be obtained by treating graphite materials with strong oxidizing agents (potassium chlorate and fuming nitric acid) where tightly stacked graphite layers are loosened by the introduction of oxygen atoms to the carbon,[128] forming a single-layer sheet of graphite oxide[129] with strong mechanical, electronic and optical properties, chemical functionalization capability and excellent features such as large surface area, high stability, and layered structure.[130-132] Based on the degree of oxidation, GO can be a semiconductor or insulator, enabling it to be used in many fields.[133] Reduced graphene oxide (rGO), another important derivative of graphene,[134] consists of few-atom-thick 2D sp^2 hybridized carbon layers with fewer oxygeneous functionalities and exhibits properties between graphene and GO.[135] Though it resembles graphene, containing residual oxygen and other heteroatoms with some structural defects degrade its electric properties.[136] While graphene derivatives (GO and rGO) can be produced in a huge quantity in their stable dispersions,[137] the major challenge for such materials is the ability to porduce high quality graphene at larger scale.[138] Hybridization of various carbonaceous compounds are also attractive due to their combined electrochemical properties, which provides enhanced capacitive performances of SC devices.[139-143]

2.2.2.2 Conducting polymers

Conducting polymers (CPs) are organic polymers, that are able to conduct electricity through a conjugated bond system along the polymer chain. In the past two decades, they are extensively explored for energy storage applications due to their reversible faradaic redox nature, high charge density, and lower cost as compared to expensive metal oxides. They are considered as promising electrode materials for flexible SCs.[144] Among CPs, PANI, PPy, and derivatives of polythiophene have widely been studied as active electrode materials for energy storage devices, *Figure 2.5b*.

PANI, a conducting polymer, has been playing a great role in energy storage and conversion devices due to its high specific capacitance, high flexibility, and low cost. It is said that the era of intrinsically conducting polymers started with the invention of polyacetylene. However, PANI attracted much more attentions from researchers due to its cheaper monomer compared to polyacetylene and ease of synthesis.[145] PANI-based electrodes for SCs provide multi-redox reactions, high conductivity and excellent flexibility.[146] However, the inferior stability of PANI

limits its application to be used alone in the fabrication of electrodes.[147] Therefore, the combination of PANI with other active materials (such as carbon materials, metal compounds or other polymers) is recommended to overcome such intrinsic disadvantage.[148-150]

PPy is a π-electron conjugated CP, which has been researched widely for energy storage applications due to its good electrical conductivity and environmental stability in ambient conditions. It has shown promise as SC electrodes because of its large theoretical capacitance, good redox properties, superior conductivity, ease of synthesis, nontoxicity, biocompatibility, and high thermal and environmental stability.[151] However, the brittleness of PPy limits its practical uses. Nevertheless, their processability and mechanical properties can be improved by either blending PPy with some other fibre polymers or forming copolymers of PPy.[152] Thus, PPy-based composites may provide the fibres or fabrics with electrical properties similar to metals or semiconductors.[153] The water solubility of pyrrole monomers and much less carcinogenic risks associated with its biprodcuts compared to PANI, makes PPy a proper material as SC electrodes. However, the poor cyclic stability and poor rate behaviour of pristine PPy-based SCs drastically restrict their practical applications.[154] Nevertheless, higher electrochemical performance can be achieved by the introduction of novel design of nanostructured PPy and its nanocomposites, which is currently being explored widely for SC electrode fabrication.[155-157]

PEDOT is one of the most promising π-conjugated polymers exhibiting some very interesting properties such as excellent conductivity (≥300 S cm^{-1}), electrooptic properties, and processability.[158, 159] PEDOT is highly conductive in its oxidized (doped) state, while in its undoped form is usually nonconductive or shows very little conductivity. Its conductivity can be increased by oxidizing or reducing with a doping agent which introduces positive charges along the backbone structure of PEDOT. These positive charges are later balanced by the anions provided by the doping agent.[159] The oxidized or doped form of PEDOT shows very high conductivity, flexibility, low-cost, and pseudocapacitance. However, the low stability and limited capacitance have limited its industrial applications. Several approaches have been undertaken to tackle these issues including the addition of conducting nanofillers to increase conductivity, and mixing or depositing metal oxide to enhance capacitance.[160] Though several studies have reported the electrochemical performance of PEDOT based SCs,[161, 162] the polymer mixture with polystyrene sulfonate (PEDOT:PSS) possess a high conductivity (up to 4,600 S cm^{-1})[163], and can be used as an electrode material for SCs.[164, 165] The hybridization of

PEDOT:PSS with other active materials have also been studied for the SC electrode fabrication.[165-168]

2.2.2.3 Metal oxides

Electrodes composed of metal oxides possess exceptional properties, qualifying them as a suitable engineering materials with a wide range of applications including sensors, semiconductors, energy storage, lithium-ion batteries and solar cells.[169] Metal oxides, due to its wide variety of oxidation states for redox charge transfer, are generally considered as one of the prime candidates for the use as electrode materials in SCs,[170] *Figure 2.5c*.

Ruthenium dioxide (RuO_2): Due to its high theoretical specific capacitance value (1,400–2,000 F g^{-1}), RuO_2 has been extensively recognized as a promising material for SC devices.[171] Additionally, it demonstrates highly reversible redox reactions, good thermal stability, high electronic conductivity (300 S cm^{-1}), superior cycle lifespan and high rate capability.[170] Despite having such outstanding properties, their higher production cost and agglomeration effects limit its practical applications. Therefore, RuO_2-based nanocomposites have widely been studied to optimize the material cost, with simultaneous improvement in the electrochemical performances.[171] Several researchers have studied RuO_2-based nanocomposites for SC fabrication[172, 173] as well as for the improvement of the electrochemical performances for next-generation SCs.[174-176]

Manganese dioxide (MnO_2): MnO_2 is considered as one of the most promising electrode materials for electrochemical capacitors, due to its low cost, high theoretical specific capacitance (~1,370 Fg^{-1}), natural abundance, environmental friendliness and nontoxicity.[177] MnO_2 is a very common material in the battery field, which has long been used as active material for the positive electrode.[178] The charge storage mechanism is based on the surface adsorption of electrolyte cations M^+ (e.g., K^+, Na^+, Li^+) as well as proton incorporation as follows:[179]

$$MnO_2 + xM^+ + yH^+ + (x+y)e^- \rightleftharpoons MnOOM_xH_y \qquad \text{Equation 1}$$

However, the poor conductivity, much lower actual specific capacitance than the theoretical specific capacitance, poor structural stability and easy dissolving nature in the electrolyte results in poor cycling ability.[180] Therefore, the combination of MnO_2 with other active components are much preferred by the researchers for SC electrode application.[181-183]

Nickel oxide (NiO): *NiO* is another attractive conversion reaction-based anode material in the field of SCs due to its low cost, ease of preparation, nontoxicity, environment friendliness and high theoretical capacity (~3,750 F g^{-1}). [184] The pseudocapacitance of *NiO* is obtained from the following redox reaction:

$$NiO + OH^- \rightleftharpoons NiOOH + e^- \quad \text{Equation 2}$$

Though theoretically advantageous enormously, the relatively poor electrical conductivity and lower specific surface area hinder their practical applications. One possible solution to these problems is to synthesize nanostructures of NiO with large surface areas, which are associated with more faradaic active sites and higher pseudo capacitance. Therefore, various nanostructured forms of nickel oxides such as nanowires, nanoflakes, nanocolumns, nanosheets, porous nanoflowers, and hollow nanospheres were successfully fabricated in the past few years by various methods[170] and investigated for SC fabrication.[185-187]

Nickel hydroxide [$Ni(OH)_2$]: *$Ni(OH)_2$* is also an attractive electrode material because of its high theoretical capacity, superior redox behaviour, and potential applications in alkaline batteries and SCs. Its main reaction mechanism as positive electrode material for SCs is shown as follows:

$$Ni(OH)_2 + OH^- \rightleftharpoons NiOOH + H_2O + e^- \quad \text{Equation 3}$$

However, *$Ni(OH)_2$* usually suffers from poor stability, lower conductivity, and large volume changes during the charge/discharge processes. Thus, composites with high surface-area conductive materials such as CNTs, activated carbon, graphene, show remarkably enhanced electrochemical performance due to improved electrical conductivity of the composites, and the shortening of the electron and ion diffusion pathways.[188-191]

Cobalt oxide (Co_3O_4) is generally considered one of the best candidates for electrode material in the field of SCs owing to its superior reversible redox behaviour, excellent cycle stability, large surface area, and outstanding corrosion stability.[192-194] The redox reactions in alkaline electrolyte solution can be expressed as follows:

$$Co_3O_4 + OH^- + H_2O \rightleftharpoons 3CoOOH + e^- \quad \text{Equation 4}$$

$$CoOOH + OH^- \rightleftharpoons CoO_2 + H_2O + e^- \quad \text{Equation 5}$$

Due to layered structure with a large interlayer spacing, Cobalt hydroxide [$Co(OH)_2$] provides a large surface area and a high ion insertion/extraction rate and offer a great potential to become

a high-performance electrode material[170] and explored for SC studies.[110, 111] The pseudofaradaic reaction at a low potential of $Co(OH)_2$ and the faradaic reaction at a higher potential can be expressed as follows:

$$Co(OH)_2 + OH^- \rightleftharpoons CoOOH + H_2O + e^- \qquad \text{Equation 6}$$

$$CoOOH + OH^- \rightleftharpoons CoO_2 + H_2O + e^- \qquad \text{Equation 7}$$

Among iron oxides, Fe_3O_4 is one of the main and naturally abundant pseudocapacitive material with a reasonable metallic electrical conductivity (~10^2–10^3 S cm^{-1}). However, the low specific capacitance limits its practical applications. TiO_2 is also considered very important material for energy storage systems because of its good intercalation/ deintercalation behaviour of metal ions (such as Li+ and Na+) without the formation of solid electrolyte interface by-products and electrode collapse caused by volume changes. These characteristics contribute to its high-power capacity and long lifespan. Non-toxicity, chemical stability, photocatalytic activity and low cost make it a promising semiconductor.[195] In terms of properties, TiO_2 is suitable for the use as negative electrode material in organic electrolyte for hybrid SCs. SnO_2 is another alternative electrode material to be used in SCs. But compared to other metal oxides, it has a much lower specific capacitance. The several oxidation states of vanadium in V_2O_5 results in both surface and bulk redox reactions. Therefore, it has been studied for its potential application in energy storage devices. V_2O_5 has a higher capacitance in KCl electrolyte than in any other electrolyte solutions. *Table 2.3* compares the basic types of electrode materials for the fabrication of SCs.

Table 2.3. Comparison of various supercapacitor materials[144]

Properties	**Carbonaceous material**	**Metal oxides**	**Conducting polymers**
Non-faradic capacitance	Very high	Medium	Medium
Faradic capacitance	Very low	Very high	Very high
Conductivity	Very high	Low	Very high
Energy density	Low	High	Medium
Power density	High	Low	Medium
Cost	Medium	High	Medium
Chemical stability	Very high	Low	High
Cycle life	Very high	Medium	Medium
Ease of fabrication	Medium	Low	High
Flexibility	Medium	Very low	High

2.2.2.4 2D materials

Since the discovery of graphene, two-dimensional (2D) materials (*Figure 2.5d*) such as hexagonal boron nitride (*hBN*), transition metal chalcogenides (*TMDs)- Molybdenum disulfide (MoS_2), Tungsten selenide (WSe_2)*, transition metal carbides/nitrides (i.e. *MXenes- Ti_2C*) and 2D metal-organic frameworks (*MOFs*) also attracted tremendous research attention due to their extraordinary properties including large surface area, good electronic conductivity, excellent electrochemical properties, and good chemical, electrochemical, and thermal stability, since these properties are promising for batteries and SCs.[196-198] 2D materials are generally defined as materials with infinite crystalline extensions along two dimensions and one crystalline dimension with few or single atomic layers thickness. Such materials are derived from most classes of known layered materials and possess strong in-plane bonds within the layers and only weak interactions between neighbouring layers.[199] However poor cyclic stability, and large structural changes during metal-ion insertion/extraction, as well as higher manufacturing cost are the major challenges for 2D materials which require further improvements to find their applications in commercial batteries and SCs.[200]

2D-hBN an isomorph of graphene with a very similar layered structure,[201] is uniquely featured by its exotic opto-electrical properties together with mechanical robustness, thermal stability, and chemical inertness. *2D-hBN* is an insulator itself but can well be tuned by several strategies in terms of properties and functionalities, such as by doping, substitution, functionalization and hybridization, making *2D-hBN* a truly versatile type of functional materials for a wide range of applications. More importantly, both theoretical and experimental results show that the *BN*–noble metal interface can also improve the electrocatalytic activity. Recent studies have also shown that it has the ability to adsorb polysulfides and Li ions, which is a greatly desired property for improving the performance of *Li–S* and solid-state batteries. Thus, *BN*-based nanomaterials have huge potential in the field of electrochemical energy storage and conversion.[202] It is also considered as one of the most promising materials, able to integrate with other 2D materials, including graphene and *TMDCs* for the next-generation microelectronic technologies,[203] as well as SC electrodes.[204-207]

MoS_2, another exciting 2D material, has been investigated to a lesser extent but are gaining increased interest recently for integration into electronic devices due to their graphene like properties. Exfoliated *MoS_2* possesses high catalytic activity which makes it an efficient hydrogen evolution catalyst as well as a useful energy storage material for the use in lithium and sodium ion batteries. In addition to conventional synthesizing processes such as

micromechanical peeling or chemical vapor deposition, currently MoS_2 is being synthesized by ultrasonic treatment similar to graphene. It creates large volumes of monolayer and few layer flakes that can then be deposited onto a substrate or formed into films.[208] The favourable electrochemical properties are mainly a result of the hydrophilicity and high electrical conductivity, as well as the ability of the exfoliated layers to dynamically expand and intercalate various ions.[209] Similar to *hBN*, MoS_2 has been explored alone[210, 211] or with other functional materials[212-215] for SC electrode fabrication.

MXene, a new family of 2D metal carbides, nitrides and carbonitrides have gained much attention due to their attractive electrical and electrochemical properties such as hydrophilicity, conductivity, surface area, topological structure, rich surface chemistry, tunable terminations, excellent processability etc.[216-218] The term *MXenes* with a formula of $M_{n+1}X_n$, are named after other 2D analog materials silicene, graphene, phosphorene, and so on, synthesized by extracting a atomic layer from ternary *MAX* ($M_{n+1}AX_n$) ceramics, where M = early transition metal elements (Ti, Zr, Mo, Nb, V, Mn, Sc, Hf, W, and so on), A = group 13 or 14 (Si, Al, Ga, and so on), X = C or/and N. Due to their unique intrinsic physical/chemical properties, *2D MXenes* materials have thoroughly been investigated and can be used in various research fields, including ceramics, conductive polymer, energy storage, sensors, water purification, catalysis, thermoelectric conversion, photothermal conversion, solar cell, biomedicine, and microwave absorption and shielding.[219, 220] Moreover, the improved coupling and hybridization of *MXene* with other materials at the nano-scale makes it one of the most intriguing materials for wearable applications.[221, 222]

2.2.3 Electrolytes for supercapacitors

Electrolytes are vital constituents of SCs, as their physical and chemical properties play an important role to obtain desired performances in terms of capacitance, power density, rate performance, cyclability and safety.[223] For the SC performance, the type, composition, and concentration of the electrolyte is as important as the electrode materials.[224] An optimized electrolyte concentration is always desired, as the ion transport within the electrode layers becomes easier at high electrolyte concentration, inducing an effective build-up for the double layer. If the concentration becomes too high, the ion activity is reduced due to less water hydration, resulting in decreased ion mobility. A good electrolyte offers a wide voltage window, high electrochemical stability, high ionic concentration and conductivity, low viscosity, and low toxicity. However, a proper cell design should also consider the key electrolyte parameters, such as: (i) sufficiently high ion conductivity, (ii) electrochemical stability on the anode and

cathode surfaces, (iii) good wetting in contact with electrode materials, (iv) suitable thermal properties, (v) adequate cost, and (vi) adequate mechanical properties.[225] Common electrolytes can be classified into three types: aqueous, organic liquid, and ionic liquid,[226] (Appendix C). Due to offering safer and more packageable construction, providing more design freedom, larger operable temperature range and electrochemical stability, polymer-based electrolytes have also garnered significant attention for SC fabrication. *Figure 2.6* summarizes some of the key features of major electrolyte families to compare their advantages and disadvantages.

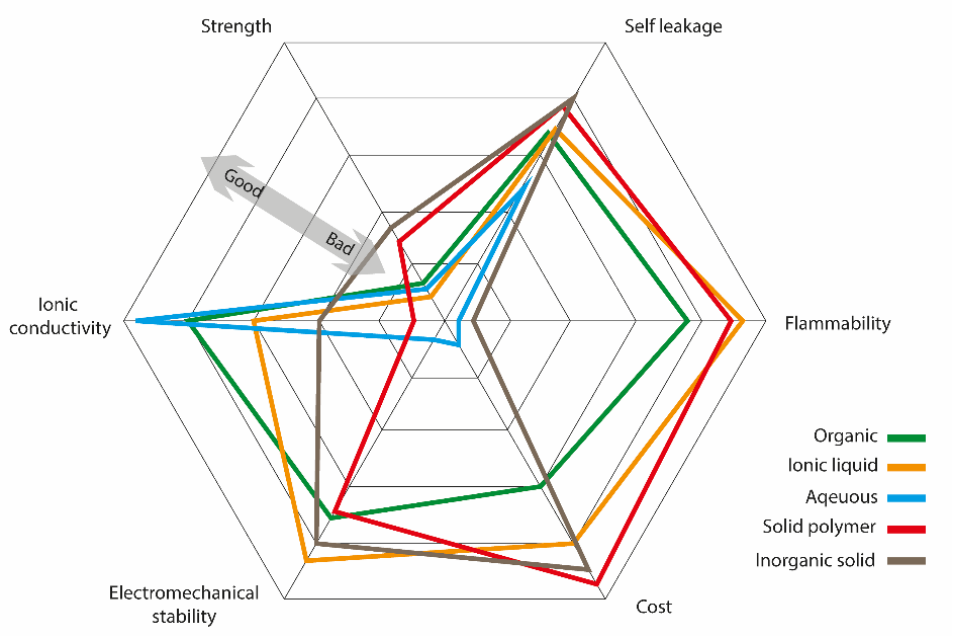

Figure 2.6. Comparison of the performance of several electrolyte types

2.3 Manufacturing of conductive electrodes

Several technologies can be utilized for the manufacturing of conductive electrode. Spinning, coating, and printing of active materials with/on textiles are the key manufacturing techniques for such electrodes. *In-situ* growth of active materials on/ in the substrate is another way of such manufacturing.

2.3.1 Coating of active materials on substrate

The conventional textile materials such as cotton, polyester, nylon is electrically nonconductive. Therefore, electrical conductivity must be introduced to such textiles to prepare a textile-based energy storage device. The coating of a layer of electrically conducting material onto non-conductive textiles can impart electronic capabilities in a facile manner. Materials such as intrinsically CPs, conducting polymer composites, metals and carbon based materials have been used to achieve this.[227] The commonly used coating techniques that have been used

to deposit such materials on textiles are dip coating, doctor-blade coating, wrapping, physical vapor deposition (VPD) and CVD.[62, 70]

Dip Coating, also termed as impregnation or saturation coating, is the simplest process of creating a uniform thin layer of conductive materials on a substrate. In such technique, textile substrates are dipped into a bath containing coating materials in liquid form, *Figure 2.7a*. The viscosity of the coating liquid is usually very low to enable it to run off while the substrate leaves the coating liquid. A pair of nip rollers are often placed to remove the excessive liquor from coated surface, providing a homogeneous liquid film on the sustrate.[228] After drying, the volatile solvents are eliminated, followed by possible chemical reactions, resulting in a thin coated film.[229] Dip coating offers a simple, low-cost, reliable and reproducible method, which is extensively effective for research purposes. However, the inconsistent quality of such coatings makes them unsuitable for industrial scale application.[154] Hu et al. reported a simple dipping and drying of SWNT ink on textiles to produce highly conductive textiles with electrical conductivity of 125 S cm^{-1} and sheet resistance < 1 Ω sq^{-1}. SCs made from such conductive textiles showed high areal capacitance, up to 0.48F cm^{-2}, and specific energy as high as 20 Wh kg^{-1} at a specific power of 10 kW kg^{-1}, *Figure 2.7*(b-d).[230] The same researcher group later demonstrated the coating of polyester fabric with solution-exfoliated graphene nanosheets and further electrodeposition of MnO_2 nanomaterials, yielding high specific capacitance up to 315 F g^{-1}. They also successfully fabricated asymmetric electrochemical capacitors with graphene/MnO_2-textile as the positive electrode and SWNTs-textile as the negative electrode with aqueous Na_2SO_4 electrolyte, exhibiting promising characteristics with a maximum power density of 110 kW kg^{-1}, an energy density of 12.5 Wh kg^{-1}, and excellent cycling performance with ~95% capacitance retention over 5,000 cycles, *Figure 2.7(e, f)*.[231] Dip coating is a simple and scalable process, however the loading of active materials depends on the surface properties as well as deposition position of the textile substrate. The repeated dipping-drying cycles are usually employed to achieve sufficient material loading which lowers the efficiency of fabrication process. Padding is a modified version of dip coating, used for continuous treatment of textiles for various chemical treatments and finishes. Textile substrate after impregnated with the solution is squeezed through nip rollers.[8] In a previous study,[26] the lowest sheet resistances was reported ~11.9 Ω sq^{-1} on graphene e-textiles, through a simple and scalable pad−dry−cure method with subsequent roller compression and a fine encapsulation of graphene flakes. The graphene coated textiles were highly conductive even after 10 home laundry washing cycles with extremely high flexibility, bendability, and

compressibility as it shows repeatable response in both forward and backward directions before and after home laundry washing cycles. The potential applications of such conductive textiles were demonstrated as ultra-flexible SC and skin-mounted strain sensors, *Figure 2.7(g, i)*.

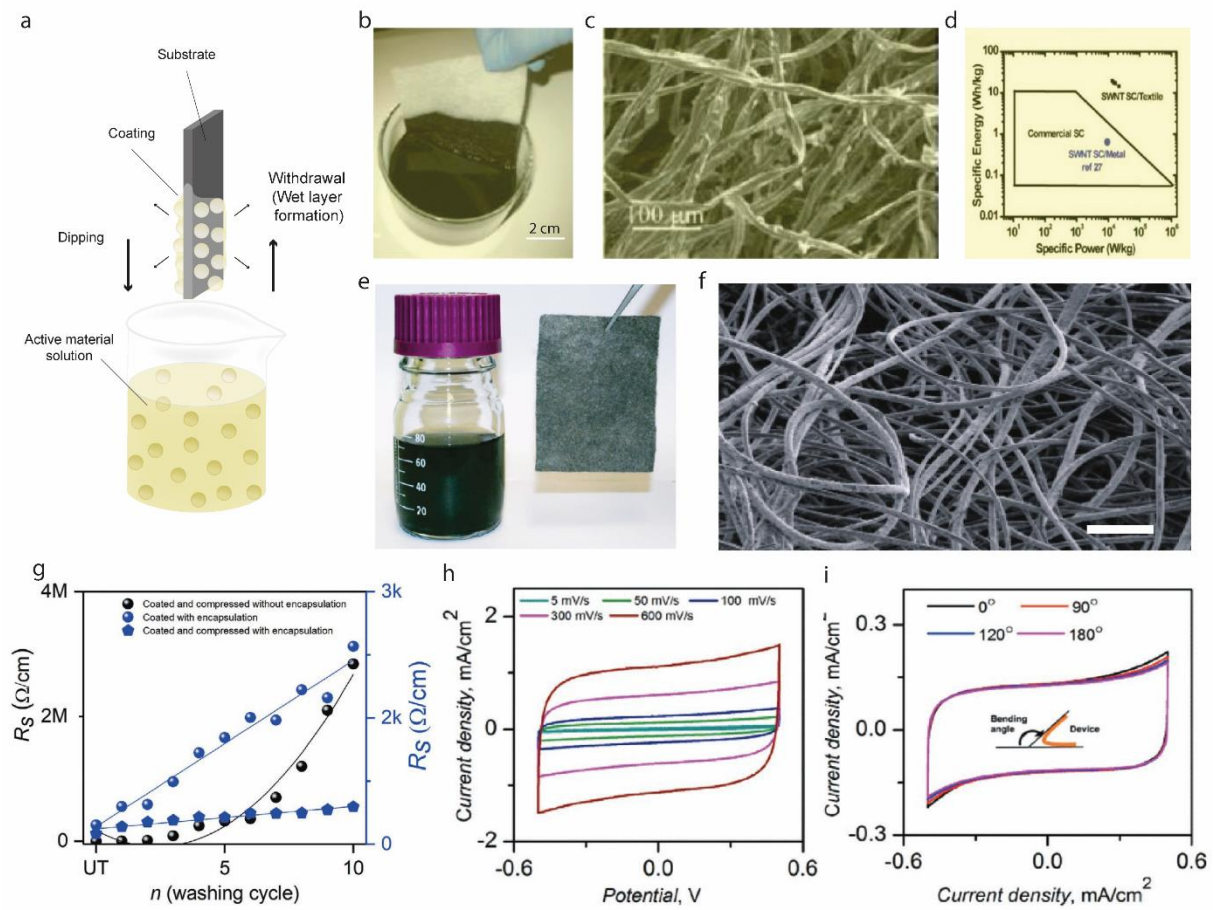

Figure 2.7. a) Schematic diagram of dip coating technique b) Conductive textiles fabricated by dipping textile into an aqueous SWNT ink followed by drying in oven at 120 °C for 10 min c) SEM image of coated cotton reveals the macroporous structure of the cotton sheet coated with SWNTs on the cotton fibre surface. (d) Ragone plot of commercial SCs, SWNT SC on metal substrates, and SWNT SC on porous conductors including all the weight. Reproduced with permission.[230] Copyright 2010, American Chemical Society. e) Photograph of a stable, solution-exfoliated graphene ink suspension prepared by ultrasonication of the graphite powder in a water sodium cholate solution, and a 6 cm X 8 cm graphene-coated conductive textile sheet (polyester) (f) SEM image of a sheet of graphene-coated textile after 60 min MnO_2 electrodeposition showing large-scale, uniform deposition of MnO_2 nanomaterials achieved on almost entire fabric fibre surfaces, Scale bar: 200 µm. Reproduced with permission.[231] Copyright 2011, American Chemical Society. g) The change in resistance with the number of washing cycles of G-coated compressed (with encapsulation) poly-cotton fabric, G-coated only

(with encapsulation) poly-cotton fabric, and G-coated compressed (without encapsulation) poly-cotton fabric. h) CV recorded for the supercapacitor device at different scan rates i) CV curves for the ASC device at different bending angle. Reproduced with permission.[26] Copyright 2020, Wiley-VCH.

Doctor blade coating, also called knife coating or blade coating or tape casting, is another widely used technique for producing thin films on surfaces with large area. The process involves a constant relative movement between a blade over the substrate or a substrate underneath the blade, resulting in a spread of the coating material on the substrate to form a thin film on the substrate upon drying. The operating speed of such technique can reach up to several meters per minute, and coat substrate with a very wide range of wet film thicknesses ranging from 20 to several hundred microns.[232] This process can create thin uniform films over large surface areas quickly and efficiently, though cannot offer the nanoscale uniformity or extreme thin film. Nevertheless, the scalability, versatility, and simplicity of this technique make it perfect for industrial applications. In comparison to dip coating, doctor blade technique allows a much more precise and uniform control over the coating amount of active materials in a continuous process.[16] Though few literatures are available on fabric or thin-film-based lithium-ion batteries fabricated using doctor blade coating,[233] the fabrication of SCs using such technique is rare.

2.3.2 Printing of active material on substrate

The process described as printing involves the controlled deposition of a material, either for decorative or functional purposes, onto a substrate in such a manner that a pre-defined pattern is produced. Other deposition processes, such as painting or spraying, have much in common, but printing is further defined because the process can rapidly produce identical multiples of the original. There are three basic methods of printing: positive contact, negative contact, and non-contact printing. The first two methods are described as contact printing since the substrate is touched by the print master. The positive contact type resembles the principle of stamping, examples include printing presses and woodcuts. Gravure or screen printing are the examples of negative contact type printing. In non-contact printing, the printer does not contact the substrate. The most common examples of non-contact printing is inkjet printing, where ink droplets are ejected from a nozzle, and deposited on a substrate.[234]

Surface wettability of a polymeric material is of great importance when it comes to different applications in material science.[235] This is a basic feature of printing substrate which is a direct

intermolecular interaction occurring when liquid and solid medium are brought together. The study of wettability involves the measurements of contact angle (CA), indicating the degree of wetting when a solid and liquid interact. CA when low (<90°) corresponds to high wettability, meaning that the fluid will spread over a large surface area. A high CA (>90°) represents low wettability, so the fluid will minimize contact with the surface and form a compact liquid droplet. CA>150° indicates minimal contact between the liquid droplet and the surface and it corresponds to a super hydrophobic behaviour.

Surface tension, or *surface free energy*, both similar parameter, corresponds to the residual binding capacity of a material surface, i.e., the binding capacity of atoms or group of atoms that constitute the border surface of the material of interest.[236] When talking about solid surfaces only, the term 'free surface energy' is usually used. Both the terms refer to the same physical quantity and share the same symbol. The unit of the free surface energy is Jm^{-2}, and the unit of surface tension is Nm^{-1}, which is, once multiplied by m m^{-1} the same unit.[237]

2.3.2.1 Textile surface engineering and post treatment

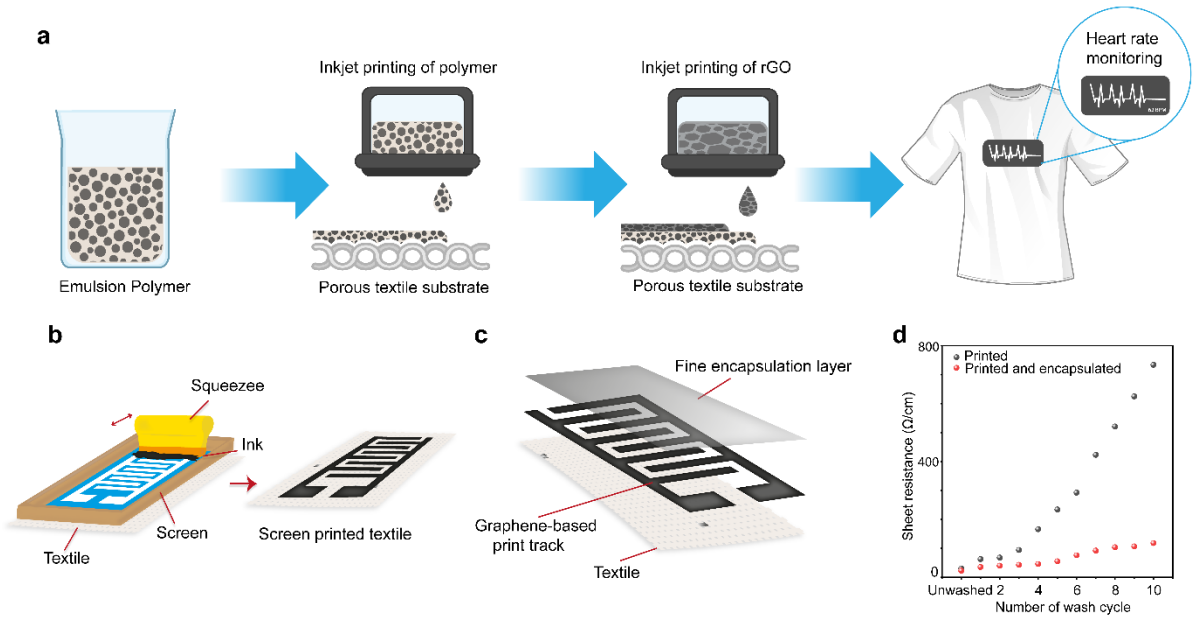

Figure 2.8 Textile surface pre-treatment and post treatment for e-textiles. a) Inkjet printing of organic nanoparticle coating followed by inkjet printing of conductive rGO to prepare conductive textile.[22] Screen printing of b) graphene ink on textiles c) polyurethane (PU) based encapsulation post-treatment to improve washability d) Comparison on the change of electrical resistance of printed textiles with and without encapsulation layer.[238]

Printed electronics often require a uniform and smooth substrate that is also solvent resistance, chemically and thermally stable, stretchable, conformal, flexible, and light weight. One of the key challenges with printed e-textiles is the ability to achieve continuous highly conductive electrical tracks on a rough and porous textile substrate. Due to the orientation of fibres or yarns, textile fabrics demonstrate an intrinsic planar anisotropy of the general properties.[239] Also, the morphology of the fibre changes constantly due to the exchange of water molecules with surroundings, which makes it extremely difficult to produce uniform and continuous conductive paths using low viscous inkjet inks.[22] Number of researches have been conducted to introduce interface layer for reducing such roughness and porosity of textiles. Previous studies have suggested polyurethane acrylate-based interface layers,[240] however the deposition of such interface layer suffer from few draw backs. These usually constrains the potential feature resolution, not suitable for small quantity of material deposition or roll to roll manufacturing. In a previous work,[22] an organic nanoparticle-based inkjet printable textile surface pre-treatment was reported which enables production of all inkjet-printed graphene-based wearable e-textiles which is breathable, comfortable and environmentally friendly, *Figure 2.8*a.

Another key challenge of wide commercial adoption textile-based wearable electronics is their poor stability on repeated laundry washing.[241] A good washability is essential for e-textiles to survive intense mechanical deformations and water invasion of washing cycles used during their life cycles.[242] The delamination of the conductive functional materials due to the mechanical forces experienced during washing cycles, results in losing the electrical performance.[238] The wash stability of wearable e-textiles can be improved via a number of methods including a textile surface pre-treatment with BSA, or by a post-treatment for instance embedding with PDMS, PU sealing, a screen-printed PU top layer or, hot melt encapsulation to seal conductive track on the textile surface.[26] In our another work,[238] we used a translucent, thin, and stretchable PU-based encapsulant to protect screen-printed graphene-printed wearable e-textiles, *Figure 2.8*b-c. Such encapsulation material adheres with textile materials, keeping the printed graphene layer attached to textiles but covered and protected even during repeated wash cycles, *Figure 2.8*d.

2.3.2.1 Printing techniques for e-textiles

The printing process involves a controlled deposition of material, either for decorative or functional purposes, onto a substrate in such a manner that a pre-defined pattern is produced. Though other deposition processes including painting or spraying are there, printing is further

highlighted because it can rapidly produce identical multiples of the original. Three basic methods of printing are there: positive contact, negative contact, and non-contact printing. Since the substrate is touched by the print master during printing, the first two methods are described as contact printing. Positive contact type resembles the stamping principle, examples include printing presses and woodcuts. Gravure or screen printing are examples of the negative contact printing. In non-contact printing process, the printer does not meet the substrate. The most common examples of non-contact printing is inkjet printing where ink is ejected on a substrate from a nozzle.[234] The available print technologies are briefly introduced in the following section.

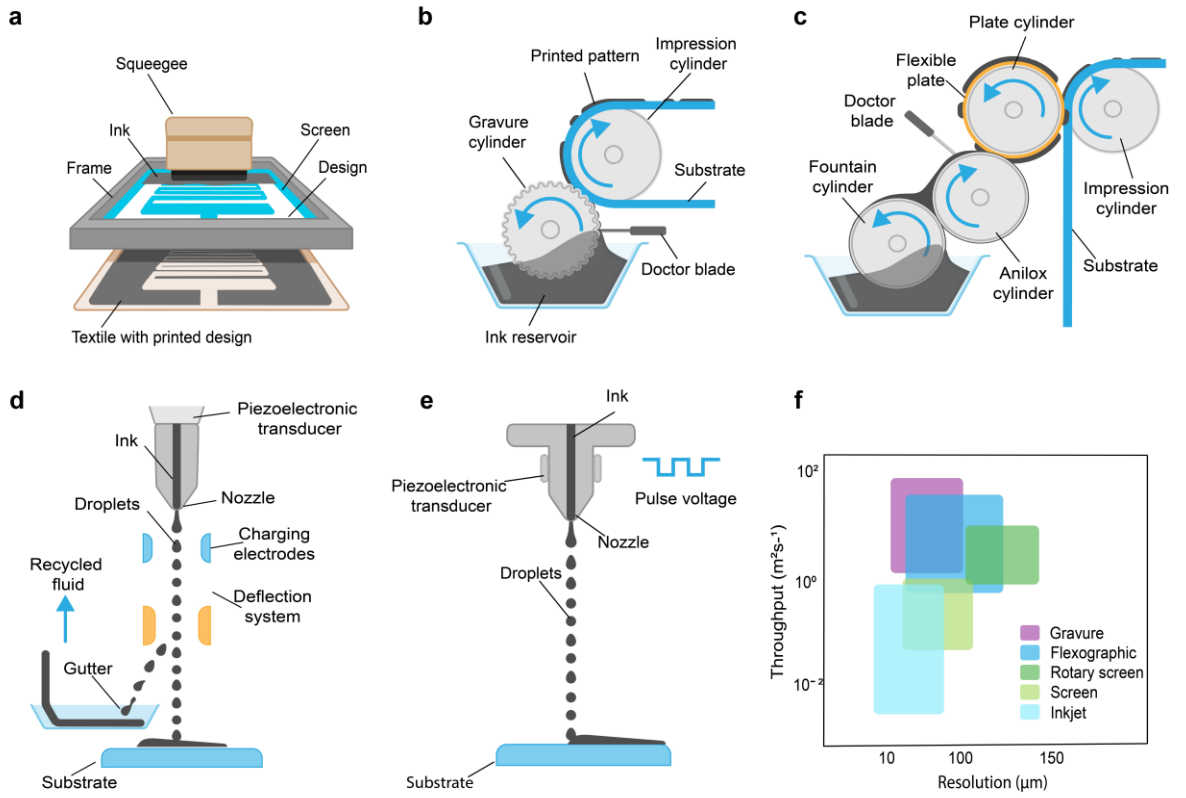

Figure 2.9 Printing technologies for e-textiles fabrication, a) screen printing b) gravure printing c) flexographic printing d) continuous inkjet printing and e) drop-on-demand inkjet printing f) Comparison of print throughput and best achievable resolution ranges of print technologies.[23]

2.3.2.3 Screen printing

Screen printing (*Figure 2.9*a) generally uses a screen mask which includes a fabric mesh with the patterns of image. The ink is pressed using a squeegee such that the ink penetrates the substrate through the portion of the mesh not covered with the fabric material, forming a printed

pattern.[243-245] Basically, this is a selective transfer process of ink through the open areas of the unmasked portions of a screen. Masking of the screen is accomplished by the transfer of a photographically produced image from its temporary film base support to the screen.[246] Low cost and high processing speeds are some potential advantages of the screen printing, however, changes in shear force can continually influence ink viscosity, leading to a pattern distortion. Here, the printing resolution is limited by the printing speed. Thus, there is a need to optimize the formulation of conductive inks suitable for screen printing while maintaining the good conductivity and fidelity of printed patterns.[245] One of the biggest advantages of screen printing is the versatility of the substrates including paper, paperboard, polymer materials, textiles, wood, metal, ceramics, glass, and leather. In addition, the screen printing process enables ink application not just to flat surfaces but to irregular ones too, as long as the thick ink adheres properly to the printed substrate and the screen can adapt to the substrate's shape consistently without distortion.[247] The wide variety of polymer substrates requires different types of inks. Printing inks must be selected according to the type and surface characteristics of printing substrates. A sharp edge of printed image requires ink with higher viscosity in screen printing than in other printing techniques. Screen printing inks can be categorized by the drying process in the following groups: evaporative (water-based and solvent-based), oxidizing, catalytic, and UV inks. Solvent-based inks are very common in polymer screen printing applications, but there are some other inks that are dried by a slower process of oxidation and polymerization, too. Few inks also use UV energy for curing by polymerization.[247] Screen printing is by far the most widely used method for wearable e-textiles application. Researchers have attempted screen printing for the fabrication of textile-based strain, [248] pressure,[249] temperature,[250] and humidity sensors.[251] Several textile-based biosensors such as for electrocardiogram (ECG), [252, 253] electroencephalography (EEG), [254] electromyography (EMG)[255] and electro-oculography (EOG)[255, 256] were also reported via screen printing method. In addition to these, several screen-printed textile-based supercapacitor,[19] heating elements[257] were also demonstrated. We will discuss in detailed about screen-printed wearable e-textiles in the subsequent sections.

Jost et al.,[258] investigated traditional screen printing of porous carbon materials on woven cotton and polyester fabric for fabricating flexible and lightweight SC electrodes as a possible energy source for smart garments. A high gravimetric capacitance (85 F g^{-1}) and areal capacitance (~0.43 Fcm^{-2}) on both cotton lawn and polyester microfibre was obtained. In another study, Abdelkader et al.[259] reported a solid-state flexible textiles SC device, produced *via* screen printing of GO ink on textiles. After the *in-situ* reduction of GO, the printed

electrodes exhibited excellent mechanical stability and flexibility, as well as outstanding cyclic stability over 10,000 cycles, which are necessary for wearable applications, *Figure 2.10*(a-c). Lu et al.[260] synthesised FeOOH/MnO_2 composites which was screen-printed as SC electrode on different substrates, including PET, paper and textiles. The all-printed solid-state flexible SC device exhibited high area specific capacitance of 5.7 mF cm^{-2} with 80% retention up to 2,000 charge-discharge cycles, and high mechanical flexibility. Additionally, they demonstrated printed SCs on different substrates, which are capable of lighting up a 1.9 V yellow light emitting diode (LED), even after bending and stretching, *Figure 2.10(d-g)*.

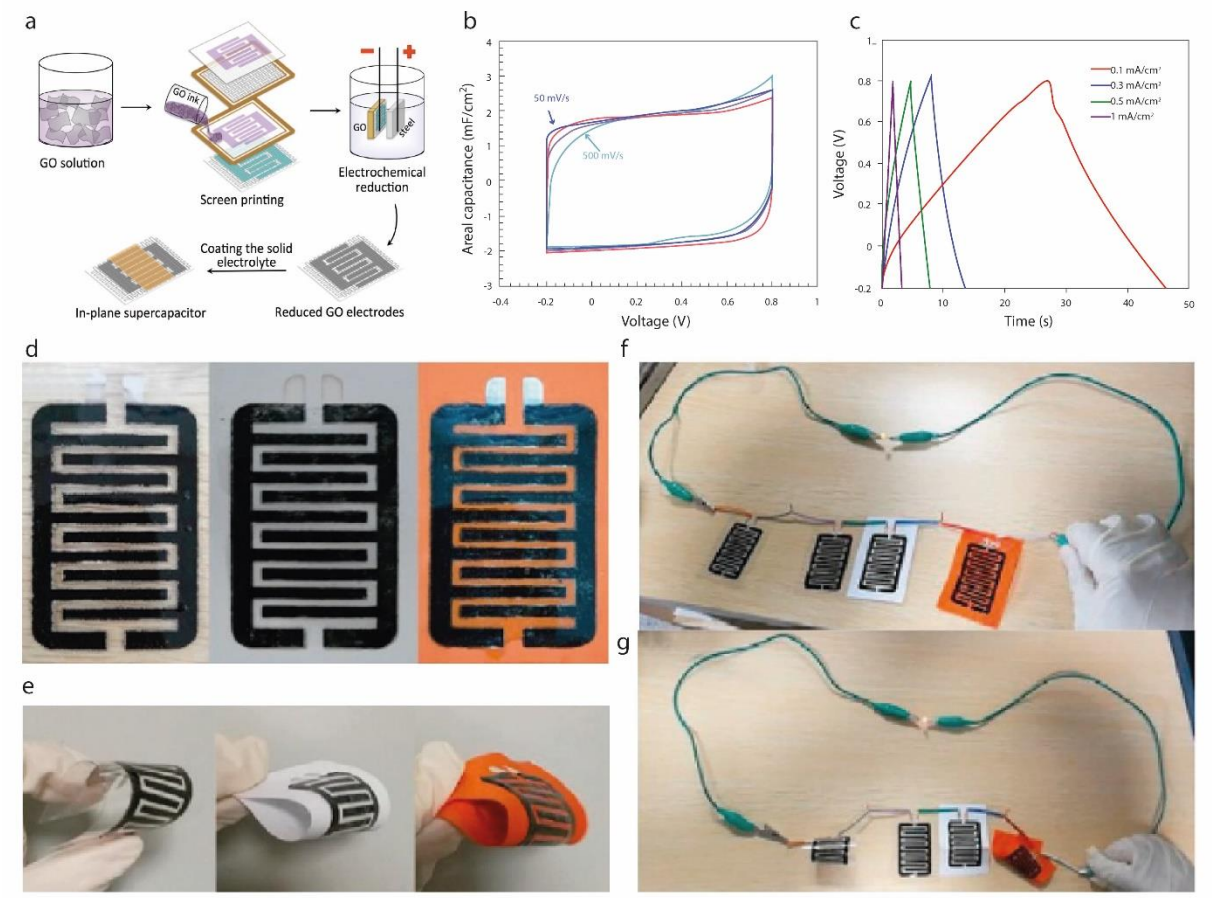

Figure 2.10. a) Schematic representation of the printed in-plane SC fabrication process. Electrochemical characterisation of printed graphene on textile (b) CV at different scan rates and (c) GCD curves at different current densities. Reproduced with Permission.[259] Copyright 2017, IOP Publishing Ltd. D) Images of all printed solid-state flexible SC devices on PET, paper, textile substrates, e) images of the SCs after bending f) image of these SCs in series lighting up a yellow LED, and g) images of the same after bending these SCs. Reproduced with permission.[260] Copyright 2017, Elsevier B.V.

2.3.2.4 Gravure printing

Gravure is a widely used roll-to-roll printing method (*Figure 2.9*b), characterized by excellent print quality with high speed, often used for large volumes of magazines and catalogues printing.[261, 262] An engraved metal roll is used in gravure printing to transfer the ink directly to the substrate. The depression in the engraved surface forms the print pattern. The roll is immersed in the ink bath where the etched portions pick up and hold the ink followed by a blade removes the excess ink. An impression cylinder pushes the substrate film with the depressed, ink-filled regions of the gravure roll, thus transferring the ink to the film. A dryer after that drives off the solvent creating the final layer of coating.[263, 264] The depressions in the gravure rolls, to hold the ink can be etched chemically, mechanically, or by laser. One of the advantages of gravure printing is that the rolls are hard, durable, thus is cost-effective for long runs though the initial costs are high. The printing quality depends on the ink viscosity, substrate speeds as well as the pressure of the impression roller. A relatively high print pressure (1–5 MPa) and quite low-viscosity inks (50–200 mPa) performs a good ink transfer. Another advantage is stretchy and unstable fabrics can also be printed by this technique efficiently.[265] The printing rate in gravure printing may be achieved up to 25-1000 m min^{-1}.[262] Liquid gravure printing inks are dried by using physical method, i.e., by evaporation of the solvents, and inks of two components by chemical curing. The solvents speed up the drying process, but volatile organic chemicals (VOCs) are emitted, which need to be recovered (typically 87-98%). Since gravure printing is widely used for large scale roll-to-roll textile batches, for lab-scale e-textiles it is not a very popular method. However, few researchers reported gravure printing for textile-based humidity sensors.[266, 267] We assume, upon commercialization, gravure printing might be a high-speed production choice for large scale e-textiles fabrication.

2.3.2.5 Flexographic printing

Like gravure printing, the flexographic (shortly named as flexo) printing is another high-speed roll-to-roll printing technique, *Figure 2.9*c. The printing process involves transferring ink, from the surface of a flexible plate to the substrate. The pattern is made into plates that are attached to a roll. The printing ink is metered onto the surface of the plate by an 'anilox'- an engraved/ etched roller of chrome or ceramic similar to a gravure cylinder but with a uniform distribution of cells (size, shape and depth). The volume of ink to the transferred to the printing plate depends on this specification of the anilox. The ink is taken into these cells and a doctor blade assembly wipes the excess ink subsequently. The plate transfers the ink film from the anilox to the substrate by impression.[268] Flexo plates use vulcanized rubber or photopolymer materials

that are attached to rotating cylinders.[269] The difference of flexographic printing with the gravure printing is, instead of relying on impressing the film into the ink containing cavities of the roll, the ink on the flexographic plates relies on the ridges of the pattern.[263] The relatively inexpensive plates, advanced quality and productivity of flexographic printing often makes a printer difficult to choose between flexographic and gravure printing. Flexography is now dominant process for labelling, leaflets and cartons markets in packaging.[268] Flexographic printing allows to achieve increased printing speeds, of approximately 10 m^2 s^{-1}. Resolutions of approximately 50–100 μm can be achieved. This technique is also suitable for the creation of RF circuits, where very good conductivities are necessary since a thicker ink layer can also be deposited (5 μm).[270] Flexographic inks maybe solvent-based, water-based or UV-curable inks. To ensure the regular ink flow in the printing unit, low-viscosity printing inks are required in flexographic printing, generally lower than 0.05–0.5 Pas with a flow time equal to 18–35 s. Concentrates of both solvent- and water-based flexographic have relatively higher viscosity in the range of 0.1–0.25 Pa·s.[271] Similar to gravure printing, flexography is suitable for large scale production. We assume for large scale production of commercial grade e-textiles, flexography could be a suitable choice.

2.3.2.6 Inkjet printing

Inkjet printing (IJP) also known as digital printing of functional materials with specific electrical, chemical, biological, optical, or structural functionalities has gained significant research interest due to its wide range of application in different processes and purposes, from the batch coding of soft drink cans to smart electronic textiles.[272, 273] IJP allows the deposition of tiny droplets onto substrate without depending on the high-speed operation of mechanical printing elements. Nozzle sizes for the printers are usually 20–30 μm with ink droplets as small as 1.5 pL with an achievement of high resolution (dots per inch).[274] Besides 2D print results, in ink jet printing, "structural" fluids can also print layers that harden to form three-dimensional (3D) structures. In spite of all these, several consideration such as the printing speed, cost–benefit issues, printed film uniformity and material, and fluids' jet-ability as ink – are still points of concern for the printers.[275] Two distinct modes of inkjet printing are there, (1) Continuous inkjet (CIJ), suitable for industrial scale and mass-production and (2) Drop-on-demand (DOD), used for small-volume and prototype sample production.

CIJ utilizes a pressurized fluid stream and a piezoelectric element at high frequencies (~20 - 80 kHz), to form droplets, *Figure 2.9*d. A continuous and consistent stream of fluid droplets of uniform size and spacing can be generated by the careful adjustment of the voltage and

frequency of the piezoelectric device. A conductive material placed in the fluid can impart an electric charge on selected drops breaking them off from the fluid stream which are further deflected by means of high voltage deflector plates to form various patterns onto the substrate. Uncharged droplets are captured by a gutter mechanism and re-circulated through the system. A "catcher," a plate situated below the nozzle to perform patterning, actuates into and out of the path of the droplets, only allowing the droplets to pass when pattern material is required. For industrial environments CIJ offers cheaper alternate and high print rate by minimizing transient and clogging issues, which is a limitation of DOD.[276] CIJ printing possess high flexibility, precision, and speed allowing it to be used in applications in high-speed graphical application such as coding, marking, and labelling, as well as textiles and micro-manufacturing industries. The benefits of CIJ over DOD are improved image quality, throw distance, and the ability to deflect droplets independent of gravity.[277] Since the CIJ printing produces large-diameter droplets (~ 40 mm), the print resolution is relatively low.

DOD printing, today, is the most commonly used printing technique in laboratory and small-volume printers, *Figure 2.9*e. Due to the flexibility of the variety of inks used and simplicity of application, it works very well with the prototype environments. The printer nozzle while passing over the substrate, an actuator ejects a droplet wherever patterned material is required,[276] the production of each drop occurs rapidly in response to a trigger signal. Typically, DOD print head contains multiple nozzles and instead of drop ejection resulting from external fluid pressure as in CIJ printing, the drop's kinetic energy derives from sources located within the print head, very close to each nozzle. In DOD printing, the liquid emerging from the print head in the form of a jet, is then detached from the nozzle and collapses under surface tension forces to form one or more droplets.[278] Typical drop volumes of individual ink drops in DOD are in the range of 1–70 pL, produces print spot size in the range of 10–50 μm in diameter. The slower speed (5000–20 000 Hz per second) of making drops is the limitation of DOD.[279] The high accuracy and small droplet size of DOD inkjet printers are the key advantages for the direct patterning of functional materials.

IJP delivers a small amount of materials as an ink to a specific location of substrate, which opens the door of design versatility.[275] It does not require stencils; achieving cost-effective printing choice for a much smaller print run than does conventional screen printing.[280] Being highly adaptive, it can be applied to a wide range of different processes and purposes, from batch to rapid prototyping in product design.[272] It also provides possibilities for new workflows, short production runs, sustainable printing environments, quick response time, and

customization.[265] Considering all these benefits, inkjet printing is considered to be the future of e-textiles. Therefore, after screen printing, inkjet printing is most widely used technique to fabricate e-textiles. It's worth noting that, the amount of active functional material deposited on textiles via inkjet printing is much less than the screen printing. Therefore, achieving an optimum conductivity requires more print passes than the screen-printing process. Researchers have already reported inkjet printing method to fabricate textile-based strain,[281] pressure,[282] temperature,[283] and humidity sensors.[284] Several biosensors such as ECG,[22] EEG,[285] and EMG[285] are also reported. Inkjet printing has also been used to fabricate textile supercapacitor electrodes.[28]

2.3.2.7 Formulation of printable inks

Conventional printable inks usually contain four components: dye or pigment, binder, solvent, and additive. All these combinedly provide viscosity and flow properties to the printing ink. [286] Functional inks on the other hand, have an electrically functional element instead of or along with the pigment. They usually possess electromagnetic, thermal, chemical, and/or optical properties, and are classified into conductive, semi-conductive, dielectric and resistive ink categories.[287] Binder (also called thickener) holds the functional components and contributes to the properties such as hardness, gloss, adhesion and flexibility. They become an integral part of the pigment-binder-substrate system by crosslinking after evaporation (by drying or curing) is carried out of the printing ink. Alkyds, polyamides, polyimides, rubber, ketone, acrylic, epoxide etc. resins are typical binders used in printing ink formulation. It is important to mention here that, the main component of wearable e-textiles is the conductive track obtained through coating and/or various methods of printing. Binders are usually insulator materials; the presence of excess quantity of binder materials can hamper the conductivity of the functional material. Therefore, an optimization of the proper functional material to binder ratio is important to formulate any printable ink. Since various print technique demand printable paste/ink of different rheological properties, the specific print method should also be taken into consideration for the formulation of specific print paste/ink. The main objective of using solvent is to prevent the agglomeration of materials along with keeping the ink paste in fluid form, sufficient to apply on a substrate. For dissolving polar molecules, polar solvents such as water, alcohol, esters are widely used. Liquid hydrocarbons are used for nonpolar molecules. Sometimes co-solvents are combined with solvents to cut the cost. An ideal solvent dissolves the resin/polymer without dissolving or degrading the pigment; evaporates at a compatible rate with desired printing process, possess required viscosity and should be compatible with image

carrier. Modifiers and/or additives are added in the print ink to either enhance the printability of the ink or of the cloth. Modifiers may tailor the viscosity or surface tension of the print ink to enhance the printing performance of the print ink. Several type of additives include hygroscopic agents, anti-oxidizing agents, fastness enhancers, or functional agents such as anti-flammable agents, antiseptics, and disinfectants.[288] Additives are incorporated into ink formulations in amounts not exceeding 5%,[287] *Table 2.4* presents a typical composition of various print inks.

Table 2.4 Typical composition of printable inks [23]

Composition	Screen	Gravure	Flexographic	Inkjet
Pigment	12-20	12-17	12-17	5-10
Binder	45-65	20-35	40-45	5-20
Solvent	20-30	60-65	25-45	65-95
Modifier and/or additive	1-5	1-2	1-5	1-5

2.3.2.8 Requirements of conductive inks

A liquid has an internal resistance to flow, "*viscosity*" is a measure of this resistance to flow or shear. It can also be termed as a drag force and is a measure of the frictional properties of the fluid.[289] According to viscosity, printing inks may be classified to either low-viscosity printing inks or high-viscosity print pastes. Liquid printing inks like flexographic, gravure, and inkjet inks fall under low-viscosity category.[271, 290] In case of offset, screen printing, and pad printing inks, the viscosity remains higher than 1 Pa-s, are categorized as high-viscosity printing inks. The term 'rheology', a key feature to describe the print paste behaviour, is 'the study of the deformation and flow of matter'.[291] For a print ink (for lower viscosity formulation, usually used for gravure, flexographic or inkjet process), density, viscosity, surface tension, drying rate, flow behaviour, flow time etc. are important factors determining the efficient output of the print process. Though the viscosity of a print paste or ink can be modified; it is challenging to keep the same electrical properties with changing the viscosity. Increasing the temperature decreases the viscosity whereas the evaporation of solvent increases the viscosity. Solvent might be used to tune the viscosity of the ink. In addition to this, increasing the dispersant concentration decreases the viscosity of the ink.[290]

Surface tension of the ink is another important parameter of the print paste or ink, required for the formation of drops, which also affects the interaction between the ink and the substrate i.e., wettability and printability. Surface tension depends on the composition; polar liquids have

higher and the nonpolar one has lower surface tension. Thus, water (surface tension 73 mN m^{-1}) based inks have higher values, and ethyl alcohol (24 mN m^{-1}) or other nonpolar solvents based inks have lower values of surface tension.[292] A proper bonding exists between a liquid and a substrate surface when the surface tension of the liquid is 2-10 mN m^{-1} lower than the surface energy of the substrates.[293]An increase in the temperature or increase in solid content can decrease the surface tension of an ink.[290]

According to the viscous flow behaviour, liquids may either be *Newtonian fluids* or *non-Newtonian fluids*. The viscosity of a Newtonian fluid remains constant and they exhibit ideal viscous flow behaviour. Any physical or chemical modification to the ideal Newtonian fluid may affect the flow behavior.[294] *Non-Newtonian fluids* are two types; *Shear-thinning* or *pseudo-plastic fluids* are characterized by an apparent viscosity, which decreases with increasing shear rate.[295] The usual printing pastes exhibit shear-thinning flow behaviour. [271] In case of *shear thickening* (or *dilatant) fluids*, the apparent viscosity increases reversibly as the shear rate increases..[296] Shear thickening fluids are not recommended in printing, since the fluid do not distribute properly, particularly with fast-running presses related to the occurrence of the high shearing stresses.

Another characteristic is important for print ink named "*thixotropy*". This is a time-dependent phenomenon means that the viscosity of the fluid depends on time as well as shear rate; i.e., the viscosity of thixotropic fluids decreases with time.[297] When stirring at a constant shear rate, the gel structures in the ink break, then a gradual recovery of the structure occurs, when the stress is removed, thus thicken when the ink is kept standing. The highly viscous printing inks, in most cases, are thixotropic; therefore, the viscosity of a printed ink is higher than when the ink is in the printing unit rollers.[271]

Particle size is also an important parameter for functional print ink. Decreasing the particle size increases the surface area and increases the amount of stabilizing agents required. It also results to a high surface to volume ratio, lowering the required sintering temperature. Small particle size and uniform size distribution in the ink produce higher viscosity inks and denser printed patterns; therefore, improves the functionality. Moreover, particle morphologies, e.g., nanospheres (NS) and nanowires (NW), also affect both the electrical conductivity and energy needed for sintering. Higher electrical conductivity can also be achieved by using inks with higher solid content. An increase in the solid content also leads to viscosity decrease under shear stress, allowing the ink to flow more smoothly from one surface to another while still

preventing excessive spreading of the ink after printing. The rheological behaviour of the ink can thus be tailored by changing the solid content of the ink.[290] *Table 2.5* provides a typical comparison among various print inks properties.

Table 2.5 Comparison among various printable ink parameters[271, 290]

Ink viscosity	Print technology	Viscosity (Pa.s)	Surface tension (mN/m)	Layer thickness (µm)	Feature size (µm)	Maximum particle size (nm)	Maximum preferred particle size (nm)	Maximum solid content (%)	Flow Properties
Low viscosity printing inks	Flexography	0.01-2	28-38	0.04-2.5	80	15000	3000	40	Newtonian or non-Newtonian shear thinning with small deviation
	Gravure	0.01-1.1	41-44	0.1-8	70-80	15000	3000	30	Non-Newtonian
	Inkjet	0.001-0.05	25-50	0.05-20	20-50	$1/10^{th}$ of nozzle diameter	50	20	Non-Newtonian
High viscosity printing ink (paste inks)	offset	20-100	30-37	0.5-2	10-50	10000	1000	90	Non-Newtonian, shear thinning, thixotropic
	Screen printing	0.1-1000	30-50	0.015-100	20-100	$1/10^{th}$ of mesh opening	100	90	Thixotropic

Printability (i.e., the ability to absorb inks or lacquers or other liquid and paste substances) of any substrate depends on its porosity, surface free energy (SFE), structure and dimension, durability, hydrophilic property, and optical properties. Besides these, selection of an ink with an appropriate level of surface tension is also necessary. It is generally believed that surface tension of the ink should be lower than surface free energy of the substrate. Printability of polymer substrates may be improved by increasing in surface free energy of the material (by

any means of activation), by the reduction of surface tension of applied inks; and by the maximum reduction of the polar component of substrate SFE.[292]

Fluid properties such as viscosity and surface tension have influence on the formation of droplets from an inkjet printer. The spreading behaviour of the inks is determined by the hydrodynamic properties namely; Reynolds number, (Re=vαρ/η, is the ratio of inertial to viscous forces), and the Weber number, (We=v2αρ/η, is a balance between inertial and capillary forces).[298] Both are combined to form the Ohnesorge number (Oh). The inverse of the Ohnesorge number is termed as printability. This is usually expressed by the Z number. The Ohnesorge number is given as √We/Re or,

$$Oh = \frac{\eta}{\sqrt{(\gamma \rho a)}} \quad \ldots\ldots\ldots\ldots\ldots \text{ Equation 8}$$

Where, η is dynamic viscosity, γ is surface tension, ρ is density and a is the characteristic length (usually the diameter of the print head's nozzle). The printability,

$$Z = \frac{1}{Oh} = \frac{\sqrt{(\gamma \rho a)}}{\eta} \quad \ldots\ldots\ldots\ldots\ldots \text{ Equation 9}$$

Such a fluid velocity independent, dimensionless number has advantages as a suitable metric for fluid selection. Fromm suggested that $Z > 2$ for stable drop formation because viscous dissipation prevents drop ejection at lower values. Reis and Derby proposed, on the basis of computational fluid dynamics (CFD) modelling, that Z should be in the range $1 < Z < 10$, with viscous dissipation preventing drop ejection when $Z < 1$, while satellite drops were predicted to form together with the primary drop when $Z > 10$.[299] It was also found that Z has an influence on droplet volume too. As Z increases there is an increase in volume. Moon and co-workers have said that Z should be between 4 and 14 for an ink to be printable.[300] Jang et al. observed inks were easily ejected by the applied pressure without significant viscous dissipation, when Z>14,. The primary droplet fell with a high relative travel velocity, so that the separated tail which formed transient satellites could not catch up with the droplet head. The large oscillatory kinetic energy and the high surface tension tend to induce a secondary rupture, which generated a primary droplet and permanent satellites. So fluids with Z>14 are not printable fluids.[298]

Considering the drop generation, drop flight and drop impact, the optimal value of the physical condition for a robust DOD inkjet printing are typically with surface tension lying in the range of 20-50 mN m^{-1} and viscosity within the range of 2-20 mPa.s. This range broadly meets the criteria of a suitable ink for DOD inkjet printing to achieve high resolution print on desired

trajectory, where narrower and specified range would be more applicable for specific print heads.[125] *Figure 2.11*a shows the ink properties suitable for inkjet printing. *Figure 2.11*b displays a drop watcher image showing five nozzles jetting 3 wt./wt. % polyDADMAC solution with a 30 µs delay. *Figure 2.11*c shows a grayscale image of ink jetting captured by the drop watcher system with the time sequence of the waveform.

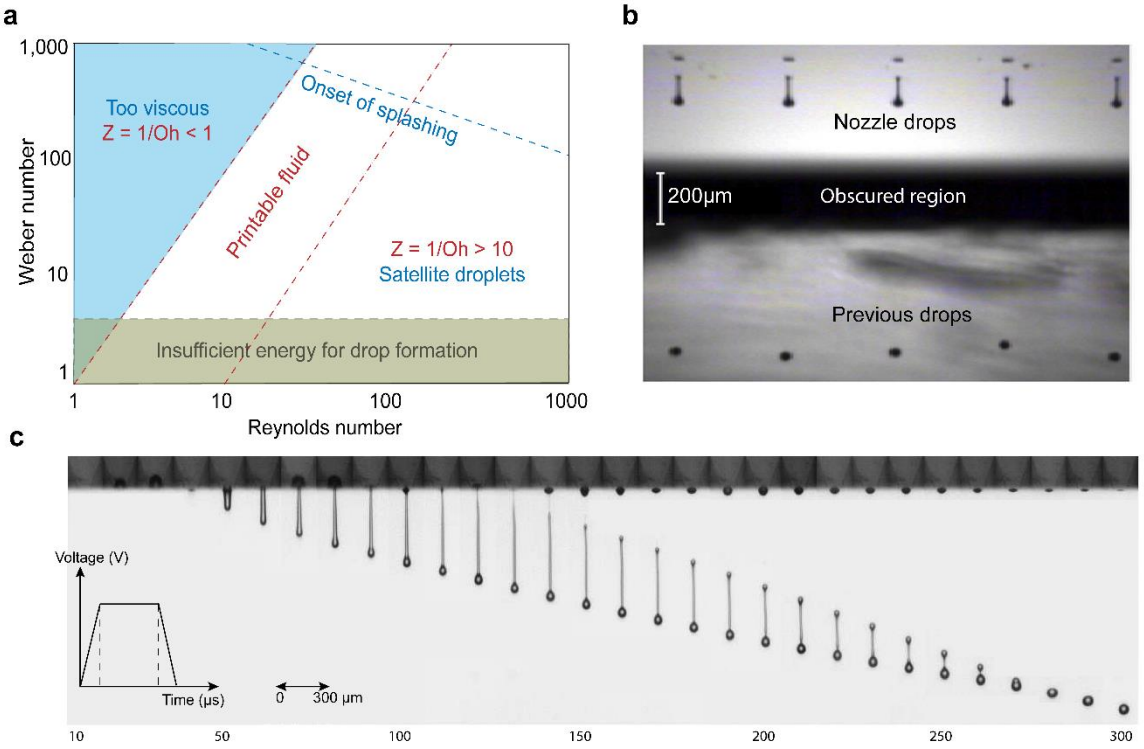

Figure 2.11 *Inkjet Ink property requirement and drop formation. a. Graphical means of assessing ink suitability using nondimensional numbers*[301] *b. Example of a drop watcher image on DMP-2831, showing five nozzles jetting 3 wt./wt. % polyDADMAC solution with a 30 µs strobe delay.*[302] *c. Grayscale images of the ink jetting captured by the drop watcher system with the time sequence of the waveform.*[303]

High-performance devices can be produced by printing and stacking the functional inks in desired locations,[304] *Figure 2.12a*. IJP allows the deposition of tiny droplets onto substrate without depending on the high-speed operation of mechanical printing elements. The nozzle size for such printers are typically ~20–30 µm and ink droplets can be as small as 1.0 pL to achieve high print resolution (dots per inch).[274, 305] In addition to 2D prints, IJP can print layers of "structural" fluids that harden to form three-dimensional (3D) structures. In spite of all these benefits, print speed, higher cost, printed film uniformity and fluids' jet-ability as ink, are still points of concern for inkjet printers.[275]

There are two distinct modes of inkjet printing: Continuous inkjet (CIJ), suitable for industrial scale and mass-production, and Drop-on-demand (DOD), used for small-volume and prototype sample production.[276] The high accuracy and small droplet size of DOD inkjet printers are the key advantages for the direct patterning of functional materials.[278, 279] There are several parameters of an ink such as viscosity, surface tension, density and size are important for successful inkjet printing of a fluid. The spreading behaviour of the ink is determined by the Ohnesorge number (*Oh*). The inverse of the Ohnesorge number is used to determine the printability of DOD inkjet inks. This is known as the Z number.[298] The printability,

$$Z = \frac{1}{Oh} = \frac{\sqrt{(\gamma \rho a)}}{\eta} \quad \text{Equation 10}$$

Where, η represents dynamic viscosity, γ is surface tension, ρ is density and a is the characteristic length (usually the diameter of the print head's nozzle). Several research groups studied the printability of inkjet inks.[298, 299] Moon et al.[300] summarized Z values for inkjet ink to be in between 4 and 14 to be ideally printable. Considering the drop generation, drop flight and drop impact, the optimal value of the physical conditions for a robust DOD inkjet printing are typically with surface tension lying in the range of 20-50 mN m^{-1} and viscosity within the range of 2-20 mPa.s. to achieve high resolution print on desired trajectory, where narrower and specified range would be more applicable for specific print heads.[125]

For e-textile fabrication, inkjet printing offers a number of advantages over conventional manufacturing techniques including the ability to deposit controlled quantities of materials at precise locations of the fabric, combined with a reduction in both material waste and water utilization.[306] However, the key challenge with inkjet printing of e-textiles is the ability to achieve uniform and continuous highly conductive electrical tracks on a rough and porous textile substrate using low viscosity inkjet inks. To solve this, we developed a novel surface pre-treatment that was inkjet-printed onto rough and porous textiles before inkjet printing of electrically conductive graphene-based inks for wearable e-textiles applications.[43] Later, we formulated graphene-Ag composite inks for inkjet printing onto surface pre-treated cotton fabrics, to enable all-inkjet-printed highly conductive e-textiles with a sheet resistance in the range of ~0.08–4.74 Ω sq^{-1}.[306]

Stempien et al.[307] propose an inkjet printing method to prepare PPy layers on textile fabrics using direct freezing of inks under varying temperature up to −16 °C. The as-coated PPy layers on PP textile substrates were further assembled as the electrodes in symmetric all-solid-state

SC device, *Figure 2.12b*. The electrochemical results demonstrate that the symmetric SC device made with the PPy prepared at −12 °C, showed the highest specific capacitance of 72.3 F g^{-1} at a current density of 0.6 A g^{-1}, and delivers an energy density of 6.12 Wh kg^{-1} with a corresponding power density of 139 W kg^{-1}. Sundriyal et al.[308] reported an inkjet-printed, solid-state, planar, and asymmetric micro-supercapacitor (PAμSC) desk-jet printed on cellulose paper substrate. They digitally designed interdigitated electrode patterns and printed on paper with rGO ink to construct a conducting matrix. The negative electrode was printed using activated carbon–Bi_2O_3 ink and the positive electrode was printed with rGO-MnO_2 ink. After that, they demonstrated bamboo fabric as a sustainable substrate for developing SC device with a replicable inkjet printing process.[28] Different metal oxide inks such as MnO_2–$NiCo_2O_4$ was used as a positive and rGO as a negative electrode. With LiCl-PVA gel electrolyte, the textile-based MnO_2–$NiCo_2O_4$//rGO asymmetric SC displayed excellent electrochemical performance with an overall high areal capacitance of 2.12 F cm^{-2} (1,766 F g^{-1}) at a current density of 2 mA cm^{-2}, excellent energy density of 37.8 mW cm^{-3}, a maximum power density of 2,678.4 mW cm^{-3} and good cycle life, *Figure 2.12(c-e)*.

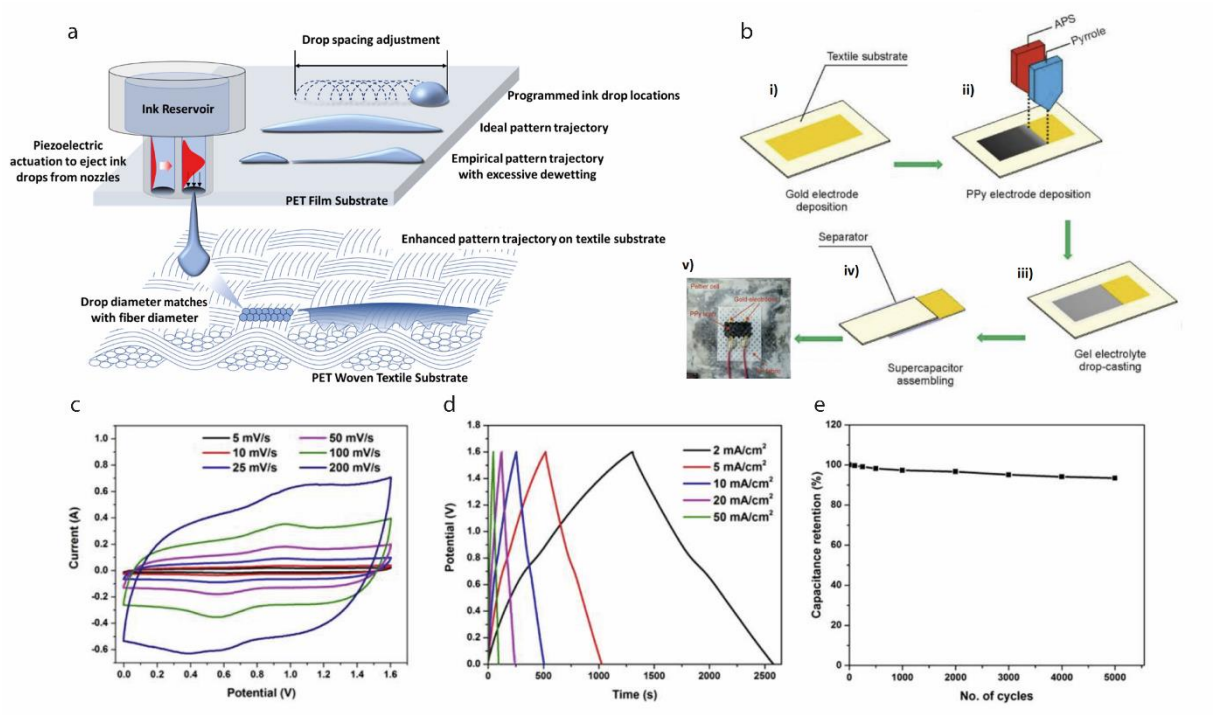

Figure 2.12. a) Schematic drawing of the inkjet process and ink spreading behaviour on the film and textile substrates. Reproduced with permission.[304] Copyright 2021, American Chemical Society. b) Detailed steps of fabrication of inkjet-printed textile supercapacitor and printed samples. Reproduced with permission.[307] Copyright 2021, The Authors. c) CV curves of MnO_2–$NiCo_2O_4$//rGO asymmetric device at different scan rates d) GCD profiles of the

MnO_2–$NiCo_2O_4$//rGO asymmetric device at various current densities and e) Capacitance retention of the device with the different number of charge–discharge cycles. Reproduced with permission. [28] Copyright 2020, The Authors.

2.3.3 Spinning technology

Spinning of polymer fibres, is an interdisciplinary field applying the principles of engineering and material science toward the development of textile substitutes. Electrically conducting textile materials can be spun in the form of staple fibre or filament yarn based on intrinsic CPs. An extruded liquid polymer filament is continuously drawn and simultaneously solidified to form a continuous synthetic fibre in this process.[309] This is based on a special extrusion process that uses spinneret (a nozzle type device) to form multiple continuous filaments or mono filaments. Available spinning technologies such as dry, wet, melt or electrospinning can be exploited for this purpose. The polymer, needed to form fibre, is first converted into spinnable solution. The solidification of the ejected solution is carried out by the removal of heat and/or solvent by contacting the liquid with a suitable moving fluid, either with gas or liquid.[310, 311]

The basic dry spinning process involves dissolving the polymer in organic solvents followed by blending with additives and filtering to produce low viscosity polymer solution, called as 'dope.' The dope is filtered, de-aired and pre-heated, and pumped through filters to achieve the right consistency. The dope is then extruded in a spinning tube where the solution is forced through the fine orifices of spinneret (or jet). The exiting jets of the polymer solution, when come in contact with a stream of hot gas, vaporizes the solvent in the gas stream, increasing the polymer concentration in the filament and thus solidifying it without the need for further drying.[312] This complex process makes dry spun fibres very expensive. Additionally, the poor solubility of most conducting polymers in organic solvents, makes them unsuitable for the production of conductive polymer filaments using such technique.

Wet spinning is another technique, which requires pumping of the polymer solution through the fine orifices of a spinneret into a coagulating bath and drawing off as continuous filaments by means of take-up rollers. The bath removes the solvent from the as-spun filaments so that they become solidified. They are collected together to form a continuous tow or rope.[313] Wet spinning is slower than other spinning processes due to mass transfer of the solvent and non-solvent for fibre solidification. Zhang et al.,[314] exploited the solubility properties of PANI to blend with poly-ω-aminoundecanoyle (PA11) in concentrated sulfuric acid (c-H_2SO_4) to form a spinning dope solution to spin conductive PANI/PA11 fibres by wet-spinning technology.

Kou et al,[315] proposed a coaxial wet-spinning assembly to spin polyelectrolyte-wrapped graphene/carbon nanotube core-sheath fibres continuously, which were used directly as safe electrodes to assemble two-ply yarn SCs, *Figure 2.13(a-d)*. The yarn SCs using liquid and solid electrolytes exhibited ultra-high capacitances of 269 and 177 mF cm^{-2} and energy densities of 5.91 and 3.84mWh cm^{-2}, respectively.

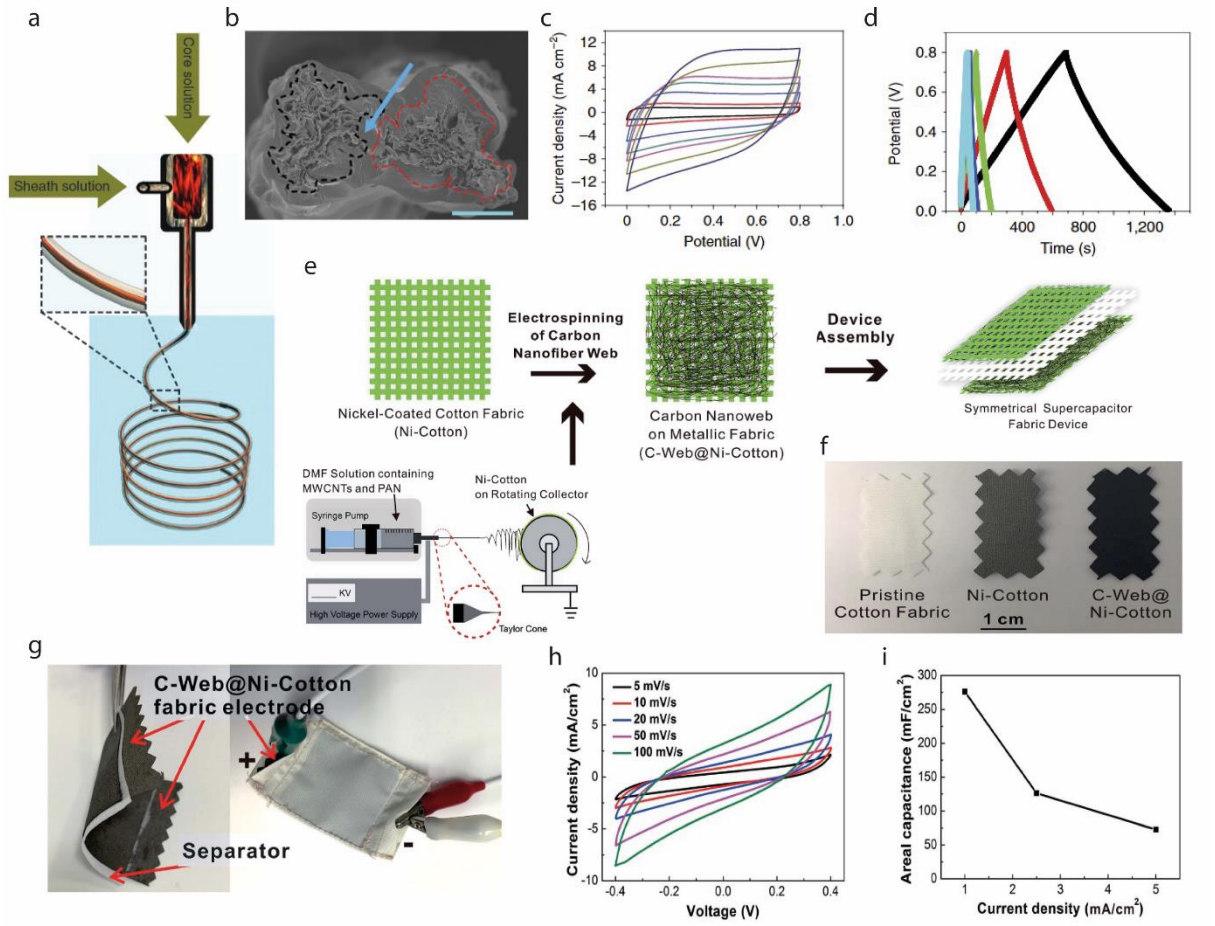

Figure 2.13. a) Schematic illustration showing the coaxial spinning process. Two-ply YSCs and their electrochemical properties- b) SEM images of cross-sectional view of a two-ply YSC. The arrow area is PVA/H_3PO_4 electrolyte (scale bar: 50 μm) c) CV curves of RGO+CNT@CMC d) GCD curves of RGO+CNT@CMC. Reproduced with permission.[315] *Copyright 2014, The Authors. e) Schematic illustration of textile-based SC fabrication process. The inset shows details of one-step electrospinning setup f) Photographs of the pristine cotton fabric, Ni-coated cotton fabric (Ni–cotton) and carbon nanofibre web coated Ni–cotton fabric (C-web@Ni–cotton) g) Photographs of a large supercapacitor fabric (active area: 4 cm× 4 cm) enclosed with commercial nonconductive fabrics h) CV curves of solid-state C-web@Ni–cotton supercapacitor fabric i) Summary of the areal capacitance of the supercapacitor at*

different current densities. Reproduced with permission.[316] *Copyright 2016, The Royal Society of Chemistry.*

Melt spinning is one of the most popular methods for manufacturing synthetic fibre filaments. It requires no solvents, thus simple and economical process. In melt-spinning process, the polymer pellets or granules are fed into an extruder for melting by heating, and then the polymer melt is pumped through a spinneret under pressure. After extrusion, it is quenched with cold air which solidify the molten mass to form filaments. Spinning is followed by a mechanical drawing to improve the degree of crystallinity, which contributes to improve physical, mechanical and chemical properties.[317] Kim et al.,[318] melt-mixed polyaniline emeraldine salt (PANI-ES), PPy and graphite with PP and low-density polyethylene (LDPE) using a co-rotating twin screw extruder. However, the electrical conductivity of conductive materials/PP monofilament obtained by melt spinning process was not found satisfactory, due to the problems of structure homogeneity and the aggregation of conductive materials.

Electrospinning is another fibre spinning process, which is used to produce ultrafine fibres by charging and ejecting a polymer melt or solution through a spinneret under a high-voltage electric field and to solidify or coagulate to form filaments.[319] This is a relatively simpler and cheaper spinning process, as well as a versatile method to produce continuous, long and fine (in the range of nano to sub-micron size range) fibres. These fibres possess high surface to volume ratio, high aspect ratio, controlled pore size and superior mechanical properties than conventional fibres. Electrospinning can be used to produce novel fibres with diameters between 100 nm and 10 μm. Electro-spun fibres have been investigated as sensor, light emitting diodes, rechargeable batteries, electroactive actuators, nano-electronic devices, electromagnetic shielding for wearable electronics applications.[320, 321] Wei et al.,[322] prepared core-sheath nanofibres with conductive polyaniline as the core and an insulating polymer as the sheath by electrospinning of blends of polyaniline with polystyrene and polycarbonate. These unique core-sheath structures offer potential in a number of applications including nanoelectronics. Huang et al., reported the development of high-performance wearable SC fabrics based on flexible metallic fabrics (Ni–cotton), in which MWCNTs-based nano-fibre webs were directly electro-spun, showing a high areal capacitance of 973.5 mF cm^{-2} (2.5 mA cm^{-2}), *Figure 2.13(e-i)*. The SC fabrics was also integrated into commercial textiles with desirable forms, demonstrating its the potential for wearable electronics applications.[316]

2.3.4 In-situ growth of active material on substrate

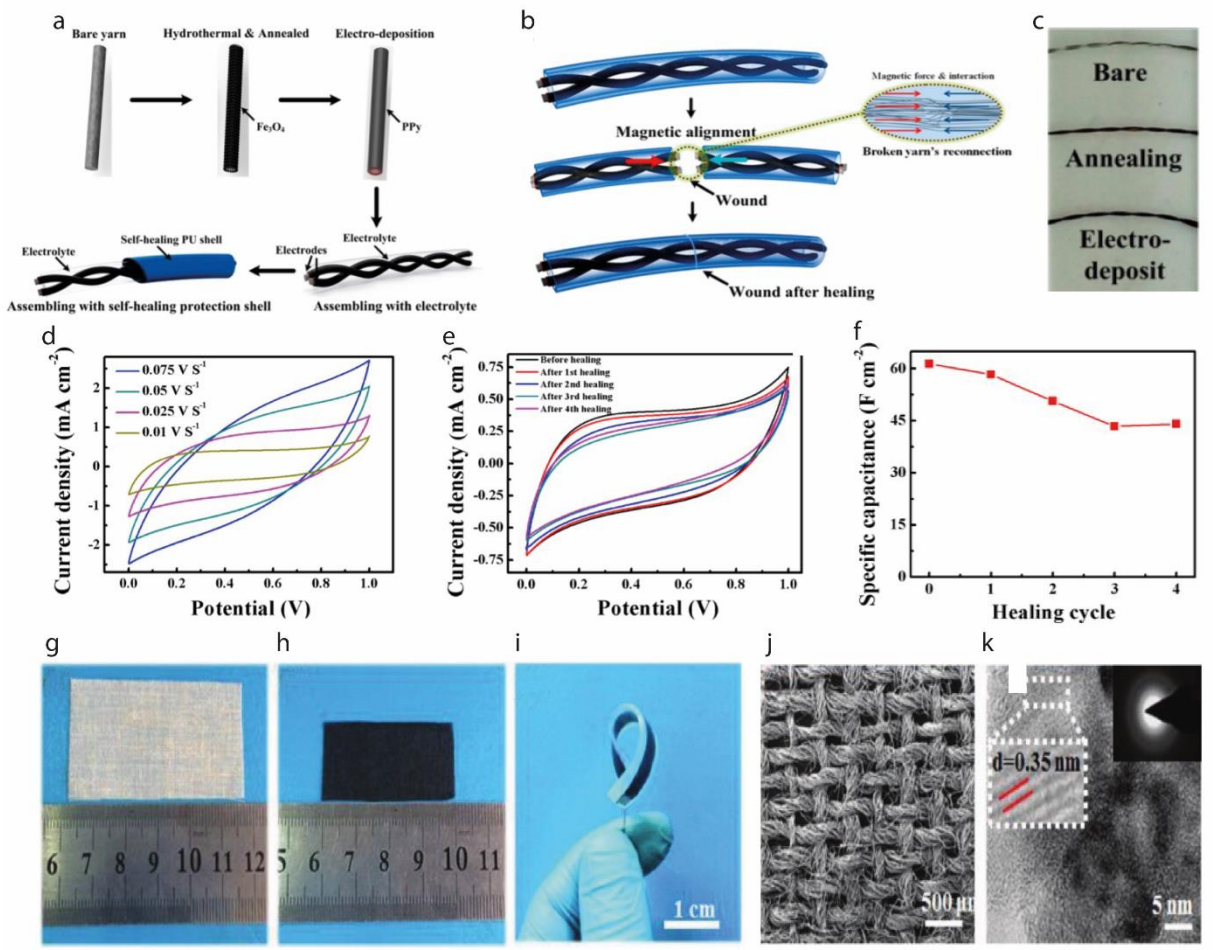

Figure 2.14. a) Design and manufacturing process flow of magnetic-assisted self-healable supercapacitor. Fe_3O_4 nanoparticles anchor on the surface of yarn by a microwave-assisted hydrothermal method. The processed yarn is annealed to ensure the magnetic particles anchor on the yarn tightly. To achieve a better electrochemical performance, a layer of PPy is electrodeposited on the annealed yarn. Finally, two yarns as a set of electrodes are assembled with a solid electrolyte and a self-healing shell to form a self-healing supercapacitor b) Schematic illustration of supercapacitor's self-healing process. The magnetic alignment could assist the reconnection of fibres in broken yarn electrodes when they are brought together, as shown in inset image. c) From top to bottom, pristine yarn, hydrothermal and annealing-treated yarn, and PPy-electrodeposited yarn. Electrochemical measurements for as-prepared capacitor. d) CVs obtained at various scan rates e) CVs after healing for different cycles. (f) Specific capacitance of the original device and after healing for different cycles. Reproduced with permission.[323] *Copyright 2015, American Chemical Society. g) Fabrication process and characterization of carbonized plain weave cotton fabric (CPCF)- Photograph of a pristine*

cotton fabric h) Photograph of the CPCF made from (g) i) A flexible CPCF-based strain sensor. j–k) SEM image and TEM image of the CPCF. Reproduced with permission.[324] *Copyright 2016, Wiley-VCH.*

Electrodeposition is a well-known method of producing in-situ metallic coatings or thin films of oxides and/or hydroxides by applying an electric current to a conductive material immersed in a solution containing a metal salt. By controlling several experimental parameters including potential, current density, deposition time and plating solution composition, the morphology and texture of the film can be modified.[325] The process may either be an anodic or cathodic. In anodic process, a metal anode is electrochemically oxidized in the solution, and then deposited on anode. In a cathodic process, components (ions, clusters, or NPs) are deposited onto cathode from solution precursors. The increase in the reaction time causes more source materials deposition resulting in larger film thickness. The deposition rate can be maintained by the variation of current with time.[326] E. Gasana et al.[327] reported an electroconductive polyaramide woven textile structure produced *via* electroless deposition of PPy and copper at a deposition time of 240 seconds, providing the resistance of 5±1 Ω with a surface coverage of 100±1%. Zhao et al.,[328] deposited copper galvanostatically in the copper citrate complex anions on poly PET fabric treated with PANI to produce flexible Cu– PANI/PET conducting textiles.

Hydrothermal reaction is a synthesis mechanism, which involves chemical reactions of substances in a sealed and heated aqueous solution or organic solvent at an appropriate temperature (100-1,000°C) and pressure (1-100 MPa). Many compounds or materials with special structures and properties, which cannot be prepared from solid-state synthesis, can be obtained *via* hydrothermal reactions. In some cases, it offers an alternative and mild synthetic method for solid-state reactions by lowering the reaction temperature. Hydrothermal synthesis has been successful for the preparation of important solids such as zeolites, open-framework compounds, organic-inorganic hybrid materials, MOF materials, superionic conductors, chemical sensors, electronically conducting solids, complex oxide ceramics and fluorides, magnetic materials, and luminescence phosphors. It is also a route to unique condensed materials including nanometer particles, gels, thin films, equilibrium defect solids, distinguished helical and chiral structures, and particularly stacking-sequence materials.[329] Hydrothermal synthesis relies on the forced hydrolysis of the reactants in order to produce the oxide ceramics. This is achieved at moderate temperatures (<200 °C) and high pressures by placing the reagents in a sealed container and heating the system to the reaction temperatures. The solvent is usually water; a metal hydroxide (e.g. NaOH) is added as a mineralizer while

metal alkoxides or metal salts serve as the source of metal ions. As in precipitation systems, the nucleation is followed by particle growth to yield a powder with a certain particle-size distribution.[330] Huang et al.[323] demonstrated the synthesis of Fe_3O_4 through hydrothermal reaction, wrapped on stainless steel fibre which assisted the self-healing of a yarn-based SC to enhance the reliability and lifetime of a SC in practical usage, *Figure 2.14 (a-f)*. The specific capacitance was restored up to 71.8% even after four breaking/healing cycles with great maintenance of the whole device's mechanical properties. Li et al. [331] reported the fabrication of hierarchical graphene fibre fabrics (GFFs) with significantly enlarged specific surface area using a hydrothermal activation strategy. The achieved areal capacitance was 1,060 mF cm^{-2} with a very thin thickness (150 μm) and further magnified up to 7398 mF cm^{-2} by overlaying several layers of HAGFFs.

In-situ polymerization is another fabrication technique for conductive electrodes. This is typically a chemical encapsulation process similar to interfacial polymerization except there are no reactive monomers in the organic phase. All polymerization occurs in the continuous phase rather than in the interface as in interfacial polymerization. The most common example of this method is the condensation polymerization of urea or melamine with formaldehyde to form cross-linked urea-formaldehyde or melamine-formaldehyde capsule shells. In this method, an oil-phase is emulsified in water using water-soluble polymers and high-shear mixers, yielding a stable emulsion at the required droplet size. A water-soluble melamine resin is added and dispersed. The pH of the system is then lowered, initiating the polycondensation which yields crosslinked resins that deposit at the interface between the oil droplets and the water phase. During hardening of the wall material, the microcapsules are formed and the aqueous dispersion of polymer-encapsulated oil droplets is produced.[332, 333] Lee et al.[334] reported one-dimensional metal oxide nanostructure-based SC of multiscale architecture. In their work, MnO_2-micronodules were deposited on carbon cloth, followed by coating with partially carbonized-PPy through vapour deposition polymerization (VDP). Then, the PPy-coated MnO_2-based multiscale micronodules were assembled within a PVA–KOH polymer electrolyte as the positive-electrodes of solid-state asymmetric SCs (ASCs) which demonstrated ultrahigh performance (59.5 F cm^{-3} of capacitance, 27.0 mWh cm^{-3} of energy and 1.31 W cm^{-3} power density).

Carbon fibre, though exhibit high conductivity, suffer from agglomeration problem which creates obstacle during application in several fields. Additionally, the small surface area and low specific capacitance limits the wide scale use as conductive material, therefore surface

functionalization offers scopes to overcome the limitations and exploit the fibre properties fully. Oxidation (wet and dry), amidation, silanization, silylation, polymer grafting, polymer wrapping, surfactant adsorption, thermal annealing and encapsulation are some of the functionalization techniques.[335] Cotton, the most popular fibre ever, can be considered as an innovative platform for wearable, smart and interactive electronic devices, like batteries, SCs, and various sensors if their electrochemical performances be ensured. It is a natural polymer of cellulose, burns readily, but in low oxygen concentration, it chars leaving a carbon skeleton, which improves the conductivity.[336] Carbonization/Pyrolysis of cotton fibres can be an alternative option to produce conductive electrodes. Zhang et al.,[324] simply annealed pristine woven cotton fabric in an inert atmosphere, producing flexible and highly conductive fabric, which was used as strain sensor to demonstrate its superior performance in the detection of both large and subtle human body motions, *Figure 2.14(g-k)*. However, the release of toxic substances during carbonization process limits the viability of the process.

2.4 Fabrication of textiles supercapacitors

2.4.1 Device configurations

Textile-based flexible energy storage devices that are used for wearable applications can be categorized into: 1D fibre/yarn shaped device and 2D fabric shaped device. Additionally, there are very few 3D shaped energy storage devices that have been reported in the literatures.[337] *Figure 2.15* represents the schematic diagram of textile substrates that have been exploited as 1D and 2D shaped storage devices.

2.4.1.1 1D fibre/yarn shaped supercapacitors

In this type, energy storage device or SC components (i.e., the current collector, electrode, separator and electrolyte) are all integrated into one-dimensional system, possibly in fibre or wire or cable shaped SCs. Several forms of 1D shaped textiles are filament or staple fibres converted into two -or multi-plied yarn, split film, core sheath yarn, multi- or mono- filament and staple yarn, *Figure 2.15(a-i)*. They are generally small in size, light in weight, and possess dimensions typically ranging from tens to hundreds of micrometres in diameter, and several millimetres to meters in length.[338, 339] For instance, the electrode materials with separator are twisted to form ply yarn or all the electrodes and electrolyte are wrapped together to form a single yarn of core-sheath configuration, *Figure 2.15n*. 1D EES devices offer several potential advantages over other conventional SCs including mechanical flexibility and deformability under various bending and twisting conditions, enabling better wearability and integrability into flexible textiles. The ease of integration via weaving, knitting, stitching or embroidery

provides scopes to get assembled into various shapes at different desirable locations in several wearable devices. It enables a greater design versatility and scope of integration with 1D energy harvesting or other devices such as displays and sensors, to create multifunctional wearable systems.[340] However, the increased electrical resistance along the device length is a major challenge that affects the electrochemical performance of such devices.[225]

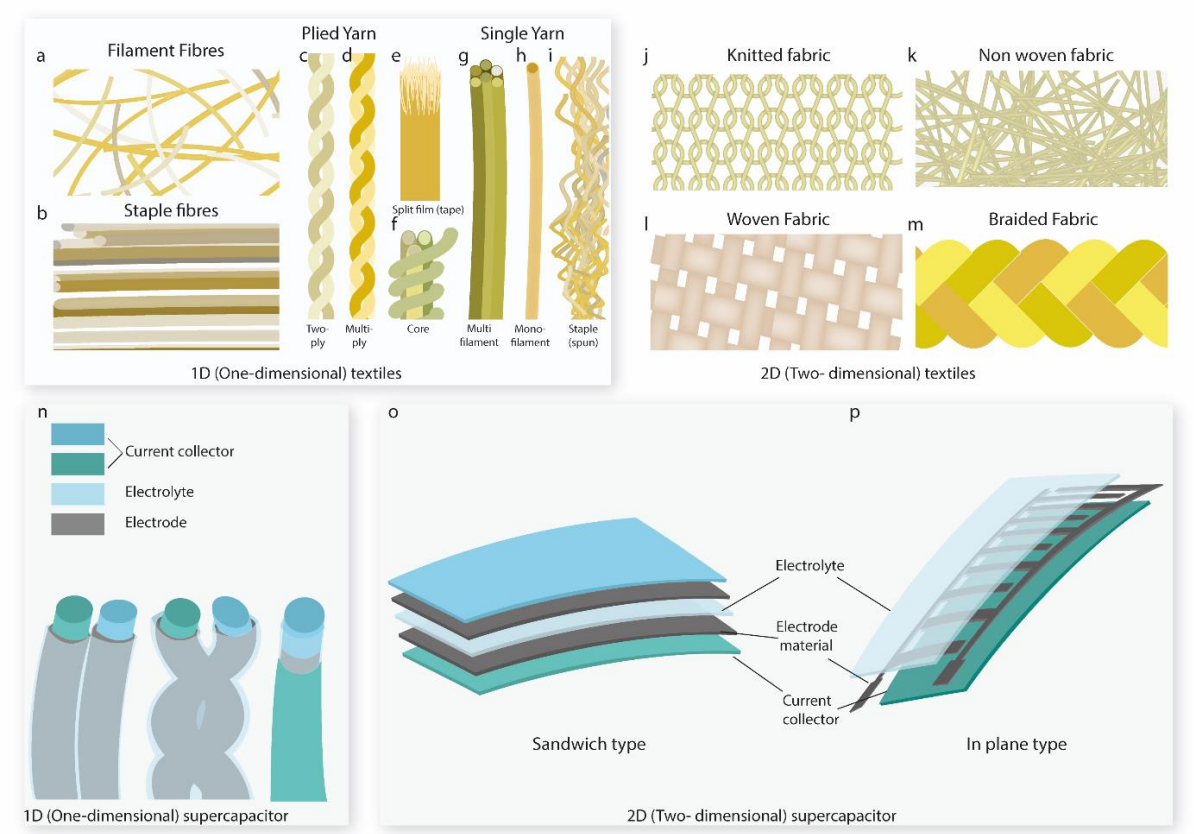

Figure 2.15. Textile-based energy storage device configuration. 1D substrate forms a) filament fibres b) staple fibres c) two plied d) multiplied e) split film and f) core sheath yarn g) multi filament h) mono filament and i) staple yarn. 2D substrate forms j) knitted k) non-woven l) woven and m) braided fabric. Textile supercapacitor forms n) 1D fibre or yarn shaped o) Sandwich type and p) in plane type 2D supercapacitor.

2.4.1.2 2D fabric shaped supercapacitors

2D planar SC devices are particularly suitable for the use in thin or layered products, such as smart cards, packaging and labels, magazines, books, skin patches and healthcare devices, jewelleries, and a broad range of other products comprising flexible electronic components.[225] Different substrates are usually used to fabricate 2D SCs including plastic films, sponge, metal sheets, papers and textiles.[341] Among them, textile fabrics offer excellent flexibility due to their intrinsic mechanical properties and ability to be integrated directly with any other textile fabrics

or garments for wearable applications *via* any simple methods of joining (e.g., sewing technology).[30] Any form of fabrics including woven, knit, non-woven or braided can be used for 2D SCs, *Figure 2.15(j-m)*. In such 2D configuration, a pair of fabric electrodes are usually separated by an electrolyte and a separator in a sandwich or planar structure, *Figure 2.15(o-p)*. However, it is challenging to maintain appropriate dimension/thickness of such configurations in order to achieve high areal device performance, flexibility and comfort.[16]

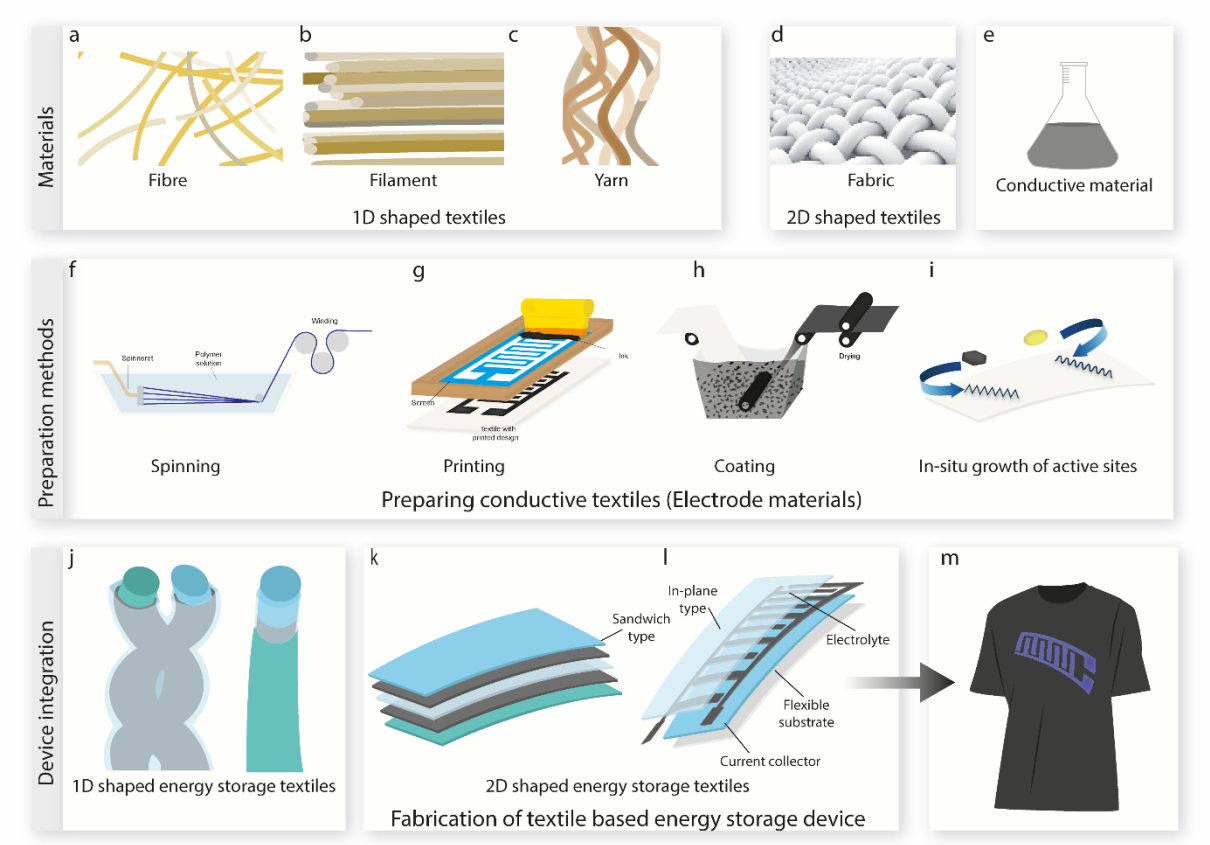

Figure 2.16. Fabrication of textile-based supercapacitor devices. 1D shaped textiles, a) fibre b) filament c) yarn and 2D shaped fabric and c) conductive materials. Preparation of conductive textiles by f) spinning g) printing h) coating and i) in-situ growth of active sites on textiles to produce j) 1D shaped energy storage textiles, 2D shaped k) sandwich type and l) in-plane type supercapacitor and m) the final e-textiles.

2.4.2 Integration of the EES device

After the formation of the electrode materials (*Figure 2.16*a-i), there comes the final but critical stage of the integration of the components to complete the full SC. LIB cells are typically parallel assembled in modules (with internal electrical circuits), which are then integrated within a battery management system. Cable-shaped 1D devices (e.g., for smart textiles) can be

embedded into textiles by weaving, knitting or embroidery.[225] Conductive electrodes and separators along with electrolytes are all integrated on a simple wire/cable shape, *Figure 2.16j*. 2D planar or thicker 3D devices may be integrated on a chip or a soft substrate into planar flexible objects. Electrodes with separator and/or electrolytes can be sandwiched by compression and/or encapsulation to form the integrated device, *Figure 2.16(k-l)*. However, there exist requirements for simpler and low-cost assemblies for flexible and wearable device architectures. Additionally, the encapsulation of the integrated device is crucial to improve the washability and durability of wearable e-textiles devices. Several methods have been used, either as surface pre-treatments (e.g., Bovine Serum Albumin (BSA) treatment) or post-treatments (e.g., polydimethylsiloxane (PDMS), polyurethane (PU) coatings), to seal conductive track and encapsulate integrated devices, protecting them from the exposure to harsh treatments during daily usages.[26]

2.4.3 Combined energy harvesting and storage

The energy harvesting (EH) devices harvest energy that dissipates around us, in the form of electromagnetic waves, heat and vibration, and then convert them into easy-to-use electric energy with relatively small levels of power in nW-mW range.[342, 343] The principle is similar to large- scale renewable energy generations such as wind turbines, but with a smaller amount of energy produced from such devices. EH is a promising technique for solving the global energy challenge without depleting natural resources and as an everlasting source of power supply.[344] It can reduce greenhouse gas emission generated with traditional energy sources.[345] Though cheap, conventional batteries limit in amount of energy, therefore requires periodic replacement or recharging. In addition to that, rigid bulky structure limits their usage in smart fabrics applications.[346] Flexible EH devices thus have potential to replace the conventional power sources for wearable electronics.

EH sources are classified into two groups according to characteristics of their source, (i) Natural sources are those available readily from the environment such as sun light, wind, and geothermal heat and (ii) artificial sources are those generated from human or system activities including human motion, pressure on floors/shoe inserts when walking or running, and system vibration when operating.[347] Biomechanical EH from human motion has attracted attention in the past decade for potential applications in charging portable electronic device, batteries and self-powered sensor systems.[348, 349]

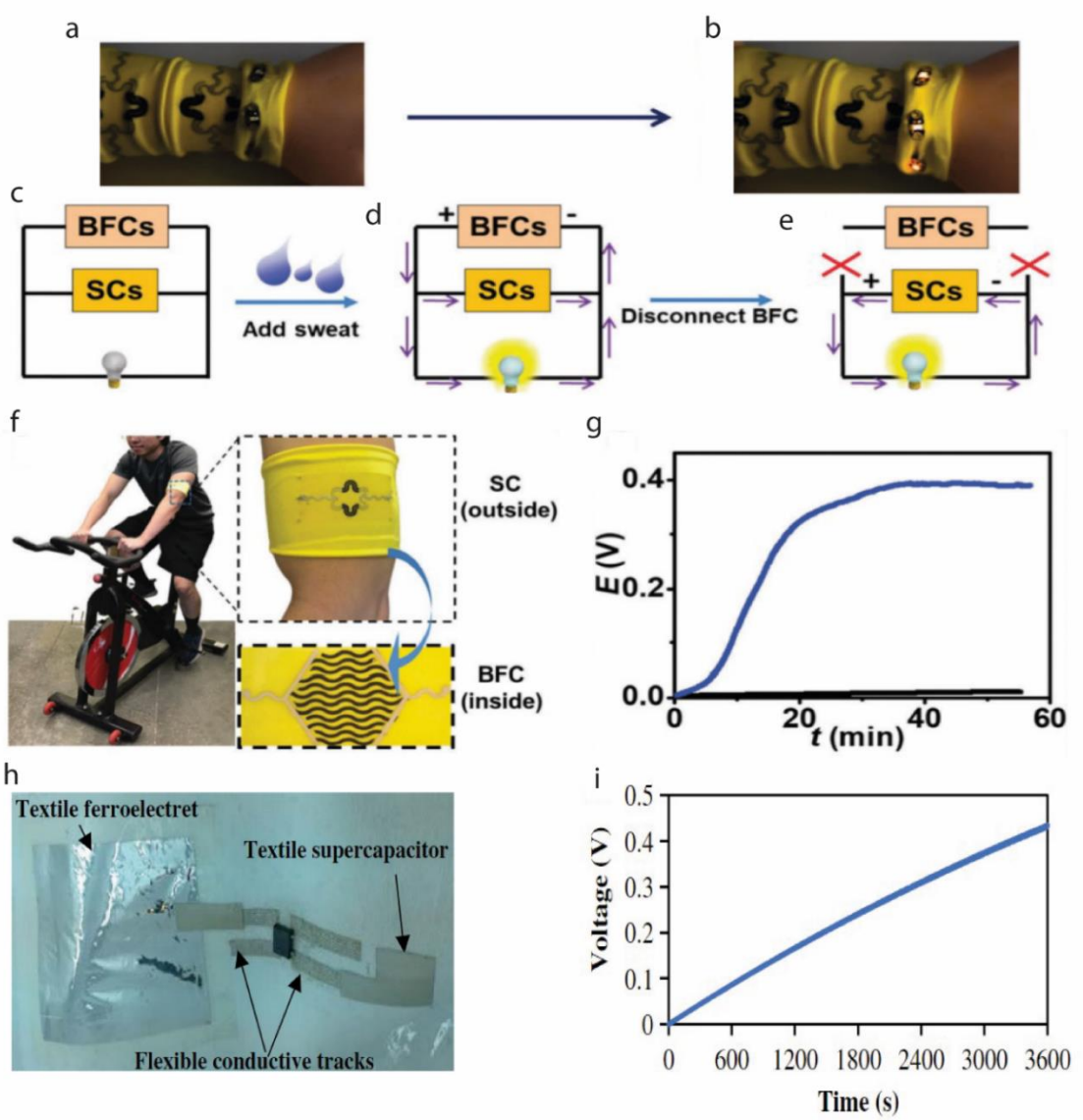

Figure 2.17. Demonstration of the hybrid SC–BFC device (a and b), Photographs showing the application of three SCs charged by five BFCs to light LEDs using the following procedure: (c) without lactate, no power; (d) with lactate, LEDs were turned on; (e) upon disconnecting BFCs and SCs, LEDs could still be turned on, (f) The integrated chemical self-powered system on one piece of textile was applied to the arm of a volunteer. The SC and BFC were printed outside and inside the textile band, respectively (g) The real-time voltage of the printed SC charged from the on-body BFC during a constant cycling exercise for 56 minutes. The SC charged by lactate BFC immobilized with LOx (blue plot) and without LOx as a control (black plot). Reproduced with permission.[350] Copyright 2018, The Royal Society of Chemistry. h) Assembled textile power module and i) FEP-textile ferroelectret charging the 2 mF textile capacitor. Reproduced with permission.[351] Copyright 2019, Wiley-VCH.

Satharasinghe et al.[352] presented an innovative solar energy harvesting fabric and demonstrated its suitability for powering wearable and mobile devices. A large solar EH fabric containing 200 miniature solar cells was demonstrated which can charge a 110 mF textile SC bank within 37s. Lv et al.[350] demonstrated the first example of a stretchable and wearable textile-based hybrid SC–biofuel cell (SC–BFC) system, screen-printed on both sides of the fabric, designed to scavenge biochemical energy from the wearer's sweat and to store it in the SC module for subsequent uses, *Figure 2.17(a-g)*. Yong et al.[351] presented a textile-based power module for the first time that combines a ferroelectric biomechanical energy harvester and solid-state SC-based energy storage device, fabricated in a single woven cotton textile layer, *Figure 2.17(h-i)*. The textile power module was highly flexible, and the fluorinated ethylene propylene (FEP) based ferroelectret was able to generate electric energy with an instantaneous output voltage of ~10V and power density of ~2.5 μW cm^{-2}, with a solid-state SC having capacitance of 5.55 mF cm^{-2}.

2.5 Electrochemical performance of textile-based supercapacitor devices

Capacitance/capacity per unit length (F cm^{-1}), area (F cm^{-2}), or volume (F cm^{-3}) are usually reported to evaluate the performance of a textile-based SC. However, the gravimetric capacitance of electrode materials does not necessarily represent the full device capacitive performance. In addition to capacitance, the other two key parameters for evaluating the SC performance are energy density and power density. Maintaining higher energy and power density is still a major challenge for such energy storage devices. SCs, in comparison with lithium-ion batteries, usually exhibit relatively lower energy density but higher power density. Whereas for LIBs, it is desirable to improve the power density while keeping the high energy density. The major challenge in achieving high-performance SC textile is to enhance the energy density while maintaining the high-power density.[16]

The capacitance retention of textile-based energy storage devices is another important property for wearable applications since the replacement of such devices would be difficult during the product lifetime. In most cases, 10,000 cycles of charge-discharge are employed for the capacitance retention assessment. For 1D shaped energy storage devices, several configurations were reported with full capacitance retention up to 10,000 cycles.[353, 354] Additionally, Fu et al.[355] reported a fibre shaped SC, developed by pen ink, which retains full capacitance even after 15,000 of charge-discharge cycles. For 2D shaped energy storage devices, full capacitance retentions were reported for even after longer (20,000-25,000) charge-discharge cycles.[356, 357] Wang et al.[358] developed a fabric type asymmetric SC using

electrochemically activated carbon cloth as anode, TiN@MnO_2 on carbon cloth as cathode and LiCl solution as electrolyte, which significantly boosted the energy storage capability. The device showed no capacitive decay even at 70,000 cycles of charge discharge. In another study, Hu et al.[230] reported a fabric-based SC device made of Cotton/SWNTs, exhibiting extremely good cycling stability of 98% capacitance retention over a remarkably large cycle number of 130,000 charge discharge cycles. As we previously classified the active materials into four categories, in this section we will discuss active materials of textile-based SCs. Each subsection focusses on both 1D and 2D shaped textile SCs. Combining any of the two or more types are also summarized under hybrid materials section. In addition, we throw light on SCs based on fibre types, particularly focusing on most widely used natural cotton, manmade polyester and carbon fibres.

2.5.1 Carbon-based textiles supercapacitors

Among all the active materials, carbonaceous compounds i.e., carbon nanotubes, graphene and its derivatives have mostly been studied for the fabrication of textile-based SC devices. Appendix D.1 summarizes the electrochemical performances of carbon-based one-dimensional fibre/yarn shaped and two-dimensional fabric shaped SCs.

Several research groups reported graphene fibre,[359] GO fibre,[360] rGO fibre[361] and modified rGO[362] fibre as SC electrodes. Kou et al. [315] twisted two coaxial fibres composed of polyelectrolyte-wrapped carbon nanomaterial core-sheath fibre, rGO@CMC, CNT@CMC, rGO+CNT@CMC, together to form a two-ply SC electrode, and then coated with PVA electrolyte. In presence of 1 M H_2SO_4 liquid electrolyte the device exhibited length, areal and volumetric capacitance of 8.0 mF cm^{-1}, 269 mF cm^{-2}, 239 F cm^{-3}, respectively. Zhai et al.[363] drop-casted activated carbon on carbon fibre yarn to prepare SC electrode. For the fabrication of yarn shaped SC, two coated strands were twisted together and finally dipped in PVA-H_3PO_4 electrolyte. The resultant device exhibited a specific length capacitance of 45.2 mF cm^{-1} at a scan rate of 2 mV s^{-1}.

For 2D fabric shaped SC cotton, polyester, poly-cotton, PP and carbon fibre textiles were investigated. Several research groups[230, 364] coated cotton fabric with SWCNT or MWCNT, however better performances were obtained while using graphene or its derivatives. For example, Hu et al.[230] coated cotton fabric with SWNT ink by simple dipping and drying method to obtain SC electrode. In the presence of $LiPF_6$ electrolyte, the device exhibited specific capacitance of 140 Fg^{-1} at 20 μA cm^{-2} and an areal capacitance of 0.48 F cm^{-2}. The energy

density was as high as 20 Wh kg^{-1} at 10 kW kg^{-1} with an outstanding cyclic stability of 98% after 130,000 charge-discharge cycles. In another study by Li et al.,[364] the gravimetric capacitance was enhanced by coating cotton fabric with rGO and using coated fabrics as SC electrode. The sandwiched shaped SC device combined with raw cotton fabric separator and H_3PO_4-PVA gel electrolyte exhibited a gravimetric capacitance of 464 F g^{-1} at 0.25 A g^{-1} and a higher energy density of 27.05 W h kg^{-1}.

The highest areal capacitance for conventional textiles SC prepared by carbonaceous compounds was reported by Jost et al.[365] They screen printed AC on both cotton and polyester fabric. The fabric SC achieved a high areal capacitance of 430 mF cm^{-2} at 5 mA cm^{-2} and a gravimetric capacitance of 85-95 F g^{-1} at 10 mV s^{-1}. The device also exhibited very good cyclic stability of 92% after 10,000 charge-discharge cycles. Additionally, they screen printed activated carbon on carbon fibre fabric and achieved even higher areal capacitance.[19] They achieved gravimetric capacitance of 88 F g^{-1} and areal capacitance of 510 mF cm^{-2} for knitted carbon fibre fabric, and that of 66 Fg^{-1} and 190 mFcm^{-2} for the woven carbon fibre fabric. The highest areal capacitance for both electrode (3,350 mF cm^{-2}) and SC device (2,700 mF cm^{-2}) was obtained through composite electroactive materials, as reported by Dong et al.[366] CNTs and graphene (Gn) were coated on activated carbon fibre felt (ACFF) to prepare electrodes. The asymmetric SC was fabricated by as prepared CNT/ACFF and Gn/ACFF composite textile electrodes with a non-woven fabric separator, and KOH aqueous electrolyte. The energy and power densities were reported as 112 μW h cm^{-2} and 490 μW cm^{-2}, respectively. Furthermore, several research groups have investigated stainless steel fabric and silver fibre fabric for fabric based SCs. Yu et al.[367] prepared two chemically converted graphene (CCG) on stainless steel fabrics electrode with 1 M H_2SO_4 to form flexible solid-state symmetrical SC. The areal capacitance was reported as high as 730.8 mF cm^{-2} at 2 mA cm^{-2} and 180.4 mF cm^{-2} at 1 mA cm^{-2}. The energy density was reported 19.2 W h cm^{-2} at 386.2 W cm^{-2}. The device was able to retain the capacitance up to 96.8% after 7,500 charge-discharge cycles and 96.4% after 800 stretching-bending cycles.

2.5.2. Conductive polymer-based textiles supercapacitors

CPs are pseudo-capacitive materials, the bulk of the material undergoes a fast redox reaction to provide the capacitive response exhibiting superior specific energies to the carbon-based EDL SCs.[368] Appendix D.2 summarizes the conducting polymer-based 1D fibre or yarn-shaped and 2D fabric-shaped SCs. Only a few works have been reported for fibre or yarn-shaped textile SCs. For example, Wei et al.[369] directly coated cotton yarns by PPy nanotubes *via* in-situ

polymerization of pyrrole in presence of methyl orange. The electrode thus obtained was used to fabricate an all-solid-state yarn SC, which provided high areal-specific capacitance of 74.0 mF cm^{-2} and an energy density of 7.5 μWh cm^{-2}.

However, several works[370-372] have been reported on 2D fabric-shaped SCs. For instance, Wang et al.[370] prepared flexible and stretchable electrodes *via in-situ* polymerization of conducting PPy polymers on knitted cotton fabrics. The areal capacitances of symmetric all-solid-state SC based on those electrodes were found to be 101 and 450 mF cm^{-2} at 5 mV s^{-1} and 1 mA cm^{-2}, respectively. The capacitance retention of such devices was reported 53% after 5,000 charge-discharge cycles. In another study by Lv et al.,[371] the electrochemical performances of several woven and knitted fabrics-based electrodes of cotton, wool, silk, and polyester fibres were enhanced *via* an improved *in-situ* polymerization method. The conjugate length of the PPy molecule and doping levels were improved to provide a thin and dense conductive polymer coating on the fabric surface with a sheet resistance <10 Ω sq^{-1}. The highest specific capacitance of 4,848 mF cm^{-2} at 1 mA cm^{-2} was reported for PPy-coated knitted electrodes of cotton fibres, with a capacitance retention of 88% after 5,000 cycles, which is 35% higher than the previously report work. The electrical conductivity of electrodes were also found to be almost unchanged even after washing in dichloromethane up to 20 laundering cycles.[371] The same research group further improved the capacitive performance of knitted electrodes of cotton fibres using an improved chemical polymerization technique.[372] The PPy-coated fabric electrode showed a superior specific areal capacitance of 5,073 mF cm^{-2}, and the fabric-based symmetric all-solid-state SC exhibited an enhanced specific areal capacitance of 1,167.9 mF cm^{-2} at 1 mA cm^{-2} which are highest among conductive polymer-based textile SCs of cotton fibres. Additionally, the same device provided a very high energy density of 102.4 μWh cm^{-2} at a power density of 0.39 mW cm^{-2} which maintained ~90% capacitance after 2,000 cycles.

Few researchers also investigated polyester fabric-based electrodes for fabricating textiles SCs. Cárdenas-Martínez et al.[373] deposited electro-spun PEDOT: PSS nanofibres on flexible polyester textiles. The all-solid-state SC exhibited an areal capacitance of 1.8 mF cm^{-2} and gravimetric capacitances of 3.6 Fg^{-1} at a discharge current of 5 μA cm^{-2}. However, like cotton textiles, *in-situ* polymerization of PPy resulted in better capacitive performances for polyester fabrics. Such PPy coating on polyester fabrics exhibited an areal capacitance of 1,213 mF cm^{-2} at 1 mA cm^{-2}.[371] Additionally, an *in-situ* polymerization of aniline and pyrrole on polyester (PET) was reported by Xie et al.[374] to produce SC electrodes. The electrode exhibited an areal

capacitance of 1,046 mF cm^{-2} at 2 mA cm^{-2} when the monomer ration of aniline to pyrrole was 0.75:0.25. The SC device showed areal capacitance of 537 mF cm^{-2}, volumetric capacitance of 1.13 F cm^{-3} at 2 mA cm^{-2} with energy and power densities of 0.043 mWhcm^{-3} and 0.005 Wcm^{-3}, respectively. In addition to cotton and polyester, Lv et al.[371] also used protein fibres as SC substrate. The in-situ polymerization of PPy exhibited an areal capacitance of 1,349 mFcm^{-2} in case of silk and 1,007 mFcm^{-2} in case of wool gauze fabric at 1 mA cm^{-2}. Few other research groups also investigated carbon fabric as SC substrates. The highest gravimetric capacitance on carbon cloth was reported by Wang et al.[375] They drop casted PANI on functionalized carbon cloth, the SC showed a gravimetric capacitance of 319.5 Fg^{-1} at 0.2 A g^{-1} with cyclic stability up to 82% after 1,000 charge-discharge cycle.

2.5.3 Metal-based textiles supercapacitors

Distinguished by particular physical and chemical properties, metal and metal oxide materials have been a focus of research and exploitation for applications in SCs,[376] Appendix D.3. Carbon nanotubes were studied mostly as substrate for the fabrication of metal based one dimensional fibre or yarn shaped SCs. Su et el.[377] produced high performance asymmetric two-ply yarn SC from spun CNT yarn (as negative electrode) and CNT@MnO_2 composite yarn (as positive electrode) in aqueous electrolyte. This asymmetric architecture resulted in areal capacitance of 12.5 Fg^{-1} with higher energy and power densities compared to the reference symmetric two-ply yarn SCs, 42.0 $Whkg^{-1}$ at a lower power density of 483.7 Wkg^{-1}, and 28.02 $Whkg^{-1}$ at a higher power density of 19,250 W kg^{-1}. Co_3O_4 was also studied by several research groups for enhancing the capacitive performance. Abouali et al.[378] employed a facile electrospinning method with subsequent heat treatments to prepare carbon nanofibres (CNFs) electrodes for SCs. The electrodes possessed a remarkable capacitance of 586 F g^{-1} at a current density of 1 Ag^{-1} with excellent cyclic stability of 74% upto 2,000 cycles at 2 A g^{-1}. Su et al.[379] in another study, further compared the electrochemical performance of CNT yarn electrodeposited with NiO along with Co_3O_4. The two-ply SCs formed from CNT@Co_3O_4 composite yarns and displayed excellent electrochemical properties with high capacitance of 52.6 mF cm^{-2} and energy density of 1.10 μWh cm^{-2}.

Among conventional textiles, polyester and silk were studied for two-dimensional fabric shaped SC. Shahidi et al.[380] deposited Ni nanoparticle on polyester to prepare flexible electrode for SC application. The device achieved a high areal capacitance of 450 mF cm^{-2} at 7.5 mA cm^{-2}. Similar to 1D type, carbon fabrics were investigated mostly for the two dimensional fabric shaped textile SC. Javed et al.[381] hydrothermally grew zinc sulfide (ZnS) nanospheres on a

flexible carbon textile. The flexible and light weight electrode exhibited a higher capacitance of 747 F g^{-1} at a scan rate of 5 mV s^{-1} in the LiCl aqueous electrolyte. The SC device demonstrated specific capacitance of 540 F g^{-1} and areal capacitance of 56.25 F cm^{-2} with excellent cycling stability of 94.6% after 5,000 cycles. The energy density was reported as high as 51 W h kg^{-1} at a power density of 205 W kg^{-1}. However, the highest capacitance for the metal-based textile SC was achieved utilizing the Co_3O_4. Howli et al.[382] hydrothermally fabricated Co_3O_4 nanowires on carbon fabric substrate to form SC electrode. With PVA-KOH electrolyte the electrode exhibited gravimetric capacitance of 3,290 F g^{-1} at a scan rate of 5 mV s^{-1} with high energy and power densities of 6.7 Wh kg^{-1} and 5,000 W kg^{-1}, respectively, and capacitance retention of 95.3% after 5,000 cycles.

2.5.4 2D material-based textile supercapacitor

Very recently several 2D materials are explored for the fabrication of SC electrodes. It is evident from literature that carbon, and cotton textiles were mainly studied for two-dimensional fabric shaped SCs, Appendix D.4. Uzun et al.[383] coated cellulose yarns with $Ti_3C_2T_x$ to produce conductive yarns. The yarn electrode exhibited linear, areal and volumetric capacitance of ~759.5 mF cm^{-1}, ~3,965.0 mF cm^{-2} and ~260.0 mF cm^{-3} respectively at 2 mV s^{-1}. With PVA–H_2SO_4 gel electrolyte, the SC device showed linear, areal and volumetric capacitance of ~306.9 mF cm^{-1}, ~1,865.3 mF cm^{-2} and ~142.4 mF cm^{-3} respectively. Levitt et al.[337] coated cotton yarn with $Ti_3C_2T_x$ (referred as MXene), knitted the yarn three dimensionally and used 1M H_3PO_4-PVA gel electrolyte for analyzing the structure performance as SC. The areal capacitance was reported 519 mF cm^{-2} at 2 mV s^{-1}. They further replaced the electrolyte with 1M H_3PO_4 electrolyte and the capacitance increased up to 707 mF cm^{-2} at 2 mV s^{-1}. The device showed >100% capacitance over 10,000 charge-discharge cycles and coulombic efficiency of ~100%.

2.5.5 Hybrid materials

The hybridization of the active materials from one or more subgroups (e.g. carbonaceous compounds, conducting polymers, metal based and other 2D materials) is one of the attractive routes to fabricate high performance energy storage textiles, Appendix D.5. Several research groups have focused on hybridizing carbonaceous compounds with conductive polymers or metal oxides to prepare one dimensional fibre or yarn shaped SC. For example, several articles reported cotton fibre or yarn-based SC devices as hybrid active compounds. Liu et al.[384] reported a fully cable-type SC composed of two PPy-MnO_2-CNT-cotton thread electrodes,

separated by cotton textiles wrapped with 0.5 M Na_2SO_4 electrolyte in a transparent silicone pipeline package shell. The cotton threads were coated with SWCNT, followed by electrochemical deposition of MnO_2 nanostructures and PPy film. The resulted electrodes achieved a high areal capacitance of 1,490 mF cm^{-2} at a scan rate of 1 mVs^{-1}, which is one of the highest among cotton fibre-based SC electrodes. The device prepared from such electrode achieved an energy density of 33 μWh cm^{-2} at a power density of 0.67 $mWcm^{-2}$. In another study,[385] almost similar capacitive performances was obtained by Wang et al. with considerably higher energy and power densities. They modified cotton yarns with three-dimensional metallic Ni conductive network and pseudocapacitive Co-Ni layered double hydroxide nanosheet array. The flexible yarn electrodes achieved areal capacitance of 1,260 mF cm^{-2} (121,571.1 C cm^{-2}) at a scan rate of 5 mV s^{-1}. The SC device was prepared by twisting two as-made yarn together, and then painted with PVA/KOH gel electrolyte, which provided an areal capacitance of 221 $mFcm^{-2}$ (21,323.2 C cm^{-2}) at 0.04 mA cm^{-2}. The energy and power densities were reported as 9.3 mWh cm^{-2} and 43.99 mW cm^{-2}, respectively.

The pseudocapacitive properties of PEDOT:PSS in combination with PPy was utilised to obtain cotton fibre-based one dimensional SC device. Ma et al.[386] blended short-staple length SSFs with cotton fibres to spin SSF/cotton blended yarn. PPy was deposited on PEDOT:PSS coated composite yarn, followed by a coating with PVA-H_3PO_4 electrolyte. Two pieces of yarns were placed in parallel and twisted together to produce a solid-state two-ply nanocomposite yarn SC. The cotton-based SC device exhibited maximum areal capacitance of 1,360 mF cm^{-2} at 0.16 mWh cm^{-2} energy density. In another study, Yang et al.[387] reported one of the highest gravimetric capacitances (~506.6 F g^{-1} at 1 A g^{-1}) on cotton-based 1D SC electrode, where PPy and MXene composite was grown on cotton fibre to prepare fibre-based electrodes. Li et al.[388] obtained the highest volumetric capacitance of 221.9 F cm^{-3} at a current of 50 mA, by modifying GO nanosheets (NSs) with ultrathin and large area MoS_2 NSs followed by reduction and using PVA-H_3PO_4 electrolyte to produce all-solid-state hybrid fibre shaped SC. Such composite device also retained 100% capacitance even after bending at 30 and 60 degrees.

Unlike cotton fibre or yarn-based SCs, only a very few reports are available on hybridizing carbonaceous compounds with conductive polymers or metal oxides for producing one dimensional fibre or yarn-shaped SCs based on synthetic textiles including polyester,[389] polyaniline,[390] nylon[391] and some elastic[392-394] fibres. For example, Zhang et al.[395] reported a high specific capacitance of 278.6 mF cm^{-2} for stretchable textiles (CNTF). The process involved electrochemical activation of pristine carbon nanotube fibres (OCNTF) and coating

of PEDOT:PSS, followed by electrochemical deposition of MnO_2 to form MnO_2@PEDOT:PSS@OCNTF positive electrode and hydrothermal synthesis of MoS_2 on CNTF to form MoS_2 @CNTF negative electrode, with LiCl-PVA gel electrolyte placed on a stretchable substrate.

Among carbon-based materials, CNT and graphene alone and/or in combination with other active materials were studied for one dimensional fibre or yarn shaped SCs. Wang et al.[396] reported biscrolled MXene with CNTs, which was used to prepare a freestanding asymmetric yarn SC prototype *via* pairing biscrolled RuO_2 yarns with 3 M H_2SO_4 electrolyte. The areal, volumetric and gravimetric capacitance of the yarn electrode were reported as high as 3,188 mF cm^{-2}, 1,083 F cm^{-3} and 523 F g^{-1}, respectively, at a current density of 2 mA cm^{-2}. The SC device also exhibited high energy and power densities of 61.6 mWh cm^{-3} (168 μWh cm^{-2} and 8.4 μWh cm^{-1}) and 5,428 mW cm^{-3} (14.8 mW cm^{-2} and 741 μW cm^{-1}), respectively, with outstanding cycle stability of ~90% up to 10,000 charge-discharge cycle. Similarly, He et al.[397] reported electrolyte mediation of hybrid fibre made of rGO and MXene, which were assembled into fibres *via* wet spinning with PVA-H_2SO_4 electrolyte. Such hybrid fibre provided an areal and gravimetric capacitance of 550.96 mF cm^{-2} and 110.89 F g^{-1}, respectively at 20 mV s^{-1}. The device also exhibited energy and power densities of 12 μWh cm^{-2} and 9.85 mWh cm^{-3} at power densities of 8.8 mW cm^{-2} and 7.1 W cm^{-3}, respectively. Additionally, Zhang et al.[398] reported $Ti_3C_2T_x$ in combination with PEDOT:PSS to form wet-spun hybrid fibre electrode for SC applications. Such electrode provided areal, gravimetric and volumetric capacitance of 676 mF cm^{-2}, 258 F g^{-1}, 615 F cm^{-3} respectively. The device fabricated with PVA-H_2SO_4 electrolyte achieved energy density of ~7.13 Wh cm^{-3} and ~8249 mW cm^{-3} with excellent stability of ~95% after 10,000 charge-discharge cycles. The device showed outstanding flexibility of 96% when stretched to 100% strain. Furthermore, Tao et al.[399] reported carbon fibres or yarns-based one dimensional SC with a volumetric capacitance of 69.3 F cm^{-3} at 0.1 A cm^{-3}. A hybrid structure was prepared by depositing PPy on MnO_2 nanoflakes coated carbon fibre (CF/MnO_2/PPy). Two PPy-MnO_2-CFs were fixed on a preservative film substrate and assembled into a SC by sandwiching with PVA-H_3PO_4 membrane as a separator and electrolyte between electrodes. Naderi et al.[400] drop coated PEDOT:PSS- rGO and deposited MnO_2 on carbon fibre to form yarn shaped SC. MnO_2/PEDOT:PSS-rGO and PEDOT:PSS-rGO were used as positive and negative electrodes, respectively, with Na_2SO_4-CMC as a solid-state electrolyte. The electrodes exhibited capacitance of 2.92 F cm^{-2} (194 F cm^{-3}, 550 mF cm^{-1}) at 5 mA cm^{-2}, which is the highest among such SCs. The energy and power densities were reported

as 295 μWh cm^{-2} (19 mWh cm^{-3}, 55 μWh cm^{-1}) and 2,900 μWcm^{-2} (190 mW cm^{-3}, 545 μWcm^{-1}), respectively. The device was also able to retain 96% of its initial capacitance after 5,000 cycles.

Platinum,[96] gold[401] and stainless-steel fibre yarns[323] were also studied as wearable SC substrate. For example, Huang et al.[402] deposited rGO hydrothermally, and MnO_2 and PPy electrically on spun stainless steel yarn. The PPy@MnO_2@rGO-conductive yarns worked as both active materials and current collectors. The length and areal capacitances made from this yarn were reported as 36.6 mF cm^{-1} and 486 mF cm^{-2} in aqueous Na_2SO_4 electrolyte or 31 mF cm^{-1} and 411 mF cm^{-2} in all solid-state PVA/H_3PO_4 electrolyte. The capacitance retained up to 92% over 4,950 charge-discharge cycles, and even 80% after 1,000 cycles at 90 bending, 91% after 1,000 cycles knotting, and 103% after 1,000 cycles twisting.

For 2D fabric shaped SCs, conventional textiles such as cotton, polyester, polycotton and carbon textiles have widely been studied. In such SC devices, carbonaceous compounds are used in combination with conducting polymers and/or metal oxides for SC fabrication *via* various fabrication techniques. Huang et al.[403] electro-spun carbon nanoweb on nickel-coated cotton fabrics. The as prepared fabric SC device achieved an areal capacitance of 973.5 mF cm^{-2} at 2.5 mA cm^{-2}. A simple dip-drying method was reported by Etana et al.[404] for fabricating cotton textiles- based SC, where GO was deposited by a 'dip and dry' method and chemically reduced to form rGO/cotton fabric. MnO_2 nanoparticles were accumulated on rGO/cotton fabric by *in-situ* chemical deposition, and then PANI layer was coated. With 1 M H_2SO_4 electrolyte solution, the SC provided high gravimetric capacitance of 888 Fg^{-1} and high areal capacitance of 444 F cm^{-2}, the highest reported for such SC configuration. In another study by Li et al.,[389] PPy was electrochemically deposited on rGO painted and $SnCl_2$-modified PET textiles, which provided areal capacitance of 1,117 mF cm^{-2} at a current density of 1 mA cm^{-2} with 100% retention after 10,000 cycles. The SC device fabricated from such fabric electrodes and PVA-H_2SO_4 gel electrolyte exhibited an aerial capacitance of 474 mF cm^{-2}. Cheng et al.[405] developed strip-shaped composite electrodes, which were prepared *via* depositing PANI on aligned CNTs, exhibiting a high volumetric capacitance of 421.7 F cm^{-3}.

In addition to polyester fabrics, silk,[406] nylon[407] and stretchable[408] textiles have also been studied for the fabrication of two dimensional fabric shaped SCs. However, carbon fibre fabric has widely been used as SC substrate by several research groups.[409-411] For instance, Lv et al.[409] reported a composite SC electrode prepared by depositing aligned CNT/MnO_2/CP on carbon

fabric (CF-ACNT-MnO_2-PEDOT). With 1 M Na_2SO_4 electrolyte, the composite electrodes achieved a high areal capacitance of 1,300 mF cm^{-2} at 0.1 mV s^{-1}. Though several attempts were reported for the enhancement of the capacitive performance, the highest areal capacitance for carbon fabric based SC was reported by Zhu et al.[410] They coated carbon fibres MoO_2 by solvothermal method; covered and interconnected with rGO film to form SC electrode. The areal capacitance of the electrode was reported as high as 8,132 mF cm^{-2} at 2 mVs^{-1}. The electrode also retained 95% capacitance after 30,000 charge-discharge cycles at 120 mA cm^{-2} and 77% after 6,000 times folding tests. However, the highest gravimetric capacitance was reported by Mu et al.,[411] who hydrothermally prepared $NiMnO_3$ nanosheets on a carbon cloth. With 6M KOH electrolyte, the electrodes reached 2,330 Fg^{-1} at the current density of 1 Ag^{-1}. In addition to these electrochemical properties, other considerable key properties for wearable applications are summarized in Appendix E.

2.6 Scopes of my studies

As previously stated, the aim of this PhD research is the development of scalable, low-cost, highly functional, and flexible graphene-based energy-storage textiles. In this chapter, I have summarized the recent developments of textile-based supercapacitors fabricated from various functional materials along with their structures, fabrication and electrochemical performance. It is evident from the study that most textile supercapacitors documented to date have been limited to laboratory-scale production and mostly resembling fibres or synthesized on carbon cloth. Cotton stands as a versatile and widely embraced textile for everyday life. In addition, the unique and complementary properties of graphene and other 2D materials potentially enable a range of high-performance supercapacitors. Therefore, the following four studies report the scalable production of cotton textile-based supercapacitors via screen printing or pad-dry coating or high precision inkjet printing aiming to produce high-performance energy textile.

3. Fully printed and multifunctional graphene-based wearable e-textiles for personalized healthcare applications

Graphene-based e-textiles have received significant interests in recent years for wearable electronics applications, due to graphene's extremely high specific surface area, high thermal and electrical conductivity, and excellent mechanical properties.[134, 137, 412] It could potentially provide a multi-functional platform for manufacturing next generation highly innovative and intelligent e-textile garments that can perform as energy generators and storage devices, sensors, actuators and electrodes for bio-signal detection, all at the same time.[125, 126, 413] While several scalable techniques were reported to produce graphene-based e-textiles, screen-printing in particular is a versatile, highly scalable and cost-effective technique that has already been exploited commercially for the fabrication of biosensors and chemical sensors.[18] Previous studies reported screen printing of graphene-based active materials on textile substrates to fabricate wearable electronics,[259, 414, 415] however, such devices are limited in terms of performance and multifunctionality.

In this study, a strategy was reported that exploits highly conductive, flexible and machine-washable graphene-based e-textiles capable of capturing bio-signals and storing energy to develop next-generation multifunctional wearable garments. A simple and scalable screen printing of graphene-based ink on textiles, and subsequent fine encapsulation of conducive track, enables highly conductive and machine washable e-textiles. Their high flexibility as well as their ability to capture movements of different body parts such as index finger, wrist joint, elbow and knee joint for demonstrating their potential as activity sensors were also demonstrated. The ink was used to print in-plane electrodes for all-solid-state supercapacitors

which shows excellent performance in flexible and non-flexible devices. The characterization of the supercapacitor was carried out in collaboration with Bournemouth University, UK. Finally, in collaboration with the University of Manchester, UK the printed textiles were used to capture EEG bio-signals, offering comparable performance to standard commercial Ag/AgCl electrodes, demonstrating their ability to provide a more comfortable biosensor to current rigid clinical electrodes. As the major contributor, I wrote the manuscript as first author and published this study as a research article in *iScience.*[238]

3.1 Fully-printed and highly conductive graphene-based e-textiles

A water-based graphene dispersion (100 g/L) was prepared using Microfluidized technique.[119, 126] The rheology of graphene-based dispersions was modified using carboxymethylcellulose sodium salt to prepare printable inks and was supplied by Versarien Limited UK. Microcircuit encapsulant PE773 was purchased from Dupont (USA). 100% cotton fabric (de-sized, scoured, and bleached which are ready-to-dye fabric) was manufactured at Square Fashions Limited (Bangladesh), and donated by 2dtronics Limited (UK). The ink viscosity was characterized using a HAAKE Viscotester iQ Rheometer (ThermoFisher Scientific, UK). Shear stress and viscosity were determined at different shear rates to assess the printing ink's flow properties. The surface topography of the control cotton fabric, graphene-printed fabric, graphene-printed fabric after washing, graphene printed-encapsulated fabric and graphene-printed and encapsulated fabric after washing were analysed using a FEI Quanta 650 field emission scanning electron microscope (SEM).

*Figure 3.1*a illustrates the concept of fully-printed and multifunctional wearable e-textiles that monitor vital signs including heart rate, temperature, oxygen saturation level and human activities, as well as store energy *via* flexible textiles supercapacitors. Such e-textiles can be produced via printing highly conductive graphene-based inks using widely used scalable and high-speed screen-printing technique, *Figure 3.1*b.

An ideal screen-printing ink is pseudoplastic, which demonstrates shear thinning properties as its viscosity decreases with the increase of shear rate, allowing the ink to flow from the mesh when shear is applied, and a rapid recovery once shear is removed to yield a high resolution trace during the separation.[23] *Figure 3.1*c shows the change of viscosity from ~407.10 cP to ~92.02 cP over a shear rate up to 1000 s^{-1} for microfluidized graphene ink used in this study. The shear stress also increases up to ~90.49 Pa over the same shear rate, exhibiting the suitability of the graphene-based ink for screen-printing. Most favourable technological effects

are obtained when the screen-printing inks possess shear-thinning with slight thixotropy.[416] In agreement to this, the small, enclosed area of the hysteresis loop (Appendix F, Figure F1) of the print ink also supports the suitability of the graphene-based ink for screen printing.

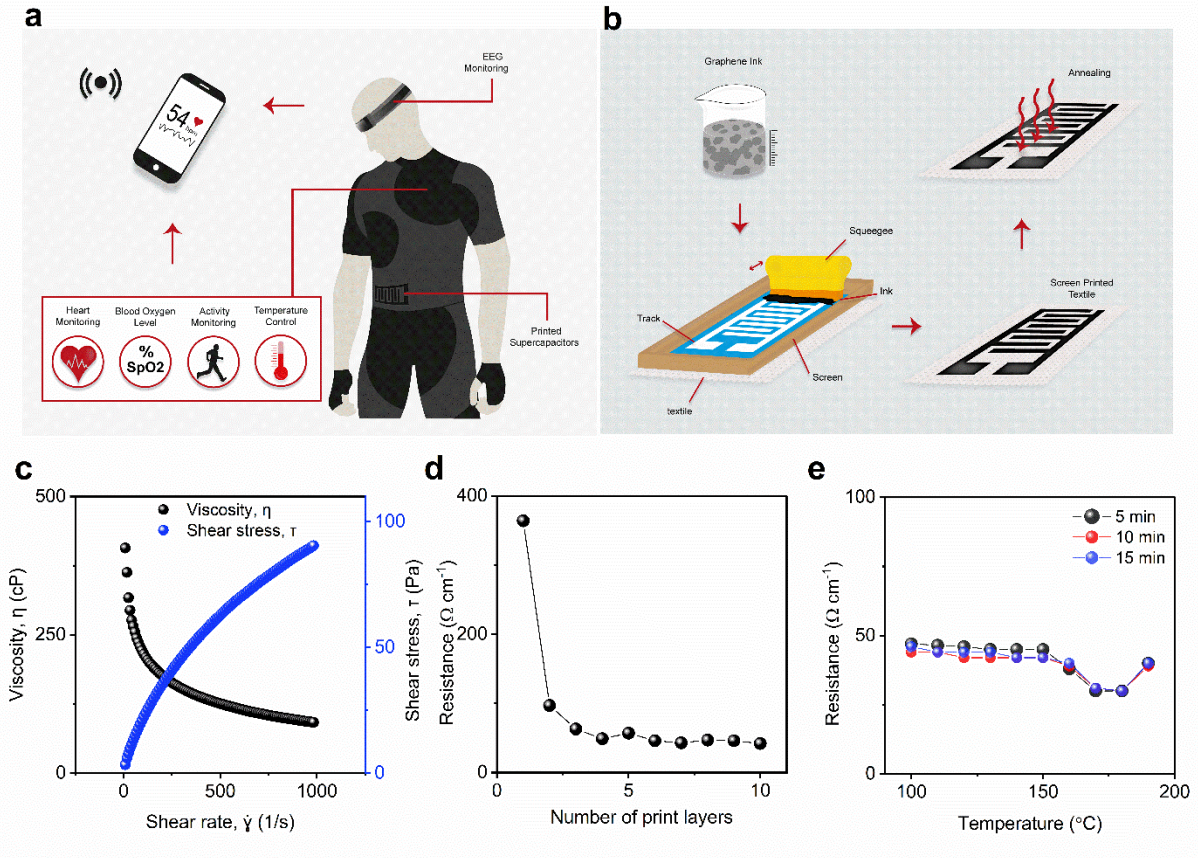

Figure 3.1 Fully-printed and multifunctional wearable e-textiles. a) Schematic diagram of multifunctional aspect of printed e-textiles b) Schematic diagram of the screen printing process for preparing graphene-based wearable e-textiles c) Rheological properties of the graphene-based ink, viscosity and shear stress expressed as a function of shear rate d) The change in the electrical resistance with the number of print layers for graphene-based ink printed cotton fabric e) The change in electrical resistance of graphene-based ink printed cotton fabric with curing time and temperature.

A basic hand screen-printing method was used to print graphene-based ink on textiles, and then printed fabric was dried at 100 °C for 10 minutes using a small table-top thermo fixation oven (Mini-Thermo, Roaches, UK). Each print cycle consisted of one printing layer (3 passes) followed by drying process. Samples were repeatedly printed and dried to optimize the number of print layers (1–10 layers). The electrical resistance of graphene printed textile was measured by a standard multi-meter. After the first print layer, the electrical resistance of the printed fabric was found to be ≈364 Ω cm^{-1}, *Figure 3.1*d. The electrical resistance reduces significantly

to ≈97 Ω cm^{-1} after the second print layer and continues to decrease steadily up to four print layers to ≈49 Ω cm^{-1} due to the permeation of an increased amount of graphene ink on the textile surface. After four print layers, the resistance reaches a saturation point and becomes steady as observed until ten print layers. Therefore, four print layers were used to prepare graphene-based printed e-textiles for subsequent processes. All the samples were dried at 100 °C for 10 min after each print layer during the print layer optimisation process.

The curing temperature and time were then optimized for graphene printed fabrics using a range of curing temperature (100 ℃–190 ℃ with 10 ℃ interval) over a time range (5–15 minutes with 5 minutes interval). *Figure 3.1*e shows that the electrical resistance of the graphene printed fabric decreases with the increase of curing temperature. The phenomenon could be attributed to the increase of contact force between conductive fillers present in the conductive ink and the shrinkage of the organic binder present in the ink, resulting in a reduced electrical resistance of the print pattern.[417] It is worth noting that after applying ~180 °C curing temperature, the cotton fabric turns into a yellow colour, as well as the electrical resistance increases, possibly due to the degradation of fibre structures, intra-macromolecular cross-linking and depolymerization.[26] Therefore, 170 °C for 5 min was selected as curing conditions for all graphene-based printed samples produced for subsequent processes.

The effect of curing treatment on fabric properties was further assessed. Tensile strength was measured for printed and/or coated e-textiles by following BS EN ISO 13934-1. Five measurements for each specimen (200 mm × 50±0.5 mm) were taken to calculate the average width and thickness. The samples were held between the caliper's external jaws by two large metal clips of a Testometric Tensile Tester. With a pretention of 1.0 N force and speed of 20 mm min^{-1}, the tensile strength and elongation at break of the samples were measured using a load cell of 2000 kgf. The annealed substrate exhibited a change in breaking force of only 2.79% in comparison with the un-treated substrate, which is very negligible (Appendix F, Table F1, Figure F2).

3.2 Machine-washable and ultra-flexible graphene-based e-textiles

The poor stability of repeated laundry washings is considered to be one of the major challenges for wide commercial adoption of e-textile products.[241] A good washability is essential for e-textiles to survive intense mechanical deformations and water invasion of washing cycles used during their life cycles.[242] The washing stability of our graphene-printed e-textiles was assessed following a British Standard (BS EN ISO 105 C06 A1S)[418] to evaluate their performance at 10

simulated home-laundry washing cycles. For wash stability tests, graphene printed textiles were encapsulated with a fine layer of a microcircuit encapsulant PE773 using the same screen-printing method followed by a drying and curing at 150 °C for 1 min. A conductive track was created with electrically conductive silver paste for measuring the electrical resistance of graphene printed and encapsulated e-textiles, Appendix F, Figure F6b.

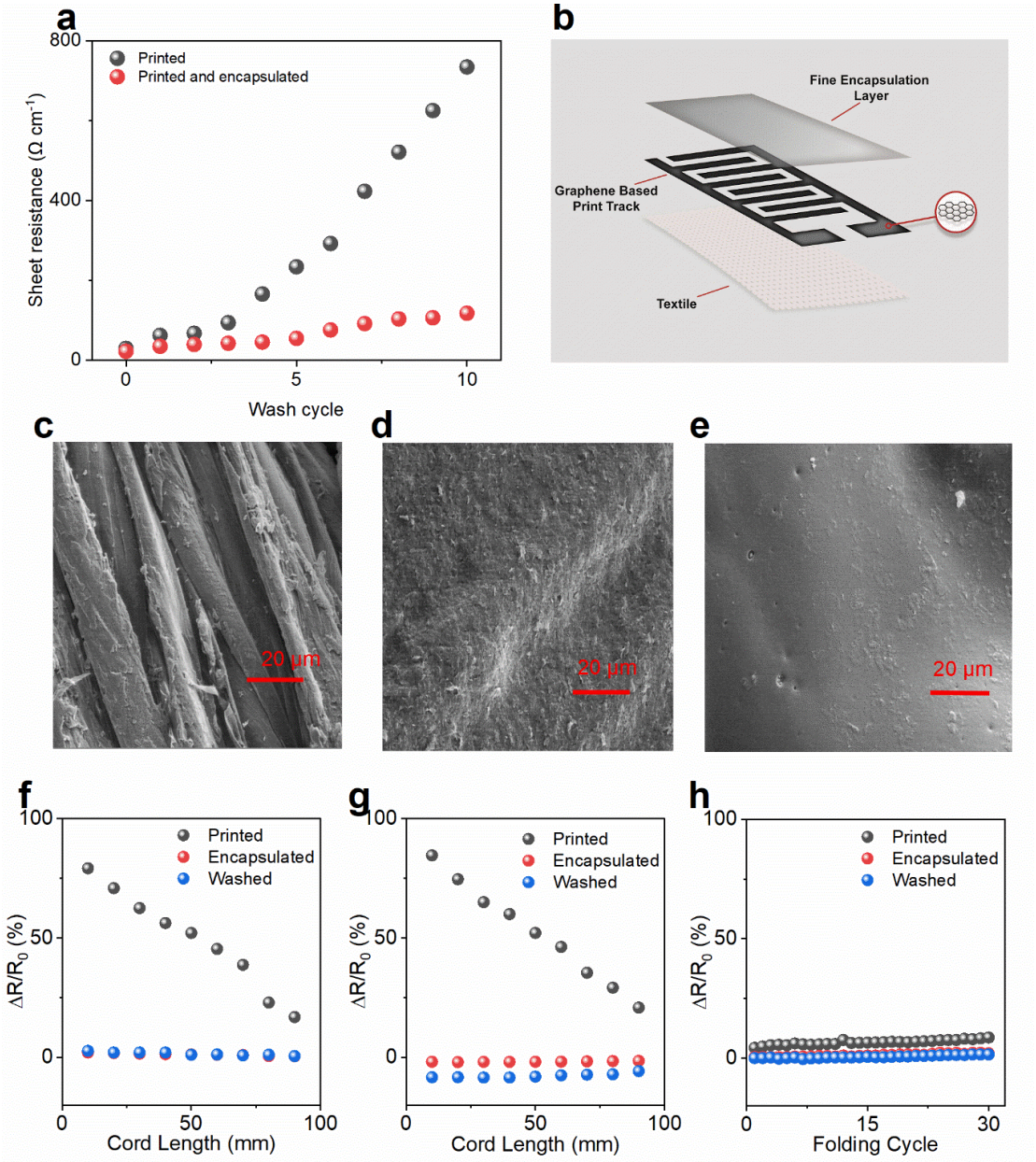

Figure 3.2 Wash stability and flexibility of printed and encapsulated graphene e-textiles. a) The change in electrical resistance with the number of washing cycles of graphene-based ink printed (without encapsulation) and graphene-based ink printed (with encapsulation) cotton fabric b) Graphical illustration of graphene-based ink pattern and encapsulation layer on textile substrate c) Scanning electron microscope (SEM) image of control cotton fibre (X2000)

d) SEM image of graphene-based ink printed (4 layers) cotton fibre (X2000) e) SEM image of graphene-based ink printed (4 layers) cotton fibre (with encapsulation) after washing (10 washing cycles) (X2000) f) The variation in resistance of the bending sensor in forward direction g) The variation in resistance of the compression sensor in forward direction h) The variation in resistance under 30 inward (printed pattern inside) folding−releasing cycles.

The printed e-textiles patterns (with 4 print layers) start to lose electrical conductivity just after one washing cycle. The electrical resistance of washed e-textiles was found to be 62.5 Ω cm^{-1} (*Figure 3.2*a) after the first washing cycle, which is double than that of the unwashed sample. After repeated washing cycles, the electrical conductivity of such e-textiles is reduced drastically, as the resistance increases significantly to 734.0 Ω cm^{-1} after 10 washing cycles, which is ~10 times higher than the first washing cycle, *Figure 3.2*a. A significant variation in the resistance was also observed at various locations of the washed sample's surface. The significant increase in the resistance of non-encapsulated samples could be explained by their more proneness to delamination due to the mechanical forces experienced during washing cycles, resulting in losses of electrical conductivity.

The wash stability of wearable e-textiles can be improved *via* a number of methods including a textiles surface pre-treatment with Bovine Serum Albumin (BSA), or by a post-treatment for instance embedding with polydimethylsiloxane (PDMS), polyurethane (PU) sealing, a screen-printed PU top layer, and transferred mould and hot melt encapsulation to seal conductive track on the textile surface.[26] In this study, a translucent, thin, and stretchable PU-based encapsulant was used to protect graphene-printed wearable e-textiles. Such encapsulation material adheres with textile materials, keeping the printed graphene layer attached to textiles but covered and protected, *Figure 3.2*b. The wash stability performance of graphene-printed textiles after encapsulation was then evaluated, where a slight linear increment in electrical resistance was observed after each washing cycle, *Figure 3.2*a. The encapsulated graphene-printed e-textiles show ≈1.5 times higher resistance (35.2 Ω cm^{-1}) after the first washing cycle in comparison to the unwashed sample. The resistance increases to 118.0 Ω cm^{-1} after 10 washing cycles, which is only about 3.5 times higher resistance in comparison to the first wash cycle. *Figure 3.2*c shows smooth and featureless the scanning electron microscope (SEM) of untreated cotton fibres, which was covered with randomly oriented graphene-based flakes after printing highly concentrated graphene inks, *Figure 3.2*d. Additionally, unlike graphene oxide (GO), reduced graphene oxide (rGO) or other functionalised graphene derivatives, graphene flakes in microfluidized graphene inks do not create chemical bonding with cellulosic fibres, as they are

mainly dominated carbon in their structure without any oxygen containing functional groups.[26] When subject to mechanical action during washing cycles, such randomly oriented flakes of printed e-textiles are removed, Appendix F, Figure F6c. Therefore, the electrical resistance of graphene-printed e-textiles decreases significantly after each washing cycle. However, the encapsulated printed fabric surface exhibits more resistance to delamination due to the protection of the graphene printed pattern with thin PU layer, Appendix F, Figure F6d. Thus, the wash stability of graphene-printed e-textiles improved substantially *via* fine encapsulation with a PU layer without any negative effect on the hand feel as well as flexibility of the conductive e-textiles.

The flexibility of printed, encapsulated and washed graphene-printed e-textiles was also evaluated, *Figure 3.2*f, g. By following previously reported methods[25, 126] various cord lengths were used to measure the change of resistance of washed and unwashed fabric (10 cm×1 cm strip) during bending (concave down) and compression (concave upward), Figure S7. Graphene-printed (4layers) and encapsulated cotton fabrics were tested both before and after 10 washing cycles. A Win Test tensile tester (Testometric, UK) was used to control the cord length both in forward and reverse directions for both bending and compression tests. The change in their electrical resistances per 10 cm length due to bending, compression (both in forward and backward direction) was measured. The cord length, which was measured by the grip distance of the sample ends during the experiment (Appendix F, Figure F7), was changed (10−90 mm) when the fabrics were bent and compressed both in forward and backward directions. *Figure 3.2*f, g exhibits repeatable responses in the change of resistance ($\Delta R/R_0$) during bending and compression in forward direction (and backward directions Appendix F, Figure F8, F9 respectively). However, the encapsulated samples show excellent repeatability in comparison with the unencapsulated samples for both before and after washing operations. Additionally, the printed samples were subjected to ten repeated folding–release cycles in both inward and outward direction. The variation of resistances was found almost stable for both unwashed and washed samples subjected to 30 inward (*Figure 3.2*h) and outward (Appendix F, Figure F10) folding−releasing operations. Printed graphene as well as the top encapsulation layer over printed graphene, when create a strong adhesion, should resist any physical damage of the conductive track. If the adhesion is not sufficient enough to hold the material on substrates, may impart cracks upon bending, losing the peel of any functional materials resulting in reduced conductivity.[419] It is worth noting that no visible changes in appearance or shape or creasing were observed due to those mechanical actions (bending, compression and

folding cycles), demonstrating excellent flexibility and bendability of encapsulated and washable graphene-based wearable e-textiles.

3.3 Activity monitoring wearables of graphene-based e-textiles

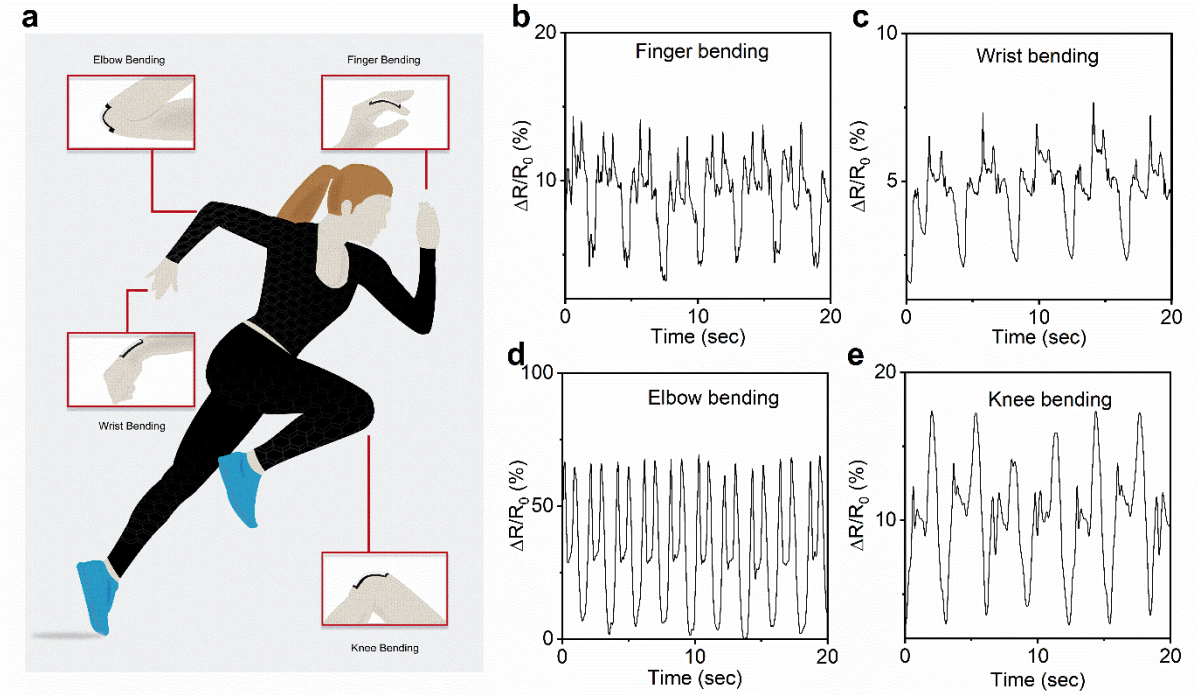

Figure 3.3 Printed graphene e-textiles as activity monitoring sensors. a) Schematic diagram showing the application of graphene-based ink printed textiles as activity monitoring sensors at different body parts. The motion detection represented by the change of resistance as a function of time during b) finger joint bending c) wrist joint bending d) elbow joint bending and e) knee joint bending by the graphene-based ink printed textiles.

Wearable sensors for monitoring individuals as well as patients' health conditions *via* gathering physiological and movement data, have received significant attention now-a-days due to their continuous and non-invasive nature.[43, 420, 421] The printed patterns on textiles, when placed on several body parts, act as sensors for collecting and monitoring several physiological information. The collected information from various sensors can then be transferred to a remote data management system wirelessly, providing the opportunity for remote monitoring of physiological parameters of adult patients, children, or people who are elderly. The strain type sensors, composed of conductive network of active materials, serve as resistor under applied voltage, the mechanism of which is known as piezoresistivity. During stretch / compression, the electrical resistance of the conductive track changes as function of the applied mechanical strain, that originates from the geometrical changes such as length and/or cross-sectional area, intrinsic resistive response of active materials, tunneling effect, and/or disconnection

mechanism. The resistance recovers to its initial values in a reversible manner after releasing from the applied strain. The deformation state, thus, can be readily measured by recording the changes in the electrical resistance of the resistive-type strain sensors.[422] Graphene printed conductive, washable and flexible e-textiles were attached on different body parts such as index finger, wrist joint, elbow and knee joint (Appendix F, Figure F13) to demonstrate their potential as activity sensors, *Figure 3.3*a. The change of the resistances with the movement of such body parts were measured (*Figure 3.3*b-e). It is noteworthy here; the similar printed patterns were utilized as piezoresistive sensors at different body parts. Though patterns were similar, the sensors placed at different body parts such as finger, wrist, elbow, and knee joints were exposed to different stress due to physical movements for different body parts. These produced different strains on the sensors, therefore the resulted repeatable responses were different for different body parts. Repeatable responses of the change of resistances were observed in all the cases over time with outstanding capability of capturing various mechanical actions. This is in agreement with previous study where similar repeatable response, and excellent capability of sensitivity measurements were achieved for both unwashed and washed (10 times) skin-mounted strain sensors.[26] Such sensors could be used to monitor physical activities such as walking, eating, running, brushing etc of patients or people who are elderly on daily basis and send to their family members or carers to inform about their health status to help them to live independent safely.[423, 424] This approach is also effective to study patient's behavioural changes and recovery processes while still living at their homes.

3.4 Sleep monitoring via electroencephalography recordings (EEG)

The effectiveness of the printed graphene-based textile electrodes to record electrophysiological information, specifically the electroencephalogram (EEG) was also demonstrated. An EEG is a non-invasive method of recording brain activity, undertaken by placing electrodes on the scalp and forehead of a person, and used in a number of areas from sleep studies to epilepsy diagnosis.[425] To verify the ability of our material to capture EEG information, a phantom head model was created using gelatine in a 1:4 ratio by mass of gelatine to water, creating a replication of the ionic conductors present in the human body, as previously reported.[426] The phantom consists of two rigid sintered silver/silver chloride (Ag/AgCl) EEG electrodes embedded inside, enabling pre-recorded EEG signals to be played-back; replicating signals present inside the human head and giving a 'known' signal to record, allowing verification. A pre-recorded EEG data from the Physionet Sleep-EDF Database,[427, 428] a dataset consisting of expert-scored PSG sleep study recordings, to generate signals in the phantom was

used. A 20-minute excerpt (03:03:00 – 03:23:00) from participant SC4001 using the Fpz-Oz channel was played back in the phantom using a current source (DS4 Biphasic Stimulus Isolator, Digitimer), set to ±10 μA, in turn connected to a digital-to-analogue voltage source (NI USB-6363, National Instruments, USA). Using silver-loaded conductive thread (Electro Fashion, Kitronik, UK) connections to two of the conductive areas on the textiles were sewn in and in turn connected to an electrophysiological amplifier (Actiwave EEG/ECG 4 channel, CamNtech), sampling at 1024 Hz and 10 bits. The textile electrodes were compared against commercially available gold-standard rigid EEG electrodes (Ag/AgCl disc electrodes and Abralyt HiCl conductive gel) commonly used in EEG studies. Frequency-domain comparisons between electrode types were made by calculating the power spectral density (PSD) using the welch method with 30 s long windows, 50% overlaps and 2^{16} FFT points. Time-domain comparisons were made after filtering with an eight-order zero-phase notch filter with f_L and f_H set to 47.5 Hz and 52.5 Hz respectively, and then filtered with a fourth-order zero-phase low-pass filter with f_L = 50 Hz. The 2D correlation coefficient between the filtered data collected from both types of graphene electrodes was calculated against the commercial rigid electrodes.

Here, the graphene-based e-textiles was used as electrodes for sleep monitoring, *Figure 3.4*a. Sleep studies which take Polysomnographic recordings (PSG), consisting principally of EEG recordings and other bio-signals are recordings taken overnight during sleep, *Figure 3.4*b. The PSG data is scored into different sleep stages by a trained expert to identify sleep disorders.[429, 430] To demonstrate the feasibility of using the e-textiles for EEG recordings, the EEG part of a PSG was stimulated using two electrodes and a gelatine head phantom,[431] *Figure 3.4*a. This setup simulates one EEG electrode placed on the central forehead (referred to as Fpz in the international 10-20 standard), and a reference electrode placed elsewhere (here we utilise the Cz location, which is in the centre of the scalp). This reference electrode could also be positioned in an alternative hairless location, such as behind the ear, but here Cz location was used to allow standardisation with other data sets.

Prior to any pre-processing or filtering of data, the frequency domain of the EEG recordings was examined by comparing the power spectral density (PSD) of the signals collected from the electrodes. This allows identification of the level of 50 Hz noise picked up by the electrodes, a common source of noise in electrophysiological recordings. This 50 Hz pickup is caused by the electrical mains (which oscillates at 50 Hz in the UK) coupling with the electrodes and measurement equipment. In *Figure 3.4*c the PSD is shown, and it is seen that over the frequency band of interest for sleep studies (0.3 – 30 Hz),[432] all electrode types follow each other very

closely. At 50 Hz, the commercial Ag/AgCl electrodes have around 12.2 dBµV Hz^{-1} of power contribution, and the graphene-based electrodes have a slightly higher contribution, around 16.4 dBµV Hz^{-1} and 17.2 dBµV Hz^{-1} for the 1 layer and 4-layer electrodes respectively.

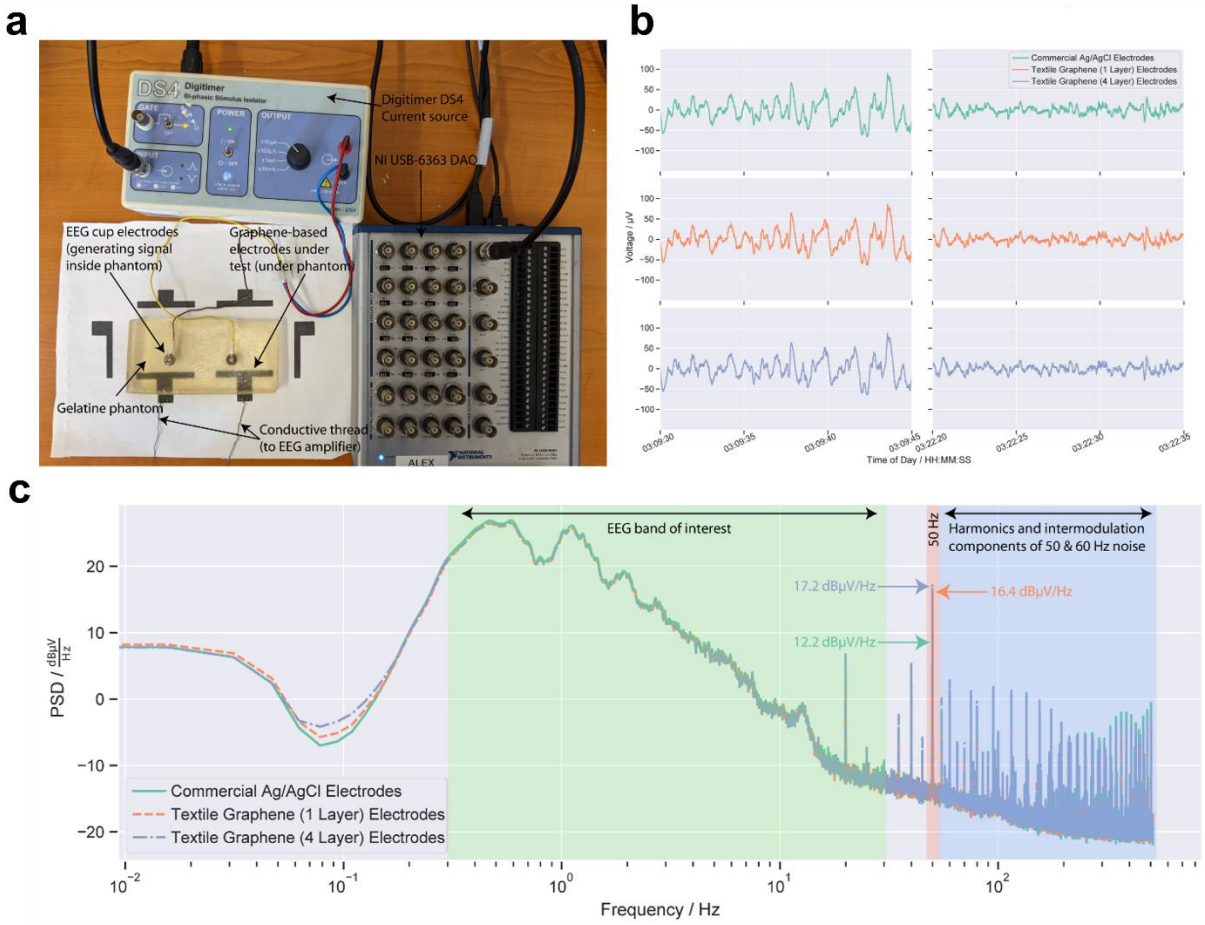

Figure 3.4 Printed graphene e-textiles for EEG applications. a) Experimental setup showing signal source (DAQ), current stimulator (Digitimer DS4), gelatine phantom, graphene-based electrodes, and conductive thread connection to EEG Amplifier. b) Data collected using the textile graphene-based electrodes against commercial Ag/AgCl electrodes from data from Fpz-Oz data in the SC4001 record from Physionet. (left) A section of the record in deepest stage of sleep (stage 4), indicated by the presence of slow oscillations in the record. (right) A lighter stage of sleep (stage 2), indicated by smaller amplitude higher frequency oscillations. c) Power spectral density of recorded signal from graphene textiles electrodes against commercial Ag/AgCl electrodes, highlighting the typical frequency band of interest in EEG studies shaded in green. The 50 Hz component and its contribution for each of the electrode types are shaded in red. Also shown are higher frequency harmonics and intermodulation components from 50 and 60 Hz noise shaded in dark blue.

It is also seen that higher frequency noise above 50 Hz in all electrodes, consist of harmonics and intermodulation components of 50 Hz and 60 Hz noise. These components arise from the 50 Hz noise that is coupled to the electrodes during our experiment and the 60 Hz noise that is present in the original EEG dataset used, (60 Hz is the mains line frequency in the US where the original dataset was collected). In this work, not only are the differences in noise between the graphene-based textiles electrodes and rigid Ag/AgCl electrodes minimal, but these noise do also not overlap with the EEG frequency bands of interest, so these power line contributions can be filtered out.

The correlation coefficient between the filtered data collected from both types of graphene-based electrodes over the 20-minute record is high at over 0.998, indicating a very strong similarity between the performance of our electrodes and the rigid Ag/AgCl electrodes. *Figure 3.4*b shows two 15 s segments of the EEG record data, at two distinct points. In the left figure, data is displayed from the participant when they are in the deepest stage of sleep (stage 4), indicated by the large-amplitude slow-wave oscillations. The right figure shows the data from the participant around 10 minutes later where they are in a lighter stage of sleep (stage 2), indicated by the higher frequency and smaller amplitude oscillations. Both features can clearly be seen both in the data collected by the graphene-based electrodes and by the rigid Ag/AgCl electrodes indicating similar levels of performance between all electrode types. The results indicate these e-textiles could be utilised for EEG recordings which overcomes the limitations of conventional rigid Ag/AgCl electrodes.

3.5 Supercapacitor device fabrication and electrochemical characterization

A solid-state symmetrical supercapacitor pattern was also printed on the textile using the same screen-printing technique. The printed device has 5 branches on both the cathode and the anode sides; each branch is 2 mm in width and 33 mm in length (Appendix F, Figure F14). The distance between each branch on the cathode and the neighbour branch from the anode is 2 mm. The supercapacitor device was prepared by following previously reported method.[259] The printed graphene textile electrodes were used as the current collector. However, copper sheets were glued to the end of every electrode to ensure good electrical contact with the measuring workstation. The printed electrodes were coated with a hydrogel-polymer electrolyte, poly (vinyl alcohol) (PVA) doped with H_2SO_4. The H_2SO_4 PVA gel electrolyte was prepared as follows: 1 g of H_2SO_4 was added into 10 ml of deionized water, and then 1 g of PVA (molecular weight: 89 000–98 000, Sigma-Aldrich) was added. The whole mixture was then heated to 85 °C under stirring until the solution became clear. The electrolyte was drop-casted and left to

dry overnight under ambient conditions to ensure that the electrolyte completely wetted the electrode and to allow for evaporation of any excess water. Two electrode system was employed for the characterization of the textile supercapacitors. The electrochemical measurements were carried out in an Ivium CompactStat. The electrochemical performances of the printed devices were investigated by cyclic voltammetry (CV), and galvanostatic charge/discharge tests. The electrochemical measurements were performed on an Iviumstat Electrochemical Interface. The CV and galvanostatic charge–discharge measures were conducted in the potential range of 0 to 1.0 V at different scan rates and current densities. For measuring the CV at different bending angles, the device was attached to a flexible polyethylene terephthalate film. The ability to collect and store energy in the form of electrical charge, per unit area, namely areal capacitance (F cm^{-2}) was calculated as per the following formula:

$$C_A = \frac{A}{2\,s\,a\,V} \qquad \text{Equation 11}$$

$$C_A = \frac{i\,\Delta t}{a\,\Delta V} \qquad \text{Equaltion 12}$$

Energy density was calculated as per the formula:

$$E = \frac{1}{2}CV^2 \qquad \text{Equation 13}$$

The following formula was used for the calculation of power density

$$P = \frac{E}{t} \qquad \text{Equation 14}$$

[Where, I= current density, V= voltage window, i=discharging current, Δv=discharge voltage, Δt= discharge time, A= integrated area of the CV curve, s= scan rate (mV s^{-1})].

As can be seen in *Figure 3.5*a, the CV curves show almost a rectangular shape at all tested scan rates, indicating ideal double-layer capacitance. The lack of any redox peak in the tested electrochemical windows suggests that graphene-based ink is of very good purity, and completely cover the cotton fibres. To calculate the areal capacitance, the charge-discharge profile was recorded at current densities ranging from 0.05 to 0.5 mA cm^{-2} (*Figure 3.5*b). In agreement with the CV results, the charge-discharge profiles exhibit an ideal double-layer behaviour with a triangular shape and equal time for charge and discharge. Also, there are no visible plateaus or bends in the profiles that might be attributed to a redox reaction. The lack of any IR (I = current and R = inner resistance) drops at the beginning of the discharge curve suggests good conductivity and low charge barriers at the electrodes. The maximum calculated areal capacitance of the symmetrical printed supercapacitor was 3.2 mF cm^{-2}, which is

comparable with many reports existing in literature (Appendix F, Table F2). Even when the current density increased by 10 times to 0.5 mA cm^{-2}, an aerial capacitance of 2.6 could be maintained, equivalent to capacitance retention of 81.3% (*Figure 3.5*c). The electrochemical stability of the supercapacitor was investigated based on long-term charge-discharge curves at a current density of 0.1 mA cm^{-2}. The devices lost only 5% of their initial capacitance after 10000 cycles, indicating excellent stability (*Figure 3.5*d). Without using any current collector or conductive agents, the printed supercapacitor could deliver a high areal energy density of 0.28 mWh cm^{-2} at the power density of 3 mW cm^{-2}.

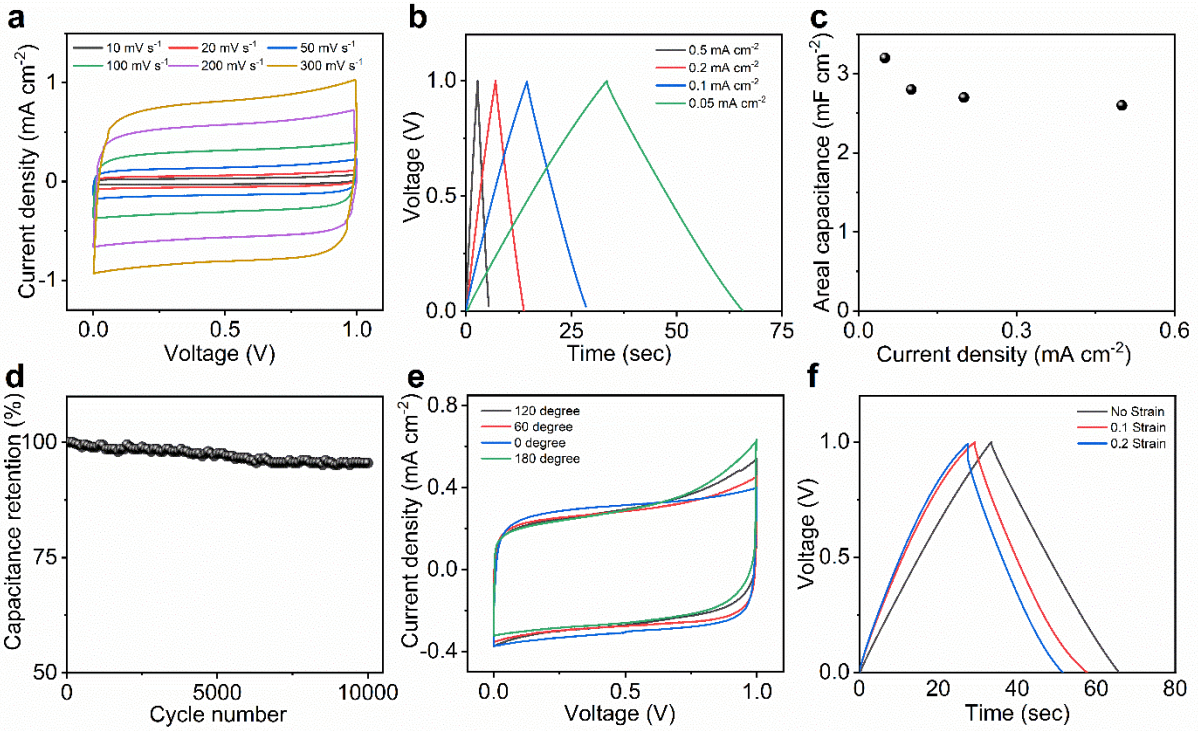

Figure 3.5 Characterization of graphene-based ink printed textile supercapacitor. a) CV curves at multiple scan rates, b) Charge-discharge curves at various current densities, c) The change of the areal capacitance with the current density, d) The cyclic stability of the printed supercapacitor measured at 0.1 mA cm^{-1}, e) CV of the printed supercapacitor at different bending angles, f) Charge-discharge profile for the supercapacitor with no strain and under strain.

For the supercapacitor to be a part of an integrated device/system on a smart textile, it is important to evaluate the performance of the printed device under various loading and strains in multiple directions. The performance of the printed supercapacitor using a bending test at various angles were assessed. The CV curves were recorded at different bending angles (*Figure 3.5*e), which show minor changes of the original unbent curve, suggesting good mechanical

stability under bending. *Figure 3.5*f shows the charge-discharge curves of the supercapacitors with no strain and under the biaxial strain of 0.1 and 0.2 strains at a constant current density of 0.1 mA cm^{-2}. Interestingly, the charge-discharge profiles of the supercapacitor under strain exhibit some bending toward the end of the discharge. This might be due to a partial exposure of the substrate cotton fibres to the supercapacitor electrolyte. It is known that the cotton fibres surface is rich with oxygen functional groups, which might introduce some faradic reaction. Obviously, the contribution of such redox reactions is limited due to the limited exposure of the fibre. There is a noticeable potential IR drop at the beginning of the discharge curve when subjected the electrodes to strain, which increases by increasing the strain. It was assumed that the increase of the electrode resistivity is related to the loss of the graphene flakes under strain, which demonstrates the possibility of using printed graphene electrodes as strain and piezoelectric sensors.

5.4 Summary

A fully-printed, highly conductive, flexible and machine washable e-textiles platform was reported that can monitor physiological conditions including bio-signals as well as can store energy. The printed conductive textiles show outstanding flexibility as well as wash stability even after 10 home laundry washing cycles. Additionally, the potential of skin-mounted wearable sensors and sleep monitoring applications of such a printed e-textiles were demonstrated. Furthermore, an in-plane flexible solid-state supercapacitor device was also fabricated from the printed e-textiles, able to provide an aerial capacitance of ~3.2 mF cm^{-2} with outstanding stability up to 10,000 cycles. These findings could potentially lead to a truly multifunctional wearable garment for personalised healthcare applications.

4. Scalable production of 2D material heterostructure textiles for high performance wearable supercapacitors

In the previous study, a graphene-based multifunctional e-textiles including their energy storage via exploiting highly versatile screen-printing technique was demonstrated. The isolation of graphene in 2004,[433] unveiled a diverse range of graphene-like 2D materials with exceptional mechanical, thermal, and electrical properties.[113, 137, 413] Transition metal dichalcogenides (TMDs) have attracted significant attention due to their unique physical properties such as magnetism, charge-density-wave order, superconductivity, and potential applications in high-performance electronic devices.[434]

Electrochemical capacitors store electrical energy either in the electrochemical double layer (EDL) formed by electrolyte ions on the electrode surface or through redox reactions involving the electrode material's surface regions, known as pseudo-capacitance.[435, 436] However, materials that possess both of these properties are rare but crucial for robust and efficient devices.[437] To address this, the fabrication of 2D material-based heterostructures combining EDLC and pseudocapacitive materials becomes essential as it increases the surface area and enhances the active electrochemical sites in the superior heterostructure. This unique architecture enables energy storage through near-surface ion adsorption and additional contribution from fast reversible faradic reactions, leading to high energy and power density.[72, 438] These heterostructures, formed by stacking 2D materials with complementary properties, exhibit unique and enhanced properties that are not found in individual materials. By carefully arranging the layers, it is possible to manipulate interlayer interactions and band structures,

resulting in the creation of diverse tailor-made heterostructures with specific and tailored properties.[439, 440] Therefore, 2D material heterostructures offer a versatile approach to enhance energy storage performance.

TMDs exhibit improved energy storage capabilities compared to traditional electrode materials and other 2D materials like graphene, thanks to their layered structures with sufficient interlayer space.[441] Among the various TMD materials, 2D MoS_2 exhibit good capacitive properties,[442] due to the tuneable band gap and a large number of active sites with extraordinary physical and chemical properties.[443] Despite their favourable properties, MoS_2 have limitations, including restacking, unsatisfactory electrical conductivity, inflexibility, and poor interface quality in electronic and electrochemical devices. To overcome these challenges, researchers have explored a wide variety of MoS_2-based heterostructures. Although graphene-MoS_2 heterostructures have been reported for other applications including non-volatile memory cells,[444] superlattice configuration,[445] fiber laser,[446] and supercapacitor electrode on nickel[447] or graphite[448] substrate; their utilization in textile-based wearable supercapacitors remains unexplored.

In this study, a scalable production method for two prominent 2D materials: graphene and MoS_2 by leveraging the unique advantages of a microfluidization technique was reported, along with their subsequent deposition hierarchically in various configurations using a highly scalable and ultrafast pad-dry method (*Figure 4.1*a). Graphene and MoS_2 were formulated through microfluidization technique and characterized them in support with University of Manchester. The number of layers of graphene coating for graphene-based and number of MoS_2 coating layers for MoS_2-based textiles supercapacitors were optimized. The supercapacitor performance fabricated from the MoS_2-graphene bi-layer coated electrodes and graphene-MoS_2-graphene tri-layer coated textile electrodes (Appendix G, Table G1) were then explored. I prepared the several heterostructure based e-textiles, analysed their flexibility, and studied their performance through fabricating several symmetric textile supercapacitors (*Figure 4.1*b). Though graphene-based supercapacitors work as EDL capacitors (*Figure 4.1*c) and MoS_2-based supercapacitors work as pseudocapacitor (*Figure 4.1*d), the heterostructure based textile supercapacitor work as hybrid capacitor, *Figure 4.1*e. I demonstrate the potential to significantly enhance the energy storage performance of heterostructure based wearable textile supercapacitors while ensuring scalability in manufacturing. I designed the experimental plan, conducted all the laboratory works and analysed the results. As I was the major contributor, I wrote the manuscript from these results and published in ACS Nano.[449]

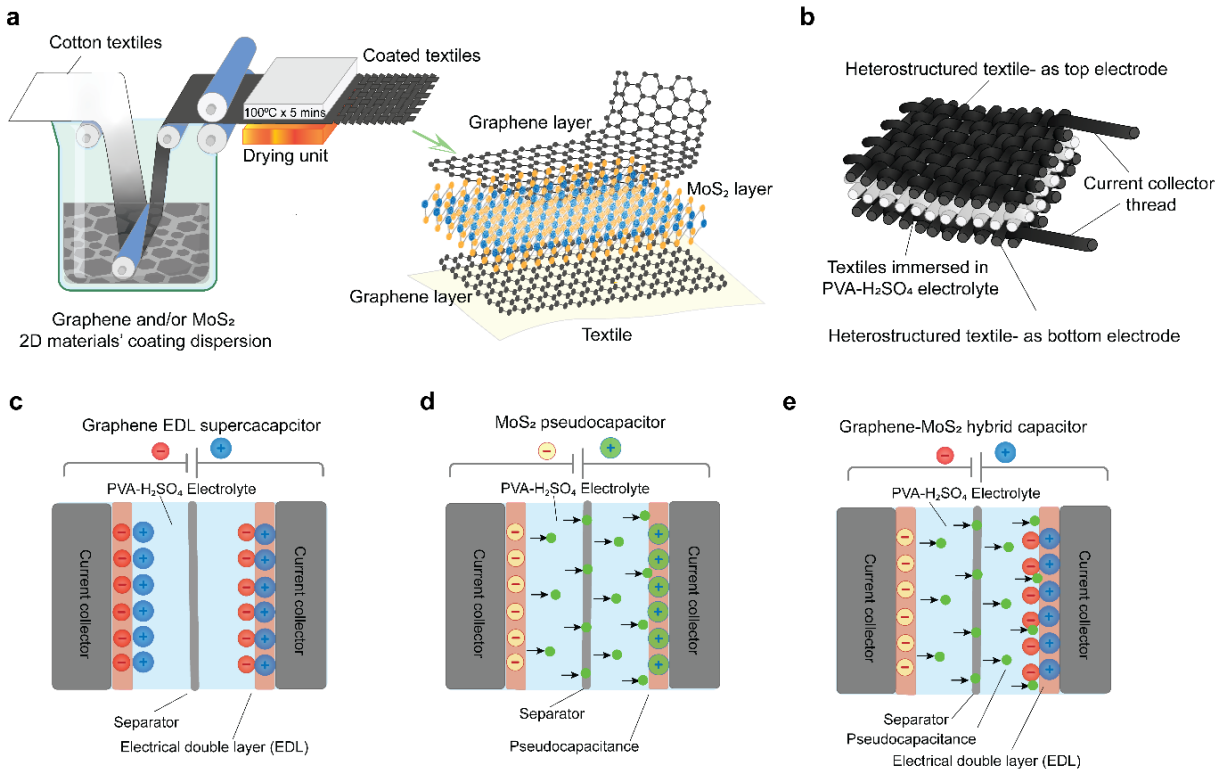

Figure 4.1 System overview of the 2D materials heterostructure textile for supercapacitor applications a. Scalable pad-dry method for coating of graphene and/or MoS_2 materials for textiles b. Schematic of the supercapacitor structure based on heterostructure textiles electrode c. Graphene based electrical double layer (EDL) supercapacitor d. MoS_2-based pseudocapacitor and e. Graphene-MoS_2-graphene heterostructure based hybrid supercapacitor.

4.1 Scalable production of 2D materials *via* microfluidization technique

Microfluidization is characterized by a homogenization technique; a high pressure (up to 207 MPa)[450] is applied to a fluid, which force the liquid to pass through a microchannel (diameter, d < 100 µm). This technique offers advantage of applying high $\gamma > 10^6$ s^{-1} to the whole dispersion,[451] unlike just locally such in case of sonication and shear-mixing. It is also a simple and environmental friendly technique with 100% exfoliation yield.[452] Previous studies reported microfluidization technique for a range of purpose such as the production of polymer nanosuspensions,[450] liposome nanoparticles,[453] aspirin nanoemulsions,[454] oil-in-water nanoemulsions,[455] and for deagglomeration and dispersion of carbon nanotubes.[456] In this study, microfluidization technique was used to exfoliate graphene and MoS_2 in a scalable quantity following previously reported methods.[452, 457] Natural flake graphite (average lateral size ~ 50 µm) and MoS_2 were purchased from Sigma Aldrich, UK. Sodium deoxycholate (SDC) powder was purchased from Sigma Aldrich, UK and used as received. Briefly, 50 g

graphite powder and 10 g SDC were added into a glass bottle and mixed with 500 ml deionised (DI) water. The mixture was then sonicated for 30 minutes using an ultrasound bath to allow homogenous dispersion and added into an input reservoir of a Microfluidizer (M-110P Microfluidizer, Microfluidics Corp, USA). The dispersion was slowly passed through 'Z-type' microfluidic channels of ~200 μm and ~87 μm diameter with diamond construction at high pressure (~200 MPa). This allows the exfoliation of graphite to few-layer graphene at 100 ml min^{-1} flow under high shear rate [$\sim 10^8\ s^{-1}$] with 100% exfoliation yield. The exfoliated dispersion was then passed through a cooling channel surrounded by cold water (~25 °C) to prevent over-heating of the dispersion and collected. This process was repeated 20 times to produce graphene flakes. MoS_2 was also produced following the same method. The obtained dispersion was used as conductive ink for textile coating.

*Figure 4.2*a shows the average lateral size of exfoliated graphene flakes is ~1.45 μm and the MoS_2 flakes is 1.25 μm. *Figure 4.2*b shows Raman spectra of exfoliated graphene flakes after 20 cycles, a typical spectra for liquid-phase exfoliated graphene, with characteristics D peak at ~1350 cm^{-1}, G peak at ~1582 cm^{-1} and an asymmetric 2D-band at ~2730 cm^{-1}.[452, 457] *Figure 4.2*c shows Raman spectra of exfoliated MoS_2 flakes. Similar to graphene, single-layer and few-layer MoS_2 has distinctive signatures in its Raman spectrum. It contains two prominent peaks: an in-plane (E_{2g}) mode located around 386 cm^{-1} and an out-of-plane (A_{1g}) mode which is located at 404 cm^{-1}. The in-plane mode corresponds to the Sulphur atoms vibrating in one direction and the Molybdenum atom in the other, while the out-of-plane mode is a mode of just the Sulphur atoms vibrating out-of-plane. The difference of these two modes (~18 cm^{-1}) can be used as a reliable identification for monolayer MoS_2.

X-ray photoelectron spectroscopy (XPS) measurements were performed to investigate the chemical composition and phase state of the as-prepared graphene and MoS_2 flakes. For XPS analysis, the exfoliated graphene and MoS_2 flakes without any surfactant were drop-casted onto a PEL paper and attached onto a carbon tape. *Figure 4.2*d shows the high resolution C1s spectra which reveals peaks for graphene flakes, dominated by C–C/C=C in aromatic rings (~284.6 eV). The high-resolution XPS spectra of the exfoliated MoS_2 acquired in the chalcogen binding energy region (226–232 eV)[458] and exhibits two obvious peaks at ~227 eV and ~230.5 eV, correspond to the Mo $3d_{5/2}$ and Mo $3d_{3/2}$, respectively, indicating the characteristic of Mo^{4+} state in MoS_2,[459] *Figure 4.2*e. The peaks of S $2p_{3/2}$ and S $2p_{1/2}$ were located at ~164.0 eV and ~165.1 eV with a spin-orbit splitting of 1.1 eV, revealing the S_2- in MoS_2,[460, 461] *Figure 4.2*f.

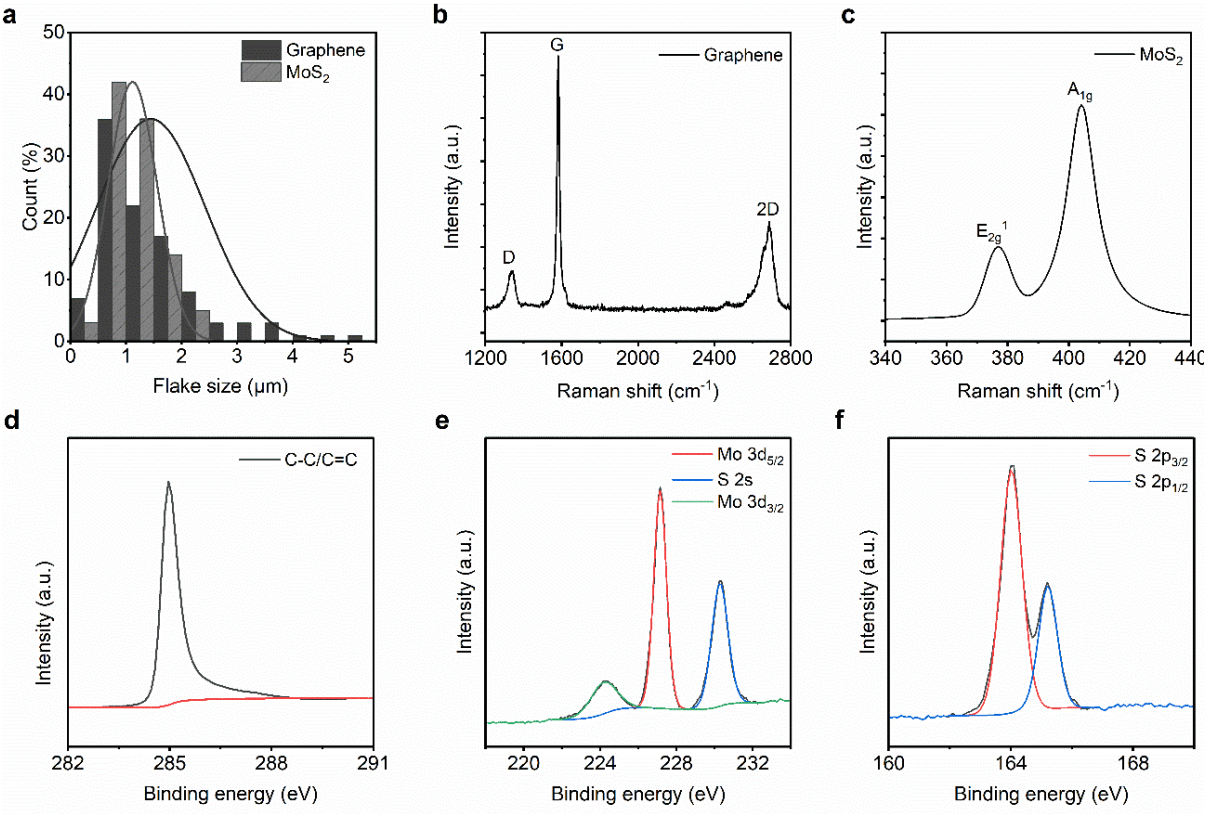

Figure 4.2. Characterization of microfluidized 2D materials a. The size distribution of graphene and MoS_2 flakes b. Raman spectra of graphene flakes c. Raman spectra of MoS_2 flakes d. High resolution XPS spectra of graphene flakes. High-resolution XPS spectra of e. Mo 3d and S 2s and f. S 2p of as-prepared MoS_2 flakes.

4.2 Scalable fabrication of highly flexible graphene-MoS_2 heterostructure for e-textiles

In the textile industry, pad-dry method is widely employed for applying functional finishes to textiles, such as anti-microbial, water repellency, wrinkle resistance, and moisture management finishes. This method offers a remarkably high production speed, capable of processing ~150m fabrics with functional finishes in just 1 minute. In this study, a laboratory-scale laboratory scale padder BVHP 2 Bowl (Roaches, UK) was utilized, demonstrating its potential for large-scale production of e-textiles was used for coating. The padding roller was set at a speed of 1m min^{-1} with a pressure of 0.74 bar. To simulate the industrial process, a 100% cotton control fabric (de-sized, scoured, and bleached which are ready-to-dye fabric) collected from Square Fashions Limited (Bangladesh), was passed, which had undergone desizing, scouring, and bleaching processes to remove impurities and colors, through a padding bath containing a 100 g L^{-1} graphene dispersion. The mangle's nip rollers were used to remove excess 2 dispersion from the fabric's surface, ensuring a uniform treatment. The padded fabrics were subsequently

dried at 100 °C for 5 min at 100°C for 5 minutes in a Type 350 Special Roaches laboratory dryer (UK) to eliminate water/solvent and fix the graphene onto the textiles and were studied for e-textiles application. Textile fabrics were padded one dip and one nip through graphene dispersions to a wet pick-up of ~80% on the weight of the fabric (o.w.f.). The wet pick-up% was calculated using following formula:

$$Pick-up\% = \frac{\text{coated fabric weight} - \text{untreated dry fabric weight}}{\text{untreated dry fabric weight}} \times 100 \qquad \text{Equation 15}$$

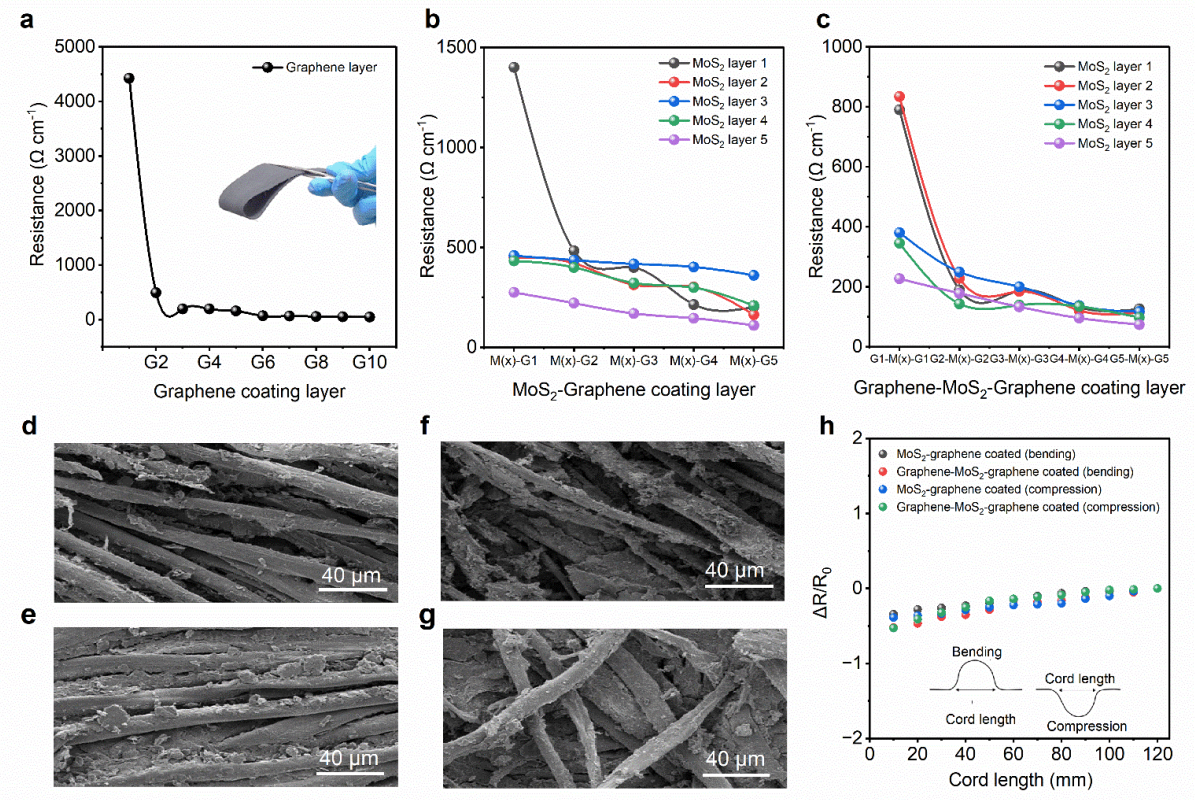

Figure 4.3. Characterization of the 2DM heterostructure based textiles. The change in the electrical resistance of a. Graphene coated, b. MoS_2-Graphene bi-layer coated and c. Graphene-MoS_2-Graphene tri-layer coated textiles. Surface morphology of the 2DM coated textiles: Scanning electron microscope (SEM) image of the d. Graphene 1 coated textiles, G1 (x 1000) e. Graphene 10 coated textiles, G10 (x 1000) f. 4 MoS_2-5 graphene coated textiles, M4G5 (x 1000) and g) 4 Graphene-3 MoS_2-4 graphene coated textiles, G4M3G4 (x 1000) and h. The variation in resistance of MoS_2-graphene bi-layer coated and graphene-MoS_2-graphene tri-layer coated textiles during bending and compression.

Several coated samples were prepared using multiple (1−10) padding passes to establish any improvement in the electrical conductivity of the coated fabrics. *Figure 4.3*a shows the changes

of electrical resistance per unit length of the graphene-coated fabric with the number of coating layers. Following the application of a single coating layer with graphene dispersion, the resistance of the fabric measured 4426.5 Ω cm^{-1}. Notably, the resistance underwent a significant reduction of ~89% after the second coating layer, reaching ~ 493.5 Ω cm^{-1}. Furthermore, the resistance continued to decrease with each additional coating layer, reaching ~71.33 Ω cm^{-1} after six layers. We continued the coating process up to ten layers, resulting in a minimum resistance of ~ 49.62 Ω cm^{-1}. This observed phenomenon can be attributed to absorption and adsorption mechanisms. Initially, the graphene dispersion is absorbed into the textile fibers, leading to a significant reduction in the resistance during the first few coating cycles. As saturation is reached, the dispersion predominantly adsorbs onto the surface of the textiles, forming a continuous conductive film by establishing improved connections between graphene flakes. The surface topography was analysed using a FEI Quanta 650 field emission scanning electron microscope (SEM). As evidenced from the scanning electron microscope (SEM) images, in comparison to the uncoated textiles, (Appendix G, Figure G1a), greater amount of graphene flakes deposited on the fiber surface during coating (*Figure 4.3*d,e) and their restacking through van der Waals forces exerted by the squeeze rollers reduce the resistance of the fabric consequently.

The similar process was repeated for the other 2D material, i.e., MoS_2 of same concentration. 10 textile samples were coated with MoS_2 from 1 to 10 successive MoS_2 layers. Both the graphene coated and MoS_2 coated textiles were utilized as control electrodes for further studies. The SEM images of the MoS_2-coated textiles also exhibit the similar phenomena (Appendix G, Figure G1b,c). It is worth noting that, being a semiconductor, MoS_2-coated textiles do not show any conductivity at initial coating layers. After 8~9 coating layers, the textiles exhibited a very high resistance of ~0.8-0.9 GΩ cm^{-1}, i.e., very poor conductivity.

After preparing graphene- and MoS_2 coated textiles, the aim was to produce heterostructures based on these two 2D materials. For bi-layered structures, the textiles were first coated with MoS_2 (one to five coating layers), followed by graphene coating (one to five layers). This resulted in 25 configurations (Appendix G, Table G1). *Figure 4.3*b illustrates the changes in the resistance for the bi-layered textiles with varying coating layers in each configuration. The single MoS_2-single graphene coated textile (M1G1) exhibited a resistance of ~1401 Ω cm^{-1}. As the number of graphene coatings on top of the MoS_2 layer increased, the sheet resistance continued to decrease. At the second graphene coating (M1G2), the resistance reached ~483.1 Ω cm^{-1}, which further reduced to ~203.43 Ω cm^{-1} after five graphene coatings (M1G5). This

phenomenon can be attributed to the increased deposition of conductive material (*Figure 4.3*f) on the MoS_2-coated textiles with each additional graphene layer. We also varied the number of MoS_2 base coating layers. It was observed that the sheet resistance decreased by ~80% (from around 1401 to 274.9 Ω cm^{-1}) between the M1G1 and M5G1 layered textiles. Ultimately, the configuration with the lowest sheet resistance was achieved with M5G5 layered textiles, measuring ~110.75 Ω cm^{-1}, which was around 60% lower than the M5G1 layered textiles.

To explore the impact of heterostructures on textiles, a tri-layered configurations for achieving conductive e-textiles were also attempted. Initially, the textiles were coated with graphene using the pad-dry method. Subsequently, MoS_2 was applied onto the graphene-coated textiles, followed by an additional graphene layer deposition using the same method. This resulted in another 25 configurations (Appendix G, Table G1). *Figure 4.3***c** illustrates the changes in sheet resistance for the tri-layered textiles with varying coating layers in each configuration. The single graphene-single MoS_2-single graphene (G1M1G1) layered textiles exhibited a resistance of ~789.8 Ω cm^{-1}. Increasing the number of MoS_2 and graphene layers contributed to a reduction in the resistance. As the number of MoS_2 layers increased between two single graphene layers (G1-M(x)-G1 configuration), the resistance progressively decreased. For the G1M5G1 layer, the resistance measured was approximately ~226.85 Ω cm^{-1}, which was ~71.27% of the initial G1M1G1 layer. Increasing the graphene layers also led to a reduction in the resistance. The G5M1G5 layer exhibited a resistance of ~126 Ω cm^{-1}, corresponding to an ~84% reduction compared to the initial G1M1G1 layer. Furthermore, increasing all coating layers, including the initial graphene, intermediate MoS_2, and final graphene layers, significantly reduced the resistance. The configuration with the lowest resistance was achieved with G5M5G5, measuring ~74 Ω cm^{-1}, representing an ~90.6% reduction compared to the initial G1M1G1 layer. Notably, the tri-layered structure demonstrated significantly lower resistance compared to the bi-layered structures due to overall more deposition of active materials (*Figure 4.3*g).

The flexibility of the several coated e-textiles were also evaluated. The change in their electrical resistances per 12 cm length during bending, compression and folding were measured. The cord length, which was measured by the grip distance of the sample ends during the experiment, was changed (10–120 mm) when the fabrics were bent and compressed. Similar to the graphene coated textiles (Appendix G, Figure G2a-left), no significant change in the resistance ($\Delta R/R_0$) were observed during bending and compression of the heterostructure coated textiles (*Figure 4.3*h). Even during folding−releasing operations, the changes in the resistance of the coated

textiles were found negligible, proving the outstanding flexibility of our heterostructure based textiles (Appendix G, Figure G2a-right). It is worth noting that no visible changes in appearance or shape or creasing were observed due to those mechanical actions (bending, compression, and folding cycles), of the heterostructure-based wearable e-textiles (Appendix G, Figure G2b-e).

4.3 Electrochemical characterization of heterostructure-based textile supercapacitors

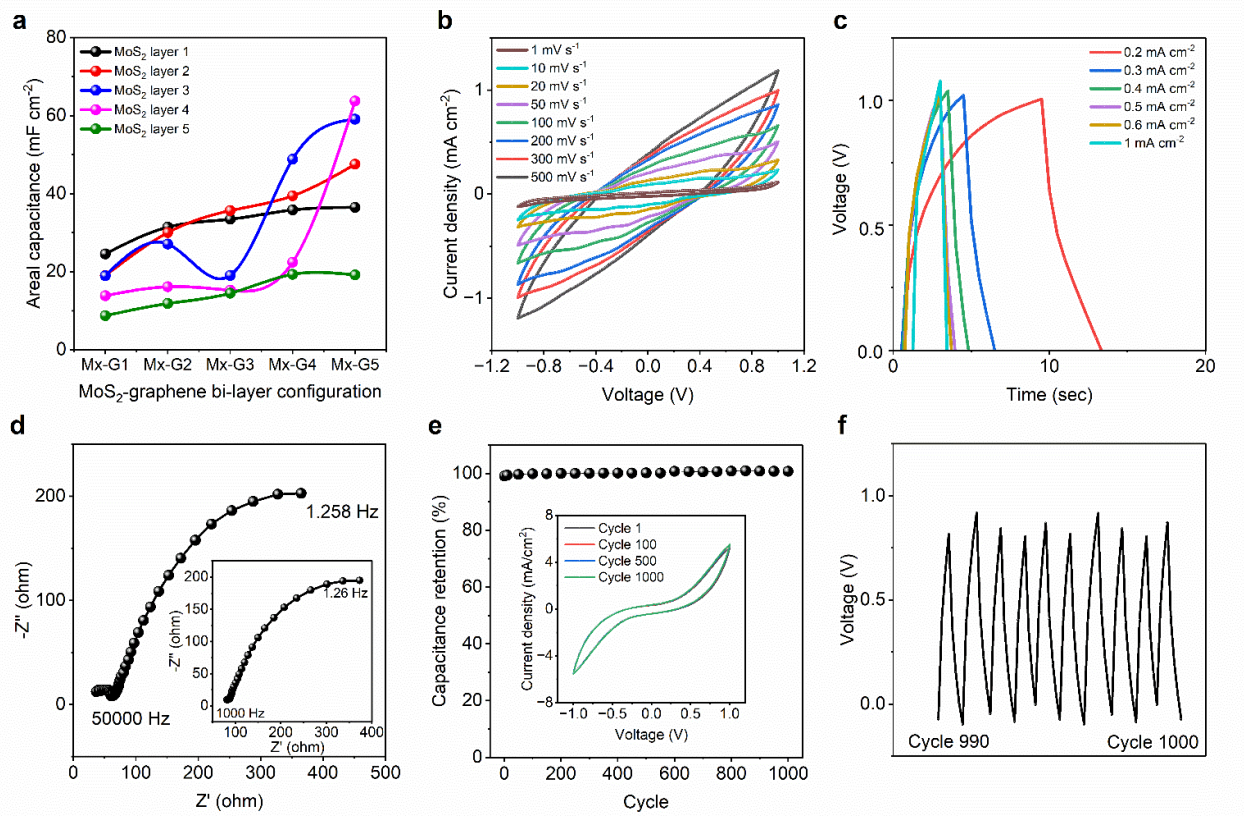

Figure 4.4. MoS_2-Graphene bi-layer coated textile supercapacitor a. Change of areal capacitance with increase of coating layers b. Cyclic voltammetry curves of the G5M4 coated textile supercapacitor at various scan rates c. Charge-discharge profile of the G5M4 coated textile supercapacitor at different current densities d. Electrical impedance spectroscopy of the device at high frequency range (inset shows the response of the supercapacitor device at low frequency range) e. Capacitance retention of the G5M4 coated textile supercapacitor device up to 1000 cycles, inset shows the CV curves at 1st, 100th, 500th and 1000th cycles and f. cyclic test of the supercapacitor (from 990th to 1000th cycles).

Initially, multiple graphene layers coated textiles were utilized as electrodes to fabricate graphene based symmetric textile supercapacitor. A thorough analysis of the cyclic

voltammetry (CV), galvanostatic charge-discharge (GCD) and electrical impedance spectroscopy (EIS) was carried out for the highest capacitance showing capacitor (Appendix G4). The supercapacitor with a single graphene coating (G1 electrodes) exhibited an areal capacitance of ~7.74 mF cm^{-2} at a scan rate of 1 mV s^{-1}. The highest areal capacitance of ~80.19 mF cm^{-2} at a scan rate of 1 mV s^{-1} was achieved with the textile supercapacitor fabricated using 10 graphene coating layered (G10). Similarly, MoS_2-based symmetric textile supercapacitors were also fabricated (Appendix G5). The highest areal capacitance with bare MoS_2 was achieved with 10 coating layers (M10) at ~ 7.1 mF cm^{-2} and a scan rate of 1 mV s^{-1}. To enhance the capacitance performance of our textile supercapacitors, a combination of heterostructures were explored by depositing both graphene and MoS_2 onto textile electrodes. Textiles were initially coated with MoS_2 at different layer configurations (Mx, where x is the number of coating layers from 1 to 5), followed by graphene coating at different layer configurations (Gx, where x is the number of coating layers from 1 to 5). These bi-layered configurations of MoS_2 and graphene (Mx-Gx) coated textiles were used as electrodes for the supercapacitors and exhibited the characteristics of a hybrid supercapacitor (ultracapacitor), combining the principles of double-layer capacitance and pseudocapacitance.

A total of 25 samples were fabricated to investigate the effect of bi-layered configurations on the areal capacitance of the textile supercapacitors. *Figure 4.4*a demonstrates the change of areal capacitance at different layer configuration. The highest areal capacitance of ~36.49 mF cm^{-2} was achieved when textiles were coated with a single layer of MoS_2 followed by five layers of graphene (M1G5 configuration) at a scan rate of 1 mVs^{-1}. However, increasing the number of MoS_2 layers under a single graphene layer led to a decrease in the areal capacitance. The lowest value of ~8.735 mF cm^{-2} was obtained when textiles were coated with five layers of MoS_2 under a single graphene layer (M5G1 configuration). Similarly, increasing the number of graphene layers while keeping a single MoS_2 layer also resulted in increased capacitance, up to ~31.435 mF cm^{-2} for the M1G2 configuration. Among the 25 configurations, the highest areal capacitance of ~63.73 mF cm^{-2} was achieved when textiles were coated with four layers of MoS_2 covered by five layers of graphene (M4G5 configuration). Interestingly, further increasing the number of MoS_2 layers under the graphene layers led to a dramatic reduction in the areal capacitance to ~19.16 mF cm^{-2}. This could be attributed to the excessive amount of graphene interfering with the conductivity of the MoS_2 flakes. There exists an optimum quantity of both graphene and MoS_2 for achieving ideal hybrid capacitance behaviour. It is to note that, the areal capacitance of MoS_2-graphene bi-layered electrode based symmetric textile

capacitor was almost similar with the graphene electrode based symmetric textile supercapacitor, exhibiting 71.62 mF cm^{-2} at 9 coating layers, reaching to 80.18 $mFcm^{-2}$ after 10th coating layer (Appendix G, Figure G3a). However, textile supercapacitor composed of only MoS_2-electrodes exhibited a highest areal capacitance of only 7.1 $mFcm^{-2}$ after 10 coating layers (Appendix G, Figure G4a).

Several electrochemical tests (CV, GCD and EIS) were carried out of the best-performing supercapacitor based on M4G5 electrodes. The CV curves exhibited near-rectangular shapes at all tested scan rates, indicating ideal capacitance behaviour, *Figure 4.4*b. Though for only graphene- and only MoS_2-based supercapacitors, the current density reaches to 1.736 mA cm^{-2} (Appendix G, Figure G3b), and 1.08 $mAcm^{-2}$ (Appendix G, Figure G4b) respectively, for the bi-layered structure, the current density reaches to a maximum of 1.186 mA cm^{-2} only. The charge-discharge profiles (*Figure 4.4*c) showed no plateaus or bends, confirming the absence of redox reactions. The slight potential drop observed at the beginning of the discharge curve was due to the device's ESR, but it did not significantly affect the conductivity or charge barrier of the electrodes. It is to note that, at a current density of 0.2 mA cm^{-2}, the charge-discharge took nearly 206 seconds for graphene-based supercapacitor (Appendix G, Figure G3c) and nearly 8.5 seconds for MoS_2-based supercapacitor (Appendix G, Figure G4c). The MoS_2-graphene bi-layered electrode-based textile supercapacitor on contrary took nearly 13 seconds at the same current density. The EIS results (*Figure 4.4*d) demonstrated an ESR of ~81.63 Ω at a lower frequency range (1 kHz), which reduced to ~36.89 Ω at a higher frequency range (50 kHz). The graphene and MoS_2 exhibited an ESR of 37.01 and 29.44 Ω at a lower frequency range (1 kHz) and 26.78 Ω at a higher frequency range (50 kHz), (Appendix G, Figure G3d and G4d). The Nyquist plot exhibited a 45-degree bend at the low-frequency range, indicating the ideal behaviour of a capacitor.

The electrochemical stability of the supercapacitor was also evaluated by examining its long-term charge-discharge behaviour at a current density of 1 mA cm^{-2}. Remarkably, even after 1,000 cycles, the device retained its initial capacitance, demonstrating exceptional stability (*Figure 4.4*e). The inset in the figure illustrates the CV profile of the supercapacitor up to 1,000 cycles, showing no deviations. To further illustrate this stability, *Figure 4.4*f displays the charge-discharge curves specifically from the 990th to the 1,000th cycle of the GCD tests. The M4G5 supercapacitor, without the use of any current collector, exhibited an impressive areal energy density of 35.405 μWh cm^{-2} (~44.55 μWh cm^{-2} for graphene, ~3.944 μWh cm^{-2} for MoS_2) and power density of 8,497.333 μW cm^{-2} (~581.05 μW cm^{-2} for graphene and ~3550

μW cm^{-2} for MoS_2). Additionally, it achieved specific energy density of 9.317 Wh kg^{-1} (~12.73 Wh kg^{-1} for graphene and 1.578 Wh kg^{-1} for MoS_2) and power density of 2,236.14 W kg-^{1}, (~166.01 W kg^{-1} for graphene and 1420 W kg^{-1} for MoS_2). The exceptionally high-power density show promise for our textile supercapacitor for next generation wearable applications.

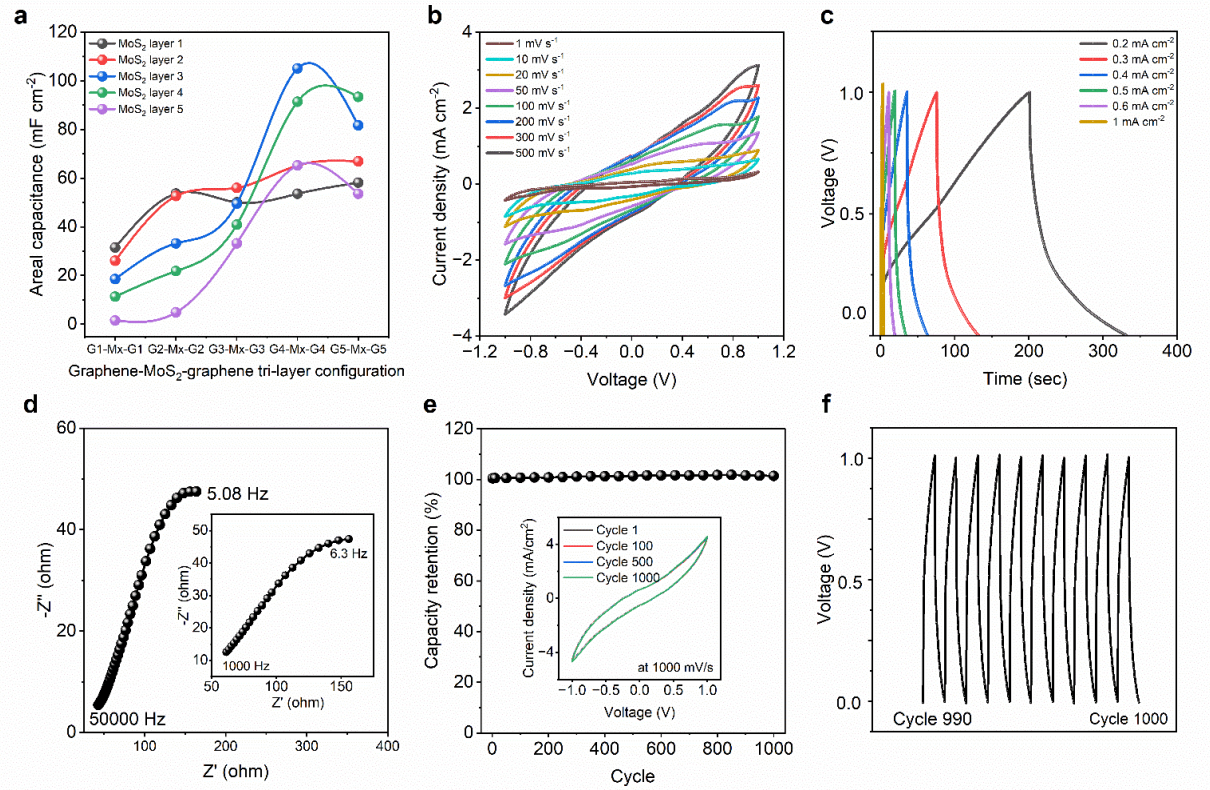

Figure 4.5. Graphene-MoS_2-Graphene tri-layer coated textile supercapacitor a. Change of areal capacitance with increase of coating layers b. Cyclic voltammetry curves of the G4M3G4 coated textile supercapacitor at various scan rates c. Charge-discharge profile of the G4M3G4 coated textile supercapacitor at different current densities d. Electrical impedance spectroscopy of the device at high frequency range (inset shows the response of the supercapacitor device at low frequency range) e. Capacitance retention of the G4M3G4 coated textile supercapacitor device up to 1000 cycles, inset shows the CV curves at 1st, 100th, 500th and 1000th cycles and f. cyclic test of the supercapacitor (from 990th to 1000th cycles).

To achieve higher capacitance performance of our textile supercapacitor, we introduced another initial graphene layer on the previous bi-layer configuration resulting in a tri-layered heterostructure component configuration. Initially, textiles were coated with graphene at different layer configurations (G_x, where x is the number of coating layer, 1 to 5). These textiles were then coated with several MoS_2 layers at varying configurations (M_x, where x is the number of coating layer, 1 to 5). Finally, the graphene-MoS_2 coated textiles were further coated with

graphene at different layer configurations (G_x, where x is the number of coating layer, 1 to 5). Textiles coated with several tri-layered configuration of 2D materials (G_x-M_x-G_x) were then utilized as supercapacitor electrodes. Similar to our bi-layered structure, the graphene-MoS_2-graphene tri-layered electrodes exhibited a hybrid capacitance behavior when fabricated into a supercapacitor.

*Figure 4.5*a demonstrates the change in the areal capacitance of the textile supercapacitors fabricated with graphene-MoS_2-graphene tri-layers in various configurations. Like the bi-layered structure, we fabricated a total of 25 coated samples to evaluate the effect of tri-layered textile electrodes for supercapacitor applications. As observed, supercapacitors fabricated with electrodes containing a single layer of graphene, followed by a single layer of MoS_2 and a final single layer of graphene (i.e., G1M1G1) exhibited an areal capacitance of ~31.48 mF cm^{-2} at a scan rate of 1 mVs^{-1}. Similar to the bi-layered textile SCs, increasing the number of graphene layers enhanced the areal capacitance, reaching values of ~53.58 mF cm^{-2} and ~58.16 mF cm^{-2} at the same scan rate for G4M1G4 and G5M1G5 configurations, respectively. Interestingly, increasing the number of MoS_2 layers between the top and bottom graphene layers further improved the supercapacitor's areal capacitance. With one MoS_2 layer in between top 4-layer and bottom 4-layer graphene the capacitance was 53.58 mF cm^{-2} which increased to 65.21 mF cm^{-2} with increasing another layer of MoS_2. The G4M3G4 configuration achieved the highest value of ~105.08 mF cm^{-2} at a scan rate of 1 mVs^{-1}. However, further increases in the number of MoS_2 layers reduced the capacitance to ~91.37 mF cm^{-2} (G4M4G4) and ~65.205 mF cm^{-2} (G4M5G4) at the same scan rate. This phenomenon could be attributed to the fact that, the addition of a layer of MoS_2 contributes to fill the voids on the graphene surface, providing additional active sites for charge storage (pseudocapacitance in case of MoS_2) and improving the overall capacitance. After a certain limit, the excess amount of MoS_2 start to interfere the overall charge storage of the structure. Since MoS_2 is a semi-conductor material, the presence of excess amount might have obstructed the capacitive behaviour of the EDL graphene material as well as the overall heterostructure.

A similar trend was observed for the G5 configuration of tri-layered structures. The supercapacitor with a G5M1G5 electrode exhibited an areal capacitance of ~58.16 mF cm^{-2} at a scan rate of 1 mV s^{-1}, which increased to ~93.4 mF cm^{-2} at the same scan rate. However, further increases in the number of MoS_2 layers reduced the capacitance to 53.58 mF cm^{-2}. This phenomenon can be attributed to the amount of active material loaded with each coating layer. For example, the total number of coating layers was 3 for G1M1G1 (~31.48 mF cm^{-2}), 11 for

G5M1G5 (58.16 mF cm^{-2}), 11 for G4M3G4 (105.08 mF cm^{-2}), and 14 for G5M4G5 (93.4 mF cm^{-2}). Textiles can absorb active material up to a certain limit, and beyond saturation, additional coating hinders performance rather than adding functionality. When considering the 11-layered structures (G5M1G5 and G4M3G4), it is evident that despite the reduced amount of highly conductive graphene, the introduction of a semiconductor material within a certain limit increases the capacitance of the fabricated supercapacitor by ~80.69%. The effect of MoS_2 presence in the supercapacitor is also evident in electrodes fabricated with G4M1G4 and G4M3G4 structures. The addition of 2 MoS_2 coating layers between the G4-Mx-G4 configuration contributes to an enhancement of ~96.14% in areal capacitance.

A comprehensive analysis of the electrochemical performance (CV, GCD and EIS) of the highest-performing supercapacitor configuration (G4M3G4) was carried out. The CV curves exhibited nearly rectangular shapes at all scan rates (*Figure 4.5*b), indicating ideal capacitance behaviour. As previously discussed, in comparison to the other configurations, the current density reaches to a maximum of 3.13 mA cm^{-2}. The absence of redox peaks within the tested electrochemical windows suggests complete coverage of cotton fibers by the graphene-based ink. The charge-discharge profile (*Figure 4.5*c) of the G4M3G4 supercapacitor showed no visible plateaus or bends associated with redox reactions. The minor potential drop observed initially can be attributed to the energy consumption of the device's equivalent series resistance (ESR), which still ensures good conductivity and low charge barrier of the electrodes. It should be noted that the charge-discharge time was extended up to 332 seconds compared to other heterostructure supercapacitors at the same current density of 0.2 mA cm^{-2}. The EIS analysis revealed a low equivalent series resistance (ESR) of ~61.47 Ω at a lower frequency range (1 kHz) that reduced to ~42.87 Ω at a higher frequency range (50 kHz), as indicated by the Nyquist plot (*Figure 4.5*d). The proximity of the vertical lines to the imaginary axis suggests that the supercapacitor behaviour closely resembles that of an ideal capacitor. The electrochemical stability of the supercapacitor was also evaluated through long-term charge-discharge curves at a current density of 1 mA cm^{-2}. Remarkably, the device maintained its initial capacitance even after 1,000 cycles, demonstrating excellent stability (*Figure 4.5*e). The inset depicts the CV profile of the supercapacitor up to 1000 cycles, showing no deviation. Furthermore, *Figure 4.5*f presents the charge-discharge curves of the 990th to 1000th cycle in the GCD tests. The G4M3G4 supercapacitor, achieved the highest areal energy density of 58.37 μWh cm^{-2} (~35.405 μWh cm^{-2} for M4G5 bi-layered supercapacitor, ~44.55 μWh cm^{-2} for graphene and ~3.944 μWh cm^{-2} for MoS_2 supercapacitor). However, the power density was 1604.27 mW

cm^{-2} (though highest was for M4G5 bi-layered supercapacitor 8,497.333 μW cm^{-2}, ~581.05 μW cm^{-2} for graphene and ~3550 μW cm^{-2} for MoS_2 supercapacitor). The specific energy density was achieved 14.59 Wh kg^{-1} whereas 9.317 Wh kg^{-1} for M4G5 bi-layered, ~12.73 Wh kg^{-1} for graphene and 1.578 Wh kg^{-1} for MoS_2 supercapacitor. The power density was reported as 401.06 W kg^{-1}, (2,236.14 W kg^{-1} for M4G5 bi-layer ~166.01 W kg^{-1} for graphene and 1,420 Wkg^{-1} for MoS_2 supercapacitor). The exceptionally high energy and power densities show promise for our textile supercapacitor for next generation wearable applications.

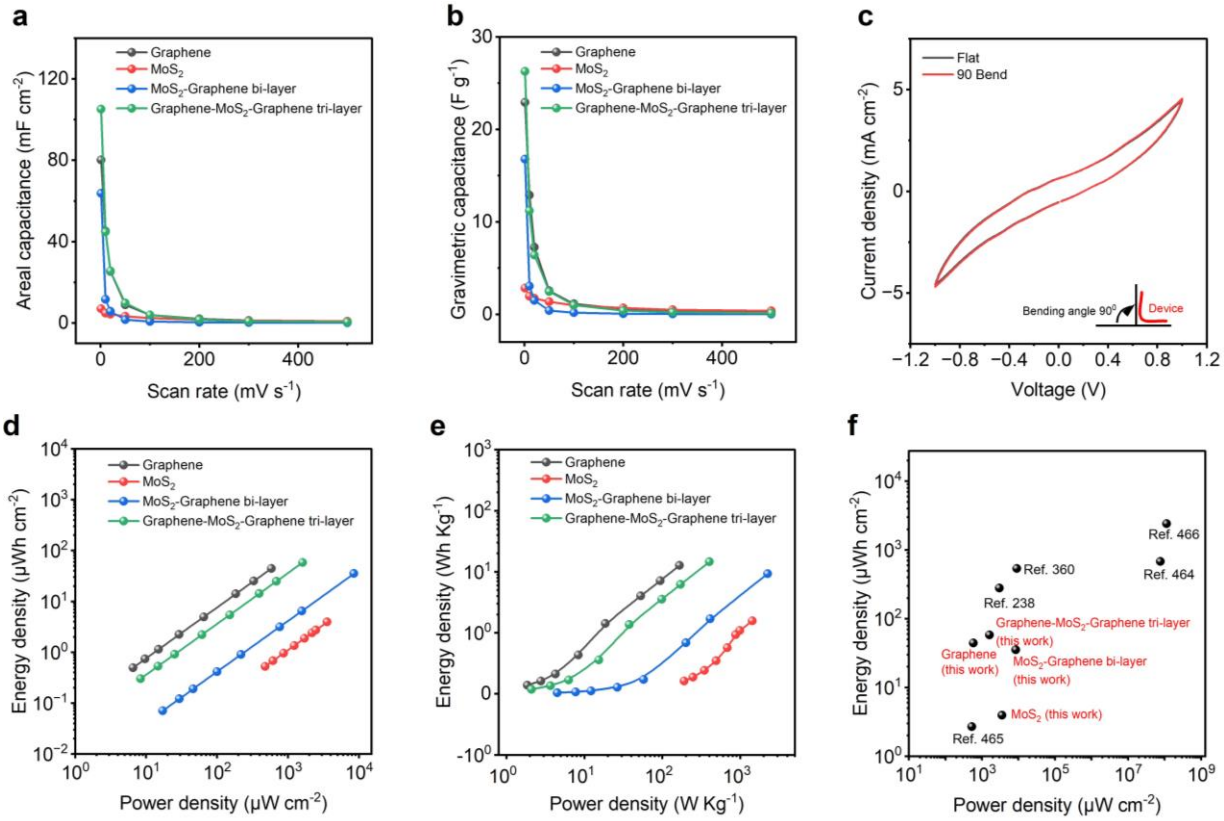

Figure 4.6. Performance of the 2DM heterostructure based textile supercapacitors. a. Areal capacitance of 4 as-fabricated textile supercapacitors at different scan rate. b. Gravimetric capacitance of 4 as-fabricated textile supercapacitors at different scan rate c. Comparison of the capacitance performance 4 as-fabricated textile supercapacitors with others in literature d. Ragone plot showing comparison of 4 as-fabricated supercapacitor performance (in terms of areal energy and power density) e. Ragone plot showing comparison of 4 as-fabricated supercapacitor performance (in terms of specific energy and power density) and f. Ragone plot showing comparison of 4 as-fabricated supercapacitor performance with others in literature.

Figure 4.6 presents the performance analysis of our fabricated supercapacitors. Areal and gravimetric capacitance, as a function of scan rate, are depicted in *Figure 4.6a* and *Figure 4.6*b,

respectively. It can be observed that higher scan rates result in lower capacitance, possibly due to insufficient time for electrolytes to adsorb and desorb on the electrode surface.[462] At lower scan rates, electrolyte ion diffusion becomes more efficient, reaching both the external surface and inner active sites of the electrode material.[463] In *Figure 4.6*c, the CV curves of the device are shown when it is both flat and bent at a 90° angle, demonstrating the device's stable electrochemical performance even under bending conditions. The Ragone plot in *Figure 4.6*d and *Figure 4.6*e showcases the energy and power densities of our fabricated supercapacitors. Notably, our graphene-MoS_2-graphene tri-layered textiles exhibit impressive energy and power densities of ~58.38 μWh cm^{-2} and 1604.27 μW cm^{-2}, respectively. These values are either superior or comparable to those reported in previous studies (*Figure 4.6*f) on graphene-based wearable supercapacitors.[212, 238, 360, 464-470]

4.4 Small scale integration of textile supercapacitors

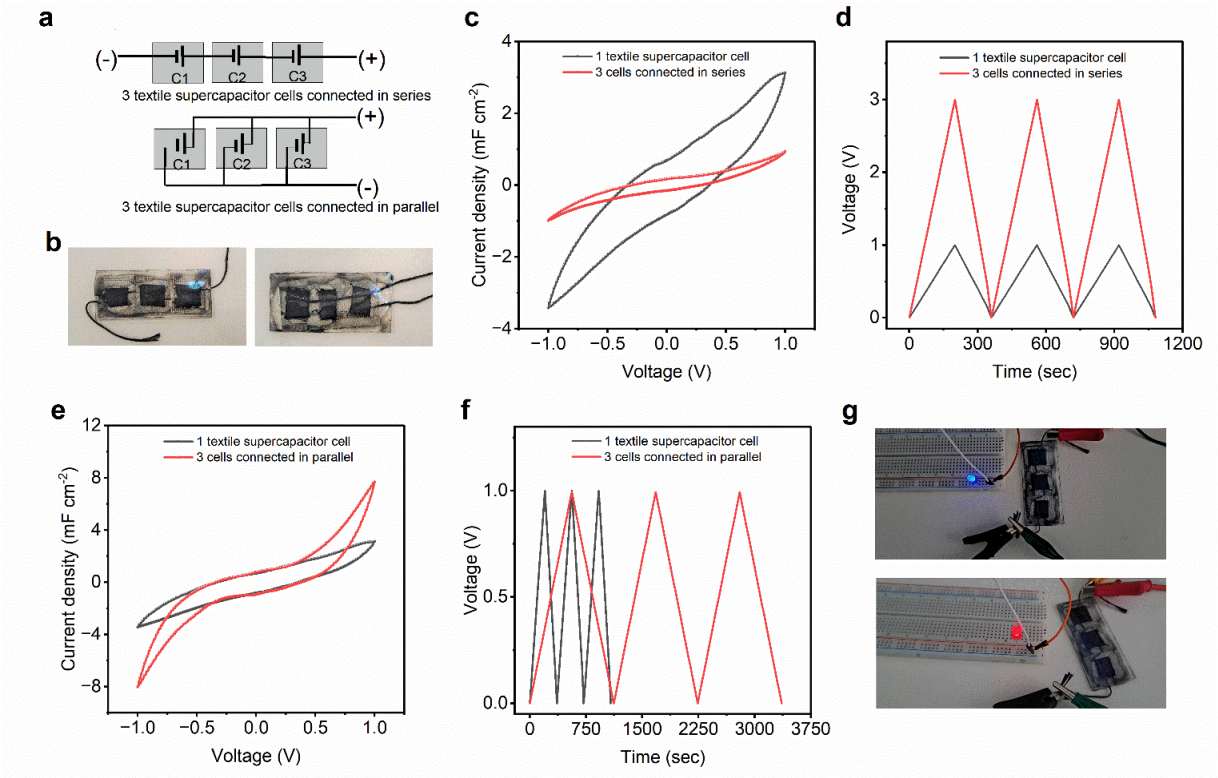

Figure 4.7. Small scale integration of 2DM heterostructure based textile supercapacitor. a. Schematic of 3 supercapacitor cells in series (top) and parallel (bottom) connection. b. 3 as-fabricated textile supercapacitor cells connected in series (left) and parallel (right) connection. c. CV profile of 1 supercapacitor cell versus 3 supercapacitor cells connected in series (at scan rate 500 mV s^{-1}) d. GCD curve of 1 supercapacitor cell versus 3 supercapacitor cells connected in series (at current density 0.2 mA cm^{-2}) e. CV profile of 1 supercapacitor cell versus 3 supercapacitor cells connected in parallel (at scan rate 500 mV s^{-1}) f. GCD curve of 1

supercapacitor cell versus 3 supercapacitor cells connected in parallel (at current density 0.2 mA cm^{-2}) and g. 3 supercapacitor cells connected in series powering LEDs.

In practical applications, a single supercapacitor often does not provide sufficient voltage and current to power circuits effectively.[471] Therefore, multiple supercapacitors are commonly connected in series and/or in parallel (*Figure 4.7*a) to form a "bank" with a specific voltage and capacitance.[472] *Figure 4.7*b shows the small-scale connection of 3 supercapacitors in series (left) and parallel (right). The conductive current collector threads were employed as connection wires for the supercapacitors. *Figure 4.7*c shows the CV profiles and *Figure 4.7*d shows the GCD curves of the three series-connected textile supercapacitors. It is evident that the series-connection increases the voltage window from 1 to 3 V, with a reduction in capacitance to approximately one-third of a single device. On the other hand, *Figure 4.7*e displays the CV profiles, and *Figure 4.7*f presents the GCD curves for the three parallel-connected textile supercapacitors. In contrast to the series connection, the parallel connection exhibits nearly three times higher capacitance compared to a single device while maintaining the same operating voltage window. Furthermore, the parallelly connected supercapacitors were capable of powering different coloured LEDs with varying voltage requirements, as depicted in *Figure 4.7*g. This highlights the capability of our textile-based flexible supercapacitors to meet the increasing energy needs of wearable electronics in the future.[5, 473, 474]

4.5 Summary

In this study, the scalable production of very promising two of the 2D materials, namely graphene and MoS_2, through microfluidization technique was reported. Considering the design flexibility of 2D materials for tuning their electronic properties, graphene and MoS_2 heterostructures for wearable electronic textile-based for supercapacitor fabrication were also reported. The highest areal capacitance was obtained from the supercapacitor fabricated from the graphene–MoS_2-graphene tri-layered textile electrodes. Though the energy density was highest for tri-layered electrode-based supercapacitor, highest power density was achieved for the MoS_2-graphene bi-layered electrode-based supercapacitor. 3 of the as-fabricated supercapacitors, when integrated, were able to power up an LED. Industrially most-known and highly scalable coating method was exploited for the fabrication of textile supercapacitors, which demonstrates the potential of the reported fabrication for the large-scale production of wearable e-textile supercapacitors.

5. [redacted]

[redacted]

[redacted]

(Image and Article redacted for copyright reasons)

[redacted]

(Image and Article redacted for copyright reasons)

[redacted]

[redacted]

[redacted]

[redacted]

(Image and Article redacted for copyright reasons)

[redacted]

[redacted]

[redacted]

[redacted]

[redacted]

(Image and Article redacted for copyright reasons)

[redacted]

[redacted]

(Image and Article redacted for copyright reasons)

[redacted]

(Image and Article redacted for copyright reasons)

[redacted]

[redacted]

(Image and Article redacted for copyright reasons)

[redacted]

[redacted]

[redacted]						
[redacted]						
[redacted]						
[redacted]						
[redacted]						
[redacted]						

6. [redacted]

[redacted]

[redacted]

[redacted]

(Image and Article redacted for copyright reasons)

[redacted]

[redacted]

[redacted]

[redacted]

(Image and Article redacted for copyright reasons)

[redacted]

[redacted]

[redacted]

(Image and Article redacted for copyright reasons)

[redacted]

[redacted]

(Image and Article redacted for copyright reasons)

[redacted]

[redacted]

[redacted]

[redacted]

(Image and Article redacted for copyright reasons)

[redacted]

[redacted]

[redacted]

[redacted]

[redacted]

(Image and Article redacted for copyright reasons)

[redacted]

[redacted]

[redacted]

(Image and Article redacted for copyright reasons)

[redacted]

[redacted]

(Image and Article redacted for copyright reasons)

[redacted]

[redacted]

7. Summary and future recommendations

As outlined in the Chapter 1, the aim of this PhD study was to develop scalable, low-cost, highly functional and flexible graphene-based energy storage textiles for powering a personalized wearable e-textile garment. Overall, the study focuses on exfoliation, preparation and application of graphene and other 2D materials namely MoS_2 and hBN for textile-based supercapacitor applications. An extensive overview of textile-based supercapacitors, their structures, manufacturing and performance is reported in Chapter 2. The following chapters then report the studies carried out in this PhD in order to achieve high performance textile-based supercapacitors. This final chapter presents the summary of the major findings from these studies and finally, recommendations are made for further research in the field of textile-based supercapacitors.

7.1 Summary of findings

As discussed in Chapter 1, the current drive to move away from metal-based e-textiles technology has facilitated the emerge of graphene and other 2D materials for their outstanding physical, mechanical and electrical properties.[22, 24-27] However, the major challenge with this technology is the ability to produce colloidally stable conductive inks in a scalable quantity. In the following studies of this PhD thesis, I have used/formulated graphene and/or other 2D materials MoS_2 and hBN to be applied to textiles for the fabrication of supercapacitor electrodes (Research objective 1).

Chapter 2 reveals that there are a range of fabrication techniques employable for textile supercapacitors; such as hydrothermal deposition,[528] drop casting,[375] electrochemical deposition,[389] electrochemical activation,[395] hydrothermal activation,[331] in-situ synthesis[529] etc.

Nevertheless, while they are all appropriate for laboratory trials, they are not suitable for large-scale production in industrial settings. Screen printing and coating are the two most common industrially known fabrication methods for realizing functional textiles.

Therefore, in Chapter 3, a commercial graphene-based ink was used on a rough and flexible textile substrate via highly scalable screen printing process (Research objective 2), followed by a fine encapsulation to produce highly conductive machine-washable e-textiles platform. With an optimized print condition, the resistance was as low as ~30 Ω cm^{-1}, i.e. highly conductive graphene based e-textiles was achieved. The flexibility and washability of the screen-printed e-textiles were assessed. The screen-printed textile was then employed as a piezoresistive sensor for activity monitoring, as an EEG electrode as well as electrode for supercapacitor application. CV and GCD and long-term cyclic stability tests were assessed for the characterization of textile supercapacitor (Research objective 3). With reliable performance for activity monitoring as well as monitoring brain signals (Research objective 4), the screen-printed textile supercapacitor exhibited an areal capacitance of 3.2 mF cm^{-2} at a scan rate of 1 mV s^{-1} with an energy density of 200 μWh cm^{-2}.

In Chapter 4, highly scalable microfluidization technique was reported to exfoliate high quality few layer two-dimensional (2D) materials (graphene and MoS_2 flakes) from bulk graphite and MoS_2. The average lateral size of exfoliated graphene flakes was ~1.45 μm and of the MoS_2 1.25 μm. The Raman spectrum of exfoliated graphene flakes exhibited typical spectrum for liquid-phase exfoliated graphene, with characteristics D peak at ~1350 cm^{-1}, G peak at ~1582 cm^{-1} and an asymmetric 2D-band at ~2730 cm^{-1}.[452, 457] Similar to graphene, MoS_2 exhibited distinctive signatures in its Raman spectrum containing two prominent peaks: E2g, ~386 cm^{-1} and A1g located at ~404 cm^{-1}. XPS measurements were performed to investigate their chemical composition and phase state; the high resolution C1s spectra reveals peaks for graphene flakes, dominated by C–C/C=C in aromatic rings (~284.6 eV). The high-resolution XPS spectra of the exfoliated MoS_2 exhibited two obvious peaks at ~227 eV and ~230.5 eV, correspond to the Mo 3d5/2 and Mo 3d3/2, respectively. The peaks of S 2p3/2 and S 2p1/2 were located at ~164.0 eV and ~165.1 eV with a spin-orbit splitting of 1.1 eV, revealing the S_2^- in MoS_2.[458-461] A simple but highly scalable pad-dry-cure technique was employed to fabricate graphene, MoS_2 and their heterostructure based textiles (Research objective 2). The flexibility of the e-textiles prepared from various heterostructures were studied. With the prepared microfluidized graphene dispersion, the resistance of textiles was obtained as low as ~49 Ω cm^{-1}. The graphene-coated textile was then used as supercapacitor electrode; exhibiting

a supercapacitor capacitance of ~80.19 mF cm^{-2}. To improve the energy storage performance, MoS_2 was then employed to realize heterostructure based textiles to be employed as supercapacitor electrodes. The highest capacitance of the textile-based supercapacitor was achieved ~105.08 mF cm^{-2} for a graphene-MoS_2-graphene tri layer configuration, an increase of 31.03% compared to the bare graphene-based supercapacitor. In addition to CV, GCD, EIS and long-term cyclic stability tests were carried out for the characterization of the heterostructure based textile supercapacitors (Research objective 3). The energy density and power density achieved was ~58.377 μWh cm^{-2} and ~1604.274 μW cm^{-2} with a cyclic stability of ~100% even after 1000 cycles. Three supercapacitors integrated together was able to power an LED bulb (Research objective 4).

[redacted]

[redacted]

[redacted]	[redacted]	[redacted]	[redacted]	[redacted]	[redacted]
[redacted]	[redacted]	[redacted]	[redacted]		[redacted]
[redacted]	[redacted]	[redacted]	[redacted]	[redacted]	[redacted]

	[redacted]	[redacted]	[redacted]	[redacted]	[redacted]
	[redacted]	[redacted]	[redacted]	[redacted]	[redacted]
	[redacted]	[redacted]	[redacted]	[redacted]	[redacted]
[redacted]	[redacted]	[redacted]	[redacted]	[redacted]	[redacted]
	[redacted]	[redacted]	[redacted]	[redacted]	[redacted]
	[redacted]	[redacted]	[redacted]	[redacted]	[redacted]
	[redacted]	[redacted]	[redacted]	[redacted]	[redacted]
[redacted]	[redacted]	[redacted]	[redacted]	[redacted]	[redacted]
	[redacted]	[redacted]	[redacted]	[redacted]	[redacted]
	[redacted]	[redacted]	[redacted]	[redacted]	[redacted]

[redacted]

[redacted]

[redacted]

[redacted]

[redacted]

References

(1) Chen, G.; Xiao, X.; Zhao, X.; Tat, T.; Bick, M.; Chen, J. Electronic Textiles for Wearable Point-of-Care Systems. *Chemical Reviews* **2022**, *122* (3), 3259-3291. DOI: 10.1021/acs.chemrev.1c00502.

(2) Chen, G.; Li, Y.; Bick, M.; Chen, J. Smart Textiles for Electricity Generation. *Chemical Reviews* **2020**, *120* (8), 3668-3720. DOI: 10.1021/acs.chemrev.9b00821.

(3) Fang, Y.; Chen, G.; Bick, M.; Chen, J. Smart textiles for personalized thermoregulation. *Chemical Society Reviews* **2021**, *50* (17), 9357-9374, 10.1039/D1CS00003A. DOI: 10.1039/D1CS00003A.

(4) Zhang, Y.; Zhu, Y.; Zheng, S.; Zhang, L.; Shi, X.; He, J.; Chou, X.; Wu, Z.-S. Ink formulation, scalable applications and challenging perspectives of screen printing for emerging printed microelectronics. *Journal of Energy Chemistry* **2021**, *63*, 498-513. DOI: 10.1016/j.jechem.2021.08.011.

(5) Tan, S.; Afroj, S.; Li, D.; Islam, M. R.; Wu, J.; Cai, G.; Karim, N.; Zhao, Z. Highly sensitive and extremely durable wearable e-textiles of graphene/carbon nanotube hybrid for cardiorespiratory monitoring. *iScience* **2023**, *26* (4), 106403. DOI: 10.1016/j.isci.2023.106403.

(6) Stoppa, M.; Chiolerio, A. Wearable electronics and smart textiles: a critical review. *Sensors (Basel)* **2014**, *14* (7), 11957-11992. DOI: 10.3390/s140711957 PubMed.

(7) Yin, J.; Wang, S.; Di Carlo, A.; Chang, A.; Wan, X.; Xu, J.; Xiao, X.; Chen, J. Smart textiles for self-powered biomonitoring. *Med-X* **2023**, *1* (1), 3. DOI: 10.1007/s44258-023-00001-3.

(8) Karim, N.; Afroj, S.; Tan, S.; Novoselov, K. S.; Yeates, S. G. All Inkjet-Printed Graphene-Silver Composite Ink on Textiles for Highly Conductive Wearable Electronics Applications. *Scientific Reports* **2019**, *9* (1), 1-10. DOI: 10.1038/s41598-019-44420-y.

(9) Libanori, A.; Chen, G.; Zhao, X.; Zhou, Y.; Chen, J. Smart textiles for personalized healthcare. *Nature Electronics* **2022**, *5* (3), 142-156. DOI: 10.1038/s41928-022-00723-z.

(10) Islam, M. R.; Afroj, S.; Novoselov, K. S.; Karim, N. Smart Electronic Textile-Based Wearable Supercapacitors. *Advanced Science* **2022**, *9* (31), 2203856. DOI: 10.1002/advs.202203856.

(11) Simon, P.; Gogotsi, Y. Materials for electrochemical capacitors. *Nature Materials* **2008**, *7* (11), 845-854. DOI: 10.1038/nmat2297.

(12) Xu, G.; Nie, P.; Dou, H.; Ding, B.; Li, L.; Zhang, X. Exploring metal organic frameworks for energy storage in batteries and supercapacitors. *Materials Today* **2017**, *20* (4), 191-209. DOI: 10.1016/j.mattod.2016.10.003.

(13) Zhang, L. L.; Zhao, X. S. Carbon-based materials as supercapacitor electrodes. *Chemical Society Reviews* **2009**, *38* (9), 2520-2531, 10.1039/B813846J. DOI: 10.1039/B813846J.
(14) Yan, J.; Wang, Q.; Wei, T.; Fan, Z. Recent Advances in Design and Fabrication of Electrochemical Supercapacitors with High Energy Densities. *Advanced Energy Materials* **2014**, *4* (4), 1300816, https://doi.org/10.1002/aenm.201300816. DOI: 10.1002/aenm.201300816 (acccessed 2023/07/21).
(15) Cui, Y.; Shi, Q.; Liu, Z.; Lv, J.; Wang, C.; Xie, X.; Zhang, S. MXene/biomass/chitosan carbon aerogel (MBC) with shared cathode and anode for the construction of high-efficiency asymmetric supercapacitor. *Chemical Engineering Journal* **2023**, *472*, 144701. DOI: 10.1016/j.cej.2023.144701.
(16) Huang, Q.; Wang, D.; Zheng, Z. Textile-Based Electrochemical Energy Storage Devices. *Advanced Energy Materials* **2016**, *6* (22), 1-28. DOI: 10.1002/aenm.201600783.
(17) Li, W. C.; Mak, C. L.; Kan, C. W.; Hui, C. Y. Enhancing the capacitive performance of a textile-based CNT supercapacitor. *RSC Advances* **2014**, *4* (110), 64890-64900, 10.1039/C4RA10450A. DOI: 10.1039/C4RA10450A.
(18) Zhang, H.; Qiao, Y.; Lu, Z. Fully printed ultraflexible supercapacitor supported by a single-textile substrate. *ACS Applied Materials and Interfaces* **2016**, *8* (47), 32317-32323. DOI: 10.1021/acsami.6b11172.
(19) Jost, K.; Stenger, D.; Perez, C. R.; McDonough, J. K.; Lian, K.; Gogotsi, Y.; Dion, G. Knitted and screen printed carbon-fiber supercapacitors for applications in wearable electronics. *Energy & Environmental Science* **2013**, *6* (9), 2698-2705, 10.1039/C3EE40515J. DOI: 10.1039/C3EE40515J.
(20) Li, L.; Wu, Z.; Yuan, S.; Zhang, X. B. Advances and challenges for flexible energy storage and conversion devices and systems. *Energy and Environmental Science* **2014**, *7* (7), 2101-2122. DOI: 10.1039/c4ee00318g.
(21) Islam, G. M. N.; Ali, A.; Collie, S. Textile sensors for wearable applications: a comprehensive review. *Cellulose* **2020**, *27* (11), 6103-6131. DOI: 10.1007/s10570-020-03215-5.
(22) Karim, N.; Afroj, S.; Malandraki, A.; Butterworth, S.; Beach, C.; Rigout, M.; Novoselov, K. S.; Casson, A. J.; Yeates, S. G. All inkjet-printed graphene-based conductive patterns for wearable e-textile applications. *Journal of Materials Chemistry C* **2017**, *5* (44), 11640-11648, 10.1039/C7TC03669H. DOI: 10.1039/C7TC03669H.

(23) Hu, G.; Kang, J.; Ng, L. W. T.; Zhu, X.; Howe, R. C. T.; Jones, C. G.; Hersam, M. C.; Hasan, T. Functional inks and printing of two-dimensional materials. *Chemical Society Reviews* **2018**, *47* (9), 3265-3300. DOI: 10.1039/c8cs00084k.

(24) Yao, L.; Zhou, C.; Hu, N.; Hu, J.; Hong, M.; Zhang, L.; Zhang, Y. Flexible graphene/carbon nanotube hybrid papers chemical-reduction-tailored by gallic acid for high-performance electrochemical capacitive energy storages. *Applied Surface Science* **2018**, *435*, 699-707. DOI: 10.1016/j.apsusc.2017.11.163.

(25) Karim, N.; Afroj, S.; Tan, S.; He, P.; Fernando, A.; Carr, C.; Novoselov, K. S. Scalable Production of Graphene-Based Wearable E-Textiles. *ACS Nano* **2017**, *11* (12), 12266-12275. DOI: 10.1021/acsnano.7b05921.

(26) Afroj, S.; Tan, S.; Abdelkader, A. M.; Novoselov, K. S.; Karim, N. Highly Conductive, Scalable, and Machine Washable Graphene-Based E-Textiles for Multifunctional Wearable Electronic Applications. *Advanced Functional Materials* **2020**. DOI: 10.1002/adfm.202000293.

(27) Mao, M.; Hu, J.; Liu, H. Graphene-based materials for flexible electrochemical energy storage. *International Journal of Energy Research* **2015**, *39* (6), 727-740. DOI: 10.1002/er.3256.

(28) Sundriyal, P.; Bhattacharya, S. Textile-based supercapacitors for flexible and wearable electronic applications. *Scientific Reports* **2020**, *10* (1), 13259. DOI: 10.1038/s41598-020-70182-z.

(29) Liu, J.; Wang, J.; Xu, C.; Jiang, H.; Li, C.; Zhang, L.; Lin, J.; Shen, Z. X. Advanced Energy Storage Devices: Basic Principles, Analytical Methods, and Rational Materials Design. *Advanced Science* **2018**, *5* (1), 1700322. DOI: 10.1002/advs.201700322.

(30) Wicaksono, I.; Tucker, C. I.; Sun, T.; Guerrero, C. A.; Liu, C.; Woo, W. M.; Pence, E. J.; Dagdeviren, C. A tailored, electronic textile conformable suit for large-scale spatiotemporal physiological sensing in vivo. *npj Flexible Electronics* **2020**, *4* (1), 5. DOI: 10.1038/s41528-020-0068-y.

(31) Ismar, E.; Kurşun Bahadir, S.; Kalaoglu, F.; Koncar, V. Futuristic Clothes: Electronic Textiles and Wearable Technologies. *Global Challenges* **2020**, *4* (7), 1900092, https://doi.org/10.1002/gch2.201900092. DOI: 10.1002/gch2.201900092 (acccessed 2021/07/06).

(32) Peng, H.; Sun, X.; Cai, F.; Chen, X.; Zhu, Y.; Liao, G.; Chen, D.; Li, Q.; Lu, Y.; Zhu, Y.; et al. Electrochromatic carbon nanotube/polydiacetylene nanocomposite fibres. *Nature Nanotechnology* **2009**, *4* (11), 738-741. DOI: 10.1038/nnano.2009.264.

(33) Shi, X.; Zuo, Y.; Zhai, P.; Shen, J.; Yang, Y.; Gao, Z.; Liao, M.; Wu, J.; Wang, J.; Xu, X.; et al. Large-area display textiles integrated with functional systems. *Nature* **2021**, *591* (7849), 240-245. DOI: 10.1038/s41586-021-03295-8.

(34) Wang, L.; Xie, S.; Wang, Z.; Liu, F.; Yang, Y.; Tang, C.; Wu, X.; Liu, P.; Li, Y.; Saiyin, H.; et al. Functionalized helical fibre bundles of carbon nanotubes as electrochemical sensors for long-term in vivo monitoring of multiple disease biomarkers. *Nature Biomedical Engineering* **2020**, *4* (2), 159-171. DOI: 10.1038/s41551-019-0462-8.

(35) Zhang, Z.; Guo, K.; Li, Y.; Li, X.; Guan, G.; Li, H.; Luo, Y.; Zhao, F.; Zhang, Q.; Wei, B.; et al. A colour-tunable, weavable fibre-shaped polymer light-emitting electrochemical cell. *Nature Photonics* **2015**, *9* (4), 233-238. DOI: 10.1038/nphoton.2015.37.

(36) Lin, R.; Kim, H.-J.; Achavananthadith, S.; Xiong, Z.; Lee, J. K. W.; Kong, Y. L.; Ho, J. S. Digitally-embroidered liquid metal electronic textiles for wearable wireless systems. *Nature Communications* **2022**, *13* (1), 2190. DOI: 10.1038/s41467-022-29859-4.

(37) Karim, N.; Afroj, S.; Lloyd, K.; Oaten, L. C.; Andreeva, D. V.; Carr, C.; Farmery, A. D.; Kim, I.-D.; Novoselov, K. S. Sustainable Personal Protective Clothing for Healthcare Applications: A Review. *ACS Nano* **2020**, *14* (10), 12313-12340. DOI: 10.1021/acsnano.0c05537.

(38) Heo, J. S.; Eom, J.; Kim, Y. H.; Park, S. K. Recent Progress of Textile-Based Wearable Electronics: A Comprehensive Review of Materials, Devices, and Applications. *Small* **2018**, *14* (3), 1-16. DOI: 10.1002/smll.201703034.

(39) Zhang, Y.; Wang, H.; Lu, H.; Li, S.; Zhang, Y. Electronic fibers and textiles: Recent progress and perspective. *iScience* **2021**, *24* (7), 102716. DOI: 10.1016/j.isci.2021.102716.

(40) Zhao, J.; Fu, Y.; Xiao, Y.; Dong, Y.; Wang, X.; Lin, L. A Naturally Integrated Smart Textile for Wearable Electronics Applications. *Advanced Materials Technologies* **2020**, *5* (1), 1900781. DOI: 10.1002/admt.201900781.

(41) Kaushik, V.; Lee, J.; Hong, J.; Lee, S.; Lee, S.; Seo, J.; Mahata, C.; Lee, T. Textile-Based Electronic Components for Energy Applications: Principles, Problems, and Perspective. *Nanomaterials (Basel)* **2015**, *5* (3), 1493-1531. DOI: 10.3390/nano5031493 PubMed.

(42) Hatamie, A.; Angizi, S.; Kumar, S.; Pandey, C. M.; Simchi, A.; Willander, M.; Malhotra, B. D. Review—Textile Based Chemical and Physical Sensors for Healthcare Monitoring. *Journal of The Electrochemical Society* **2020**, *167* (3), 037546. DOI: 10.1149/1945-7111/ab6827.

(43) Karim, N.; Afroj, S.; Malandraki, A.; Butterworth, S.; Beach, C.; Rigout, M.; Novoselov, K. S.; Casson, A. J.; Yeates, S. G. All inkjet-printed graphene-based conductive patterns for

wearable e-textile applications. *Journal of Materials Chemistry C* **2017**. DOI: 10.1039/c7tc03669h.

(44) Chen, J.; Huang, Y.; Zhang, N.; Zou, H.; Liu, R.; Tao, C.; Fan, X.; Wang, Z. L. Micro-cable structured textile for simultaneously harvesting solar and mechanical energy. *Nature Energy* **2016**, *1* (10), 16138. DOI: 10.1038/nenergy.2016.138.

(45) Yang, Y.; Huang, Q.; Niu, L.; Wang, D.; Yan, C.; She, Y.; Zheng, Z. Waterproof, Ultrahigh Areal-Capacitance, Wearable Supercapacitor Fabrics. *Advanced Materials* **2017**, *29* (19), 1606679. DOI: 10.1002/adma.201606679.

(46) Ahmed, S.; Ahmed, A.; Rafat, M. Supercapacitor performance of activated carbon derived from rotten carrot in aqueous, organic and ionic liquid based electrolytes. *Journal of Saudi Chemical Society* **2018**, *22* (8), 993-1002. DOI: 10.1016/j.jscs.2018.03.002.

(47) Palchoudhury, S.; Ramasamy, K.; Gupta, R. K.; Gupta, A. Flexible Supercapacitors: A Materials Perspective. *Frontiers in Materials* **2019**, *5* (83), Mini Review. DOI: 10.3389/fmats.2018.00083.

(48) Gu, Y.; Zhang, T.; Chen, H.; Wang, F.; Pu, Y.; Gao, C.; Li, S. Mini Review on Flexible and Wearable Electronics for Monitoring Human Health Information. *Nanoscale Research Letters* **2019**, *14* (1), 263. DOI: 10.1186/s11671-019-3084-x.

(49) Shi, S.; Xu, C.; Yang, C.; Li, J.; Du, H.; Li, B.; Kang, F. Flexible supercapacitors. *Particuology* **2013**, *11* (4), 371-377. DOI: 10.1016/j.partic.2012.12.004.

(50) Islam, M. R.; Afroj, S.; Yin, J.; Novoselov, K. S.; Chen, J.; Karim, N. Advances in Printed Electronic Textiles. *Advanced Science* **2023**, *n/a* (n/a). DOI: 10.1002/advs.202304140.

(51) Price, A. 12 - Energy storage for small and micro combined heat and power (CHP) systems. In *Small and Micro Combined Heat and Power (CHP) Systems*, Beith, R. Ed.; Woodhead Publishing, 2011; pp 307-322.

(52) Liu, G.; Qu, L.; Zeng, R.; Gao, F. 12 - Energy Internet in China. In *The Energy Internet*, Su, W., Huang, A. Q. Eds.; Woodhead Publishing, 2019; pp 265-282.

(53) Kalaiselvam, S.; Parameshwaran, R. Chapter 2 - Energy Storage. In *Thermal Energy Storage Technologies for Sustainability*, Kalaiselvam, S., Parameshwaran, R. Eds.; Academic Press, 2014; pp 21-56.

(54) Hussain, F.; Rahman, M. Z.; Sivasengaran, A. N.; Hasanuzzaman, M. Chapter 6 - Energy storage technologies. In *Energy for Sustainable Development*, Hasanuzzaman, M. D., Rahim, N. A. Eds.; Academic Press, 2020; pp 125-165.

(55) Wang, Y.; Xu, Y.; Qiu, J. Chapter 6 - Distributed finite-time control of aggregated energy storage systems for frequency regulation in multiarea microgrids. In *Distributed Control*

Methods and Cyber Security Issues in Microgrids, Meng, W., Wang, X., Liu, S. Eds.; Academic Press, 2020; pp 149-176.

(56) Pollet, B. G.; Staffell, I.; Shang, J. L.; Molkov, V. 22 - Fuel-cell (hydrogen) electric hybrid vehicles. In *Alternative Fuels and Advanced Vehicle Technologies for Improved Environmental Performance*, Folkson, R. Ed.; Woodhead Publishing, 2014; pp 685-735.

(57) Huggins, R. A. Introduction to Electrochemical Energy Storage. In *Energy Storage: Fundamentals, Materials and Applications*, Huggins, R. Ed.; Springer International Publishing, 2016; pp 119-144.

(58) Vix-Guterl, C.; Frackowiak, E.; Jurewicz, K.; Friebe, M.; Parmentier, J.; Béguin, F. Electrochemical energy storage in ordered porous carbon materials. *Carbon* **2005**, *43* (6), 1293-1302. DOI: 10.1016/j.carbon.2004.12.028.

(59) Rakhi, R. B. 16 - Preparation and properties of manipulated carbon nanotube composites and applications. In *Nanocarbon and its Composites*, Khan, A., Jawaid, M., Inamuddin, Asiri, A. M. Eds.; Woodhead Publishing, 2019; pp 489-520.

(60) Chen, K.; Xue, D. Materials chemistry toward electrochemical energy storage. *Journal of Materials Chemistry A* **2016**, *4* (20), 7522-7537, 10.1039/C6TA01527A. DOI: 10.1039/C6TA01527A.

(61) Lv, W.; Li, Z.; Deng, Y.; Yang, Q.-H.; Kang, F. Graphene-based materials for electrochemical energy storage devices: Opportunities and challenges. *Energy Storage Materials* **2016**, *2*, 107-138. DOI: 10.1016/j.ensm.2015.10.002.

(62) Jost, K.; Dion, G.; Gogotsi, Y. Textile energy storage in perspective. *Journal of Materials Chemistry A* **2014**, *2* (28), 10776-10787, 10.1039/C4TA00203B. DOI: 10.1039/C4TA00203B.

(63) Pandolfo, A. G.; Hollenkamp, A. F. Carbon properties and their role in supercapacitors. *Journal of Power Sources* **2006**, *157* (1), 11-27. DOI: https://doi.org/10.1016/j.jpowsour.2006.02.065.

(64) A, D.; Hegde, G. Activated carbon nanospheres derived from bio-waste materials for supercapacitor applications – a review. *RSC Advances* **2015**, *5* (107), 88339-88352, 10.1039/C5RA19392C. DOI: 10.1039/C5RA19392C.

(65) Zhang, S.; Pan, N. Supercapacitors Performance Evaluation. *Advanced Energy Materials* **2015**, *5* (6), 1401401, https://doi.org/10.1002/aenm.201401401. DOI: 10.1002/aenm.201401401 (acccessed 2021/03/10).

(66) Abbas, Q.; Mirzaeian, M.; Hunt, M. R. C.; Hall, P.; Raza, R. Current State and Future Prospects for Electrochemical Energy Storage and Conversion Systems. *Energies* **2020**, *13* (21), 5847. DOI: 10.3390/en13215847.

(67) Lokhande, P. E.; Chavan, U. S.; Pandey, A. Materials and Fabrication Methods for Electrochemical Supercapacitors: Overview. *Electrochemical Energy Reviews* **2020**, *3* (1), 155-186. DOI: 10.1007/s41918-019-00057-z.
(68) Zhang, Y.; Feng, H.; Wu, X.; Wang, L.; Zhang, A.; Xia, T.; Dong, H.; Li, X.; Zhang, L. Progress of electrochemical capacitor electrode materials: A review. *International Journal of Hydrogen Energy* **2009**, *34* (11), 4889-4899. DOI: 10.1016/j.ijhydene.2009.04.005.
(69) You, X.; Misra, M.; Gregori, S.; Mohanty, A. K. Preparation of an Electric Double Layer Capacitor (EDLC) Using Miscanthus-Derived Biocarbon. *ACS Sustainable Chemistry & Engineering* **2018**, *6* (1), 318-324. DOI: 10.1021/acssuschemeng.7b02563.
(70) Hui, C.-y.; Kan, C.-w.; Mak, C.-l.; Chau, K.-h. Flexible Energy Storage System—An Introductory Review of Textile-Based Flexible Supercapacitors. *Processes* **2019**, *7* (12). DOI: 10.3390/pr7120922.
(71) Miao, Y.-E.; Liu, T. Chapter 21 - Electrospun Nanofiber Electrodes: A Promising Platform for Supercapacitor Applications. In *Electrospinning: Nanofabrication and Applications*, Ding, B., Wang, X., Yu, J. Eds.; William Andrew Publishing, 2019; pp 641-669.
(72) Choi, C.; Ashby, D. S.; Butts, D. M.; DeBlock, R. H.; Wei, Q.; Lau, J.; Dunn, B. Achieving high energy density and high power density with pseudocapacitive materials. *Nature Reviews Materials* **2020**, *5* (1), 5-19. DOI: 10.1038/s41578-019-0142-z.
(73) Viswanathan, B. Chapter 13 - Supercapacitors. In *Energy Sources*, Viswanathan, B. Ed.; Elsevier, 2017; pp 315-328.
(74) Gazal, U.; Khan, I.; Usmani, M. A.; Bhat, A. H. 11 - Modification of polymer nanocomposites and significance of ionic liquid for supercapacitor application. In *Polymer-based Nanocomposites for Energy and Environmental Applications*, Jawaid, M., Khan, M. M. Eds.; Woodhead Publishing, 2018; pp 315-332.
(75) Muzaffar, A.; Ahamed, M. B.; Deshmukh, K.; Thirumalai, J. A review on recent advances in hybrid supercapacitors: Design, fabrication and applications. *Renewable and Sustainable Energy Reviews* **2019**, *101*, 123-145. DOI: https://doi.org/10.1016/j.rser.2018.10.026.
(76) Karthikeyan, K.; Amaresh, S.; Kim, K. J.; Kim, S. H.; Chung, K. Y.; Cho, B. W.; Lee, Y. S. A high performance hybrid capacitor with Li2CoPO4F cathode and activated carbon anode. *Nanoscale* **2013**, *5* (13), 5958-5964, 10.1039/C3NR00760J. DOI: 10.1039/C3NR00760J.
(77) Qian, C.; Yongji, G. Applications and Challenges of 2D Materials in Lithium Metal Batteries. *Materials Lab* **2022**, *1*, 220034-220031-220034-220035. DOI: 10.54227/mlab.20220034.

(78) Xiang-Xi, H.; Jia-Hua, Z.; Wei-Hong, L.; Zhuo, Y.; Yun, G.; Hang, Z.; Yun, Q.; Li, L.; Shu-Lei, C. Challenges and Applications of Flexible Sodium Ion Batteries. *Materials Lab* **2022**, *1* (1), 210001-210001-210001-210024. DOI: 10.54227/mlab.20210001.

(79) Ren, J.; Li, L.; Chen, C.; Chen, X.; Cai, Z.; Qiu, L.; Wang, Y.; Zhu, X.; Peng, H. Twisting Carbon Nanotube Fibers for Both Wire-Shaped Micro-Supercapacitor and Micro-Battery. *Advanced Materials* **2013**, *25* (8), 1155-1159. DOI: 10.1002/adma.201203445.

(80) He, J.; Lu, C.; Jiang, H.; Han, F.; Shi, X.; Wu, J.; Wang, L.; Chen, T.; Wang, J.; Zhang, Y.; et al. Scalable production of high-performing woven lithium-ion fibre batteries. *Nature* **2021**, *597* (7874), 57-63. DOI: 10.1038/s41586-021-03772-0.

(81) Weston, A.; Castanon, E. G.; Enaldiev, V.; Ferreira, F.; Bhattacharjee, S.; Xu, S.; Corte-León, H.; Wu, Z.; Clark, N.; Summerfield, A.; et al. Interfacial ferroelectricity in marginally twisted 2D semiconductors. *Nature Nanotechnology* **2022**, *17* (4), 390-395. DOI: 10.1038/s41565-022-01072-w.

(82) Ali, A. E.; Jeoti, V.; Stojanović, G. M. Fabric based printed-distributed battery for wearable e-textiles: a review. *Science and Technology of Advanced Materials* **2021**, *22* (1), 772-793. DOI: 10.1080/14686996.2021.1962203.

(83) Liao, M.; Wang, C.; Hong, Y.; Zhang, Y.; Cheng, X.; Sun, H.; Huang, X.; Ye, L.; Wu, J.; Shi, X.; et al. Industrial scale production of fibre batteries by a solution-extrusion method. *Nature Nanotechnology* **2022**, *17* (4), 372-377. DOI: 10.1038/s41565-021-01062-4.

(84) Zhang, Z.; Guo, X.; Wen, F.; Shi, Q.; He, T.; Dong, B.; Lee, C. Development of Triboelectric Sensors for IoT and Wearable Applications. In *Reference Module in Biomedical Sciences*, Elsevier, 2021.

(85) Lessing, J.; Glavan, A. C.; Walker, S. B.; Keplinger, C.; Lewis, J. A.; Whitesides, G. M. Inkjet Printing of Conductive Inks with High Lateral Resolution on Omniphobic "RF Paper" for Paper-Based Electronics and MEMS. *Advanced Materials* **2014**, *26* (27), 4677-4682. DOI: 10.1002/adma.201401053.

(86) Maddipatla, D.; Narakathu, B. B.; Ali, M. M.; Chlaihawi, A. A.; Atashbar, M. Z. Development of a novel carbon nanotube based printed and flexible pressure sensor. In *2017 IEEE Sensors Applications Symposium (SAS)*, 13-15 March 2017, 2017; pp 1-4. DOI: 10.1109/SAS.2017.7894034.

(87) Maddipatla, D.; Narakathu, B. B.; Atashbar, M. Recent Progress in Manufacturing Techniques of Printed and Flexible Sensors: A Review. *Biosensors* **2020**, *10* (12), 199. DOI: 10.3390/bios10120199.

(88) Sreenilayam, S. P.; Ahad, I. U.; Nicolosi, V.; Acinas Garzon, V.; Brabazon, D. Advanced materials of printed wearables for physiological parameter monitoring. *Materials Today* **2020**, *32*, 147-177. DOI: 10.1016/j.mattod.2019.08.005.

(89) Zhao, Y.; Zhang, Z.; Ren, Y.; Ran, W.; Chen, X.; Wu, J.; Gao, F. Vapor deposition polymerization of aniline on 3D hierarchical porous carbon with enhanced cycling stability as supercapacitor electrode. *Journal of Power Sources* **2015**, *286*, 1-9. DOI: 10.1016/j.jpowsour.2015.03.141.

(90) Lin, T.; Zhang, Y. Q.; Zhang, L.; Klappenberger, F. On-Surface Chemistry of Alkyne Derivatives. In *Encyclopedia of Interfacial Chemistry*, Wandelt, K. Ed.; Elsevier, 2018; pp 324-334.

(91) Liao, C.; Li, Y.; Tjong, S. C. Graphene Nanomaterials: Synthesis, Biocompatibility, and Cytotoxicity. *International Journal of Molecular Sciences* **2018**, *19* (11). DOI: 10.3390/ijms19113564.

(92) Yuansheng, J.; Shenghua, L. 24 - Superlubricity of In Situ Generated Protective Layer on Worn Metal Surfaces in Presence of Mg6Si4O10(OH)8. In *Superlubricity*, Erdemir, A., Martin, J.-M. Eds.; Elsevier Science B.V., 2007; pp 445-469.

(93) Mallakpour, S.; Rashidimoghadam, S. 9 - Carbon Nanotubes for Dyes Removal. In *Composite Nanoadsorbents*, Kyzas, G. Z., Mitropoulos, A. C. Eds.; Elsevier, 2019; pp 211-243.

(94) Eatemadi, A.; Daraee, H.; Karimkhanloo, H.; Kouhi, M.; Zarghami, N.; Akbarzadeh, A.; Abasi, M.; Hanifehpour, Y.; Joo, S. W. Carbon nanotubes: properties, synthesis, purification, and medical applications. *Nanoscale Research Letters* **2014**, *9* (1), 393. DOI: 10.1186/1556-276X-9-393.

(95) Lu, Z.; Raad, R.; Safaei, F.; Xi, J.; Liu, Z.; Foroughi, J. Carbon Nanotube Based Fiber Supercapacitor as Wearable Energy Storage. *Frontiers in Materials* **2019**, *6*, Review. DOI: 10.3389/fmats.2019.00138.

(96) Zhang, D.; Miao, M.; Niu, H.; Wei, Z. Core-spun carbon nanotube yarn supercapacitors for wearable electronic textiles. *ACS Nano* **2014**, *8* (5), 4571-4579. DOI: 10.1021/nn5001386 From NLM.

(97) Choi, C.; Park, J. W.; Kim, K. J.; Lee, D. W.; de Andrade, M. J.; Kim, S. H.; Gambhir, S.; Spinks, G. M.; Baughman, R. H.; Kim, S. J. Weavable asymmetric carbon nanotube yarn supercapacitor for electronic textiles. *RSC Advances* **2018**, *8* (24), 13112-13120, 10.1039/C8RA01384E. DOI: 10.1039/C8RA01384E.

(98) Guan, C.; Qian, X.; Wang, X.; Cao, Y.; Zhang, Q.; Li, A.; Wang, J. Atomic layer deposition of Co3O4 on carbon nanotubes/carbon cloth for high-capacitance and ultrastable supercapacitor electrode. *Nanotechnology* **2015**, *26* (9), 094001. DOI: 10.1088/0957-4484/26/9/094001.

(99) Lv, T.; Yao, Y.; Li, N.; Chen, T. Highly Stretchable Supercapacitors Based on Aligned Carbon Nanotube/Molybdenum Disulfide Composites. *Angewandte Chemie International Edition* **2016**, *55* (32), 9191-9195. DOI: 10.1002/anie.201603356.

(100) Marsh, H.; Rodríguez-Reinoso, F. CHAPTER 9 - Production and Reference Material. In *Activated Carbon*, Marsh, H., Rodríguez-Reinoso, F. Eds.; Elsevier Science Ltd, 2006; pp 454-508.

(101) Talarico, D.; Arduini, F.; Constantino, A.; Del Carlo, M.; Compagnone, D.; Moscone, D.; Palleschi, G. Carbon black as successful screen-printed electrode modifier for phenolic compound detection. *Electrochemistry Communications* **2015**, *60*, 78-82. DOI: 10.1016/j.elecom.2015.08.010.

(102) Kossyrev, P. Carbon black supercapacitors employing thin electrodes. *Journal of Power Sources* **2012**, *201*, 347-352. DOI: 10.1016/j.jpowsour.2011.10.106.

(103) Yang, K.; Cho, K.; Kim, S. Effect of carbon black addition on thermal stability and capacitive performances of supercapacitors. *Scientific Reports* **2018**, *8* (1), 11989. DOI: 10.1038/s41598-018-30507-5.

(104) Jäckel, N.; Weingarth, D.; Zeiger, M.; Aslan, M.; Grobelsek, I.; Presser, V. Comparison of carbon onions and carbon blacks as conductive additives for carbon supercapacitors in organic electrolytes. *Journal of Power Sources* **2014**, *272*, 1122-1133. DOI: 10.1016/j.jpowsour.2014.08.090.

(105) Gu, W.; Yushin, G. Review of nanostructured carbon materials for electrochemical capacitor applications: advantages and limitations of activated carbon, carbide-derived carbon, zeolite-templated carbon, carbon aerogels, carbon nanotubes, onion-like carbon, and graphene. *WIREs Energy and Environment* **2014**, *3* (5), 424-473, https://doi.org/10.1002/wene.102. DOI: 10.1002/wene.102 (acccessed 2021/03/11).

(106) Sinha, P.; Banerjee, S.; Kar, K. K. Activated Carbon as Electrode Materials for Supercapacitors. In *Handbook of Nanocomposite Supercapacitor Materials II: Performance*, Kar, K. K. Ed.; Springer International Publishing, 2020; pp 113-144.

(107) Choi, J.-H. Fabrication of a carbon electrode using activated carbon powder and application to the capacitive deionization process. *Separation and Purification Technology* **2010**, *70* (3), 362-366. DOI: 10.1016/j.seppur.2009.10.023.

(108) Merin, P.; Jimmy Joy, P.; Muralidharan, M. N.; Veena Gopalan, E.; Seema, A. Biomass-Derived Activated Carbon for High-Performance Supercapacitor Electrode Applications. *Chemical Engineering & Technology* **2021**, *44* (5), 844-851. DOI: 10.1002/ceat.202000450.
(109) Phiri, J.; Dou, J.; Vuorinen, T.; Gane, P. A. C.; Maloney, T. C. Highly Porous Willow Wood-Derived Activated Carbon for High-Performance Supercapacitor Electrodes. *ACS Omega* **2019**, *4* (19), 18108-18117. DOI: 10.1021/acsomega.9b01977.
(110) Piñeiro-Prado, I.; Salinas-Torres, D.; Ruiz-Rosas, R.; Morallón, E.; Cazorla-Amorós, D. Design of Activated Carbon/Activated Carbon Asymmetric Capacitors. *Frontiers in Materials* **2016**, *3*, Original Research. DOI: 10.3389/fmats.2016.00016.
(111) Afroj, S.; Britnell, L.; Hasan, T.; Andreeva, D. V.; Novoselov, K. S.; Karim, N. Graphene-Based Technologies for Tackling COVID-19 and Future Pandemics. *Advanced Functional Materials* **2021**, *n/a* (n/a), 2107407, https://doi.org/10.1002/adfm.202107407. DOI: https://doi.org/10.1002/adfm.202107407 (acccessed 2021/09/25).
(112) Bhattacharjee, S.; Joshi, R.; Chughtai, A. A.; Macintyre, C. R. Graphene Modified Multifunctional Personal Protective Clothing. *Advanced Materials Interfaces* **2019**, *6* (21), 1900622. DOI: 10.1002/admi.201900622.
(113) Islam, M. H.; Afroj, S.; Uddin, M. A.; Andreeva, D. V.; Novoselov, K. S.; Karim, N. Graphene and CNT-Based Smart Fiber-Reinforced Composites: A Review. *Advanced Functional Materials* **2022**, *32* (40), 2205723. DOI: 10.1002/adfm.202205723.
(114) Mutalib, M. A.; Rashid, N. M.; Aziz, F. 22 - Carbon-Based Polymer Nanocomposite for Photovoltaic Devices. In *Carbon-Based Polymer Nanocomposites for Environmental and Energy Applications*, Ismail, A. F., Goh, P. S. Eds.; Elsevier, 2018; pp 559-584.
(115) Inagaki, M.; Kang, F.; Toyoda, M.; Konno, H. Chapter 3 - Graphene: Synthesis and Preparation. In *Advanced Materials Science and Engineering of Carbon*, Inagaki, M., Kang, F., Toyoda, M., Konno, H. Eds.; Butterworth-Heinemann, 2014; pp 41-65.
(116) Kumar, R.; Sahoo, S.; Joanni, E.; Singh, R. K.; Yadav, R. M.; Verma, R. K.; Singh, D. P.; Tan, W. K.; Pérez del Pino, A.; Moshkalev, S. A.; et al. A review on synthesis of graphene, h-BN and MoS2 for energy storage applications: Recent progress and perspectives. *Nano Research* **2019**, *12* (11), 2655-2694. DOI: 10.1007/s12274-019-2467-8.
(117) Papageorgiou, D. G.; Kinloch, I. A.; Young, R. J. Graphene/elastomer nanocomposites. *Carbon* **2015**, *95*, 460-484. DOI: 10.1016/j.carbon.2015.08.055.
(118) Ciesielski, A.; Samorì, P. Graphene via sonication assisted liquid-phase exfoliation. *Chemical Society Reviews* **2014**, *43* (1), 381-398, 10.1039/C3CS60217F. DOI: 10.1039/C3CS60217F.

(119) Karim, N.; Zhang, M.; Afroj, S.; Koncherry, V.; Potluri, P.; Novoselov, K. S. Graphene-based surface heater for de-icing applications. *RSC Advances* **2018**, *8* (30), 16815-16823, 10.1039/C8RA02567C. DOI: 10.1039/C8RA02567C.

(120) Lemine, A. S.; Zagho, M. M.; Altahtamouni, T. M.; Bensalah, N. Graphene a promising electrode material for supercapacitors—A review. *International Journal of Energy Research* **2018**, *42* (14), 4284-4300, https://doi.org/10.1002/er.4170. DOI: 10.1002/er.4170 (acccessed 2021/03/10).

(121) Chakraborty, M.; Hashmi, M. S. J. Graphene as a Material@ An Overview of Its Properties and Characteristics and Development Potential for Practical Applications. 2018.

(122) Banerjee, S.; Lee, J. H.; Kuila, T.; Kim, N. H. 7 - Synthesis of graphene-based polymeric nanocomposites. In *Fillers and Reinforcements for Advanced Nanocomposites*, Dong, Y., Umer, R., Lau, A. K.-T. Eds.; Woodhead Publishing, 2015; pp 133-155.

(123) Xu, T.; Sun, L. 5 - Structural defects in graphene. In *Defects in Advanced Electronic Materials and Novel Low Dimensional Structures*, Stehr, J., Buyanova, I., Chen, W. Eds.; Woodhead Publishing, 2018; pp 137-160.

(124) Bhattacharjee, S.; Macintyre, C. R.; Bahl, P.; Kumar, U.; Wen, X.; Aguey-Zinsou, K.-F.; Chughtai, A. A.; Joshi, R. Reduced Graphene Oxide and Nanoparticles Incorporated Durable Electroconductive Silk Fabrics. *Advanced Materials Interfaces* **2020**, *7* (20), 2000814. DOI: 10.1002/admi.202000814.

(125) Karim, N.; Afroj, S.; Leech, D.; Abdelkader, A. M. Flexible and Wearable Graphene-Based E-Textiles. In *Oxide Electronics*, Ray, A. Ed.; John Wiley & Sons, Ltd.j, 2021.

(126) Afroj, S.; Karim, N.; Wang, Z.; Tan, S.; He, P.; Holwill, M.; Ghazaryan, D.; Fernando, A.; Novoselov, K. S. Engineering Graphene Flakes for Wearable Textile Sensors via Highly Scalable and Ultrafast Yarn Dyeing Technique. *ACS Nano* **2019**, *13* (4), 3847-3857. DOI: 10.1021/acsnano.9b00319.

(127) Sarker, F.; Potluri, P.; Afroj, S.; Koncherry, V.; Novoselov, K. S.; Karim, N. Ultrahigh Performance of Nanoengineered Graphene-Based Natural Jute Fiber Composites. *ACS Applied Materials & Interfaces* **2019**, *11* (23), 21166-21176. DOI: 10.1021/acsami.9b04696.

(128) Kalash, R. S.; Lakshmanan, V. K.; Cho, C.-S.; Park, I.-K. 4.4 - Theranostics. In *Biomaterials Nanoarchitectonics*, Ebara, M. Ed.; William Andrew Publishing, 2016; pp 197-215.

(129) Radhapyari, K.; Datta, S.; Dutta, S.; Jadon, N.; Khan, R. Chapter 4 - Graphene-based nanostructures for biomedical applications. In *Two-Dimensional Nanostructures for Biomedical Technology*, Khan, R., Barua, S. Eds.; Elsevier, 2020; pp 101-135.

(130) Kecili, R.; Hussain, C. M. Chapter 4 - Mechanism of Adsorption on Nanomaterials. In *Nanomaterials in Chromatography*, Hussain, C. M. Ed.; Elsevier, 2018; pp 89-115.
(131) Vandezande, P. 5 - Next-generation pervaporation membranes: recent trends, challenges and perspectives. In *Pervaporation, Vapour Permeation and Membrane Distillation*, Basile, A., Figoli, A., Khayet, M. Eds.; Woodhead Publishing, 2015; pp 107-141.
(132) Sarker, F.; Karim, N.; Afroj, S.; Koncherry, V.; Novoselov, K. S.; Potluri, P. High-Performance Graphene-Based Natural Fiber Composites. *ACS Applied Materials & Interfaces* **2018**, *10* (40), 34502-34512. DOI: 10.1021/acsami.8b13018.
(133) Inagaki, M.; Kang, F. Chapter 3 - Engineering and Applications of Carbon Materials. In *Materials Science and Engineering of Carbon: Fundamentals (Second Edition)*, Inagaki, M., Kang, F. Eds.; Butterworth-Heinemann, 2014; pp 219-525.
(134) Karim, N.; Sarker, F.; Afroj, S.; Zhang, M.; Potluri, P.; Novoselov, K. S. Sustainable and Multifunctional Composites of Graphene-Based Natural Jute Fibers. *Advanced Sustainable Systems* **2021**, *5* (3), 2000228. DOI: 10.1002/adsu.202000228.
(135) Mohan, V. B.; Brown, R.; Jayaraman, K.; Bhattacharyya, D. Characterisation of reduced graphene oxide: Effects of reduction variables on electrical conductivity. *Materials Science and Engineering: B* **2015**, *193*, 49-60. DOI: 10.1016/j.mseb.2014.11.002.
(136) Bayan, R.; Karak, N. Chapter 8 - Polymer nanocomposites based on two-dimensional nanomaterials. In *Two-Dimensional Nanostructures for Biomedical Technology*, Khan, R., Barua, S. Eds.; Elsevier, 2020; pp 249-279.
(137) Islam, M. H.; Islam, M. R.; Dulal, M.; Afroj, S.; Karim, N. The effect of surface treatments and graphene-based modifications on mechanical properties of natural jute fibre reinforced composites: a review. *iScience* **2021**, 103597. DOI: 10.1016/j.isci.2021.103597.
(138) Phiri, J.; Gane, P.; Maloney, T. C. General overview of graphene: Production, properties and application in polymer composites. *Materials Science and Engineering: B* **2017**, *215*, 9-28. DOI: 10.1016/j.mseb.2016.10.004.
(139) Jin, L.-N.; Shao, F.; Jin, C.; Zhang, J.-N.; Liu, P.; Guo, M.-X.; Bian, S.-W. High-performance textile supercapacitor electrode materials enhanced with three-dimensional carbon nanotubes/graphene conductive network and in situ polymerized polyaniline. *Electrochimica Acta* **2017**, *249*, 387-394. DOI: 10.1016/j.electacta.2017.08.035.
(140) Liu, K.; Yao, Y.; Lv, T.; Li, H.; Li, N.; Chen, Z.; Qian, G.; Chen, T. Textile-like electrodes of seamless graphene/nanotubes for wearable and stretchable supercapacitors. *Journal of Power Sources* **2020**, *446*, 227355. DOI: 10.1016/j.jpowsour.2019.227355.

(141) Li, Y.; Chen, C. Polyaniline/carbon nanotubes-decorated activated carbon fiber felt as high-performance, free-standing and flexible supercapacitor electrodes. *Journal of Materials Science* **2017**, *52* (20), 12348-12357. DOI: 10.1007/s10853-017-1291-3.
(142) Rapisarda, M.; Damasco, A.; Abbate, G.; Meo, M. Carbon Black and Reduced Graphene Oxide Nanocomposite for Binder-Free Supercapacitors with Reduced Graphene Oxide Paper as the Current Collector. *ACS Omega* **2020**, *5* (50), 32426-32435. DOI: 10.1021/acsomega.0c04530.
(143) Gürten Inal, I. I. Scalable activated carbon/graphene based supercapacitors with improved capacitance retention at high current densities. *Turk J Chem* **2021**, *45* (3), 927-941. DOI: 10.3906/kim-2012-39 PubMed.
(144) Shown, I.; Ganguly, A.; Chen, L.-C.; Chen, K.-H. Conducting polymer-based flexible supercapacitor. *Energy Science & Engineering* **2015**, *3* (1), 2-26. DOI: 10.1002/ese3.50.
(145) Bhandari, S. Chapter 2 - Polyaniline: Structure and Properties Relationship. In *Polyaniline Blends, Composites, and Nanocomposites*, Visakh, P. M., Pina, C. D., Falletta, E. Eds.; Elsevier, 2018; pp 23-60.
(146) Wang, H.; Lin, J.; Shen, Z. X. Polyaniline (PANi) based electrode materials for energy storage and conversion. *Journal of Science: Advanced Materials and Devices* **2016**, *1* (3), 225-255. DOI: 10.1016/j.jsamd.2016.08.001.
(147) Konwar, G.; Sarma, S. C.; Mahanta, D.; Peter, S. C. Polyaniline Hybrid Nanofibers via Green Interfacial Polymerization for All-Solid-State Symmetric Supercapacitors. *ACS Omega* **2020**, *5* (24), 14494-14501. DOI: 10.1021/acsomega.0c01158.
(148) Ruchi; Gupta, V.; Pal, R.; Goyal, S. L. Efficient energy storage performance of polyaniline based supercapacitor. *AIP Conference Proceedings* **2021**, *2369* (1), 020051. DOI: 10.1063/5.0061431.
(149) Horng, Y.-Y.; Lu, Y.-C.; Hsu, Y.-K.; Chen, C.-C.; Chen, L.-C.; Chen, K.-H. Flexible supercapacitor based on polyaniline nanowires/carbon cloth with both high gravimetric and area-normalized capacitance. *Journal of Power Sources* **2010**, *195* (13), 4418-4422. DOI: 10.1016/j.jpowsour.2010.01.046.
(150) Rahman, M. M.; Joy, P. M.; Uddin, M. N.; Mukhlish, M. Z. B.; Khan, M. M. R. Improvement of capacitive performance of polyaniline based hybrid supercapacitor. *Heliyon* **2021**, *7* (7), e07407. DOI: 10.1016/j.heliyon.2021.e07407.
(151) Parayangattil Jyothibasu, J.; Chen, M.-Z.; Lee, R.-H. Polypyrrole/Carbon Nanotube Freestanding Electrode with Excellent Electrochemical Properties for High-Performance All-

Solid-State Supercapacitors. *ACS Omega* **2020**, *5* (12), 6441-6451. DOI: 10.1021/acsomega.9b04029.

(152) Xue, P.; Tao, X. M.; Kwok, K. W. Y.; Leung, M. Y.; Yu, T. X. Electromechanical Behavior of Fibers Coated with an Electrically Conductive Polymer. *Textile Research Journal* **2004**, *74* (10), 929-936. DOI: 10.1177/004051750407401013.

(153) Harlin, A.; Ferenets, M. 13 - Introduction to conductive materials. In *Intelligent Textiles and Clothing*, Mattila, H. R. Ed.; Woodhead Publishing, 2006; pp 217-238.

(154) Kakaei, K.; Esrafili, M. D.; Ehsani, A. Chapter 9 - Graphene-Based Electrochemical Supercapacitors. In *Interface Science and Technology*, Kakaei, K., Esrafili, M. D., Ehsani, A. Eds.; Vol. 27; Elsevier, 2019; pp 339-386.

(155) Huang, Y.; Li, H.; Wang, Z.; Zhu, M.; Pei, Z.; Xue, Q.; Huang, Y.; Zhi, C. Nanostructured Polypyrrole as a flexible electrode material of supercapacitor. *Nano Energy* **2016**, *22*, 422-438. DOI: 10.1016/j.nanoen.2016.02.047.

(156) Feng, M.; Lu, W.; Zhou, Y.; Zhen, R.; He, H.; Wang, Y.; Li, C. Synthesis of polypyrrole/nitrogen-doped porous carbon matrix composite as the electrode material for supercapacitors. *Scientific Reports* **2020**, *10* (1), 15370. DOI: 10.1038/s41598-020-72392-x.

(157) He, Y.; Ning, X.; Wan, L. Ultrathin graphene oxide@polypyrrole nanosheets as a supercapacitor electrode with high areal specific capacitance. *Polymer Bulletin* **2021**. DOI: 10.1007/s00289-021-03948-8.

(158) Nie, S.; Li, Z.; Yao, Y.; Jin, Y. Progress in Synthesis of Conductive Polymer Poly(3,4-Ethylenedioxythiophene). *Frontiers in chemistry* **2021**, *9*, 803509-803509. DOI: 10.3389/fchem.2021.803509 PubMed.

(159) Koncar, V. 1 - Smart textiles for monitoring and measurement applications. In *Smart Textiles for In Situ Monitoring of Composites*, Koncar, V. Ed.; Woodhead Publishing, 2019; pp 1-151.

(160) Zhao, Z.; Richardson, G. F.; Meng, Q.; Zhu, S.; Kuan, H.-C.; Ma, J. PEDOT-based composites as electrode materials for supercapacitors. *Nanotechnology* **2015**, *27* (4), 042001. DOI: 10.1088/0957-4484/27/4/042001.

(161) Li, B.; Lopez-Beltran, H.; Siu, C.; Skorenko, K. H.; Zhou, H.; Bernier, W. E.; Whittingham, M. S.; Jones, W. E. Vaper Phase Polymerized PEDOT/Cellulose Paper Composite for Flexible Solid-State Supercapacitor. *ACS Applied Energy Materials* **2020**, *3* (2), 1559-1568. DOI: 10.1021/acsaem.9b02044.

(162) Rajesh, M.; Raj, C. J.; Manikandan, R.; Kim, B. C.; Park, S. Y.; Yu, K. H. A high performance PEDOT/PEDOT symmetric supercapacitor by facile in-situ hydrothermal

polymerization of PEDOT nanostructures on flexible carbon fibre cloth electrodes. *Materials Today Energy* **2017**, *6*, 96-104. DOI: 10.1016/j.mtener.2017.09.003.
(163) Worfolk, B. J.; Andrews, S. C.; Park, S.; Reinspach, J.; Liu, N.; Toney, M. F.; Mannsfeld, S. C. B.; Bao, Z. Ultrahigh electrical conductivity in solution-sheared polymeric transparent films. *Proceedings of the National Academy of Sciences* **2015**, *112* (46), 14138-14143. DOI: 10.1073/pnas.1509958112.
(164) Manjakkal, L.; Pullanchiyodan, A.; Yogeswaran, N.; Hosseini, E. S.; Dahiya, R. A Wearable Supercapacitor Based on Conductive PEDOT:PSS-Coated Cloth and a Sweat Electrolyte. *Advanced Materials* **2020**, *32* (24), 1907254. DOI: 10.1002/adma.201907254.
(165) Liu, Y.; Weng, B.; Razal, J. M.; Xu, Q.; Zhao, C.; Hou, Y.; Seyedin, S.; Jalili, R.; Wallace, G. G.; Chen, J. High-Performance Flexible All-Solid-State Supercapacitor from Large Free-Standing Graphene-PEDOT/PSS Films. *Scientific Reports* **2015**, *5* (1), 17045. DOI: 10.1038/srep17045.
(166) Liu, G.; Chen, X.; Liu, J.; Liu, C.; Xu, J.; Jiang, Q.; Jia, Y.; Jiang, F.; Duan, X.; Liu, P. Fabrication of PEDOT:PSS/rGO fibers with high flexibility and electrochemical performance for supercapacitors. *Electrochimica Acta* **2021**, *365*, 137363. DOI: 10.1016/j.electacta.2020.137363.
(167) Khasim, S.; Pasha, A.; Badi, N.; Lakshmi, M.; Mishra, Y. K. High performance flexible supercapacitors based on secondary doped PEDOT–PSS–graphene nanocomposite films for large area solid state devices. *RSC Advances* **2020**, *10* (18), 10526-10539, 10.1039/D0RA01116A. DOI: 10.1039/D0RA01116A.
(168) Yoonessi, M.; Borenstein, A.; El-Kady, M. F.; Turner, C. L.; Wang, H.; Stieg, A. Z.; Pilon, L. Hybrid Transparent PEDOT:PSS Molybdenum Oxide Battery-like Supercapacitors. *ACS Applied Energy Materials* **2019**, *2* (7), 4629-4639. DOI: 10.1021/acsaem.8b02258.
(169) Chukwuneke, C.; Madu, J. O.; Adams, F. V.; Johnson, O. T. Application of Metal Oxides Electrodes. In *Nanostructured Metal-Oxide Electrode Materials for Water Purification: Fabrication, Electrochemistry and Applications*, Ama, O. M., Ray, S. S. Eds.; Springer International Publishing, 2020; pp 127-149.
(170) Zhou, L.; Li, C.; Liu, X.; Zhu, Y.; Wu, Y.; van Ree, T. 7 - Metal oxides in supercapacitors. In *Metal Oxides in Energy Technologies*, Wu, Y. Ed.; Elsevier, 2018; pp 169-203.
(171) Majumdar, D.; Maiyalagan, T.; Jiang, Z. Recent Progress in Ruthenium Oxide-Based Composites for Supercapacitor Applications. *ChemElectroChem* **2019**, *6* (17), 4343-4372, https://doi.org/10.1002/celc.201900668. DOI: 10.1002/celc.201900668 (acccessed 2021/03/11).

(172) Xia, H.; Shirley Meng, Y.; Yuan, G.; Cui, C.; Lu, L. A Symmetric RuO2/RuO2 Supercapacitor Operating at 1.6 V by Using a Neutral Aqueous Electrolyte. *Electrochemical and Solid-State Letters* **2012**, *15* (4), A60. DOI: 10.1149/2.023204esl.
(173) Subramanian, V.; Hall, S. C.; Smith, P. H.; Rambabu, B. Mesoporous anhydrous RuO2 as a supercapacitor electrode material. *Solid State Ionics* **2004**, *175* (1), 511-515. DOI: 10.1016/j.ssi.2004.01.070.
(174) Jeon, S.; Jeong, J. H.; Yoo, H.; Yu, H. K.; Kim, B.-H.; Kim, M. H. RuO2 Nanorods on Electrospun Carbon Nanofibers for Supercapacitors. *ACS Applied Nano Materials* **2020**, *3* (4), 3847-3858. DOI: 10.1021/acsanm.0c00579.
(175) Muniraj, V. K. A.; Dwivedi, P. K.; Tamhane, P. S.; Szunerits, S.; Boukherroub, R.; Shelke, M. V. High-Energy Flexible Supercapacitor—Synergistic Effects of Polyhydroquinone and RuO2·xH2O with Microsized, Few-Layered, Self-Supportive Exfoliated-Graphite Sheets. *ACS Applied Materials & Interfaces* **2019**, *11* (20), 18349-18360. DOI: 10.1021/acsami.9b01712.
(176) Han, Z. J.; Pineda, S.; Murdock, A. T.; Seo, D. H.; Ostrikov, K.; Bendavid, A. RuO2-coated vertical graphene hybrid electrodes for high-performance solid-state supercapacitors. *Journal of Materials Chemistry A* **2017**, *5* (33), 17293-17301, 10.1039/C7TA03355A. DOI: 10.1039/C7TA03355A.
(177) Chung, D. D. L. 2 - Introduction to Carbon Composites. In *Carbon Composites (Second Edition)*, Chung, D. D. L. Ed.; Butterworth-Heinemann, 2017; pp 88-160.
(178) Nishio, K. PRIMARY BATTERIES – NONAQUEOUS SYSTEMS | Lithium–Manganese Dioxide. In *Encyclopedia of Electrochemical Power Sources*, Garche, J. Ed.; Elsevier, 2009; pp 83-92.
(179) Kordesch, K.; Taucher-Mautner, W. CHEMISTRY, ELECTROCHEMISTRY, AND ELECTROCHEMICAL APPLICATIONS | Manganese. In *Encyclopedia of Electrochemical Power Sources*, Garche, J. Ed.; Elsevier, 2009; pp 784-795.
(180) Zhang, M.; Yang, D.; Li, J. Supercapacitor performances of MnO2 and MnO2/ reduced graphene oxide prepared with various electrodeposition time. *Vacuum* **2020**, *178*, 109455. DOI: 10.1016/j.vacuum.2020.109455.
(181) Zhu, G.; He, Z.; Chen, J.; Zhao, J.; Feng, X.; Ma, Y.; Fan, Q.; Wang, L.; Huang, W. Highly conductive three-dimensional MnO2–carbon nanotube–graphene–Ni hybrid foam as a binder-free supercapacitor electrode. *Nanoscale* **2014**, *6* (2), 1079-1085, 10.1039/C3NR04495E. DOI: 10.1039/C3NR04495E.

(182) Wu, D.; Xie, X.; Zhang, Y.; Zhang, D.; Du, W.; Zhang, X.; Wang, B. MnO2/Carbon Composites for Supercapacitor: Synthesis and Electrochemical Performance. *Frontiers in Materials* **2020**, *7*, Review. DOI: 10.3389/fmats.2020.00002.

(183) Xu, L.; Jia, M.; Li, Y.; Jin, X.; Zhang, F. High-performance MnO2-deposited graphene/activated carbon film electrodes for flexible solid-state supercapacitor. *Scientific Reports* **2017**, *7* (1), 12857. DOI: 10.1038/s41598-017-11267-0.

(184) Chen, Y.; Li, X.; Zhou, L.; Mai, Y.-W.; Huang, H. Chapter 21 - High-performance electrospun nanostructured composite fiber anodes for lithium–ion batteries. In *Multifunctionality of Polymer Composites*, Friedrich, K., Breuer, U. Eds.; William Andrew Publishing, 2015; pp 662-689.

(185) Xiao, H.; Yao, S.; Liu, H.; Qu, F.; Zhang, X.; Wu, X. NiO nanosheet assembles for supercapacitor electrode materials. *Progress in Natural Science: Materials International* **2016**, *26* (3), 271-275. DOI: 10.1016/j.pnsc.2016.05.007.

(186) Dhas, S. D.; Maldar, P. S.; Patil, M. D.; Nagare, A. B.; Waikar, M. R.; Sonkawade, R. G.; Moholkar, A. V. Synthesis of NiO nanoparticles for supercapacitor application as an efficient electrode material. *Vacuum* **2020**, *181*, 109646. DOI: 10.1016/j.vacuum.2020.109646.

(187) Vijayakumar, S.; Nagamuthu, S.; Muralidharan, G. Supercapacitor Studies on NiO Nanoflakes Synthesized Through a Microwave Route. *ACS Applied Materials & Interfaces* **2013**, *5* (6), 2188-2196. DOI: 10.1021/am400012h.

(188) Ramesh, S.; Karuppasamy, K.; Yadav, H. M.; Lee, J.-J.; Kim, H.-S.; Kim, H.-S.; Kim, J.-H. Ni(OH)2-decorated nitrogen doped MWCNT nanosheets as an efficient electrode for high performance supercapacitors. *Scientific Reports* **2019**, *9* (1), 6034. DOI: 10.1038/s41598-019-42281-z.

(189) Jiang, H.; Li, C.; Sun, T.; Ma, J. High-performance supercapacitor material based on Ni(OH)2 nanowire-MnO2 nanoflakes core–shell nanostructures. *Chemical Communications* **2012**, *48* (20), 2606-2608, 10.1039/C2CC18079K. DOI: 10.1039/C2CC18079K.

(190) Cai, J.; Zhang, D.; Ding, W.-P.; Zhu, Z.-Z.; Wang, G.-Z.; He, J.-R.; Wang, H.-B.; Fei, P.; Si, T.-L. Promising Rice-Husk-Derived Carbon/Ni(OH)2 Composite Materials as a High-Performing Supercapacitor Electrode. *ACS Omega* **2020**, *5* (46), 29896-29902. DOI: 10.1021/acsomega.0c04117.

(191) Brisse, A.-L.; Stevens, P.; Toussaint, G.; Crosnier, O.; Brousse, T. Ni(OH)2 and NiO Based Composites: Battery Type Electrode Materials for Hybrid Supercapacitor Devices. *Materials* **2018**, *11* (7), 1178. DOI: 10.3390/ma11071178.

(192) Meher, S. K.; Rao, G. R. Ultralayered Co3O4 for High-Performance Supercapacitor Applications. *The Journal of Physical Chemistry C* **2011**, *115* (31), 15646-15654. DOI: 10.1021/jp201200e.

(193) Guo, C.; Yin, M.; Wu, C.; Li, J.; Sun, C.; Jia, C.; Li, T.; Hou, L.; Wei, Y. Highly Stable Gully-Network Co3O4 Nanowire Arrays as Battery-Type Electrode for Outstanding Supercapacitor Performance. *Frontiers in Chemistry* **2018**, *6*, Original Research. DOI: 10.3389/fchem.2018.00636.

(194) Rabani, I.; Yoo, J.; Kim, H.-S.; Lam, D. V.; Hussain, S.; Karuppasamy, K.; Seo, Y.-S. Highly dispersive Co3O4 nanoparticles incorporated into a cellulose nanofiber for a high-performance flexible supercapacitor. *Nanoscale* **2021**, *13* (1), 355-370, 10.1039/D0NR06982E. DOI: 10.1039/D0NR06982E.

(195) Morozova, M.; Kluson, P.; Krysa, J.; Vesely, M.; Dzik, P.; Solcova, O. Electrochemical Properties of TiO2 Electrode Prepared by Various Methods. *Procedia Engineering* **2012**, *42*, 573-580. DOI: 10.1016/j.proeng.2012.07.450.

(196) Yun, Q.; Li, L.; Hu, Z.; Lu, Q.; Chen, B.; Zhang, H. Layered Transition Metal Dichalcogenide-Based Nanomaterials for Electrochemical Energy Storage. *Adv Mater* **2020**, *32* (1), e1903826. DOI: 10.1002/adma.201903826 From NLM.

(197) Tanwar, S.; Arya, A.; Gaur, A.; Sharma, A. L. Transition metal dichalcogenide (TMDs) electrodes for supercapacitors: a comprehensive review. *Journal of Physics: Condensed Matter* **2021**, *33* (30), 303002. DOI: 10.1088/1361-648x/abfb3c.

(198) Joseph, N.; Shafi, P. M.; Bose, A. C. Recent Advances in 2D-MoS2 and its Composite Nanostructures for Supercapacitor Electrode Application. *Energy & Fuels* **2020**, *34* (6), 6558-6597. DOI: 10.1021/acs.energyfuels.0c00430.

(199) Schneemann, A.; Dong, R.; Schwotzer, F.; Zhong, H.; Senkovska, I.; Feng, X.; Kaskel, S. 2D framework materials for energy applications. *Chemical Science* **2021**, *12* (5), 1600-1619, 10.1039/D0SC05889K. DOI: 10.1039/D0SC05889K.

(200) Soares, D. M.; Mukherjee, S.; Singh, G. TMDs beyond MoS2 for Electrochemical Energy Storage. *Chemistry – A European Journal* **2020**, *26* (29), 6320-6341, https://doi.org/10.1002/chem.202000147. DOI: 10.1002/chem.202000147 (acccessed 2021/09/25).

(201) Bao, J.; Jeppson, K.; Edwards, M.; Fu, Y.; Ye, L.; Lu, X.; Liu, J. Synthesis and applications of two-dimensional hexagonal boron nitride in electronics manufacturing. *Electronic Materials Letters* **2016**, *12* (1), 1-16. DOI: 10.1007/s13391-015-5308-2.

(202) Pu, J.; Zhang, K.; Wang, Z.; Li, C.; Zhu, K.; Yao, Y.; Hong, G. Synthesis and Modification of Boron Nitride Nanomaterials for Electrochemical Energy Storage: From Theory to Application. *Advanced Functional Materials* **2021**, *31* (48), 2106315. DOI: 10.1002/adfm.202106315.

(203) Zhang, K.; Feng, Y.; Wang, F.; Yang, Z.; Wang, J. Two dimensional hexagonal boron nitride (2D-hBN): synthesis, properties and applications. *Journal of Materials Chemistry C* **2017**, *5* (46), 11992-12022, 10.1039/C7TC04300G. DOI: 10.1039/C7TC04300G.

(204) Ergen, O. Hexagonal boron nitride incorporation to achieve high performance Li4Ti5O12 electrodes. *AIP Advances* **2020**, *10* (4), 045040. DOI: 10.1063/5.0004376.

(205) Gao, T.; Gong, L.-j.; Wang, Z.; Yang, Z.-k.; Pan, W.; He, L.; Zhang, J.; Ou, E.-c.; Xiong, Y.; Xu, W. Boron nitride/reduced graphene oxide nanocomposites as supercapacitors electrodes. *Materials Letters* **2015**, *159*, 54-57. DOI: 10.1016/j.matlet.2015.06.072.

(206) Byun, S.; Kim, J. H.; Song, S. H.; Lee, M.; Park, J.-J.; Lee, G.; Hong, S. H.; Lee, D. Ordered, Scalable Heterostructure Comprising Boron Nitride and Graphene for High-Performance Flexible Supercapacitors. *Chemistry of Materials* **2016**, *28* (21), 7750-7756. DOI: 10.1021/acs.chemmater.6b02947.

(207) Gunday, S. T.; Cevik, E.; Yusuf, A.; Bozkurt, A. Nanocomposites composed of sulfonated polysulfone/hexagonal boron nitride/ionic liquid for supercapacitor applications. *Journal of Energy Storage* **2019**, *21*, 672-679. DOI: 10.1016/j.est.2019.01.008.

(208) Bissett, M. A.; Kinloch, I. A.; Dryfe, R. A. W. Characterization of MoS2–Graphene Composites for High-Performance Coin Cell Supercapacitors. *ACS Applied Materials & Interfaces* **2015**, *7* (31), 17388-17398. DOI: 10.1021/acsami.5b04672.

(209) Acerce, M.; Voiry, D.; Chhowalla, M. Metallic 1T phase MoS2 nanosheets as supercapacitor electrode materials. *Nature Nanotechnology* **2015**, *10* (4), 313-318. DOI: 10.1038/nnano.2015.40.

(210) Wei, S.; Zhou, R.; Wang, G. Enhanced Electrochemical Performance of Self-Assembled Nanoflowers of MoS2 Nanosheets as Supercapacitor Electrode Materials. *ACS Omega* **2019**, *4* (14), 15780-15788. DOI: 10.1021/acsomega.9b01058.

(211) Gupta, H.; Chakrabarti, S.; Mothkuri, S.; Padya, B.; Rao, T. N.; Jain, P. K. High performance supercapacitor based on 2D-MoS2 nanostructures. *Materials Today: Proceedings* **2020**, *26*, 20-24. DOI: 10.1016/j.matpr.2019.04.198.

(212) Ghasemi, F.; Jalali, M.; Abdollahi, A.; Mohammadi, S.; Sanaee, Z.; Mohajerzadeh, S. A high performance supercapacitor based on decoration of MoS2/reduced graphene oxide with

NiO nanoparticles. *RSC Advances* **2017**, *7* (83), 52772-52781, 10.1039/C7RA09060A. DOI: 10.1039/C7RA09060A.

(213) Wang, F.; Ma, J.; Zhou, K.; Li, X. MoS2/corncob-derived activated carbon for supercapacitor application. *Materials Chemistry and Physics* **2020**, *244*, 122215. DOI: 10.1016/j.matchemphys.2019.122215.

(214) Chen, Q.; Xie, F.; Wang, G.; Ge, K.; Ren, H.; Yan, M.; Wang, Q.; Bi, H. Hybrid MoS2@PANI materials for high-performance supercapacitor electrode. *Ionics* **2021**, *27* (9), 4083-4096. DOI: 10.1007/s11581-021-04147-1.

(215) Baig, M. M.; Pervaiz, E.; Yang, M.; Gul, I. H. High-Performance Supercapacitor Electrode Obtained by Directly Bonding 2D Materials: Hierarchal MoS2 on Reduced Graphene Oxide. *Frontiers in Materials* **2020**, *7*, Original Research. DOI: 10.3389/fmats.2020.580424.

(216) Garg, R.; Agarwal, A.; Agarwal, M. A review on MXene for energy storage application: effect of interlayer distance. *Materials Research Express* **2020**, *7* (2), 022001. DOI: 10.1088/2053-1591/ab750d.

(217) Sun, Y.; Chen, D.; Liang, Z. Two-dimensional MXenes for energy storage and conversion applications. *Materials Today Energy* **2017**, *5*, 22-36. DOI: 10.1016/j.mtener.2017.04.008.

(218) Ahmed, A.; Hossain, M. M.; Adak, B.; Mukhopadhyay, S. Recent Advances in 2D MXene Integrated Smart-Textile Interfaces for Multifunctional Applications. *Chemistry of Materials* **2020**, *32* (24), 10296-10320. DOI: 10.1021/acs.chemmater.0c03392.

(219) Li, X.; Huang, Z.; Zhi, C. Environmental Stability of MXenes as Energy Storage Materials. *Frontiers in Materials* **2019**, *6* (312), Mini Review. DOI: 10.3389/fmats.2019.00312.

(220) Anasori, B.; Lukatskaya, M. R.; Gogotsi, Y. 2D metal carbides and nitrides (MXenes) for energy storage. *Nature Reviews Materials* **2017**, *2* (2), 16098. DOI: 10.1038/natrevmats.2016.98.

(221) Ahmed, A.; Sharma, S.; Adak, B.; Hossain, M. M.; LaChance, A. M.; Mukhopadhyay, S.; Sun, L. Two-dimensional MXenes: New frontier of wearable and flexible electronics. *InfoMat n/a* (n/a), e12295. DOI: 10.1002/inf2.12295.

(222) Ahmed, A.; Sharma, S.; Adak, B.; Hossain, M. M.; LaChance, A. M.; Mukhopadhyay, S.; Sun, L. Two-dimensional MXenes: New frontier of wearable and flexible electronics. *InfoMat* **2022**, *4* (4), e12295. DOI: 10.1002/inf2.12295.

(223) Pal, B.; Yang, S.; Ramesh, S.; Thangadurai, V.; Jose, R. Electrolyte selection for supercapacitive devices: a critical review. *Nanoscale Advances* **2019**, *1* (10), 3807-3835, 10.1039/C9NA00374F. DOI: 10.1039/C9NA00374F.

(224) Balli, B.; Şavk, A.; Şen, F. 5 - Graphene and polymer composites for supercapacitor applications. In *Nanocarbon and its Composites*, Khan, A., Jawaid, M., Inamuddin, Asiri, A. M. Eds.; Woodhead Publishing, 2019; pp 123-151.
(225) Fu, W.; Turcheniuk, K.; Naumov, O.; Mysyk, R.; Wang, F.; Liu, M.; Kim, D.; Ren, X.; Magasinski, A.; Yu, M.; et al. Materials and technologies for multifunctional, flexible or integrated supercapacitors and batteries. *Materials Today* **2021**. DOI: https://doi.org/10.1016/j.mattod.2021.01.026.
(226) Wang, Q.; Chen, S.; Zhang, D. Chapter 10 - CNT yarn-based supercapacitors. In *Carbon Nanotube Fibers and Yarns*, Miao, M. Ed.; Woodhead Publishing, 2020; pp 243-270.
(227) Chatterjee, K.; Tabor, J.; Ghosh, T. K. Electrically Conductive Coatings for Fiber-Based E-Textiles. *Fibers* **2019**, *7* (6), 51. DOI: 10.3390/fib7060051.
(228) Joshi, M.; Butola, B. S. 14 - Application technologies for coating, lamination and finishing of technical textiles. In *Advances in the Dyeing and Finishing of Technical Textiles*, Gulrajani, M. L. Ed.; Woodhead Publishing, 2013; pp 355-411.
(229) Neacşu, I. A.; Nicoară, A. I.; Vasile, O. R.; Vasile, B. Ş. Chapter 9 - Inorganic micro- and nanostructured implants for tissue engineering. In *Nanobiomaterials in Hard Tissue Engineering*, Grumezescu, A. M. Ed.; William Andrew Publishing, 2016; pp 271-295.
(230) Hu, L.; Pasta, M.; La Mantia, F.; Cui, L.; Jeong, S.; Deshazer, H. D.; Choi, J. W.; Han, S. M.; Cui, Y. Stretchable, Porous, and Conductive Energy Textiles. *Nano Letters* **2010**, *10* (2), 708-714. DOI: 10.1021/nl903949m.
(231) Yu, G.; Hu, L.; Vosgueritchian, M.; Wang, H.; Xie, X.; McDonough, J. R.; Cui, X.; Cui, Y.; Bao, Z. Solution-processed graphene/MnO2 nanostructured textiles for high-performance electrochemical capacitors. *Nano Letters* **2011**, *11* (7), 2905-2911. DOI: 10.1021/nl2013828.
(232) Berni, A.; Mennig, M.; Schmidt, H. Doctor Blade. In *Sol-Gel Technologies for Glass Producers and Users*, Aegerter, M. A., Mennig, M. Eds.; Springer US, 2004; pp 89-92.
(233) Hu, L.; La Mantia, F.; Wu, H.; Xie, X.; McDonough, J.; Pasta, M.; Cui, Y. Lithium-Ion Textile Batteries with Large Areal Mass Loading. *Advanced Energy Materials* **2011**, *1* (6), 1012-1017, https://doi.org/10.1002/aenm.201100261. DOI: 10.1002/aenm.201100261 (acccessed 2021/09/22).
(234) Beedasy, V.; Smith, P. J. Printed Electronics as Prepared by Inkjet Printing. *Materials* **2020**, *13* (3). DOI: 10.3390/ma13030704.
(235) Puliyalil, H.; Filipič, G.; Cvelbar, U. Chapter 9 - Selective Plasma Etching of Polymers and Polymer Matrix Composites. In *Non-Thermal Plasma Technology for Polymeric*

Materials, Thomas, S., Mozetič, M., Cvelbar, U., Špatenka, P., K.M, P. Eds.; Elsevier, 2019; pp 241-259.
(236) Baquey, C.; Durrieu, M. C.; G. Guidoin, R. Chapter 8 - Fluorinated Biomaterials for Cardiovascular Surgery. In *Fluorine and Health*, Tressaud, A. Ed.; Elsevier, 2008; pp 379-406.
(237) Rapp, B. E. Chapter 22 - Measuring Surface Tension and Free Surface Energy. In *Microfluidics: Modelling, Mechanics and Mathematics*, Rapp, B. E. Ed.; Elsevier, 2017; pp 453-465.
(238) Islam, M. R.; Afroj, S.; Beach, C.; Islam, M. H.; Parraman, C.; Abdelkader, A.; Casson, A. J.; Novoselov, K. S.; Karim, N. Fully printed and multifunctional graphene-based wearable e-textiles for personalized healthcare applications. *iScience* **2022**, *25* (3), 103945. DOI: 10.1016/j.isci.2022.103945.
(239) Salvado, R.; Loss, C.; Gonçalves, R.; Pinho, P. Textile Materials for the Design of Wearable Antennas: A Survey. *Sensors (Basel)* **2012**, *12*, 15841 - 15857. DOI: 10.3390/s121115841.
(240) Chauraya, A.; Whittow, W. G.; Vardaxoglou, J. C.; Li, Y.; Torah, R.; Yang, K.; Beeby, S.; Tudor, J. Inkjet printed dipole antennas on textiles for wearable communications. *IET Microwaves, Antennas & Propagation* **2013**, *7* (9), 760-767. DOI: 10.1049/iet-map.2013.0076.
(241) Rotzler, S.; Kallmayer, C.; Dils, C.; von Krshiwoblozki, M.; Bauer, U.; Schneider-Ramelow, M. Improving the washability of smart textiles: influence of different washing conditions on textile integrated conductor tracks. *The Journal of The Textile Institute* **2020**, *111* (12), 1766-1777. DOI: 10.1080/00405000.2020.1729056.
(242) Niu, B.; Yang, S.; Hua, T.; Tian, X.; Koo, M. Facile fabrication of highly conductive, waterproof, and washable e-textiles for wearable applications. *Nano Research* **2021**, *14* (4), 1043-1052. DOI: 10.1007/s12274-020-3148-3.
(243) Blunden, B. W.; Birkenshaw, J. W. The Printing Processes. In *The Printing Ink Manual*, Leach, R. H., Armstrong, C., Brown, J. F., Mackenzie, M. J., Randall, L., Smith, H. G. Eds.; Springer US, 1988; pp 10-68.
(244) Miles, L. W. C. *Textile printing*; Society of Dyers and Colourists, 2003.
(245) Tang, X.; Wu, K.; Qi, X.; Kwon, H.-j.; Wang, R.; Li, Z.; Ye, H.; Hong, J.; Choi, H. H.; Kong, H.; et al. Screen Printing of Silver and Carbon Nanotube Composite Inks for Flexible and Reliable Organic Integrated Devices. *ACS Applied Nano Materials* **2022**, *5* (4), 4801-4811. DOI: 10.1021/acsanm.1c04317.
(246) Shemilt, H. R. Screen Printing. *Circuit World* **1975**, *1* (3), 7-12. DOI: 10.1108/eb043518 (acccessed 2021/03/12).

(247) Novaković, D.; Kašiković, N.; Vladić, G.; Pál, M. 15 - Screen Printing. In *Printing on Polymers*, Izdebska, J., Thomas, S. Eds.; William Andrew Publishing, 2016; pp 247-261.
(248) Filipowska, B.; Wiśniewski, B.; Zawadzka Michalak, L. Creation of electro-conductive paths and patterns by screen printing on textile bases. *Textile Research Journal* **2018**, *88* (3), 261-274. DOI: 10.1177/0040517516679146.
(249) Gerlach, C.; Krumm, D.; Illing, M.; Lange, J.; Kanoun, O.; Odenwald, S.; Hübler, A. Printed MWCNT-PDMS-Composite Pressure Sensor System for Plantar Pressure Monitoring in Ulcer Prevention. *IEEE Sensors Journal* **2015**, *15* (7), 3647-3656. DOI: 10.1109/JSEN.2015.2392084.
(250) Wu, L.; Qian, J.; Peng, J.; Wang, K.; Liu, Z.; Ma, T.; Zhou, Y.; Wang, G.; Ye, S. Screen-printed flexible temperature sensor based on FG/CNT/PDMS composite with constant TCR. *Journal of Materials Science: Materials in Electronics* **2019**, *30* (10), 9593-9601. DOI: 10.1007/s10854-019-01293-1.
(251) Komazaki, Y.; Uemura, S. Stretchable, printable, and tunable PDMS-CaCl2 microcomposite for capacitive humidity sensors on textiles. *Sensors and Actuators B: Chemical* **2019**, *297*, 126711. DOI: 10.1016/j.snb.2019.126711.
(252) Kang, T.; Merritt, C. R.; Grant, E.; Pourdeyhimi, B.; Nagle, H. T. Nonwoven Fabric Active Electrodes for Biopotential Measurement During Normal Daily Activity. *IEEE Transactions on Biomedical Engineering* **2008**, *55* (1), 188-195. DOI: 10.1109/TBME.2007.910678.
(253) Yoo, H. J.; Yoo, J.; Yan, L. Wireless fabric patch sensors for wearable healthcare. *Annu Int Conf IEEE Eng Med Biol Soc* **2010**, *2010*, 5254-5257. DOI: 10.1109/iembs.2010.5626295 From NLM.
(254) Matiko, J. W.; Wei, Y.; Torah, R.; Grabham, N.; Paul, G.; Beeby, S.; Tudor, J. Wearable EEG headband using printed electrodes and powered by energy harvesting for emotion monitoring in ambient assisted living. *Smart Materials and Structures* **2015**, *24* (12), 125028. DOI: 10.1088/0964-1726/24/12/125028.
(255) Paul, G.; Torah, R.; Beeby, S.; Tudor, J. The development of screen printed conductive networks on textiles for biopotential monitoring applications. *Sensors and Actuators A: Physical* **2014**, *206*, 35-41. DOI: 10.1016/j.sna.2013.11.026.
(256) Myllymaa, S.; Lepola, P.; Hukkanen, T.; Oun, A.; Mervaala, E.; Toyras, J.; Lappalainen, R.; Myllymaa, K. Novel screen printed electrode set for routine EEG recordings in patients with altered mental status. *Annu Int Conf IEEE Eng Med Biol Soc* **2013**, *2013*, 6724-6727. DOI: 10.1109/embc.2013.6611099 From NLM.

(257) Torah, R.; Yang, K.; Beeby, S. P.; Tudor, M. J. Screen-printed multilayer meander heater on polyester cotton. In 88th Textile Institute World Conference, Shah Alam, Selangor, Malaysia; 2012.
(258) Jost, K.; Perez, C. R.; McDonough, J. K.; Presser, V.; Heon, M.; Dion, G.; Gogotsi, Y. Carbon coated textiles for flexible energy storage. *Energy and Environmental Science* **2011**, *4* (12), 5060-5067. DOI: 10.1039/c1ee02421c.
(259) Abdelkader, A. M.; Karim, N.; Vallés, C.; Afroj, S.; Novoselov, K. S.; Yeates, S. G. Ultraflexible and robust graphene supercapacitors printed on textiles for wearable electronics applications. *2D Materials* **2017**, *4* (3). DOI: 10.1088/2053-1583/aa7d71.
(260) Lu, Q.; Liu, L.; Yang, S.; Liu, J.; Tian, Q.; Yao, W.; Xue, Q.; Li, M.; Wu, W. Facile synthesis of amorphous FeOOH/MnO2 composites as screen-printed electrode materials for all-printed solid-state flexible supercapacitors. *Journal of Power Sources* **2017**, *361*, 31-38. DOI: 10.1016/j.jpowsour.2017.06.065.
(261) Szentgyörgyvölgyi, R. 12 - Gravure Printing. In *Printing on Polymers*, Izdebska, J., Thomas, S. Eds.; William Andrew Publishing, 2016; pp 199-215.
(262) Roth, B.; Søndergaard, R. R.; Krebs, F. C. 7 - Roll-to-roll printing and coating techniques for manufacturing large-area flexible organic electronics. In *Handbook of Flexible Organic Electronics*, Logothetidis, S. Ed.; Woodhead Publishing, 2015; pp 171-197.
(263) Morris, B. A. 2 - Converting Processes. In *The Science and Technology of Flexible Packaging*, Morris, B. A. Ed.; William Andrew Publishing, 2017; pp 25-49.
(264) Bajpai, P. Chapter 13 - Printing and Graphic Arts. In *Biermann's Handbook of Pulp and Paper (Third Edition)*, Bajpai, P. Ed.; Elsevier, 2018; pp 283-310.
(265) Ujiie, H. Chapter 20 - Fabric Finishing: Printing Textiles. In *Textiles and Fashion*, Sinclair, R. Ed.; Woodhead Publishing, 2015; pp 507-529.
(266) Reddy, A. S. G.; Narakathu, B. B.; Atashbar, M. Z.; Rebros, M.; Rebrosova, E.; Bazuin, B. J.; Joyce, M. K.; Fleming, P. D.; Pekarovicova, A. Printed Capacitive Based Humidity Sensors on Flexible Substrates. *Sensor Letters* **2011**, *9* (2), 869-871. DOI: 10.1166/sl.2011.1633.
(267) Turkani, V. S.; Narakathu, B. B.; Maddipatla, D.; Bazuin, B. J.; Atashbar, M. Z. P1FW.5 - A Fully Printed CNT Based Humidity Sensor on Flexible PET Substrate. 2018.
(268) Mumby, R. 19 - Printing for packaging. In *Packaging Technology*, Emblem, A., Emblem, H. Eds.; Woodhead Publishing, 2012; pp 441-489.
(269) Dunn, T. 3 - Flexographic Printing. In *Flexible Packaging*, Dunn, T. Ed.; William Andrew Publishing, 2015; pp 27-37.

(270) Vena, A.; Perret, E.; Tedjini, S. 5 - Implementation and Measurements of Chipless RFID Tags. In *Chipless RFID based on RF Encoding Particle*, Vena, A., Perret, E., Tedjini, S. Eds.; Elsevier, 2016; pp 171-227.
(271) Żołek-Tryznowska, Z. 6 - Rheology of Printing Inks. In *Printing on Polymers*, Izdebska, J., Thomas, S. Eds.; William Andrew Publishing, 2016; pp 87-99.
(272) Cie, C. 1 - Theoretical foundations for ink jet technology. In *Ink Jet Textile Printing*, Cie, C. Ed.; Woodhead Publishing, 2015; pp 1-13.
(273) Ko, S. H. Chapter 18 - Advanced Inkjet Technology for 3D Micro-metal Structure Fabrication. In *Micromanufacturing Engineering and Technology (Second Edition)*, Qin, Y. Ed.; William Andrew Publishing, 2015; pp 425-439.
(274) Manthiram, A.; Zhao, X.; Li, W. 11 - Developments in membranes, catalysts and membrane electrode assemblies for direct methanol fuel cells (DMFCs). In *Functional Materials for Sustainable Energy Applications*, Kilner, J. A., Skinner, S. J., Irvine, S. J. C., Edwards, P. P. Eds.; Woodhead Publishing, 2012; pp 312-369.
(275) Soleimani-Gorgani, A. 14 - Inkjet Printing. In *Printing on Polymers*, Izdebska, J., Thomas, S. Eds.; William Andrew Publishing, 2016; pp 231-246.
(276) Cook, B. S.; Tehrani, B.; Cooper, J. R.; Kim, S.; Tentzeris, M. M. 8 - Integrated printing for 2D/3D flexible organic electronic devices. In *Handbook of Flexible Organic Electronics*, Logothetidis, S. Ed.; Woodhead Publishing, 2015; pp 199-216.
(277) Mei, J.; Lovell, M.; Mickle, M.; Heston, S. Continuous ink-jet printing electronic components using novel conductive inks. 2004.
(278) Daly, R.; Harrington, T. S.; Martin, G. D.; Hutchings, I. M. Inkjet printing for pharmaceutics - A review of research and manufacturing. *Int J Pharm* **2015**, *494* (2), 554-567. DOI: 10.1016/j.ijpharm.2015.03.017 From NLM.
(279) Parraman, C. 25 - Colour printing techniques and new developments in colour printing. In *Colour Design (Second Edition)*, Best, J. Ed.; Woodhead Publishing, 2017; pp 589-618.
(280) Kobayashi, H. 7 - Industrial production printers – Mimaki's Tx series. In *Digital Printing of Textiles*, Ujiie, H. Ed.; Woodhead Publishing, 2006; pp 98-122.
(281) Quintero, A. V.; Camara, M.; Mattana, G.; Gaschler, W.; Chabrecek, P.; Briand, D.; de Rooij, N. F. Capacitive Strain Sensors Inkjet-printed on PET Fibers for Integration in Industrial Textile. *Procedia Engineering* **2015**, *120*, 279-282. DOI: 10.1016/j.proeng.2015.08.613.
(282) Khan, S.; Ali, S.; Khan, A.; Bermak, A. Developing pressure sensors from impregnated textile sandwiched in inkjet-printed electrodes. *Journal of Materials Science: Materials in Electronics* **2021**. DOI: 10.1007/s10854-021-07325-z.

(283) Liew, Q. J.; Aziz, A. S. A.; Lee, H. W.; Lee, M. W.; Hawari, H. F.; Md Khir, M. H. Inkjet-Printed Flexible Temperature Sensor Based on Silver Nanoparticles Ink. *Engineering Proceedings* **2020**, *2* (1). DOI: 10.3390/ecsa-7-08216.

(284) Weremczuk, J.; Tarapata, G.; Jachowicz, R. Humidity Sensor Printed on Textile with Use of Ink-Jet Technology. *Procedia Engineering* **2012**, *47*, 1366-1369. DOI: 10.1016/j.proeng.2012.09.410.

(285) La, T.-G.; Qiu, S.; Scott, D. K.; Bakhtiari, R.; Kuziek, J. W. P.; Mathewson, K. E.; Rieger, J.; Chung, H.-J. Two-Layered and Stretchable e-Textile Patches for Wearable Healthcare Electronics. *Advanced Healthcare Materials* **2018**, *7* (22), 1801033. DOI: 10.1002/adhm.201801033.

(286) Malshe, V. C. Paints: Water-Based☆. In *Reference Module in Chemistry, Molecular Sciences and Chemical Engineering*, Elsevier, 2019.

(287) Pekarovicova, A.; Husovska, V. 3 - Printing Ink Formulations. In *Printing on Polymers*, Izdebska, J., Thomas, S. Eds.; William Andrew Publishing, 2016; pp 41-55.

(288) Cie, C. 7 - Inks for digital printing. In *Ink Jet Textile Printing*, Cie, C. Ed.; Woodhead Publishing, 2015; pp 85-97.

(289) Viswanath, D. S.; Ghosh, T. K.; Prasad, D. H. L.; Dutt, N. V. K.; Rani, K. Y. INTRODUCTION. In *Viscosity of Liquids: Theory, Estimation, Experiment, and Data*, Viswanath, D. S., Ghosh, T. K., Prasad, D. H. L., Dutt, N. V. K., Rani, K. Y. Eds.; Springer Netherlands, 2007; pp 1-8.

(290) Wiklund, J.; Karakoç, A.; Palko, T.; Yiğitler, H.; Ruttik, K.; Jäntti, R.; Paltakari, J. A Review on Printed Electronics: Fabrication Methods, Inks, Substrates, Applications and Environmental Impacts. *Journal of Manufacturing and Materials Processing* **2021**, *5* (3), 89. DOI: 10.3390/jmmp5030089.

(291) Chapter 1 - Introduction. In *Rheology Series*, Barnes, H. A., Hutton, J. F., Walters, K. Eds.; Vol. 3; Elsevier, 1989; pp 1-10.

(292) Izdebska, J. 1 - Printing on Polymers: Theory and Practice. In *Printing on Polymers*, Izdebska, J., Thomas, S. Eds.; William Andrew Publishing, 2016; pp 1-20.

(293) Aydemir, C.; Altay, B. N.; Akyol, M. Surface analysis of polymer films for wettability and ink adhesion. *Color Research & Application* **2021**, *46* (2), 489-499, https://doi.org/10.1002/col.22579. DOI: 10.1002/col.22579 (acccessed 2021/03/13).

(294) Tabbernor, A. Rheology of Printing Inks. In *The Printing Ink Manual*, Leach, R. H., Armstrong, C., Brown, J. F., Mackenzie, M. J., Randall, L., Smith, H. G. Eds.; Springer US, 1988; pp 666-698.
(295) Amoo, L. M.; Layi Fagbenle, R. 14 - Overview of non-Newtonian boundary layer flows and heat transfer. In *Applications of Heat, Mass and Fluid Boundary Layers*, Fagbenle, R. O., Amoo, O. M., Aliu, S., Falana, A. Eds.; Woodhead Publishing, 2020; pp 413-435.
(296) Braun, D. B.; Rosen, M. R. Part 1 - Practical Rheology. In *Rheology Modifiers Handbook*, Braun, D. B., Rosen, M. R. Eds.; William Andrew Publishing, 1999; pp 1-69.
(297) Eley, R. R. Rheology and Viscometry. Koleske, J. Ed.; ASTM International, 2012; pp 415-451.
(298) Yin, Z.; Huang, Y.; Bu, N.; Wang, X.; Xiong, Y. Inkjet printing for flexible electronics: Materials, processes and equipments. *Chinese Science Bulletin* **2010**, *55* (30), 3383-3407. DOI: 10.1007/s11434-010-3251-y.
(299) Liu, Y.; Derby, B. Experimental study of the parameters for stable drop-on-demand inkjet performance. *Physics of Fluids* **2019**, *31* (3), 032004. DOI: 10.1063/1.5085868 (acccessed 2021/03/13).
(300) Smith, P. J.; Morrin, A. Reactive inkjet printing. *Journal of Materials Chemistry* **2012**, *22* (22), 10965-10970, 10.1039/C2JM30649B. DOI: 10.1039/C2JM30649B.
(301) Cummins, G.; Desmulliez, M. P. Y. Inkjet printing of conductive materials: a review. *Circuit World* **2012**, *38* (4), 193-213. DOI: 10.1108/03056121211280413 (acccessed 2022/11/13).
(302) Koivunen, R.; Bollström, R.; Gane, P. Inkjet jettability and physical characterization of water–ethanol solutions of low molecular weight sodium polyacrylate and poly-diallyl dimethyl ammonium chloride (polyDADMAC). *AIP Advances* **2020**, *10* (5), 055309. DOI: 10.1063/5.0006634.
(303) Kim, S.; Choi, J. H.; Sohn, D. K.; Ko, H. S. The Effect of Ink Supply Pressure on Piezoelectric Inkjet. *Micromachines* **2022**, *13* (4), 615. DOI: 10.3390/mi13040615.
(304) Kim, I.; Ju, B.; Zhou, Y.; Li, B. M.; Jur, J. S. Microstructures in All-Inkjet-Printed Textile Capacitors with Bilayer Interfaces of Polymer Dielectrics and Metal–Organic Decomposition Silver Electrodes. *ACS Applied Materials & Interfaces* **2021**, *13* (20), 24081-24094. DOI: 10.1021/acsami.1c01827.
(305) Yang, J.; Zheng, F.; Derby, B. Stability of Lines with Zero Receding Contact Angle Produced by Inkjet Printing at Small Drop Volume. *Langmuir* **2021**, *37* (1), 26-34. DOI: 10.1021/acs.langmuir.0c01928.

(306) Karim, N.; Afroj, S.; Tan, S.; Novoselov, K. S.; Yeates, S. G. All Inkjet-Printed Graphene-Silver Composite Ink on Textiles for Highly Conductive Wearable Electronics Applications. *Scientific Reports* **2019**, *9* (1), 8035. DOI: 10.1038/s41598-019-44420-y.

(307) Stempien, Z.; Khalid, M.; Kozanecki, M.; Filipczak, P.; Wrzesińska, A.; Korzeniewska, E.; Sąsiadek, E. Inkjet Printing of Polypyrrole Electroconductive Layers Based on Direct Inks Freezing and Their Use in Textile Solid-State Supercapacitors. *Materials (Basel)* **2021**, *14* (13), 3577. DOI: 10.3390/ma14133577 PubMed.

(308) Sundriyal, P.; Bhattacharya, S. Scalable Micro-fabrication of Flexible, Solid-State, Inexpensive, and High-Performance Planar Micro-supercapacitors through Inkjet Printing. *ACS Applied Energy Materials* **2019**, *2* (3), 1876-1890. DOI: 10.1021/acsaem.8b02006.

(309) Denn, M. M. Fibre Spinning. In *Computational Analysis of Polymer Processing*, Pearson, J. R. A., Richardson, S. M. Eds.; Springer Netherlands, 1983; pp 179-216.

(310) Mirabedini, A.; Foroughi, J.; Wallace, G. G. Developments in conducting polymer fibres: from established spinning methods toward advanced applications. *RSC Advances* **2016**, *6* (50), 44687-44716, 10.1039/C6RA05626A. DOI: 10.1039/C6RA05626A.

(311) Onggar, T.; Kruppke, I.; Cherif, C. Techniques and Processes for the Realization of Electrically Conducting Textile Materials from Intrinsically Conducting Polymers and Their Application Potential. *Polymers (Basel)* **2020**, *12* (12). DOI: 10.3390/polym12122867 From NLM.

(312) Imura, Y.; Hogan, R. M. C.; Jaffe, M. 10 - Dry spinning of synthetic polymer fibers. In *Advances in Filament Yarn Spinning of Textiles and Polymers*, Zhang, D. Ed.; Woodhead Publishing, 2014; pp 187-202.

(313) Ozipek, B.; Karakas, H. 9 - Wet spinning of synthetic polymer fibers. In *Advances in Filament Yarn Spinning of Textiles and Polymers*, Zhang, D. Ed.; Woodhead Publishing, 2014; pp 174-186.

(314) Zhang, Q.; Wang, X.; Chen, D.; Jing, X. Preparation and properties of conductive polyaniline/poly-ω-aminoundecanoyle fibers. *Journal of Applied Polymer Science* **2002**, *85* (7), 1458-1464, https://doi.org/10.1002/app.10748. DOI: 10.1002/app.10748 (acccessed 2021/03/12).

(315) Kou, L.; Huang, T.; Zheng, B.; Han, Y.; Zhao, X.; Gopalsamy, K.; Sun, H.; Gao, C. Coaxial wet-spun yarn supercapacitors for high-energy density and safe wearable electronics. *Nature Communications* **2014**. DOI: 10.1038/ncomms4754.

(316) Huang, Q.; Liu, L.; Wang, D.; Liu, J.; Huang, Z.; Zheng, Z. One-step electrospinning of carbon nanowebs on metallic textiles for high-capacitance supercapacitor fabrics. *Journal of Materials Chemistry A* **2016**. DOI: 10.1039/c5ta09309k.
(317) Rawal, A.; Mukhopadhyay, S. 4 - Melt spinning of synthetic polymeric filaments. In *Advances in Filament Yarn Spinning of Textiles and Polymers*, Zhang, D. Ed.; Woodhead Publishing, 2014; pp 75-99.
(318) Kim, B.; Koncar, V.; Devaux, E.; Dufour, C.; Viallier, P. Electrical and morphological properties of PP and PET conductive polymer fibers. *Synthetic Metals* **2004**, *146* (2), 167-174. DOI: 10.1016/j.synthmet.2004.06.023.
(319) Zhong, W. 3 - Nanofibres for medical textiles. In *Advances in Smart Medical Textiles*, van Langenhove, L. Ed.; Woodhead Publishing, 2016; pp 57-70.
(320) Ni, Q. Q.; Jin, X. D.; Xia, H.; Liu, F. 7 - Electrospinning, processing and characterization of polymer-based nano-composite fibers. In *Advances in Filament Yarn Spinning of Textiles and Polymers*, Zhang, D. Ed.; Woodhead Publishing, 2014; pp 128-148.
(321) Arica, T. A.; Isık, T.; Guner, T.; Horzum, N.; Demir, M. M. Advances in Electrospun Fiber-Based Flexible Nanogenerators for Wearable Applications. *Macromolecular Materials and Engineering* **2021**, *306* (8), 2100143. DOI: 10.1002/mame.202100143.
(322) Wei, M.; Lee, J.; Kang, B.; Mead, J. Preparation of Core-Sheath Nanofibers from Conducting Polymer Blends. *Macromolecular Rapid Communications* **2005**, *26* (14), 1127-1132, https://doi.org/10.1002/marc.200500212. DOI: 10.1002/marc.200500212 (acccessed 2021/03/12).
(323) Huang, Y.; Huang, Y.; Zhu, M.; Meng, W.; Pei, Z.; Liu, C.; Hu, H.; Zhi, C. Magnetic-Assisted, Self-Healable, Yarn-Based Supercapacitor. *ACS Nano* **2015**, *9* (6), 6242-6251. DOI: 10.1021/acsnano.5b01602.
(324) Zhang, M.; Wang, C.; Wang, H.; Jian, M.; Hao, X.; Zhang, Y. Carbonized Cotton Fabric for High-Performance Wearable Strain Sensors. *Advanced Functional Materials* **2017**, *27* (2), 1604795, https://doi.org/10.1002/adfm.201604795. DOI: 10.1002/adfm.201604795 (acccessed 2021/09/23).
(325) Basile, F.; Benito, P.; Fornasari, G.; Monti, M.; Scavetta, E.; Tonelli, D.; Vaccari, A. A novel electrochemical route for the catalytic coating of metallic supports. In *Studies in Surface Science and Catalysis*, Gaigneaux, E. M., Devillers, M., Hermans, S., Jacobs, P. A., Martens, J. A., Ruiz, P. Eds.; Vol. 175; Elsevier, 2010; pp 51-58.

(326) Karatutlu, A.; Barhoum, A.; Sapelkin, A. Chapter 1 - Liquid-phase synthesis of nanoparticles and nanostructured materials. In *Emerging Applications of Nanoparticles and Architecture Nanostructures*, Barhoum, A., Makhlouf, A. S. H. Eds.; Elsevier, 2018; pp 1-28.
(327) Gasana, E.; Westbroek, P.; Hakuzimana, J.; De Clerck, K.; Priniotakis, G.; Kiekens, P.; Tseles, D. Electroconductive textile structures through electroless deposition of polypyrrole and copper at polyaramide surfaces. *Surface and Coatings Technology* **2006**, *201* (6), 3547-3551. DOI: https://doi.org/10.1016/j.surfcoat.2006.08.128.
(328) Zhao, Y.; Cai, Z.; Fu, X.; Song, B.; Zhu, H. Electrochemical deposition and characterization of copper crystals on polyaniline/poly(ethylene terephthalate) conductive textiles. *Synthetic Metals* **2013**, *175*, 1-8. DOI: 10.1016/j.synthmet.2013.04.018.
(329) Feng, S. H.; Li, G. H. Chapter 4 - Hydrothermal and Solvothermal Syntheses. In *Modern Inorganic Synthetic Chemistry (Second Edition)*, Xu, R., Xu, Y. Eds.; Elsevier, 2017; pp 73-104.
(330) Dorey, R. Chapter 2 - Routes to thick films: What is a thick film? How is it made? In *Ceramic Thick Films for MEMS and Microdevices*, Dorey, R. Ed.; William Andrew Publishing, 2012; pp 35-61.
(331) Li, Z.; Huang, T.; Gao, W.; Xu, Z.; Chang, D.; Zhang, C.; Gao, C. Hydrothermally Activated Graphene Fiber Fabrics for Textile Electrodes of Supercapacitors. *ACS Nano* **2017**, *11* (11), 11056-11065. DOI: 10.1021/acsnano.7b05092.
(332) Nelson, G. 4 - Microencapsulated colourants for technical textile application. In *Advances in the Dyeing and Finishing of Technical Textiles*, Gulrajani, M. L. Ed.; Woodhead Publishing, 2013; pp 78-104.
(333) Al Shannaq, R.; Farid, M. M. 10 - Microencapsulation of phase change materials (PCMs) for thermal energy storage systems. In *Advances in Thermal Energy Storage Systems*, Cabeza, L. F. Ed.; Woodhead Publishing, 2015; pp 247-284.
(334) Lee, J. S.; Shin, D. H.; Jang, J. Polypyrrole-coated manganese dioxide with multiscale architectures for ultrahigh capacity energy storage. *Energy & Environmental Science* **2015**, *8* (10), 3030-3039, 10.1039/C5EE02076J. DOI: 10.1039/C5EE02076J.
(335) Nayak, L.; Rahaman, M.; Giri, R. Surface Modification/Functionalization of Carbon Materials by Different Techniques: An Overview. In *Carbon-Containing Polymer Composites*, Rahaman, M., Khastgir, D., Aldalbahi, A. K. Eds.; Springer Singapore, 2019; pp 65-98.
(336) Lam, D. V.; Won, S.; Shim, H. C.; Kim, J.-H.; Lee, S.-M. Turning cotton into tough energy textile via metal oxide assisted carbonization. *Carbon* **2019**, *153*, 257-264. DOI: 10.1016/j.carbon.2019.07.010.

(337) Levitt, A.; Hegh, D.; Phillips, P.; Uzun, S.; Anayee, M.; Razal, J. M.; Gogotsi, Y.; Dion, G. 3D knitted energy storage textiles using MXene-coated yarns. *Materials Today* **2020**, *34*, 17-29. DOI: https://doi.org/10.1016/j.mattod.2020.02.005.

(338) Yu, D.; Qian, Q.; Wei, L.; Jiang, W.; Goh, K.; Wei, J.; Zhang, J.; Chen, Y. Emergence of fiber supercapacitors. *Chemical Society Reviews* **2015**, *44* (3), 647-662, 10.1039/C4CS00286E. DOI: 10.1039/C4CS00286E.

(339) Zhai, S.; Karahan, H. E.; Wang, C.; Pei, Z.; Wei, L.; Chen, Y. 1D Supercapacitors for Emerging Electronics: Current Status and Future Directions. *Advanced Materials* **2020**, *32* (5), 1902387, https://doi.org/10.1002/adma.201902387. DOI: 10.1002/adma.201902387 (acccessed 2021/09/25).

(340) Zhai, S.; Wei, L.; Karahan, H. E.; Chen, X.; Wang, C.; Zhang, X.; Chen, J.; Wang, X.; Chen, Y. 2D materials for 1D electrochemical energy storage devices. *Energy Storage Materials* **2019**, *19*, 102-123. DOI: 10.1016/j.ensm.2019.02.020.

(341) Dubal, D. P.; Kim, J. G.; Kim, Y.; Holze, R.; Lokhande, C. D.; Kim, W. B. Supercapacitors Based on Flexible Substrates: An Overview. *Energy Technology* **2014**, *2* (4), 325-341. DOI: 10.1002/ente.201300144.

(342) Soin, N. Chapter 10 - Magnetic Nanoparticles—Piezoelectric Polymer Nanocomposites for Energy Harvesting. In *Magnetic Nanostructured Materials*, El-Gendy, A. A., Barandiarán, J. M., Hadimani, R. L. Eds.; Elsevier, 2018; pp 295-322.

(343) Akinaga, H. Recent advances and future prospects in energy harvesting technologies. *Japanese Journal of Applied Physics* **2020**, *59* (11), 110201. DOI: 10.35848/1347-4065/abbfa0.

(344) Saha, C. R.; Donnell, T. O.; Loder, H.; Beeby, S.; Tudor, J. Optimization of an Electromagnetic Energy Harvesting Device. *IEEE Transactions on Magnetics* **2006**, *42* (10), 3509-3511. DOI: 10.1109/TMAG.2006.879447.

(345) Wang, H.; Jasim, A. 14 - Piezoelectric energy harvesting from pavement. In *Eco-Efficient Pavement Construction Materials*, Pacheco-Torgal, F., Amirkhanian, S., Wang, H., Schlangen, E. Eds.; Woodhead Publishing, 2020; pp 367-382.

(346) Beeby, S. P.; Cao, Z.; Almussallam, A. 11 - Kinetic, thermoelectric and solar energy harvesting technologies for smart textiles. In *Multidisciplinary Know-How for Smart-Textiles Developers*, Kirstein, T. Ed.; Woodhead Publishing, 2013; pp 306-328.

(347) Dang, N.; Bozorgzadeh, E.; Venkatasubramanian, N. Chapter 6 - Energy Harvesting for Sustainable Smart Spaces. In *Advances in Computers*, Hurson, A., Memon, A. Eds.; Vol. 87; Elsevier, 2012; pp 203-251.

(348) Yang, Y.; Zhang, H.; Lin, Z.-H.; Zhou, Y. S.; Jing, Q.; Su, Y.; Yang, J.; Chen, J.; Hu, C.; Wang, Z. L. Human Skin Based Triboelectric Nanogenerators for Harvesting Biomechanical Energy and as Self-Powered Active Tactile Sensor System. *ACS Nano* **2013**, *7* (10), 9213-9222. DOI: 10.1021/nn403838y.

(349) Yang, W.; Chen, J.; Zhu, G.; Yang, J.; Bai, P.; Su, Y.; Jing, Q.; Cao, X.; Wang, Z. L. Harvesting Energy from the Natural Vibration of Human Walking. *ACS Nano* **2013**, *7* (12), 11317-11324. DOI: 10.1021/nn405175z.

(350) Lv, J.; Jeerapan, I.; Tehrani, F.; Yin, L.; Silva-Lopez, C. A.; Jang, J.-H.; Joshuia, D.; Shah, R.; Liang, Y.; Xie, L.; et al. Sweat-based wearable energy harvesting-storage hybrid textile devices. *Energy & Environmental Science* **2018**, *11* (12), 3431-3442, 10.1039/C8EE02792G. DOI: 10.1039/C8EE02792G.

(351) Yong, S.; Shi, J.; Beeby, S. Wearable Textile Power Module Based on Flexible Ferroelectret and Supercapacitor. *Energy Technology* **2019**, *7* (5), 1800938. DOI: 10.1002/ente.201800938.

(352) Satharasinghe, A.; Hughes-Riley, T.; Dias, T. Solar Energy-Harvesting E-Textiles to Power Wearable Devices. *Proceedings* **2019**, *32* (1). DOI: 10.3390/proceedings2019032001.

(353) Dyatkin, B.; Presser, V.; Heon, M.; Lukatskaya, M. R.; Beidaghi, M.; Gogotsi, Y. Development of a Green Supercapacitor Composed Entirely of Environmentally Friendly Materials. *ChemSusChem* **2013**, *6* (12), 2269-2280, https://doi.org/10.1002/cssc.201300852. DOI: 10.1002/cssc.201300852 (acccessed 2021/03/14).

(354) Wang, B.; Fang, X.; Sun, H.; He, S.; Ren, J.; Zhang, Y.; Peng, H. Fabricating Continuous Supercapacitor Fibers with High Performances by Integrating All Building Materials and Steps into One Process. *Adv Mater* **2015**, *27* (47), 7854-7860. DOI: 10.1002/adma.201503441 From NLM.

(355) Fu, Y.; Cai, X.; Wu, H.; Lv, Z.; Hou, S.; Peng, M.; Yu, X.; Zou, D. Fiber Supercapacitors Utilizing Pen Ink for Flexible/Wearable Energy Storage. *Advanced Materials* **2012**, *24* (42), 5713-5718, https://doi.org/10.1002/adma.201202930. DOI: https://doi.org/10.1002/adma.201202930 (acccessed 2021/03/14).

(356) Wang, G.; Wang, H.; Lu, X.; Ling, Y.; Yu, M.; Zhai, T.; Tong, Y.; Li, Y. Solid-State Supercapacitor Based on Activated Carbon Cloths Exhibits Excellent Rate Capability. *Advanced Materials* **2014**, *26* (17), 2676-2682, https://doi.org/10.1002/adma.201304756. DOI: https://doi.org/10.1002/adma.201304756 (acccessed 2021/03/14).

(357) Han, Y.; Lu, Y.; Shen, S.; Zhong, Y.; Liu, S.; Xia, X.; Tong, Y.; Lu, X. Enhancing the Capacitive Storage Performance of Carbon Fiber Textile by Surface and Structural Modulation

for Advanced Flexible Asymmetric Supercapacitors. *Advanced Functional Materials* **2019**, *29* (7), 1806329, https://doi.org/10.1002/adfm.201806329. DOI: https://doi.org/10.1002/adfm.201806329 (acccessed 2021/03/14).

(358) Wang, W.; Liu, W.; Zeng, Y.; Han, Y.; Yu, M.; Lu, X.; Tong, Y. A Novel Exfoliation Strategy to Significantly Boost the Energy Storage Capability of Commercial Carbon Cloth. *Adv Mater* **2015**, *27* (23), 3572-3578. DOI: 10.1002/adma.201500707 From NLM.

(359) Zhao, X.; Zheng, B.; Huang, T.; Gao, C. Graphene-based single fiber supercapacitor with a coaxial structure. *Nanoscale* **2015**, *7* (21), 9399-9404, 10.1039/C5NR01737H. DOI: 10.1039/C5NR01737H.

(360) Hu, Y.; Cheng, H.; Zhao, F.; Chen, N.; Jiang, L.; Feng, Z.; Qu, L. All-in-one graphene fiber supercapacitor. *Nanoscale* **2014**, *6* (12), 6448-6451, 10.1039/C4NR01220H. DOI: 10.1039/C4NR01220H.

(361) Aboutalebi, S. H.; Jalili, R.; Esrafilzadeh, D.; Salari, M.; Gholamvand, Z.; Aminorroaya Yamini, S.; Konstantinov, K.; Shepherd, R. L.; Chen, J.; Moulton, S. E.; et al. High-performance multifunctional Graphene yarns: Toward wearable all-carbon energy storage textiles. *ACS Nano* **2014**, *8* (3), 2456-2466. DOI: 10.1021/nn406026z.

(362) Chen, S.; Ma, W.; Xiang, H.; Cheng, Y.; Yang, S.; Weng, W.; Zhu, M. Conductive, tough, hydrophilic poly(vinyl alcohol)/graphene hybrid fibers for wearable supercapacitors. *Journal of Power Sources* **2016**, *319*, 271-280. DOI: 10.1016/j.jpowsour.2016.04.030.

(363) Zhai, S.; Jiang, W.; Wei, L.; Karahan, H. E.; Yuan, Y.; Ng, A. K.; Chen, Y. All-carbon solid-state yarn supercapacitors from activated carbon and carbon fibers for smart textiles. *Materials Horizons* **2015**, *2* (6), 598-605, 10.1039/C5MH00108K. DOI: 10.1039/C5MH00108K.

(364) Li, Y.; Zhang, Y.; Zhang, H.; Xing, T.-l.; Chen, G.-q. A facile approach to prepare a flexible sandwich-structured supercapacitor with rGO-coated cotton fabric as electrodes. *RSC Advances* **2019**, *9* (8), 4180-4189, 10.1039/C9RA00171A. DOI: 10.1039/C9RA00171A.

(365) Jost, K.; Perez, C. R.; McDonough, J. K.; Presser, V.; Heon, M.; Dion, G.; Gogotsi, Y. Carbon coated textiles for flexible energy storage. *Energy & Environmental Science* **2011**, *4* (12), 5060-5067, 10.1039/C1EE02421C. DOI: 10.1039/C1EE02421C.

(366) Dong, L.; Xu, C.; Yang, Q.; Fang, J.; Li, Y.; Kang, F. High-performance compressible supercapacitors based on functionally synergic multiscale carbon composite textiles. *Journal of Materials Chemistry A* **2015**, *3* (8), 4729-4737, 10.1039/C4TA06494A. DOI: 10.1039/C4TA06494A.

(367) Yu, J.; Wu, J.; Wang, H.; Zhou, A.; Huang, C.; Bai, H.; Li, L. Metallic Fabrics as the Current Collector for High-Performance Graphene-Based Flexible Solid-State Supercapacitor. *ACS Applied Materials & Interfaces* **2016**, *8* (7), 4724-4729. DOI: 10.1021/acsami.5b12180.
(368) Snook, G. A.; Kao, P.; Best, A. S. Conducting-polymer-based supercapacitor devices and electrodes. *Journal of Power Sources* **2011**, *196* (1), 1-12. DOI: 10.1016/j.jpowsour.2010.06.084.
(369) Wei, C.; Xu, Q.; Chen, Z.; Rao, W.; Fan, L.; Yuan, Y.; Bai, Z.; Xu, J. An all-solid-state yarn supercapacitor using cotton yarn electrodes coated with polypyrrole nanotubes. *Carbohydrate Polymers* **2017**, *169*, 50-57. DOI: https://doi.org/10.1016/j.carbpol.2017.04.002.
(370) Wang, B.; Song, W.; Gu, P.; Fan, L.; Yin, Y.; Wang, C. A stretchable and hydrophobic polypyrrole/knitted cotton fabric electrode for all-solid-state supercapacitor with excellent strain capacitance. *Electrochimica Acta* **2019**, *297*, 794-804. DOI: 10.1016/j.electacta.2018.12.042.
(371) Lv, J.; Zhou, P.; Zhang, L.; Zhong, Y.; Sui, X.; Wang, B.; Chen, Z.; Xu, H.; Mao, Z. High-performance textile electrodes for wearable electronics obtained by an improved in situ polymerization method. *Chemical Engineering Journal* **2019**, *361*, 897-907. DOI: 10.1016/j.cej.2018.12.083.
(372) Lv, J.; Zhang, L.; Zhong, Y.; Sui, X.; Wang, B.; Chen, Z.; Feng, X.; Xu, H.; Mao, Z. High-performance polypyrrole coated knitted cotton fabric electrodes for wearable energy storage. *Organic Electronics* **2019**, *74*, 59-68. DOI: 10.1016/j.orgel.2019.06.027.
(373) Cárdenas-Martínez, J.; España-Sánchez, B. L.; Esparza, R.; Ávila-Niño, J. A. Flexible and transparent supercapacitors using electrospun PEDOT:PSS electrodes. *Synthetic Metals* **2020**, *267*, 116436. DOI: 10.1016/j.synthmet.2020.116436.
(374) Xie, X.; Xin, B.; Chen, Z.; Xu, Y. Preparation and characterization of PANI-PPY/PET fabric conductive composite for supercapacitors. *The Journal of The Textile Institute* **2021**, 1-8. DOI: 10.1080/00405000.2021.1992848.
(375) Wang, Y.; Lv, X.; Zou, S.; Lin, X.; Ni, Y. MoS2/polyaniline/functionalized carbon cloth electrode materials for excellent supercapacitor performance. *RSC Advances* **2021**, *11* (18), 10941-10950, 10.1039/D0RA09126J. DOI: 10.1039/D0RA09126J.
(376) An, C.; Zhang, Y.; Guo, H.; Wang, Y. Metal oxide-based supercapacitors: progress and prospectives. *Nanoscale Advances* **2019**, *1* (12), 4644-4658, 10.1039/C9NA00543A. DOI: 10.1039/C9NA00543A.

(377) Su, F.; Miao, M. Asymmetric carbon nanotube–MnO2two-ply yarn supercapacitors for wearable electronics. *Nanotechnology* **2014**, *25* (13), 135401. DOI: 10.1088/0957-4484/25/13/135401.
(378) Abouali, S.; Akbari Garakani, M.; Zhang, B.; Xu, Z.-L.; Kamali Heidari, E.; Huang, J.-q.; Huang, J.; Kim, J.-K. Electrospun Carbon Nanofibers with in Situ Encapsulated Co3O4 Nanoparticles as Electrodes for High-Performance Supercapacitors. *ACS Applied Materials & Interfaces* **2015**, *7* (24), 13503-13511. DOI: 10.1021/acsami.5b02787.
(379) Su, F.; Lv, X.; Miao, M. High-Performance Two-Ply Yarn Supercapacitors Based on Carbon Nanotube Yarns Dotted with Co3O4 and NiO Nanoparticles. *Small* **2015**, *11* (7), 854-861, https://doi.org/10.1002/smll.201401862. DOI: 10.1002/smll.201401862 (acccessed 2021/03/13).
(380) Shahidi, S.; Kalaoglu, F. In situ deposition of nickel nano particles on polyester fabric and its application as a flexible electrode in supercapacitor. *Journal of Industrial Textiles* **2020**, *0* (0), 1528083720944252. DOI: 10.1177/1528083720944252.
(381) Javed, M. S.; Chen, J.; Chen, L.; Xi, Y.; Zhang, C.; Wan, B.; Hu, C. Flexible full-solid state supercapacitors based on zinc sulfide spheres growing on carbon textile with superior charge storage. *Journal of Materials Chemistry A* **2016**, *4* (2), 667-674, 10.1039/C5TA08752J. DOI: 10.1039/C5TA08752J.
(382) Howli, P.; Das, S.; Sarkar, S.; Samanta, M.; Panigrahi, K.; Das, N. S.; Chattopadhyay, K. K. Co3O4 Nanowires on Flexible Carbon Fabric as a Binder-Free Electrode for All Solid-State Symmetric Supercapacitor. *ACS Omega* **2017**, *2* (8), 4216-4226. DOI: 10.1021/acsomega.7b00702.
(383) Uzun, S.; Seyedin, S.; Stoltzfus, A. L.; Levitt, A. S.; Alhabeb, M.; Anayee, M.; Strobel, C. J.; Razal, J. M.; Dion, G.; Gogotsi, Y. Knittable and Washable Multifunctional MXene-Coated Cellulose Yarns. *Advanced Functional Materials* **2019**, *29* (45), 1905015. DOI: 10.1002/adfm.201905015.
(384) Liu, N.; Ma, W.; Tao, J.; Zhang, X.; Su, J.; Li, L.; Yang, C.; Gao, Y.; Golberg, D.; Bando, Y. Cable-Type Supercapacitors of Three-Dimensional Cotton Thread Based Multi-Grade Nanostructures for Wearable Energy Storage. *Advanced Materials* **2013**, *25* (35), 4925-4931, https://doi.org/10.1002/adma.201301311. DOI: 10.1002/adma.201301311 (acccessed 2021/03/13).
(385) Wang, H. T.; Jin, C.; Liu, Y. N.; Kang, X. H.; Bian, S. W.; Zhu, Q. Cotton yarns modified with three-dimensional metallic Ni conductive network and pseudocapacitive Co-Ni layered

double hydroxide nanosheet array as electrode materials for flexible yarn supercapacitors. *Electrochimica Acta* **2018**, *283*, 1789-1797. DOI: 10.1016/j.electacta.2018.07.090.

(386) Ma, Y.; Wang, Q.; Liang, X.; Zhang, D.; Miao, M. Wearable supercapacitors based on conductive cotton yarns. *Journal of Materials Science* **2018**, *53* (20), 14586-14597. DOI: 10.1007/s10853-018-2655-z.

(387) Yang, L.; Lin, F.; Zabihi, F.; Yang, S.; Zhu, M. High specific capacitance cotton fiber electrode enhanced with PPy and MXene by in situ hybrid polymerization. *International Journal of Biological Macromolecules* **2021**, *181*, 1063-1071. DOI: 10.1016/j.ijbiomac.2021.04.112.

(388) Li, J.; Shao, Y.; Jiang, P.; Zhang, Q.; Hou, C.; Li, Y.; Wang, H. 1T-Molybdenum disulfide/reduced graphene oxide hybrid fibers as high strength fibrous electrodes for wearable energy storage. *Journal of Materials Chemistry A* **2019**, *7* (7), 3143-3149, 10.1039/C8TA09328H. DOI: 10.1039/C8TA09328H.

(389) Li, X.; Liu, R.; Xu, C.; Bai, Y.; Zhou, X.; Wang, Y.; Yuan, G. High-Performance Polypyrrole/Graphene/SnCl2 Modified Polyester Textile Electrodes and Yarn Electrodes for Wearable Energy Storage. *Advanced Functional Materials* **2018**, *28* (22), 1800064. DOI: 10.1002/adfm.201800064.

(390) Cai, Z.; Li, L.; Ren, J.; Qiu, L.; Lin, H.; Peng, H. Flexible, weavable and efficient microsupercapacitor wires based on polyaniline composite fibers incorporated with aligned carbon nanotubes. *Journal of Materials Chemistry A* **2013**, *1* (2), 258-261, 10.1039/C2TA00274D. DOI: 10.1039/C2TA00274D.

(391) Choi, C.; Kim, S. H.; Sim, H. J.; Lee, J. A.; Choi, A. Y.; Kim, Y. T.; Lepró, X.; Spinks, G. M.; Baughman, R. H.; Kim, S. J. Stretchable, Weavable Coiled Carbon Nanotube/MnO2/Polymer Fiber Solid-State Supercapacitors. *Scientific Reports* **2015**, *5* (1), 9387. DOI: 10.1038/srep09387.

(392) Chen, X.; Lin, H.; Deng, J.; Zhang, Y.; Sun, X.; Chen, P.; Fang, X.; Zhang, Z.; Guan, G.; Peng, H. Electrochromic Fiber-Shaped Supercapacitors. *Advanced Materials* **2014**, *26* (48), 8126-8132, https://doi.org/10.1002/adma.201403243. DOI: 10.1002/adma.201403243 (acccessed 2021/03/12).

(393) Deng, J.; Zhang, Y.; Zhao, Y.; Chen, P.; Cheng, X.; Peng, H. A Shape-Memory Supercapacitor Fiber. *Angewandte Chemie International Edition* **2015**, *54* (51), 15419-15423, https://doi.org/10.1002/anie.201508293. DOI: https://doi.org/10.1002/anie.201508293 (acccessed 2021/03/14).

(394) Sun, J.; Huang, Y.; Fu, C.; Wang, Z.; Huang, Y.; Zhu, M.; Zhi, C.; Hu, H. High-performance stretchable yarn supercapacitor based on PPy@CNTs@urethane elastic fiber core spun yarn. *Nano Energy* **2016**, *27*, 230-237. DOI: https://doi.org/10.1016/j.nanoen.2016.07.008.

(395) Zhang, Q.; Sun, J.; Pan, Z.; Zhang, J.; Zhao, J.; Wang, X.; Zhang, C.; Yao, Y.; Lu, W.; Li, Q.; et al. Stretchable fiber-shaped asymmetric supercapacitors with ultrahigh energy density. *Nano Energy* **2017**, *39*, 219-228. DOI: 10.1016/j.nanoen.2017.06.052.

(396) Wang, Z.; Qin, S.; Seyedin, S.; Zhang, J.; Wang, J.; Levitt, A.; Li, N.; Haines, C.; Ovalle-Robles, R.; Lei, W.; et al. High-Performance Biscrolled MXene/Carbon Nanotube Yarn Supercapacitors. *Small* **2018**, *14* (37), 1802225. DOI: 10.1002/smll.201802225.

(397) He, N.; Patil, S.; Qu, J.; Liao, J.; Zhao, F.; Gao, W. Effects of Electrolyte Mediation and MXene Size in Fiber-Shaped Supercapacitors. *ACS Applied Energy Materials* **2020**, *3* (3), 2949-2958. DOI: 10.1021/acsaem.0c00024.

(398) Zhang, J.; Seyedin, S.; Qin, S.; Wang, Z.; Moradi, S.; Yang, F.; Lynch, P. A.; Yang, W.; Liu, J.; Wang, X.; et al. Highly Conductive Ti3C2Tx MXene Hybrid Fibers for Flexible and Elastic Fiber-Shaped Supercapacitors. *Small* **2019**, *15* (8), 1804732. DOI: 10.1002/smll.201804732.

(399) Tao, J.; Liu, N.; Ma, W.; Ding, L.; Li, L.; Su, J.; Gao, Y. Solid-State High Performance Flexible Supercapacitors Based on Polypyrrole-MnO2-Carbon Fiber Hybrid Structure. *Scientific Reports* **2013**, *3* (1), 2286. DOI: 10.1038/srep02286.

(400) Naderi, L.; Shahrokhian, S.; Soavi, F. Fabrication of a 2.8 V high-performance aqueous flexible fiber-shaped asymmetric micro-supercapacitor based on MnO2/PEDOT:PSS-reduced graphene oxide nanocomposite grown on carbon fiber electrode. *Journal of Materials Chemistry A* **2020**, *8* (37), 19588-19602, 10.1039/D0TA06561G. DOI: 10.1039/D0TA06561G.

(401) Keum, K.; Lee, G.; Lee, H.; Yun, J.; Park, H.; Hong, S. Y.; Song, C.; Kim, J. W.; Ha, J. S. Wire-Shaped Supercapacitors with Organic Electrolytes Fabricated via Layer-by-Layer Assembly. *ACS Appl Mater Interfaces* **2018**, *10* (31), 26248-26257. DOI: 10.1021/acsami.8b07113 From NLM.

(402) Huang, Y.; Hu, H.; Huang, Y.; Zhu, M.; Meng, W.; Liu, C.; Pei, Z.; Hao, C.; Wang, Z.; Zhi, C. From Industrially Weavable and Knittable Highly Conductive Yarns to Large Wearable Energy Storage Textiles. *ACS Nano* **2015**, *9* (5), 4766-4775. DOI: 10.1021/acsnano.5b00860.

(403) Huang, Q.; Liu, L.; Wang, D.; Liu, J.; Huang, Z.; Zheng, Z. One-step electrospinning of carbon nanowebs on metallic textiles for high-capacitance supercapacitor fabrics. *Journal of*

Materials Chemistry A **2016**, *4* (18), 6802-6808, 10.1039/C5TA09309K. DOI: 10.1039/C5TA09309K.

(404) Etana, B. B.; Ramakrishnan, S.; Dhakshnamoorthy, M.; Saravanan, S.; C Ramamurthy, P.; Demissie, T. A. Functionalization of textile cotton fabric with reduced graphene oxide/MnO2/polyaniline based electrode for supercapacitor. *Materials Research Express* **2020**, *6* (12), 125708. DOI: 10.1088/2053-1591/ab669d.

(405) Cheng, X.; Fang, X.; Chen, P.; Doo, S. G.; Son, I. H.; Huang, X.; Zhang, Y.; Weng, W.; Zhang, Z.; Deng, J.; et al. Designing one-dimensional supercapacitors in a strip shape for high performance energy storage fabrics. *Journal of Materials Chemistry A* **2015**. DOI: 10.1039/c5ta06317e.

(406) Zhang, H.; Qiao, Y.; Lu, Z. Fully Printed Ultraflexible Supercapacitor Supported by a Single-Textile Substrate. *ACS Applied Materials & Interfaces* **2016**, *8* (47), 32317-32323. DOI: 10.1021/acsami.6b11172.

(407) Kim, T.; Samuel, E. P.; Park, C.; Kim, Y.-I.; Aldalbahi, A.; Alotaibi, F.; Yoon, S. S. Wearable fabric supercapacitors using supersonically sprayed reduced graphene and tin oxide. *Journal of Alloys and Compounds* **2021**, *856*, 157902. DOI: 10.1016/j.jallcom.2020.157902.

(408) Liu, L.; Tian, Q.; Yao, W.; Li, M.; Li, Y.; Wu, W. All-printed ultraflexible and stretchable asymmetric in-plane solid-state supercapacitors (ASCs) for wearable electronics. *Journal of Power Sources* **2018**, *397*, 59-67. DOI: https://doi.org/10.1016/j.jpowsour.2018.07.013.

(409) Lv, P.; Feng, Y. Y.; Li, Y.; Feng, W. Carbon fabric-aligned carbon nanotube/MnO2/conducting polymers ternary composite electrodes with high utilization and mass loading of MnO2 for super-capacitors. *Journal of Power Sources* **2012**, *220*, 160-168. DOI: 10.1016/j.jpowsour.2012.07.073.

(410) Zhu, J.; Zhao, S.-X.; Wu, X.; Wang, Y.-F.; Yu, L.; Nan, C.-W. Wrapping RGO/MoO2/carbon textile as supercapacitor electrode with enhanced flexibility and areal capacitance. *Electrochimica Acta* **2018**, *282*, 784-791. DOI: 10.1016/j.electacta.2018.06.089.

(411) Mu, F.; Zhao, J.; Gu, C. Ultrathin porous NiMnO3 nanosheets on carbon cloth for use as supercapacitor electrode. *AIP Advances* **2020**, *10* (6), 065002. DOI: 10.1063/5.0009246.

(412) Wang, H.; Wang, H.; Wang, Y.; Su, X.; Wang, C.; Zhang, M.; Jian, M.; Xia, K.; Liang, X.; Lu, H.; et al. Laser Writing of Janus Graphene/Kevlar Textile for Intelligent Protective Clothing. *ACS Nano* **2020**, *14* (3), 3219-3226. DOI: 10.1021/acsnano.9b08638.

(413) Afroj, S.; Britnell, L.; Hasan, T.; Andreeva, D. V.; Novoselov, K. S.; Karim, N. Graphene-Based Technologies for Tackling COVID-19 and Future Pandemics. *Advanced Functional Materials* **2021**, *31* (52), 2107407. DOI: https://doi.org/10.1002/adfm.202107407.

(414) Qu, J.; He, N.; Patil, S. V.; Wang, Y.; Banerjee, D.; Gao, W. Screen Printing of Graphene Oxide Patterns onto Viscose Nonwovens with Tunable Penetration Depth and Electrical Conductivity. *ACS Applied Materials & Interfaces* **2019**, *11* (16), 14944-14951. DOI: 10.1021/acsami.9b00715.

(415) Xu, X.; Luo, M.; He, P.; Guo, X.; Yang, J. Screen printed graphene electrodes on textile for wearable electrocardiogram monitoring. *Applied Physics A* **2019**, *125* (10), 714. DOI: 10.1007/s00339-019-3006-x.

(416) Izak, P.; Mastalska-Poplawska, J.; Lis, J.; Stempkowska, A. Modification of the rheological properties of screen printing ceramic paints containing gold. *Journal of Physics: Conference Series* **2017**, *790*, 012011. DOI: 10.1088/1742-6596/790/1/012011.

(417) Koshi, T.; Nomura, K.-I.; Yoshida, M. Resistance Reduction of Conductive Patterns Printed on Textile by Curing Shrinkage of Passivation Layers. *Micromachines* **2020**, *11* (6), 539. DOI: 10.3390/mi11060539 PubMed.

(418) Standard, B. *Textiles — Tests for colour fastness*; 2010.

(419) Yang, K.; Torah, R.; Wei, Y.; Beeby, S.; Tudor, J. Waterproof and durable screen printed silver conductive tracks on textiles. *Textile Research Journal* **2013**, *83* (19), 2023-2031. DOI: 10.1177/0040517513490063.

(420) Teymourian, H.; Parrilla, M.; Sempionatto, J. R.; Montiel, N. F.; Barfidokht, A.; Van Echelpoel, R.; De Wael, K.; Wang, J. Wearable Electrochemical Sensors for the Monitoring and Screening of Drugs. *ACS Sens* **2020**, *5* (9), 2679-2700. DOI: 10.1021/acssensors.0c01318 From NLM.

(421) Wang, Q.; Ling, S.; Liang, X.; Wang, H.; Lu, H.; Zhang, Y. Self-Healable Multifunctional Electronic Tattoos Based on Silk and Graphene. *Advanced Functional Materials* **2019**, *29* (16), 1808695. DOI: 10.1002/adfm.201808695.

(422) Souri, H.; Banerjee, H.; Jusufi, A.; Radacsi, N.; Stokes, A. A.; Park, I.; Sitti, M.; Amjadi, M. Wearable and Stretchable Strain Sensors: Materials, Sensing Mechanisms, and Applications. *Advanced Intelligent Systems* **2020**, *2* (8), 2000039. DOI: 10.1002/aisy.202000039.

(423) Al-khafajiy, M.; Baker, T.; Chalmers, C.; Asim, M.; Kolivand, H.; Fahim, M.; Waraich, A. Remote health monitoring of elderly through wearable sensors. *Multimedia Tools and Applications* **2019**, *78* (17), 24681-24706. DOI: 10.1007/s11042-018-7134-7.

(424) Kabiri Ameri, S.; Ho, R.; Jang, H.; Tao, L.; Wang, Y.; Wang, L.; Schnyer, D. M.; Akinwande, D.; Lu, N. Graphene Electronic Tattoo Sensors. *ACS Nano* **2017**, *11* (8), 7634-7641. DOI: 10.1021/acsnano.7b02182.

(425) Biasiucci, A.; Franceschiello, B.; Murray, M. M. Electroencephalography. *Current Biology* **2019**, *29* (3), R80-R85. DOI: 10.1016/j.cub.2018.11.052.
(426) Velcescu, A.; Lindley, A.; Cursio, C.; Krachunov, S.; Beach, C.; Brown, C. A.; Jones, A. K. P.; Casson, A. J. Flexible 3D-Printed EEG Electrodes. *Sensors (Basel)* **2019**, *19* (7), 1650. DOI: 10.3390/s19071650 PubMed.
(427) Goldberger, A. L.; Amaral, L. A.; Glass, L.; Hausdorff, J. M.; Ivanov, P. C.; Mark, R. G.; Mietus, J. E.; Moody, G. B.; Peng, C. K.; Stanley, H. E. PhysioBank, PhysioToolkit, and PhysioNet: components of a new research resource for complex physiologic signals. *Circulation* **2000**, *101* (23), E215-220. DOI: 10.1161/01.cir.101.23.e215 From NLM.
(428) Kemp, B.; Zwinderman, A. H.; Tuk, B.; Kamphuisen, H. A. C.; Oberye, J. J. L. Analysis of a sleep-dependent neuronal feedback loop: the slow-wave microcontinuity of the EEG. *IEEE Transactions on Biomedical Engineering* **2000**, *47* (9), 1185-1194. DOI: 10.1109/10.867928.
(429) Sharma, M.; Tiwari, J.; Acharya, U. R. Automatic Sleep-Stage Scoring in Healthy and Sleep Disorder Patients Using Optimal Wavelet Filter Bank Technique with EEG Signals. *International Journal of Environmental Research and Public Health* **2021**, *18* (6). DOI: 10.3390/ijerph18063087.
(430) Yildirim, O.; Baloglu, U. B.; Acharya, U. R. A Deep Learning Model for Automated Sleep Stages Classification Using PSG Signals. *International journal of environmental research and public health* **2019**, *16* (4), 599. DOI: 10.3390/ijerph16040599 PubMed.
(431) Owda, A. Y.; Casson, A. J. Investigating Gelatine Based Head Phantoms for Electroencephalography Compared to Electrical and Ex Vivo Porcine Skin Models. *IEEE Access* **2021**, *9*, 96722-96738. DOI: 10.1109/ACCESS.2021.3095220.
(432) Baker, F. C.; Turlington, S. R.; Colrain, I. Developmental changes in the sleep electroencephalogram of adolescent boys and girls. *J Sleep Res* **2012**, *21* (1), 59-67. DOI: 10.1111/j.1365-2869.2011.00930.x PubMed.
(433) Geim, A. K.; Novoselov, K. S. The rise of graphene. *Nature Materials* **2007**, *6* (3), 183-191. DOI: 10.1038/nmat1849.
(434) Zhao, B.; Shen, D.; Zhang, Z.; Lu, P.; Hossain, M.; Li, J.; Li, B.; Duan, X. 2D Metallic Transition-Metal Dichalcogenides: Structures, Synthesis, Properties, and Applications. *Advanced Functional Materials* **2021**, *31* (48), 2105132. DOI: 10.1002/adfm.202105132.
(435) Wu, J. Understanding the Electric Double-Layer Structure, Capacitance, and Charging Dynamics. *Chemical Reviews* **2022**, *122* (12), 10821-10859. DOI: 10.1021/acs.chemrev.2c00097.

(436) Fleischmann, S.; Mitchell, J. B.; Wang, R.; Zhan, C.; Jiang, D.-e.; Presser, V.; Augustyn, V. Pseudocapacitance: From Fundamental Understanding to High Power Energy Storage Materials. *Chemical Reviews* **2020**, *120* (14), 6738-6782. DOI: 10.1021/acs.chemrev.0c00170.
(437) Sheberla, D.; Bachman, J. C.; Elias, J. S.; Sun, C.-J.; Shao-Horn, Y.; Dincă, M. Conductive MOF electrodes for stable supercapacitors with high areal capacitance. *Nature Materials* **2017**, *16* (2), 220-224. DOI: 10.1038/nmat4766.
(438) Lee, J.-S. M.; Briggs, M. E.; Hu, C.-C.; Cooper, A. I. Controlling electric double-layer capacitance and pseudocapacitance in heteroatom-doped carbons derived from hypercrosslinked microporous polymers. *Nano Energy* **2018**, *46*, 277-289. DOI: 10.1016/j.nanoen.2018.01.042.
(439) Guo, H.-W.; Hu, Z.; Liu, Z.-B.; Tian, J.-G. Stacking of 2D Materials. *Advanced Functional Materials* **2021**, *31* (4), 2007810. DOI: 10.1002/adfm.202007810.
(440) Wang, X.; Xia, F. Stacked 2D materials shed light. *Nature Materials* **2015**, *14* (3), 264-265. DOI: 10.1038/nmat4218.
(441) Kumar, P.; Abuhimd, H.; Wahyudi, W.; Li, M.; Ming, J.; Li, L.-J. Review—Two-Dimensional Layered Materials for Energy Storage Applications. *ECS Journal of Solid State Science and Technology* **2016**, *5* (11), Q3021-Q3025. DOI: 10.1149/2.0051611jss.
(442) Bello, I. T.; Adio, S. A.; Oladipo, A. O.; Adedokun, O.; Mathevula, L. E.; Dhlamini, M. S. Molybdenum sulfide-based supercapacitors: From synthetic, bibliometric, and qualitative perspectives. *International Journal of Energy Research* **2021**, *45* (9), 12665-12692. DOI: 10.1002/er.6690.
(443) Lee, C.-S.; Kim, T. H. Large-Scale Preparation of MoS2/Graphene Composites for Electrochemical Detection of Morin. *ACS Applied Nano Materials* **2021**, *4* (7), 6668-6677. DOI: 10.1021/acsanm.1c00622.
(444) Bertolazzi, S.; Krasnozhon, D.; Kis, A. Nonvolatile Memory Cells Based on MoS2/Graphene Heterostructures. *ACS Nano* **2013**, *7* (4), 3246-3252. DOI: 10.1021/nn3059136.
(445) Rendón-Patiño, A.; Domenech-Carbó, A.; Primo, A.; García, H. Superior Electrocatalytic Activity of MoS2-Graphene as Superlattice. *Nanomaterials* **2020**, *10* (5), 839. DOI: 10.3390/nano10050839.
(446) Liu, H.; Li, Z.; Song, W.; Yu, Y.; Pang, F.; Wang, T. MoS2/graphene heterostructure incorporated passively mode-locked fiber laser: from anomalous to normal average dispersion. *Opt. Mater. Express* **2020**, *10* (1), 46-56. DOI: 10.1364/OME.10.000046.

(447) Vikraman, D.; Rabani, I.; Hussain, S.; Sundaram, K.; Ramesh, S.; Kim, H.-S.; Seo, Y.-S.; Jung, J.; Kim, H.-S. Mixed-phase MoS2 decorated reduced graphene oxide hybrid composites for efficient symmetric supercapacitors. *International Journal of Energy Research* **2021**, *45* (6), 9193-9209. DOI: 10.1002/er.6448.

(448) Singh, K.; Kumar, S.; Agarwal, K.; Soni, K.; Ramana Gedela, V.; Ghosh, K. Three-dimensional Graphene with MoS2Nanohybrid as Potential Energy Storage/Transfer Device. *Scientific Reports* **2017**, *7* (1), 9458. DOI: 10.1038/s41598-017-09266-2.

(449) Islam, M. R.; Afroj, S.; Karim, N. Scalable Production of 2D Material Heterostructure Textiles for High-Performance Wearable Supercapacitors. *ACS Nano* **2023**, *17* (18), 18481-18493. DOI: 10.1021/acsnano.3c06181.

(450) Panagiotou, T.; Bernard, J.; Chomistek, K. J.; Fisher, R. Production of Polymer Nanosuspensions Using Microfluidizer® Processor Based Technologies. 2008.

(451) Goldberg, S. Mechanical/Physical Methods of Cell Disruption and Tissue Homogenization. In *2D PAGE: Sample Preparation and Fractionation*, Posch, A. Ed.; Humana Press, 2008; pp 3-22.

(452) Karagiannidis, P. G.; Hodge, S. A.; Lombardi, L.; Tomarchio, F.; Decorde, N.; Milana, S.; Goykhman, I.; Su, Y.; Mesite, S. V.; Johnstone, D. N.; et al. Microfluidization of Graphite and Formulation of Graphene-Based Conductive Inks. *ACS Nano* **2017**, *11* (3), 2742-2755. DOI: 10.1021/acsnano.6b07735.

(453) Lajunen, T.; Hisazumi, K.; Kanazawa, T.; Okada, H.; Seta, Y.; Yliperttula, M.; Urtti, A.; Takashima, Y. Topical drug delivery to retinal pigment epithelium with microfluidizer produced small liposomes. *European Journal of Pharmaceutical Sciences* **2014**, *62*, 23-32. DOI: 10.1016/j.ejps.2014.04.018.

(454) Tang, S. Y.; Shridharan, P.; Sivakumar, M. Impact of process parameters in the generation of novel aspirin nanoemulsions – Comparative studies between ultrasound cavitation and microfluidizer. *Ultrasonics Sonochemistry* **2013**, *20* (1), 485-497. DOI: 10.1016/j.ultsonch.2012.04.005.

(455) Jafari, S. M.; He, Y.; Bhandari, B. Production of sub-micron emulsions by ultrasound and microfluidization techniques. *Journal of Food Engineering* **2007**, *82* (4), 478-488. DOI: 10.1016/j.jfoodeng.2007.03.007.

(456) Panagiotou, T.; Bernard, J. M.; Mesite, S. V. Deagglomeration and dispersion of carbon nanotubes using microfluidizer high shear fluid processors. In *Nano Science and Technology Institute (NSTI) conference and expo proceedings*, 2008; Vol. 1, pp 39-42.

(457) Paton, K. R.; Anderson, J.; Pollard, A. J.; Sainsbury, T. Production of few-layer graphene by microfluidization. *Materials Research Express* **2017**, *4* (2), 025604. DOI: 10.1088/2053-1591/aa5b24.

(458) Pace, G.; del Rio Castillo, A. E.; Lamperti, A.; Lauciello, S.; Bonaccorso, F. 2D Materials-based Electrochemical Triboelectric Nanogenerators. *Advanced Materials n/a* (n/a), 2211037. DOI: 10.1002/adma.202211037.

(459) Li, Y.; Chen, Q.; Zhang, Z.; Li, Q.; Qiao, X. Effects of morphology and crystallinity of MoS2 nanocrystals on the catalytic reduction of p-nitrophenol. *Journal of Nanoparticle Research* **2018**, *20* (12), 327. DOI: 10.1007/s11051-018-4432-y.

(460) Liu, N.; Kim, P.; Kim, J. H.; Ye, J. H.; Kim, S.; Lee, C. J. Large-Area Atomically Thin MoS2 Nanosheets Prepared Using Electrochemical Exfoliation. *ACS Nano* **2014**, *8* (7), 6902-6910. DOI: 10.1021/nn5016242.

(461) Zhou, S.; Gao, J.; Wang, S.; Fan, H.; Huang, J.; Liu, Y. Highly efficient removal of Cr(VI) from water based on graphene oxide incorporated flower-like MoS2 nanocomposite prepared in situ hydrothermal synthesis. *Environmental Science and Pollution Research* **2020**, *27* (12), 13882-13894. DOI: 10.1007/s11356-020-07978-z.

(462) Alkhalaf, S.; Ranaweera, C. K.; Kahol, P. K.; Siam, K.; Adhikari, H.; Mishra, S. R.; Perez, F.; Gupta, B. K.; Ramasamy, K.; Gupta, R. K. Electrochemical energy storage performance of electrospun CoMn2O4 nanofibers. *Journal of Alloys and Compounds* **2017**, *692*, 59-66. DOI: 10.1016/j.jallcom.2016.09.005.

(463) Xie, Y.; Du, H. Electrochemical capacitance of a carbon quantum dots–polypyrrole/titania nanotube hybrid. *RSC Advances* **2015**, *5* (109), 89689-89697, 10.1039/C5RA16538E. DOI: 10.1039/C5RA16538E.

(464) Beidaghi, M.; Wang, C. Micro-Supercapacitors Based on Interdigital Electrodes of Reduced Graphene Oxide and Carbon Nanotube Composites with Ultrahigh Power Handling Performance. *Advanced Functional Materials* **2012**, *22* (21), 4501-4510. DOI: 10.1002/adfm.201201292.

(465) Noh, J.; Yoon, C. M.; Kim, Y. K.; Jang, J. High performance asymmetric supercapacitor twisted from carbon fiber/MnO2 and carbon fiber/MoO3. *Carbon* **2017**, *116*, 470-478. DOI: 10.1016/j.carbon.2017.02.033.

(466) Lin, J.; Zhang, C.; Yan, Z.; Zhu, Y.; Peng, Z.; Hauge, R. H.; Natelson, D.; Tour, J. M. 3-Dimensional Graphene Carbon Nanotube Carpet-Based Microsupercapacitors with High Electrochemical Performance. *Nano Letters* **2013**, *13* (1), 72-78. DOI: 10.1021/nl3034976.

(467) Cai, F.; Tao, C.-a.; Li, Y.; Yin, W.; Wang, X.; Wang, J. Effects of amount of graphene oxide and the times of LightScribe on the performance of all-solid-state flexible graphene-based micro-supercapacitors. *Materials Research Express* **2017**, *4* (3), 036304. DOI: 10.1088/2053-1591/aa65fb.

(468) Gao, W.; Singh, N.; Song, L.; Liu, Z.; Reddy, A. L. M.; Ci, L.; Vajtai, R.; Zhang, Q.; Wei, B.; Ajayan, P. M. Direct laser writing of micro-supercapacitors on hydrated graphite oxide films. *Nature Nanotechnology* **2011**, *6* (8), 496-500. DOI: 10.1038/nnano.2011.110.

(469) Wang, H.; Lu, Z.; Kong, D.; Sun, J.; Hymel, T. M.; Cui, Y. Electrochemical Tuning of MoS2 Nanoparticles on Three-Dimensional Substrate for Efficient Hydrogen Evolution. *ACS Nano* **2014**, *8* (5), 4940-4947. DOI: 10.1021/nn500959v.

(470) Winchester, A.; Ghosh, S.; Feng, S.; Elias, A. L.; Mallouk, T.; Terrones, M.; Talapatra, S. Electrochemical Characterization of Liquid Phase Exfoliated Two-Dimensional Layers of Molybdenum Disulfide. *ACS Applied Materials & Interfaces* **2014**, *6* (3), 2125-2130. DOI: 10.1021/am4051316.

(471) Li, J.; Sollami Delekta, S.; Zhang, P.; Yang, S.; Lohe, M. R.; Zhuang, X.; Feng, X.; Östling, M. Scalable Fabrication and Integration of Graphene Microsupercapacitors through Full Inkjet Printing. *ACS Nano* **2017**, *11* (8), 8249-8256. DOI: 10.1021/acsnano.7b03354.

(472) El-Kady, M. F.; Kaner, R. B. Scalable fabrication of high-power graphene micro-supercapacitors for flexible and on-chip energy storage. *Nature Communications* **2013**, *4* (1), 1475. DOI: 10.1038/ncomms2446.

(473) Dulal, M.; Afroj, S.; Ahn, J.; Cho, Y.; Carr, C.; Kim, I.-D.; Karim, N. Toward Sustainable Wearable Electronic Textiles. *ACS Nano* **2022**, *16* (12), 19755-19788. DOI: 10.1021/acsnano.2c07723.

(474) Tan, S.; Islam, M. R.; Li, H.; Fernando, A.; Afroj, S.; Karim, N. Highly Scalable, Sensitive and Ultraflexible Graphene-Based Wearable E-Textiles Sensor for Bio-Signal Detection. *Advanced Sensor Research* **2022**, *1* (1), 2200010. DOI: 10.1002/adsr.202200010.

(475) Secor, E. B.; Prabhumirashi, P. L.; Puntambekar, K.; Geier, M. L.; Hersam, M. C. Inkjet Printing of High Conductivity, Flexible Graphene Patterns. *The Journal of Physical Chemistry Letters* **2013**, *4* (8), 1347-1351. DOI: 10.1021/jz400644c.

(476) Karim, M. N.; Afroj, S.; Rigout, M.; Yeates, S. G.; Carr, C. Towards UV-curable inkjet printing of biodegradable poly (lactic acid) fabrics. *Journal of Materials Science* **2015**, *50* (13), 4576-4585. DOI: 10.1007/s10853-015-9006-0.

(477) Maiti, S.; Islam, M. R.; Uddin, M. A.; Afroj, S.; Eichhorn, S. J.; Karim, N. Sustainable Fiber-Reinforced Composites: A Review. *Advanced Sustainable Systems* **2022**, 2200258. DOI: 10.1002/adsu.202200258.

(478) Islam, M. H.; Afroj, S.; Karim, N. Toward Sustainable Composites: Graphene-Modified Jute Fiber Composites with Bio-Based Epoxy Resin. *Global Challenges n/a* (n/a), 2300111. DOI: 10.1002/gch2.202300111.

(479) Afroj, S.; Islam, M. H.; Karim, N. Multifunctional Graphene-Based Wearable E-Textiles. *Proceedings* **2021**, *68* (1). DOI: 10.3390/proceedings2021068011.

(480) Paton, K. R.; Varrla, E.; Backes, C.; Smith, R. J.; Khan, U.; O'Neill, A.; Boland, C.; Lotya, M.; Istrate, O. M.; King, P.; et al. Scalable production of large quantities of defect-free few-layer graphene by shear exfoliation in liquids. *Nature Materials* **2014**, *13* (6), 624-630. DOI: 10.1038/nmat3944.

(481) Tao, H.; Fan, Q.; Ma, T.; Liu, S.; Gysling, H.; Texter, J.; Guo, F.; Sun, Z. Two-dimensional materials for energy conversion and storage. *Progress in Materials Science* **2020**, *111*, 100637. DOI: 10.1016/j.pmatsci.2020.100637.

(482) Wu, Z.; Qi, J.; Wang, W.; Zeng, Z.; He, Q. Emerging elemental two-dimensional materials for energy applications. *Journal of Materials Chemistry A* **2021**, *9* (35), 18793-18817, 10.1039/D1TA03676A. DOI: 10.1039/D1TA03676A.

(483) Pomerantseva, E.; Gogotsi, Y. Two-dimensional heterostructures for energy storage. *Nature Energy* **2017**, *2* (7), 17089. DOI: 10.1038/nenergy.2017.89.

(484) Fang, Q.; Li, M.; Zhao, X.; Yuan, L.; Wang, B.; Xia, C.; Ma, F. van der Waals graphene/MoS2 heterostructures: tuning the electronic properties and Schottky barrier by applying a biaxial strain. *Materials Advances* **2022**, *3* (1), 624-631, 10.1039/D1MA00806D. DOI: 10.1039/D1MA00806D.

(485) Gao, S.; Wang, Z.; Wang, H.; Meng, F.; Wang, P.; Chen, S.; Zeng, Y.; Zhao, J.; Hu, H.; Cao, R.; et al. Graphene/MoS2/Graphene Vertical Heterostructure-Based Broadband Photodetector with High Performance. *Advanced Materials Interfaces* **2021**, *8* (3), 2001730. DOI: 10.1002/admi.202001730.

(486) Novoselov, K. S.; Mishchenko, A.; Carvalho, A.; Castro Neto, A. H. 2D materials and van der Waals heterostructures. *Science* **2016**, *353* (6298), aac9439. DOI: 10.1126/science.aac9439.

(487) Cho, K.; Lee, T.; Chung, S. Inkjet printing of two-dimensional van der Waals materials: a new route towards emerging electronic device applications. *Nanoscale Horizons* **2022**, *7* (10), 1161-1176, 10.1039/D2NH00162D. DOI: 10.1039/D2NH00162D.

(488) Withers, F.; Del Pozo-Zamudio, O.; Mishchenko, A.; Rooney, A. P.; Gholinia, A.; Watanabe, K.; Taniguchi, T.; Haigh, S. J.; Geim, A. K.; Tartakovskii, A. I.; et al. Light-emitting diodes by band-structure engineering in van der Waals heterostructures. *Nature Materials* **2015**, *14* (3), 301-306. DOI: 10.1038/nmat4205.

(489) McManus, D.; Vranic, S.; Withers, F.; Sanchez-Romaguera, V.; Macucci, M.; Yang, H.; Sorrentino, R.; Parvez, K.; Son, S.-K.; Iannaccone, G.; et al. Water-based and biocompatible 2D crystal inks for all-inkjet-printed heterostructures. *Nature Nanotechnology* **2017**, *12* (4), 343-350. DOI: 10.1038/nnano.2016.281.

(490) Dulal, M.; Islam, M. R.; Maiti, S.; Islam, M. H.; Ali, I.; Abdelkader, A. M.; Novoselov, K. S.; Afroj, S.; Karim, N. Smart and Multifunctional Fiber-Reinforced Composites of 2D Heterostructure-Based Textiles. *Advanced Functional Materials* **2023**, *33* (40), 2305901. DOI: 10.1002/adfm.202305901.

(491) Abbas, Q.; Raza, R.; Shabbir, I.; Olabi, A. G. Heteroatom doped high porosity carbon nanomaterials as electrodes for energy storage in electrochemical capacitors: A review. *Journal of Science: Advanced Materials and Devices* **2019**, *4* (3), 341-352. DOI: 10.1016/j.jsamd.2019.07.007.

(492) Maity, C. K.; Sahoo, S.; Verma, K.; Behera, A. K.; Nayak, G. C. Facile functionalization of boron nitride (BN) for the development of high-performance asymmetric supercapacitors. *New Journal of Chemistry* **2020**, *44* (19), 8106-8119, 10.1039/C9NJ06284J. DOI: 10.1039/C9NJ06284J.

(493) Fan, M.; Wu, J.; Yuan, J.; Deng, L.; Zhong, N.; He, L.; Cui, J.; Wang, Z.; Behera, S. K.; Zhang, C.; et al. Doping Nanoscale Graphene Domains Improves Magnetism in Hexagonal Boron Nitride. *Advanced Materials* **2019**, *31* (12), 1805778. DOI: 10.1002/adma.201805778.

(494) Gautam, C.; Tiwary, C. S.; Jose, S.; Brunetto, G.; Ozden, S.; Vinod, S.; Raghavan, P.; Biradar, S.; Galvao, D. S.; Ajayan, P. M. Synthesis of Low-Density, Carbon-Doped, Porous Hexagonal Boron Nitride Solids. *ACS Nano* **2015**, *9* (12), 12088-12095. DOI: 10.1021/acsnano.5b05847.

(495) Azadmanjiri, J.; Srivastava, V. K.; Kumar, P.; Wang, J.; Yu, A. Graphene-supported 2D transition metal oxide heterostructures. *Journal of Materials Chemistry A* **2018**, *6* (28), 13509-13537, 10.1039/C8TA03404D. DOI: 10.1039/C8TA03404D.

(496) Solís-Fernández, P.; Bissett, M.; Ago, H. Synthesis, structure and applications of graphene-based 2D heterostructures. *Chemical Society Reviews* **2017**, *46* (15), 4572-4613, 10.1039/C7CS00160F. DOI: 10.1039/C7CS00160F.

(497) Saha, S.; Jana, M.; Khanra, P.; Samanta, P.; Koo, H.; Murmu, N. C.; Kuila, T. Band Gap Engineering of Boron Nitride by Graphene and Its Application as Positive Electrode Material in Asymmetric Supercapacitor Device. *ACS Applied Materials & Interfaces* **2015**, *7* (26), 14211-14222. DOI: 10.1021/acsami.5b03562.

(498) Saha, S.; Jana, M.; Samanta, P.; Murmu, N. C.; Kim, N. H.; Kuila, T.; Lee, J. H. Investigation of band structure and electrochemical properties of h-BN/rGO composites for asymmetric supercapacitor applications. *Materials Chemistry and Physics* **2017**, *190*, 153-165. DOI: 10.1016/j.matchemphys.2017.01.025.

(499) Althubaiti, N.; Mussa, Y.; Bongu, C. S.; Bayhan, Z.; Arsalan, M.; Soliman, A.; Alsharaeh, E. Reduced graphene oxide/hexagonal boron nitride-based composite as a positive electrode in asymmetric supercapacitors. *Journal of Materials Science* **2022**, *57* (30), 14371-14385. DOI: 10.1007/s10853-022-07525-w.

(500) Li, T.; Jiao, X.; You, T.; Dai, F.; Zhang, P.; Yu, F.; Hu, L.; Ding, L.; Zhang, L.; Wen, Z.; et al. Hexagonal boron nitride nanosheet/carbon nanocomposite as a high-performance cathode material towards aqueous asymmetric supercapacitors. *Ceramics International* **2019**, *45* (4), 4283-4289. DOI: 10.1016/j.ceramint.2018.11.101.

(501) Patil, I. M.; Kapse, S.; Parse, H.; Thapa, R.; Andersson, G.; Kakade, B. 2D/3D heterostructure of h-BN/reduced graphite oxide as a remarkable electrode Material for supercapacitor. *Journal of Power Sources* **2020**, *479*, 229092. DOI: 10.1016/j.jpowsour.2020.229092.

(502) Worsley, R.; Pimpolari, L.; McManus, D.; Ge, N.; Ionescu, R.; Wittkopf, J. A.; Alieva, A.; Basso, G.; Macucci, M.; Iannaccone, G.; et al. All-2D Material Inkjet-Printed Capacitors: Toward Fully Printed Integrated Circuits. *ACS Nano* **2019**, *13* (1), 54-60. DOI: 10.1021/acsnano.8b06464.

(503) Zhou, K.-G.; Withers, F.; Cao, Y.; Hu, S.; Yu, G.; Casiraghi, C. Raman Modes of MoS2 Used as Fingerprint of van der Waals Interactions in 2-D Crystal-Based Heterostructures. *ACS Nano* **2014**, *8* (10), 9914-9924. DOI: 10.1021/nn5042703.

(504) Gołasa, K.; Grzeszczyk, M.; Bożek, R.; Leszczyński, P.; Wysmołek, A.; Potemski, M.; Babiński, A. Resonant Raman scattering in MoS2—From bulk to monolayer. *Solid State Communications* **2014**, *197*, 53-56. DOI: 10.1016/j.ssc.2014.08.009.

(505) Basu, N.; Satya Bharathi, M. S.; Sharma, M.; Yadav, K.; Parmar, A. S.; Soma, V. R.; Lahiri, J. Large Area Few-Layer Hexagonal Boron Nitride as a Raman Enhancement Material. In *Nanomaterials*, 2021; Vol. 11.

(506) Skorupska, M.; Kamedulski, P.; Lukaszewicz, J. P.; Ilnicka, A. The Improvement of Energy Storage Performance by Sucrose-Derived Carbon Foams via Incorporating Nitrogen Atoms. In *Nanomaterials*, 2021; Vol. 11.

(507) Chen, Y.; Wang, X.; Yu, C.; Ding, J.; Deng, C.; Zhu, H. Low temperature synthesis via molten-salt method of r-BN nanoflakes, and their properties. *Scientific Reports* **2019**, *9* (1), 16338. DOI: 10.1038/s41598-019-52788-0.

(508) Salvado, R.; Loss, C.; Gonçalves, R.; Pinho, P. Textile Materials for the Design of Wearable Antennas: A Survey. In *Sensors*, 2012; Vol. 12, pp 15841-15857.

(509) Carey, T.; Cacovich, S.; Divitini, G.; Ren, J.; Mansouri, A.; Kim, J. M.; Wang, C.; Ducati, C.; Sordan, R.; Torrisi, F. Fully inkjet-printed two-dimensional material field-effect heterojunctions for wearable and textile electronics. *Nature Communications* **2017**, *8* (1), 1202. DOI: 10.1038/s41467-017-01210-2.

(510) Li, B.; Hu, N.; Su, Y.; Yang, Z.; Shao, F.; Li, G.; Zhang, C.; Zhang, Y. Direct Inkjet Printing of Aqueous Inks to Flexible All-Solid-State Graphene Hybrid Micro-Supercapacitors. *ACS Applied Materials & Interfaces* **2019**, *11* (49), 46044-46053. DOI: 10.1021/acsami.9b12225.

(511) Sollami Delekta, S.; Smith, A. D.; Li, J.; Östling, M. Inkjet printed highly transparent and flexible graphene micro-supercapacitors. *Nanoscale* **2017**, *9* (21), 6998-7005, 10.1039/C7NR02204B. DOI: 10.1039/C7NR02204B.

(512) Li, Z.; Ruiz, V.; Mishukova, V.; Wan, Q.; Liu, H.; Xue, H.; Gao, Y.; Cao, G.; Li, Y.; Zhuang, X.; et al. Inkjet Printed Disposable High-Rate On-Paper Microsupercapacitors. *Advanced Functional Materials* **2022**, *32* (1), 2108773. DOI: 10.1002/adfm.202108773.

(513) Wang, H.; Zhu, Q.-L.; Zou, R.; Xu, Q. Metal-Organic Frameworks for Energy Applications. *Chem* **2017**, *2* (1), 52-80. DOI: 10.1016/j.chempr.2016.12.002.

(514) Qi, K.; Hou, R.; Zaman, S.; Qiu, Y.; Xia, B. Y.; Duan, H. Construction of Metal–Organic Framework/Conductive Polymer Hybrid for All-Solid-State Fabric Supercapacitor. *ACS Applied Materials & Interfaces* **2018**, *10* (21), 18021-18028. DOI: 10.1021/acsami.8b05802.

(515) Cheng, C.; Xu, J.; Gao, W.; Jiang, S.; Guo, R. Preparation of flexible supercapacitor with RGO/Ni-MOF film on Ni-coated polyester fabric. *Electrochimica Acta* **2019**, *318*, 23-31. DOI: 10.1016/j.electacta.2019.06.055.

(516) A. Grande, C.; I. Águeda, V.; Spjelkavik, A.; Blom, R. An efficient recipe for formulation of metal-organic Frameworks. *Chemical Engineering Science* **2015**, *124*, 154-158. DOI: 10.1016/j.ces.2014.06.048.

(517) Jiao, L.; Seow, J. Y. R.; Skinner, W. S.; Wang, Z. U.; Jiang, H.-L. Metal–organic frameworks: Structures and functional applications. *Materials Today* **2019**, *27*, 43-68. DOI: 10.1016/j.mattod.2018.10.038.

(518) Rauf, S.; Vijjapu, M. T.; Andrés, M. A.; Gascón, I.; Roubeau, O.; Eddaoudi, M.; Salama, K. N. Highly Selective Metal–Organic Framework Textile Humidity Sensor. *ACS Applied Materials & Interfaces* **2020**, *12* (26), 29999-30006. DOI: 10.1021/acsami.0c07532.

(519) Cao, Z.; Momen, R.; Tao, S.; Xiong, D.; Song, Z.; Xiao, X.; Deng, W.; Hou, H.; Yasar, S.; Altin, S.; et al. Metal–Organic Framework Materials for Electrochemical Supercapacitors. *Nano-Micro Letters* **2022**, *14* (1), 181. DOI: 10.1007/s40820-022-00910-9.

(520) Liang, J.; Luo, S.; Pan, D.; Xu, P.; Zhan, F.; Li, J. Metal organic framework derived CoNiOOH nanorods anchored on carbon cloth as electrodes for asymmetric supercapacitors. *Chemical Engineering Journal* **2023**, *464*, 142646. DOI: 10.1016/j.cej.2023.142646.

(521) Peterson, G. W.; Lee, D. T.; Barton, H. F.; Epps, T. H.; Parsons, G. N. Fibre-based composites from the integration of metal–organic frameworks and polymers. *Nature Reviews Materials* **2021**, *6* (7), 605-621. DOI: 10.1038/s41578-021-00291-2.

(522) Raphael Ezeigwe, E.; Dong, L.; Wang, J.; Wang, L.; Yan, W.; Zhang, J. MOF-deviated zinc-nickel–cobalt ZIF-67 electrode material for high-performance symmetrical coin-shaped supercapacitors. *Journal of Colloid and Interface Science* **2020**, *574*, 140-151. DOI: 10.1016/j.jcis.2020.04.025.

(523) Zhang, W.; Liu, X.; Gao, M.; Shang, H.; Liu, X. Co-Zn-MOFs Derived N-Doped Carbon Nanotubes with Crystalline Co Nanoparticles Embedded as Effective Oxygen Electrocatalysts. In *Nanomaterials*, 2021; Vol. 11.

(524) Lara, G. G.; Andrade, G. F.; Cipreste, M. F.; da Silva, W. M.; Gastelois, P. L.; Gomes, D. A.; de Miranda, M. C.; de Almeida Macedo, W. A.; Neves, M. J.; de Sousa, E. M. B. Protection of normal cells from irradiation bystander effects by silica-flufenamic acid nanoparticles. *Journal of Materials Science: Materials in Medicine* **2018**, *29* (8), 130. DOI: 10.1007/s10856-018-6134-5.

(525) Zhang, T.; Wu, J.; Xu, Y.; Wang, X.; Ni, J.; Li, Y.; Niemantsverdriet, J. W. Cobalt and cobalt carbide on alumina/NiAl(110) as model catalysts. *Catalysis Science & Technology* **2017**, *7* (24), 5893-5899, 10.1039/C7CY01806A. DOI: 10.1039/C7CY01806A.

(526) Han, H.; Bai, Z.; Wang, X.; Chao, S.; Liu, J.; Kong, Q.; Yang, X.; Yang, L. Highly dispersed Co nanoparticles inlayed in S, N-doped hierarchical carbon nanoprisms derived from Co-MOFs as efficient electrocatalysts for oxygen reduction reaction. *Catalysis Today* **2018**, *318*, 126-131. DOI: 10.1016/j.cattod.2018.03.032.

(527) Ou, J.; Wang, J.; Zhao, G.; Zou, L.; Lei, Y. Buckwheat derived nitrogen-rich porous carbon material with a high-performance Na-storage. *Journal of Porous Materials* **2020**, *27* (4), 1139-1147. DOI: 10.1007/s10934-020-00893-1.

(528) Luo, W.; Li, X.; Chen, J. Y. All-fabric flexible supercapacitor for energy storage. *Journal of Industrial Textiles* **2018**, *49* (8), 1061-1077. DOI: 10.1177/1528083718804208 (acccessed 2021/03/14).

(529) Chu, X.; Zhang, H.; Su, H.; Liu, F.; Gu, B.; Huang, H.; Zhang, H.; Deng, W.; Zheng, X.; Yang, W. A novel stretchable supercapacitor electrode with high linear capacitance. *Chemical Engineering Journal* **2018**, *349*, 168-175. DOI: https://doi.org/10.1016/j.cej.2018.05.090.

(530) Wang, J.; Malgras, V.; Sugahara, Y.; Yamauchi, Y. Electrochemical energy storage performance of 2D nanoarchitectured hybrid materials. *Nature Communications* **2021**, *12* (1), 3563. DOI: 10.1038/s41467-021-23819-0.

(531) Sun, Y.; Shi, G. Graphene/polymer composites for energy applications. *Journal of Polymer Science Part B: Polymer Physics* **2013**, *51* (4), 231-253. DOI: https://doi.org/10.1002/polb.23226 (acccessed 2023/08/29).

(532) Wang, K.; Hui, K. N.; San Hui, K.; Peng, S.; Xu, Y. Recent progress in metal–organic framework/graphene-derived materials for energy storage and conversion: design, preparation, and application. *Chemical Science* **2021**, *12* (16), 5737-5766, 10.1039/D1SC00095K. DOI: 10.1039/D1SC00095K.

(533) Zheng, Y.; Zheng, S.; Xue, H.; Pang, H. Metal-Organic Frameworks/Graphene-Based Materials: Preparations and Applications. *Advanced Functional Materials* **2018**, *28* (47), 1804950. DOI: https://doi.org/10.1002/adfm.201804950 (acccessed 2023/08/29).

(534) Choudhary, P.; Kumari Ola, S.; Chopra, I.; Dhayal, V.; Singh Shekhawat, D. Metal–organic framework (MOF)/graphene–oxide (GO) nanocomposites materials: A potential formulation for anti-corrosive coatings- a review. *Materials Today: Proceedings* **2023**, *79*, 172-178. DOI: https://doi.org/10.1016/j.matpr.2022.09.603.

(535) Qu, H.-j.; Huang, L.-j.; Han, Z.-y.; Wang, Y.-x.; Zhang, Z.-j.; Wang, Y.; Chang, Q.-r.; Wei, N.; Kipper, M. J.; Tang, J.-g. A review of graphene-oxide/metal–organic framework composites materials: characteristics, preparation and applications. *Journal of Porous Materials* **2021**, *28* (6), 1837-1865. DOI: 10.1007/s10934-021-01125-w.

(536) Weng, W.; Chen, P.; He, S.; Sun, X.; Peng, H. Smart Electronic Textiles. *Angewandte Chemie International Edition* **2016**, *55* (21), 6140-6169. DOI: 10.1002/anie.201507333.

(537) Rotzler, S.; Schneider-Ramelow, M. Washability of E-Textiles: Failure Modes and Influences on Washing Reliability. *Textiles* **2021**, *1* (1), 37-54. DOI: 10.3390/textiles1010004.

(538) Rotzler, S.; Krshiwoblozki, M. v.; Schneider-Ramelow, M. Washability of e-textiles: current testing practices and the need for standardization. *Textile Research Journal* **2021**, 0040517521996727. DOI: 10.1177/0040517521996727 (acccessed 2021/05/18).